REGIONAL SEDIMENT MANAGEMENT PLAN

APPENDICES

APPENDIX A

BIBLIOGRAPHY

Bibliography

1. Barry, J., et al. (1997), A New Broad Band Frequency Modulated Subbottom Profiling Developed for Hawaii, paper presented at Seventh Annual International Offshore and Polar Engineering Conference

2. Society of Offshore and Polar Engineers (ISOPE), Honolulu, HI, 1997.

3. Cacchione, D., et al. (2002), Sand transport within a reef channel off Kailua, paper presented at Ocean Science Meeting, American Geophysical Union, Honolulu.

4. Campbell, J.H. (1972), Erosion and Accretion of Selected Hawaiian Beaches, 1962-1972: Honolulu, NOAA Sea Grant Program, p. 1-30.

5. Chien, Y., and C. Murray (1999), Sand Thickness Exploration Model - Kailua Bay, Pacific Northwest National Laboratory.

6. Coastal Engineering Manual (2006), EM 1110-2-1100, USACE, Coastal and Hydraulics Laboratory.

7. Conger, C. L. F., C.H., and M. Barbee (2005), Artificial neural network classification of sand in all visible submarine and subaerial regions of a digital image, Journal of Coastal Research, 21, 1173-1177.

8. Department of Planning and Permitting, City and County of Honolulu (2000), Ko`olaupoko Sustainable Communities Plan, Ch 3, 1-47.

9. Edward K. Noda and Associates Inc., and DHM inc (1989), Hawaii shoreline erosion management study, 34-75 pp, Hawaii Coastal Zone Managment Program, Honolulu.

10. Ericksen, M. C., et al. (1997), Sub-bottom imaging of the Hawaiian shelf. , in Sea Technology, edited, pp. 89-92.

11. Fletcher, C. H., et al. (1996), Coastal erosion management on the island of Oahu., 102-111 pp, University of Hawaii, DLNR, Honolulu.

12. Fletcher, C. H., et al. (1997), Beach loss Along Armored Shorelines on Oahu, Journal of Coastal Research, 13, 209-215.

13. Gerritsen, F. (1978), Beach and Surf Parameters in Hawaii: Honolulu, NOAA Sea Grant, p. 1-178.

14. Grossman, E. C., and C. H. Fletcher (2004), Holocene Reef Development Where Wave Energy Reduces Accommodation Space. Kailua Bay, Windward Oahu, Hawaii, USA, Journal of Sedimentary Research, 74, 49-63.

15. Hampton, M. A., et al. (2004), Carbonate Sediment Deposits on the Reef Front Around Oahu, Hawaii, Marine Georesources and Geotechnology, 22, 65-102.

16. Harney, J. N. (2000), Carbonate Sedimentology of a Windward Shoreface: Kailua Bay, Oahu, Hawaiian Islands, 232 pp, University, Honolulu.

17. Harney, J. N., and C. H. Fletcher (2003), A budget of Carbonate Framework and Sediment Production, Kailua Bay, Oahu, Hawaii, Journal of Sedimentary Research, 73, 856-868.

18. Harney, J. N., et al. (2000), Age and composition of carbonate shoreface sediments, Kailua Bay, Oahu, Hawaii, Coral Reefs, 19, 141-154.

19. Harney, J. N., et al. (1999), Standing crop and sediment production of reef-dwelling foraminifera on Oahu, Hawaii, Pacific Science, 53, 61-73.

20. Hawaii State Department of Health (2001), Total Maximum daily Loads Estimated for Waimanalo Stream - Island of Oahu, Hawaii-, 35 pp, U.S. Environmental Protection Agency Specifications, Hawaii.

21. Ho, F. P., and L. A. Sherretz (1969), A preliminary study of ocean waves in the Hawaiian area, 36 pp, University of Hawaii, HIG-69-16, Seagrant 69-2, Honolulu.

22. Hwang, D. (1981), Beach changes on Oahu as revealed by aerial photographs: Honolulu, Urban and Regional Planning Program and Hawaii Institute of Geophysics, p. 1-146.

23. Isoun, E. (2001), A remote sensing study of coral reefs; Kailua bay, Oahu, 99 pp, University of Hawaii, Honolulu.

24. Isoun, E., et al. (2003), Multi-spectral mapping of the reef bathymetry and coral cover Kailua Bay, Hawaii, Coral Reefs, 22, 68-82.

25. Krock, H. J., and H. Sundararaghavan (1993), Kailua Bay Circulation (KB-5), 24 pp, Univ. of Hawaii, Water Resources Research Center, Honolulu.

26. Laevastu, T., Avery, D. E., Cox, D. C. (1964), Coastal currents and sewage disposal in the Hawaiian Islands: Honolulu, Department of Planning and Economic Development, State of Hawaii, p. 1-101.

27. Laevastu, T., et al. (1964), Coastal currents and sewage disposal in the Hawaiian Islands., 36-38 pp, Univ. of Hawaii, HIG-64-1, Honolulu.

28. Lander, J. F., and P. A. Lockridge (1989), United States Tsunamis, 17-23 pp, National Geophysical Data Center, Boulder.

29. Laws, E. A., and L. Ferentinos (2003), Human Impacts on Fluxes of Nutrients and Sediment in Waimanalo Stream, Oahu, Hawaiian Islands., Pacific Science, 57, 119-140.

30. Laws, E. A., and L. Roth (2004), Impact of Stream Hardening on Water Quality and Metabolic Characteristics of Waimanalo and Kaneohe Stream, Oahu, Hawaiian Islands, Pacific Science, 58, 261-280.

31. Lipp, D.G. (1995), Changes in beach profiles due to wave reflections off seawalls at Lanikai, Hawaii [unpublished Masters thesis]: University of Hawaii, Honolulu, 76 p.

32. Moberly, R., Jr. et al. (1965), Source and Variation of Hawaiian Littoral Sand, Journal of Sedimentary Petrology, 35, 589-598.

33. Moberly, R., Jr. and T. Chamberlain (1964), Hawaiian Beach Systems, 64-65 pp, Univ. of Hawaii, Honolulu.

34. Mullane, Robert and D. Suzuki (1997), Beach Management Plan for Maui, County of Maui Planning Department, p. 1-35.

35. Norcross, Z.M. (2001), Large-scale alongshore meanders on a carbonate beach substitute for seasonal morphology in response to wave state [unpublished Masters thesis]: University of Hawaii, Honolulu, 37 p.

36. Norcross, Z. M., et al. (2002), Annual and terannual changes on a reef-fringed pocket beach: Kailua Bay, Hawaii, Marine Geology, 190, 553-580.

37. Pararas-Carayannis, G., and J. P. L. Calbaugh (1977), Catalog of Tsunamis in Hawaii, 25, 29, 50 pp, World Data Center A for Solid Earth Geophysics, Report SE-4, Boulder.

38. Regional Sediment Management (RSM) Demonstration Program Technical Note, U.S. Army Corps of Engineers Engineer Research and Development Center, ERDC/RSM-TN-2, June 2003.

39. Richmond, B. M., et al. (2002), Sand transport within a reef channel off Kailua, Oahu, Hawaii, paper presented at Ocean Science meeting, American Geophysical Union, Honolulu.

40. Sea Engineering Inc. (1989), Oahu Shoreline Study, Part 2, Management Strategies: Waimanalo, HI.

41. Sea Engineering Inc. (1993), Beach Nourishment: Waimanalo, HI, p. 1-33.

42. Shaw, S. L. (1981), A history of tropical cyclones in the central North Pacific and the Hawaiian Islands 1832-1979, 125 pp, NOAA, National Weather Service, Silver Spring.

43. Smith, D.A. (2003), Effect of particle shape on grain size, hydraulic, and transport characteristics of calcareous sand [unpublished dissertation]: University of Hawaii, Honolulu, 94 p.

44. Smith, T. D. and J. R. Hayes, Southeast Oahu Regional Sediment Management: Identifying Sediment Pathways in the Vicinity of Wailea Point, Regional Sediment Management, Winter/Spring 2006

45. Tetra Tech EM Inc (2003), Kailua Waterways Improvement Plan, 95 pp, Kailua Bay Advisory Council, Honolulu.

46. US Army Corps of Engineers (2004), Regional Sediment Management Primer.

47. Walker, D. A. (1994), Tsunami Facts, 31-37 pp, University of Hawaii, SOEST Tech. Report 94-03, Honolulu.

48. Wyrtki, K., et al. (1969), Current observations in the Hawaiian archipelago, 1-27 pp, Univ. of Hawaii, Office of Naval Research - Contract nonr-3748(06), Honolulu.

APPENDIX B

SOUTHEAST OAHU REGIONAL SEDIMENT MANAGEMENT DEMONSTRATION PROJECT SCOPE OF WORK

SOUTHEAST OAHU REGIONAL SEDIMENT MANAGEMENT DEMONSTRATION PROJECT

Regional Beach Management Plan
Scope of Work
August 7, 2006

BACKGROUND: The Southeast Oahu Regional Sediment Management (SEO/RSM) demonstration project is being conducted to (1) document long-term trends in wave climate for the windward side of Oahu, Hawaii, (2) develop a regional sediment budget and a geographic information system (GIS) for three littoral cells along the southeast Oahu coast, (3) identify suitable sand sources, and (4) develop/calibrate a sediment transport model for the region. The SEO region is located on the southeast shoreline of the island of Oahu, Hawaii. There are three littoral cells, Kailua in the north, Lanikai in the middle, and Waimanalo in the south part of the study area. There are geologic controls (both sub-aerial and offshore) affecting sediment transports within these cells. The offshore region is a sloping reef along which waves break on its outer edge. Waves are depth-limited by the reef as they approach the shoreline. SEO/RSM investigations are being conducted to determine if there is sediment transport between the cells. Long-term (decadal or more) shifts in wind, wave direction, and wave period may shift sediment transport patterns and magnitudes. As a result, sediment transport processes of these beaches are difficult to understand, and RSM solutions are not readily apparent. The final products from this study will be a sand source inventory, web-enabled GIS platform and regional beach management plan for the SEO region.

REGIONAL BEACH MANAGEMENT PLAN: The work to be performed under this task order is the preparation of the SEO/RSM Regional Beach Management Plan (RBMP) report. The RBMP report will document all of the activities that have been conducted since the beginning of the SEO/RSM investigations in fiscal year 2005 (see attached SEO/RSM scope of work). Work that has been performed by the Honolulu District, Coastal & Hydraulics Laboratory, Geotechnical and Structures Laboratory and the University of Hawaii (UH) will be documented in the RBMP report along with the results of the study workshops (the next workshop is to be held on August 23, 2006). Descriptions of the various tasks that have been completed are provided as attachments to this document. Reference is also made to the “Beach Management Plan for Maui” dated December 1997 as prepared for the County of Maui Planning Department by UH Sea Grant Extension Service. Many of the SEO/RSM products can be found online at the following web site.

http://gis.poh.usace.army.mil/rsm/pages/index.htm

RBMP Report: The RBMP report will consist at a minimum of the follow sections that compile the study results to date:

Executive Summary
Introduction
Regional Sediment Management
Southeast Oahu Regional Sediment Management Demonstration Project
Coastal Ecosystem
Coastal Erosion, Beach Loss and Coral Reef Degredation
Objectives
- Identification of Erosion Hotspots and Erosion Watchspots
- Guidelines for Shoreline Protection Measures
- Beach Nourishment
  - Sand Sources for Beach Nourishment
  - Pilot Beach Nourishment Project
- Dune Preservation and Restoration
- Coral Reef Ecosystems, Water Quality, and Upland Activities
- Shoreline Setbacks and Coastal Erosion Hazard Data
- Proactive Development of Coastal Lands
- Inter-agency Coordination
- Structures and Activities within the Shoreline Area
  - Minor Structures
  - Major Structures
- Beach Management Districts
- Public Awareness and Education

Coastal Processes Modeling
- Wave Climate
- Water Circulation
- Littoral Sediment Transport
- Regional Sediment Budget

Geomorphology
Shoreline Change
Sediment Trend Analysis
Sand Source Investigations
Workshops
Web-based GIS
Literature Search/Inventory
Potential Demonstration Projects (PDP)
PDP Alternatives (to be developed as part of this report)
Appendices (to include documentation of all study products covered in the attachments to this SOW and the SEO/RSM web site).

SPECIFICATIONS: The report is to be prepared in Microsoft Office Word as a "doc" file. All products generated in the process of report preparation will be provided to the Government upon completion of the task order work. Arial 12 font will be used for the text portion of the report.

MEETINGS: The A/E firm will meet individually with Oahu representatives having input into the various study products (such as employees of the Honolulu District, Hawaii Department of Land and Natural Resources (DLNR) and the University of Hawaii) to attain an in depth perspective on SEO/RSM related activities. The A/E will also make telephone contact with mainland contributors to the study. The A/E will arrange at least four progress meetings with SEO/RSM project delivery team (PDT members include Honolulu District, DLNR and UH personnel) to discuss progress on the report and issues to be resolved. The A/E will prepare draft minutes from each meeting and provide them to the PDT for review and comment. The A/E will prepare final meeting minutes based on comments received from the PDT.

DELIVERABLES: Deliverables will consist of meeting minutes as well as preliminary, draft and final RBMP reports. All products generated in the preparation of the final RBMP report will be provided to the Government prior to issuance of final payment.

SCHEDULE:

TASK	DATE
Preliminary FBMP Report	September 28, 2006
Draft FBMP Report	October 27, 2006
Final FBMP Report	November 30, 2006
Associated Products	November 30, 2006
Final Meeting Minutes	10 days after meetings

ATTACHMENT 1:

Regional Sediment Management
Southeast Oahu
Hawaii

Purpose: This study will (1) document long-term trends in wave climate for the windward side of Oahu, Hawaii, (2) develop a regional sediment budget and a geographic information system (GIS) for three interconnected littoral cells along the southeast Oahu coast, (3) identify suitable sand sources, and (4) develop/calibrate a sediment transport model for the region. The final products from this study will be a sand source inventory, regional sediment management (RSM) plan and web-enabled GIS platform for the South East Oahu (SEO) Region.

Problem: The SEO Region is located on the southeast shoreline of the island of Oahu, Hawaii. There are three littoral cells, Kailua in the north, Lanikai in the middle, and Waimanalo in the south part of the study area (Figure 1). There are geologic controls (both subaerial and offshore) affecting sediment transport within these cells. The offshore region is a sloping reef along which waves break on its outer edge. Waves are depth-limited by the reef as they approach the shoreline. The cells are not believed to share sediment with each other. The long-term average rate of shoreline retreat is nominally 2 feet/year. Long-term (decadal or more) shifts in wind, wave direction, and wave period may shift sediment transport patterns and magnitudes. As a result, sediment transport processes of these beaches are difficult to understand, and RSM solutions are not readily apparent. In addition, sand sources for this region have not been identified.

Proposal: A description of the tasks is presented below. Figure 2 shows a timeline of the various tasks.
Total duration: 4 years.

Task 1: Develop long-term wave climate.
Time: 12 mos.
From observations of shoreline position on the northeast side of Oahu, it appears that there is a long-term trend (20 or more years) of erosion and accretion. These cycles of beach change may be caused by shifts in wave climate, including multi-decadal shifts in storm activity associated with the Pacific Decadal Oscillation. Task 1 will utilize or generate updated Wave Information Study hindcast for the project area. Directional wave buoy data are available for the years 2000-2002, and non-direction wave buoy data are available for more than 20 years. These data will be used for validation of the hindcast. This task will provide a regional wave climate for Task 5, regional shoreline modeling.

Task 2: Nearshore circulation.
Time: 8 mos.
Because waves are depth-limited as they approach the study area, it is believed that nearshore circulation (wave- and wind-induced) may be a significant process controlling sediment transport. This task will setup and run the Advanced Circulation model for the study area. There are no current data available for validation; thus, three separate drogue studies are planned under a range of wave and wind conditions.

Task 3: Geomorphic analysis of study area.
Time: 10 mos.
Historical shoreline position, beach profile, aerial photography, bathymetric, and geologic information for the study area will be evaluated to identify (a) long-term trends in shoreline position; (b) long-term trends in bathymetric change; (c) locations with possible sources of beach nourishment material, and (d) geologic controls on littoral processes. Historical shoreline position data are available from the University of Hawaii. Sand samples will be taken for each littoral cell, and sediment cores will be collected and analyzed for possible offshore sources of material. Because of the low hardness value of the sediment, it is possible that abrasion or mechanical disintegration is a significant process in shoreline retreat. The abrasive characteristics of beach sediments will be quantified. This task will provide data for Task 4, development of the regional sediment budget, and the calibration and verification data set for Task 5, regional shoreline modeling.

Task 4A: Develop a regional sediment budget.
Time: 10 mos.
Volumetric change for historical and present-day time periods will be developed for the active littoral region. These data, together with knowledge of the long-term wave and wind climate (Task 1) and regional shoreline modeling (Task 5), will be used to develop sediment budgets for each littoral cell. Sediment sources and sinks will be defined and quantified. A regional budget will be developed, including an assessment of whether long-term sand sharing between littoral cells occurs. The regional sediment budget will be used to develop a RSM plan, and a with-project regional sediment budget will be forecasted.

Task 4B: Develop a web-enabled GIS platform.
Time: 10 mos.
A web-based GIS platform will be developed for the SEO Region. The GIS will contain georeferenced maps, attributes and metadata corresponding to SEO Region RSM requirements. Aerial photography, digital elevation models, geotechnical information, survey data, wave parameters and other pertinent georeferenced information will be automated via the GIS. The GIS will utilize state-of-the-art web enabling software to provide real-time access of products through the internet. The GIS will reside at the Mobile District.

Task 5: Regional shoreline change modeling.
Time: 12 mos.
The regional shoreline change model presently in developmental testing, Cascade, will be calibrated and verified for the study region. The wave climate produced in Task 1 will drive the model, and shoreline positions, geologic controls, and bathymetric contours defined in Task 3 will be used for calibration and verification. The regional modeling will work hand-in-hand with development of the regional sediment budget (Task 4A). A RSM plan will be developed using results from each task. This RSM plan will document long-term trends in beach change, and identify possible sources of sand, to management of sediment within the region. Travel funding for trips to/from the mainland for various team members is also included in the estimate.

Task 6B: Sand source investigations.
Time: 4 years
Sand sources will be identified in areas offshore and upland of the region. Research and development of sand manufacturing techniques will also be carried out under the task.

Schedule and Funding: As indicated in Figure 2, the RSM demonstration project for the SEO Region will take four years to complete.

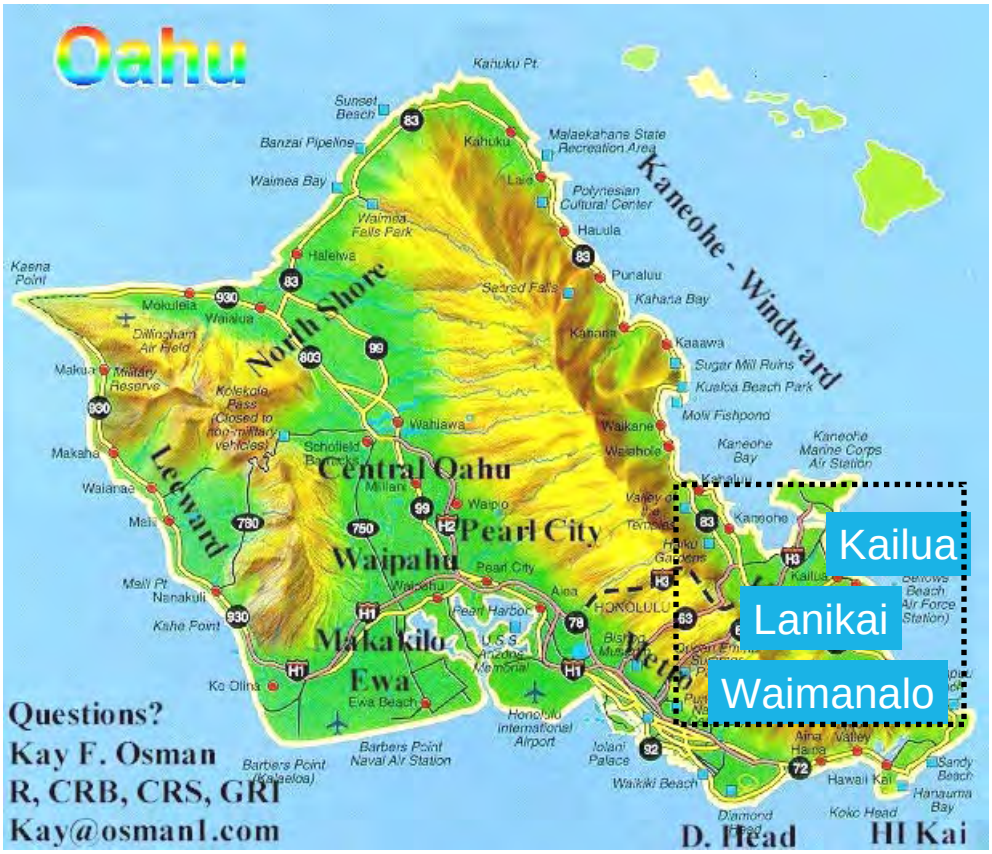

Figure 1. Project study area

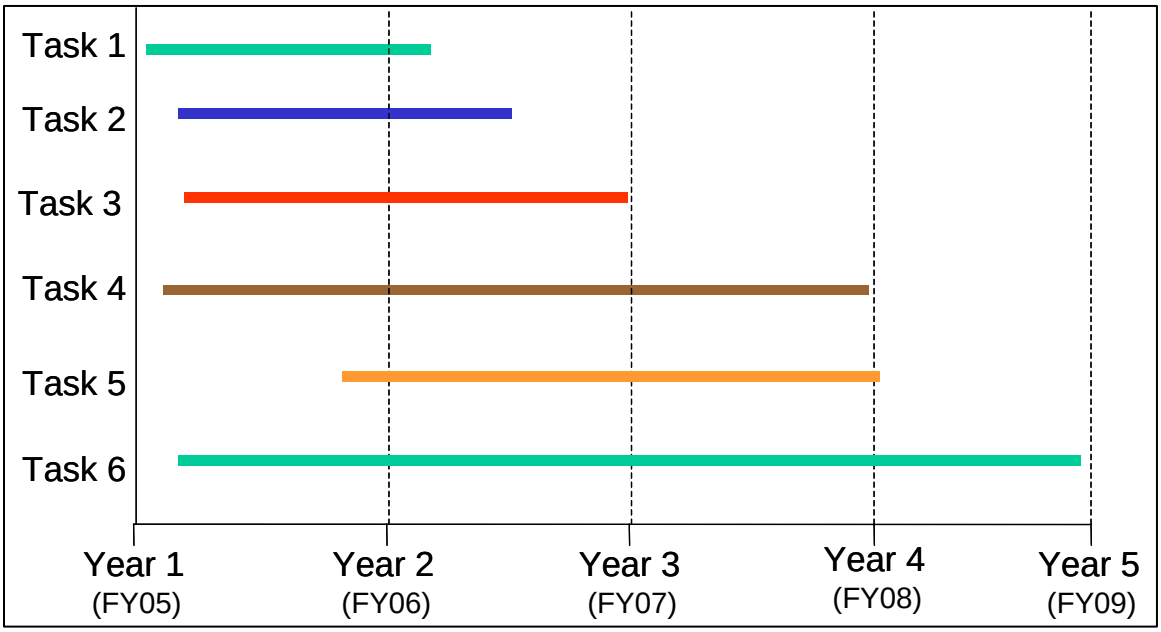

Figure 2. FY schedule and funding levels for the Southeast Oahu RSM demonstration project.

ATTACHEMENT 5

DRAFT Scope of Work
CHL Nearshore Circulation Modeling for Southeast Oahu, Hawaii

The proposed work includes six technical tasks: data collection/assessment, finite element and finite difference grid development, development of model forcing conditions, model calibration, model simulations, and simulation analysis. The tasks are linked and sequential, however, the first three tasks may be accomplished in parallel. The final product from these tasks is a calibrated hydrodynamic model for the project site. The models applied will be as follows:

a) Long-Wave Hydrodynamic Model – ADCIRC. The ADCIRC long-wave hydrodynamic model simulates the circulation and water levels associated with both tides and storms. A two-dimensional (depth-averaged) version of ADCIRC will be applied. ADCIRC has been extensively applied in the Atlantic and Pacific Oceans (and world wide) to simulate tidal circulation and associated storm surge and currents. The hydrodynamic modeling component will require the following tasks:

1. Grid development to include recent bathymetry and shoreline data.
2. Calibration and verification of the bathymetric grid to known tidal constituents. This phase of the investigation will provide circulation patterns for determining placement of water elevation and current measurement gages.
3. Re-verify model by comparison to measurements made for this study.
4. Development/selection of alternative forcing conditions.

b) Short-Wave Modeling – STWAVE. *STWAVE is a spectral wave transformation model, which is capable of representing wave-current interaction (wave-action equation, current-induced breaking, and wave blocking by a current). The ADCIRC and STWAVE models will be coupled to allow the interchange of radiation stresses from STWAVE to ADCIRC, and tide-, wind-, and wave-generated currents from ADCIRC to STWAVE. Application of STWAVE will require the following:*

1. Development of computational grid to simulate wave propagation.
2. Verification of calculated waves by comparison to measurements.
3. Generation of wave climate.

Study Phases

An approach toward development of a “turn-key” hydrodynamic modeling system should be pursued in a phased process. Activities including identifying and assembling data, grid development, tidal and wind-driven current and water level calibration, and nearshore wave transformation will be accomplished via a cooperative effort between POH and CHL personnel with in the field assistance provided by CHL.

Phase 1:

POH and CHL will jointly develop the geographic, bathymetric, hydrodynamic (waves and circulation), and meteorological data necessary to develop and calibrate the modeling system. An assessment of the quality of available data will aid in the specification of necessary additional field measurements. In addition, a decision will be reached as to what computer platform will be utilized to exercise the modeling system. CHL and POH will develop and calibrate the ADCIRC model for tidal constituent forcing, including in the field assistance if desired. Development of the finite element grid for the overall project will focus on a coarse resolution at the seaward, deep-water boundaries and detailed resolution in the nearshore regions of interest. Any recently collected bathymetric data will be evaluated and incorporated into the model grid and bathymetric databases will be used to supplement bathymetry for the grid domain.

Phase 2:

CHL will establish the range of atmospheric forcing required for accurate simulations. CHL and POH will develop and calibrate the STWAVE grid and perform an additional ADCIRC calibration including atmospheric forcing and coupling with STWAVE. This effort will include in the field assistance by CHL. These calibration simulations will utilize the POH current field measurement effort. Tidal forcing conditions will be developed for the ocean boundary condition using the LeProvost or OSU Pacific constituent database. Offshore wind and pressure fields generated by a combination of NCEP/NCAR winds and pressures adjusted for local observations will also be used as forcing conditions for the hydrodynamic model.

Phase 3:

CHL will assist POH in developing recommendations for alternative simulations, will document the methodologies and procedures, and will provide consultation in executing simulations and analyzing simulation results. The transfer of the completed modeling system to POH will be accomplished within the SMS framework.

ATTACHMENT 6:

Project: Southeast Oahu Regional Sediment Management Demonstration Project – Identification of Beach Quality Sand Sources and Investigation of Sand Manufacturing Techniques

Scope and Purpose: Carbonate sand is needed for the repair and restoration of beaches in Southeast Oahu, Hawaii. This project is directed to:

1) Locating sources of coral-based carbonate rock or gravel that can be ground to provide a clean carbonate sand.

2) Developing protocols for manufacturing carbonate sand by crushing and grinding coral-derived rock or gravel. Specifically this would involve the development of techniques for processing the carbonate to produce sand that will not re-cement when placed above the tidal zone on a beach.

3) Locating any alternate sand sources both onshore and offshore that could be used in beach construction. The goal of this project is to locate coral-reef derived carbonate material for the beach construction in sufficient quality to allow the development of a plan for the reconstruction effort and to determine the methods, equipment and material requirements needed for the production of a non-cementing carbonate beach sand. Additionally the project will complete a survey of the general availability of beach construction materials both on-shore and offshore. The time constraints and the level of funding for this phase of the work do not allow for dredging to obtain any new underwater carbonate samples.

Approach: A preliminary investigation of the carbonate supply problem will be undertaken to determine the availability of carbonate deposits using data developed in the investigations that have been undertaken by researchers from the U.S. Geological Survey, the University of Hawaii, and contractors. Archived sediment samples will be requested from past investigations. A preliminary assessment will be followed up with the collection of additional data and archived or stockpiled samples of the most promising deposits that occur within distances from the project area that make transport realistic economically.

Re-cementation of carbonate sand that is above sea level and subjected to leaching in fresh water is a significant problem. In Florida and Bermuda, natural carbonate beaches rarely have re-cementation problems that impact beach usage. The lack of dissolution of calcium carbonate and recrystallization of carbonate as cement is thought to be related to the presence of natural organic coatings on the carbonate sands. Extraction and analysis of organics from natural organic sands

shows that the surface of the grains has a coating of calcium salts of naturally occurring fatty acids (calcium stearate or calcium laurate). The coatings prevent the surface of the calcium carbonate from wetting effectively and disrupt any epitaxial growth of carbonate cements. In manufactured calcium carbonate sand, the freshly crushed material has clean surfaces that can act as templates form the formation of more crystalline calcium carbonate that can cement adjacent surfaces together. Additionally the presence of fine-grained material and sand-sized material with sharp edges and corners can contributed to the dissolution and reprecipitation that make beach rock out of beach sand.

The investigation of methods of manufacturing non-cementing beach sand will concentrate on the usefulness of using a well-sorted sand-sized particles that are tumbled to produce rounded grains and on the effects of adding coatings calcium salts of fatty acids. Phosphates in small quantities retard carbonate crystal formation and many fatty acids occur in nature with phosphate groups attached. As a coating material these compounds could be very effective crystal growth (cement) inhibitors. The systems proposed for investigation are all natural process that are being reintroduced into an manufactured sand to reproduce the non-cementing phenomenon occurring on normal carbonate beaches.

To support the development a sand manufacturing protocol, lab bench scale test will be set up to evaluate the importance of grain size and shape and the usefulness of coating materials. A test matrix will be developed with a variety of control samples to allow the evaluation of the separate properties of the sand treatments.

An overall assessment of aggregates (carbonate and non-carbonate and on-shore and off-shore) will also be included in this investigation. This survey of availability to assure that the most economical sources of material are located from the project and no useful resource that could make the project more effective or economical is overlooked. This phase of the investigation will allow the beach repair planners to optimize the use of resources and justify their selection of specific materials and specific sources. The program will include characterization of selected materials and estimates of amounts available and transport to the construction site.

APPENDIX C

TR-08-9: SOUTHEAST OAHU COASTAL HYDRODYNAMIC MODELING WITH ADCIRC AND STWAVE

ERDC/CHL TR-08-9

Coastal and Hydraulics Laboratory

US Army Corps of Engineers®
Engineer Research and Development Center

Southeast Oahu Coastal Hydrodynamic Modeling with ADCIRC and STWAVE

Mary A. Cialone, Mitchell E. Brown, Jane M. Smith, and Kent K. Hathaway

July 2008

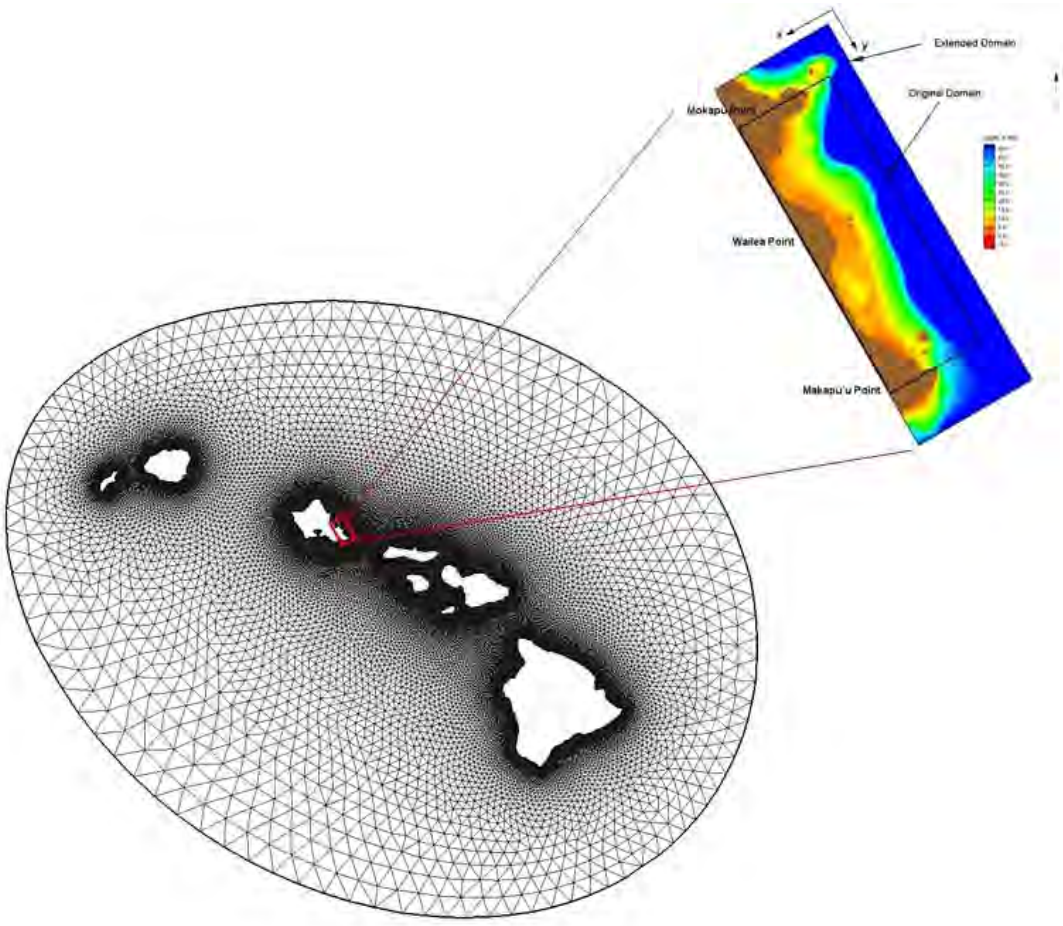

ERDC/CHL TR-08-9
July 2008

Southeast Oahu Coastal Hydrodynamic Modeling with ADCIRC and STWAVE

Mary A. Cialone, Mitchell E. Brown, Jane M. Smith, and Kent K. Hathaway

Coastal and Hydraulics Laboratory
U.S. Army Engineer Research and Development Center
3909 Halls Ferry Road
Vicksburg, MS 39180-6199

Final report

Prepared for U.S. Army Engineer District, Honolulu
Building 230
Fort Shafter, HI 96858-5440

Abstract: This study provides the Honolulu District (POH) with numerical modeling tools for understanding nearshore circulation and sediment transport for Southeast Oahu (SEO). Circulation and wave models are developed and validated for this region and can be applied to assess sediment transport potential for various forcing conditions and to determine the likelihood of accretional and erosional areas within the model domain.

Application of a wave model includes the generation of a wave climate. In the wave climate development technique, nearshore conditions are extracted from the wave model results for each simulation. A transformation correlation between the offshore and nearshore condition is then determined for each simulation. By applying the appropriate transfer function to each wave condition in the offshore time series, a long-term nearshore time series is generated. The nearshore time series demonstrates that there is a reduction in wave height from the offshore location to the nearshore location, landward of the extensive reef system as expected. The technique of developing a nearshore wave climate by applying the wave model for a range of offshore wave conditions provides a permanent "look up" table of nearshore wave conditions at any location in the computational domain and can be applied to any time period for which offshore data are available, provided that bathymetric conditions within the model domain remain similar. POH is applying the database-generated time series to develop sediment transport potential estimates in the project area.

Development of a bottom friction capability in the wave model was completed for application to the extensive reefs in the SEO study area. It is shown that bottom friction is extremely important and has a pronounced effect on modeling transformation over reefs, decreasing wave heights from the without-friction condition by 71-76% for a constant JONSWAP bottom friction value of 0.05.

Contents

Figures and Tables

Figures

Tables

Preface

This technical report describes a hydrodynamic modeling study for Southeast Oahu, Hawaii. The purpose of the nearshore circulation modeling study for the Southeast Oahu Regional Sediment Management (SEO/RSM) demonstration project was for the U.S. Army Engineer Research and Development Center (ERDC), Coastal and Hydraulics Laboratory (CHL) to provide the U.S. Army Engineer District, Honolulu, with a tool for understanding nearshore circulation and sediment transport in the study area. RSM supported field data collection and initial modeling and the Surge and Wave Island Modeling Studies Project supported refinement of STeady-state spectral WAVE model (STWAVE) friction capability and publication of this report. The study was conducted during the period April 2005 through September 2006.

The numerical modeling investigation was conducted by Mary A. Cialone, Coastal Processes Branch (CBP), CHL; and Mitchell E. Brown, Senior Scientist Group, CHL; with technical assistance from Jane M. Smith, CBP, CHL; and data reduction from Dr. Lihwa Lin, Coastal Engineering Branch, CHL. The field data collection was conducted by Kent K. Hathaway, Field Research Facility, CHL; and Raymond Chapman, CBP, CHL; with local assistance from Thomas Smith, Jessica Hays, and Stan Boc, Honolulu District; Chip Fletcher, University of Hawaii at Manoa; and Oliver Vetter, University of Hawaii at Manoa, now of the National Oceanic and Atmospheric Administration.

This project was conducted under the direct supervision of Ty Wamsley, Chief, CPB. General supervision was provided by Dr. William D. Martin, Deputy Director, CHL; and Thomas W. Richardson, Director, CHL.

COL Richard B. Jenkins was Commander and Executive Director of ERDC. Dr. James R. Houston was Director.

1 Introduction

The project area for the hydrodynamic modeling study described in this report is located along the southeast shoreline of the island of Oahu, Hawaii from Mokapu Point to Makapu'u Point (Figure 1). This stretch of coast is considered part of the "windward" side of the island, that is, where the predominant wind travels from the sea to land. Tradewinds and North Pacific waves affect the island's windward side. Tradewind waves occur throughout the year, but are most persistent in the summer, ranging between 1 and 3 m high with periods of 6 to 10 sec. The direction of approach, like the tradewinds themselves, varies between north-northeast and east-southeast and is centered on the east-northeast direction.

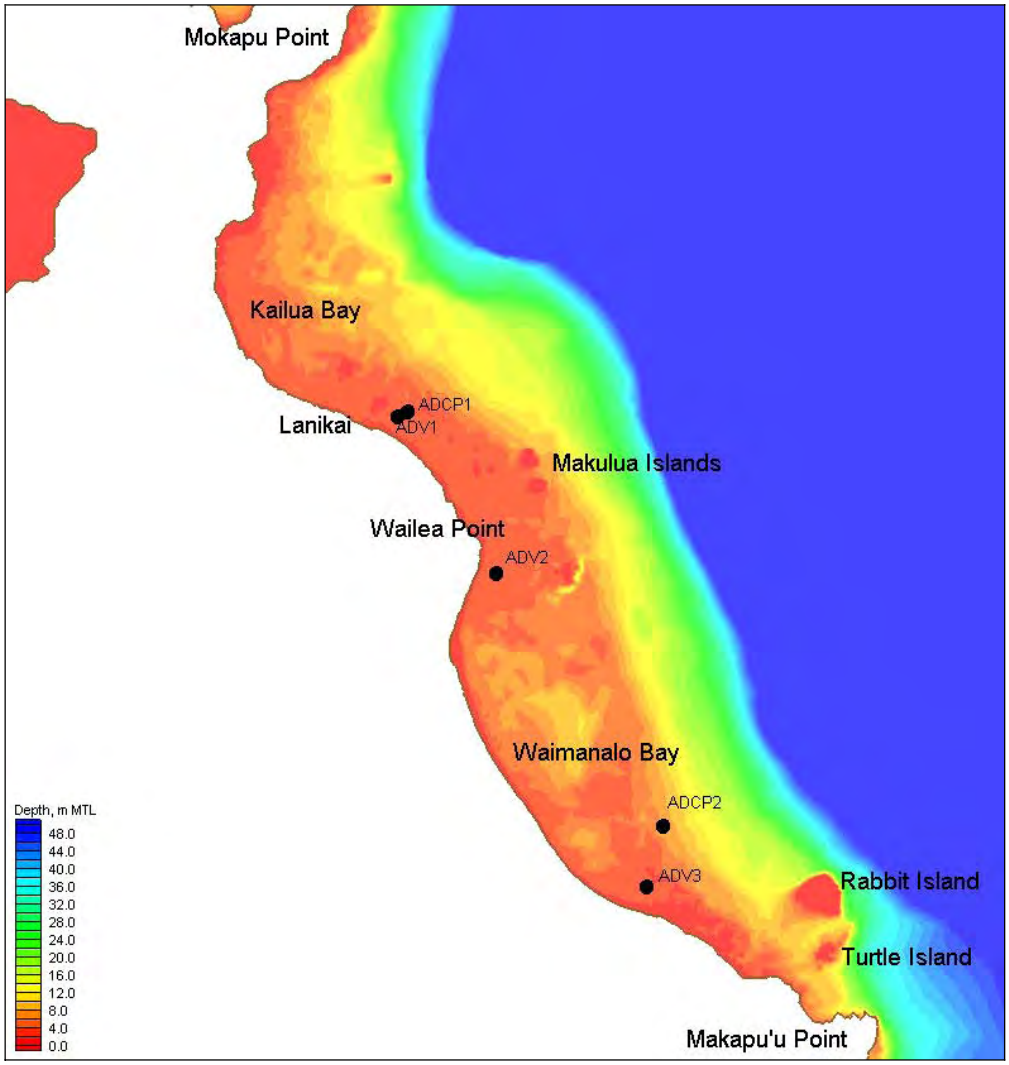

Figure 1. Project area location map and instrument locations.

During the winter months, storms generate large North Pacific swells that range in direction from west-northwest to northeast and arrive at the northern Hawaiian shores with little attenuation of wave energy. Deep-water wave heights often reach 5 m and, in extreme cases, can reach 9 m with periods of 12 to 20 sec. In the study area, offshore waves are generally from the east-northeast and range in height from 0.5 to 6.0 m. Peak wave periods are generally 6 to 16 sec (Sea Engineering 2008).

The ultimate goal for the Honolulu District (POH) was to understand sediment transport potential in the region and determine the likelihood of accretional and erosional areas within the model domain. There are three littoral cells along the project reach: Kailua in the north, Lanikai in the central portion, and Waimanalo in the southern part of the study area in which geologic controls (both subaerial and offshore) affect sediment transport. The offshore region is a sloping reef along which depth-limited waves break. Long-term (decadal or longer) shifts in wind, wave direction, and wave period have the potential to shift sediment transport patterns and magnitudes, therefore making sediment transport processes for this region difficult to understand. The focus of the work presented in this report, however, is the nearshore circulation study project, which included six technical tasks:

1. data collection/assessment,
2. finite-element and finite-difference grid development,
3. development of model forcing conditions,
4. model validation,
5. model simulations, and
6. simulation analysis.

The final product from these tasks was validated hydrodynamic and wave models for the Southeast Oahu (SEO) region. The Honolulu District could then apply the models with various forcing conditions to achieve their goal in better understanding the nearshore circulation and sediment transport potential in the region and determining the likelihood of accretional and erosional areas within the model domain.

Circulation (ADCIRC) and wave (STWAVE) models were applied in this study. The ADvanced CIRCulation (ADCIRC) long-wave hydrodynamic model simulates the circulation and water levels associated with both tides and atmospheric conditions (Luettich et al. 1992).

The two-dimensional, depth-averaged version of ADCIRC was applied in this study. ADCIRC has been extensively applied in the Atlantic and Pacific Oceans (and world wide) to simulate tidal circulation and associated storm surge and currents (U.S. Army Corps of Engineers (USACE) 2006; USACE, Mobile District, 2008; Kraus and Arden 2003; Kraus 2006). The hydrodynamic modeling component for this study required:

1. grid development to include recent bathymetry and shoreline data,
2. validation of the bathymetric grid to known tidal constituents and wind forcing, and
3. comparison of the ADCIRC simulation model results for the bathymetric grid forced with known tidal constituents, wind, and waves to measurements for the field data collection time period.

The application and validation of ADCIRC for the SEO study provides POH with the capability of simulating circulation in the study area for any required time period.

The STeady-state spectral WAVE model (STWAVE) is a spectral wave transformation model, which is capable of representing depth-induced wave refraction and shoaling, current-induced refraction and shoaling, depth- and steepness-induced wave breaking, diffraction, wind-wave growth, wave-wave interaction and whitecapping (Resio 1988; Smith et al. 2001). The purpose of applying nearshore wave transformation models such as STWAVE is to describe quantitatively the change in wave parameters between the offshore and the nearshore. Offshore time-series wave data are typically available; however, nearshore wave information is required for the design of almost all coastal engineering projects. STWAVE has previously been applied to numerous sites with a gently sloping seafloor or small areas of hardbottom. Due to the wide and relatively shallow reef fronting the shoreline of the SEO region, this application of STWAVE required the added feature of simulating wave transformation over a reef. Development of a bottom friction capability in STWAVE was completed to address this unique bathymetry specific to the island environment. Application of STWAVE for this project required development of a computational grid to simulate wave propagation, verification of calculated waves by comparison to measurements, and generation of a wave climate. The ADCIRC and STWAVE models were then coupled to allow the STWAVE radiation stresses to force circulation within ADCIRC.

The approach toward development of a “turn-key” hydrodynamic modeling system for this region was pursued in a phased process. In the first phase, the Honolulu District and the Coastal and Hydraulics Laboratory (CHL) jointly developed the geographic, bathymetric, hydrodynamic (waves and circulation), and meteorological data necessary to develop and validate the modeling system. An assessment of the quality of available data aided in the specification of additional field measurements that were to be collected for this project. CHL developed and validated the ADCIRC model for tidal constituent forcing at the ocean boundary condition using the Oregon State University (OSU) Pacific constituent database. Development of the finite-element grid for the overall project focused on a coarse resolution at the seaward, deepwater boundaries and detailed resolution in the nearshore region of interest. All recently collected bathymetric data, including SHOALS (Wozencraft and Irish 2000) data collected in 2000, were evaluated and incorporated into the model grid, and bathymetric databases were used to supplement bathymetry for the grid domain.

In Phase 2 development, CHL established the range of atmospheric forcing required for accurate simulations. CHL developed the STWAVE grid, validated the STWAVE model, and performed an additional ADCIRC validation including atmospheric forcing and coupling with STWAVE. These validation simulations utilized the field measurement effort for comparison to model results. Tidal forcing conditions were developed for the ocean boundary condition with the LeProvost tidal constituent database, which provided a stable solution for the linked model validation time period (LeProvost et al. 1994). Offshore wind and pressure fields generated by a combination of wind fields and pressures adjusted for local observations were used as forcing conditions for the hydrodynamic model. These fields are discussed in detail in Chapter 3, section on “Wind sources.” Wave conditions from a Coastal Data Information Program (CDIP) buoy near the study site were used to generate boundary forcing conditions for the wave model. STWAVE was validated by comparing model-predicted and field measurements of wave conditions at the field data collection locations. The bottom friction was calibrated in the model to represent the reef and non-reef areas until a close comparison was achieved. ADCIRC was validated by comparing model-predicted and field measurements of water level and velocity at the field data collection locations. A hybrid friction formulation in ADCIRC and a range of wave radiation stress gradients from STWAVE were applied to achieve the best comparison.

In Phase 3, CHL assisted POH in developing recommendations for alternative simulations, documented the methodologies and procedures, and provided consultation in executing simulations and analyzing simulation results. The completed modeling system has been transferred to the Honolulu District within the Surface Water Modeling System (SMS) framework and training has been provided to the Honolulu District for future applications.

2 Field Data Collection

Wave and current data were collected for this project from 9 August to 14 September 2005 with two RD Instruments Workhorse Acoustic Doppler Current Profilers (ADCPs) and three Sontek Hydra Acoustic Doppler Velocimeters (ADVs). The field data collection deployment period was dominated by tradewind weather (typically occurring from April through September in Hawaii) as characterized by consistent winds from the northeast and occasional swells from the southeast and southwest. Large wave events affecting the windward coast are not typical during this season. Waves along the windward coast during these months are typically generated from local winds, and this is evident in the relatively small wave heights and northeasterly incident direction of the waves recorded during the deployment period. Instrument locations and additional information are shown in Figure 1 and Table 1. All recording gauges were referenced to coordinated universal time (UTC).

Table 1. Instrument identification and location (Hawaii RSM gauge locations, August–September 2005).

Gauge		Latitude deg min	Longitude deg min	Recording Time Period	Nominal Depth, m
Type	Name				
ADCP	ADCP1	21 23.905	157 42.994	9 August–14 September	3.3
ADCP	ADCP2	21 20.318	157 40.786	10 August–4 September	6.6
ADV	ADV1	21 23.861	157.43.079	9 August–14 September	2.5
ADV	ADV2	21 22.509	157 42.233	9 August–14 September	2.7
ADV	ADV3	21 19.795	157 40.930	9 August–14 September	2.5

ADCP gauges

For this study, two RD Instruments 1200 kHz Workhorse ADCP gauges were deployed for approximately 1 month. The ADCPs were bottom mounted, facing upward with the sensor head approximately 0.4 m off the bottom. The water depth at ADCP1 was approximately 3.3 m and the water depth at ADCP2 was approximately 6.6 m, located near the seaward edge of the reef flat. These gauges have four acoustic transducers for measuring currents and a pressure sensor, from which horizontal and vertical current profiles were computed at 0.2 m vertical spacing. Waves were calculated from the decay in orbital velocities. These instruments sampled at 2 Hz for

directional wave measurements. Each hourly wave burst was approximately 34 min long, starting at the top of each hour, and consisted of 4096 points. The instruments have a 0.44-m blanking distance from the transducer head, and a 0.2-m bin width makes the first sample 0.72 m above the transducer. The profiles, therefore, span from 1.12 m off the ocean bed to the moving free surface position. Current profiles were collected every 10 min from a 200 point average.

The ADCP deployments were on 9 August 2005 and retrieval was on 14 September 2005. ADCP2 was reprogrammed on 10 August so data collection started a day later than the other instruments, and the batteries were depleted on 4 September, about 10 days before retrieval of all gauges. The ADCP2 data record was, therefore, 11 days shorter than the other gauge records.

ADV gauges

In addition to the two ADCPs, three ADV gauges were deployed for the same 1-month time period. ADV deployments were on 9 August 2005 and retrieval was on 14 September 2005. The three ADV gauges were Sontek's Hydra model that samples a single-point current velocity (U, V, and W) and contains an external pressure sensor. With these instruments, wave height, period, and direction are determined from PUV analysis (pressure and orbital velocities) (Guza and Thornton 1980). The sample volume for the current measurement is approximately 1–2 cm in size and about 0.17 m above the center transducer. This instrument uses three beams to determine the three current components. Both the ADCP and ADV instruments and their mounts are shown in Figure 2. Figure 3 shows wave height, peak period, and mean direction for the three ADV gauges. Figure 4 depicts wave roses (peak direction) for the two ADCP gauges.

Current drogues

Four current drogues (drifters) were designed and built at the CHL Field Research Facility (FRF) in Duck, NC, for deployment at the beginning (10 August 2005) and end (13 September 2005) of the ADCP/ADV deployment period. The approximately 1-m by 1-m drogues were constructed with polyvinyl chloride (PVC) pipe, vertical risers, rubber unions (connectors), hose clamps, and sails. They used Global Positioning System (GPS) receivers for tracking and radio telemetry for positioning (Figure 5).

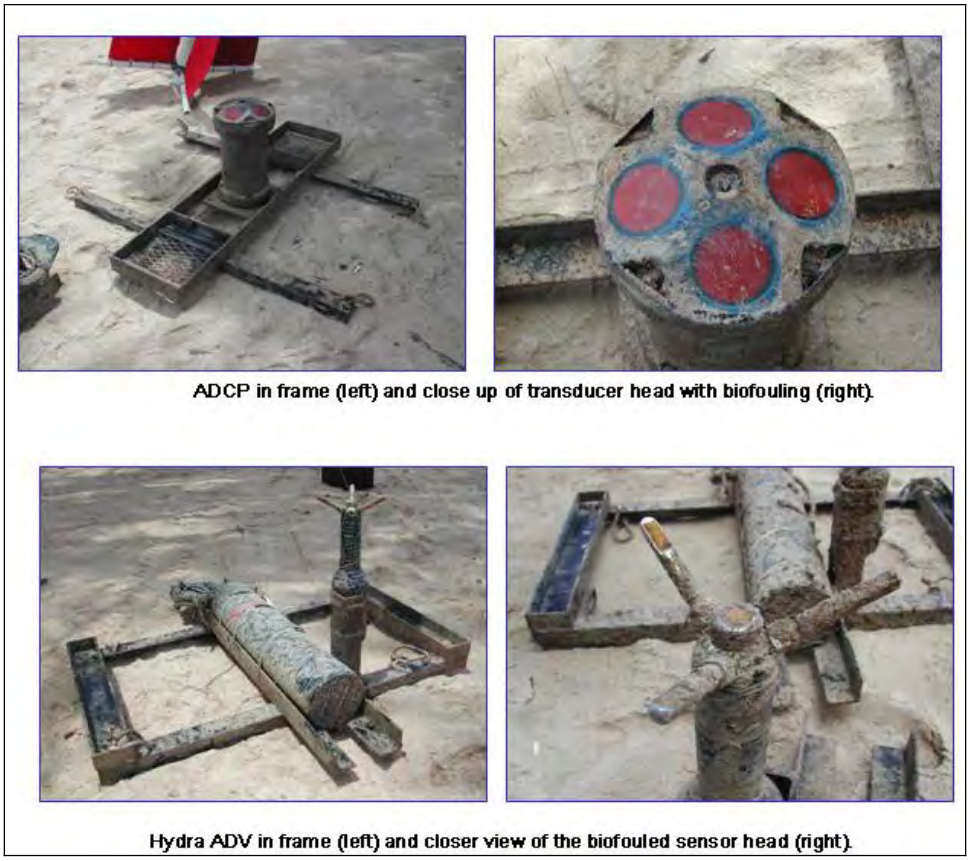

Figure 2. Images of gauges and mounts.

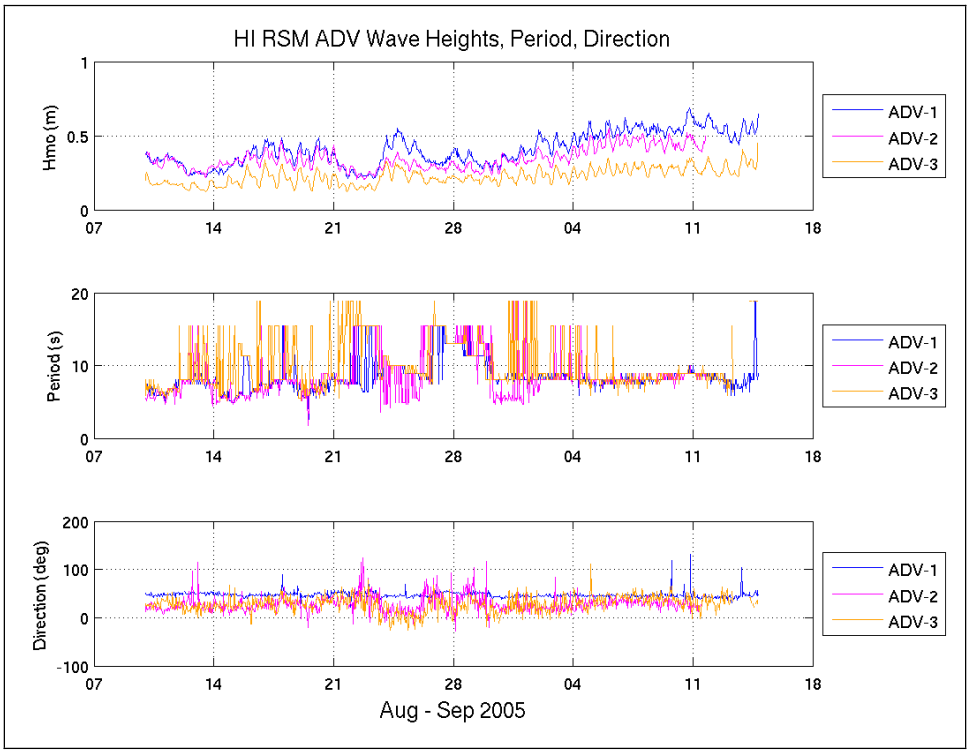

Figure 3. Wave height, period, and direction from the three ADV gauges.

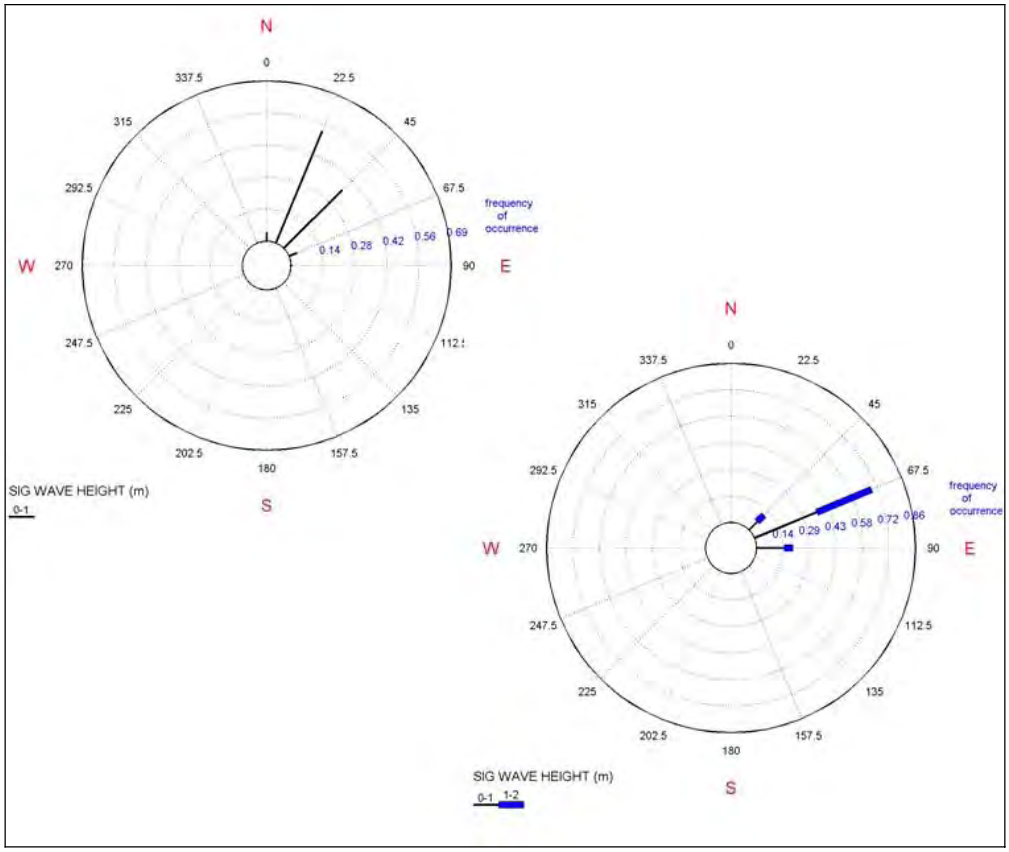

Figure 4. Wave roses for ADCP #1 (left) and #2 (right).

Figure 5. GPS current drogue (left) with traditional drifter (behind grapefruit) and Hawaiian drifter (coconut). Drifter floats just below surface (right).

The drogues floated just below the surface, which placed the bottom of the sail about 1 m from the ocean surface. Difficulty with the radio tracking was experienced because it required line of sight to receive signals from the drifters. Since the drifters were in two different locations (Kailua Bay and Waimanalo Bay), partial tracking was all that could be accomplished. In addition, two antennas and connectors were broken during deployment.

Current drogue tracks for 10 August 2005 and 13 September 2005 are shown in Figure 6. There were two deployments on 10 August, hence the numbers 1 through 8. Some drogues were deployed in the vicinity of the ADV and ADCP gauges for inter-comparison. A track direction reversal of Drogue #2 was observed shortly after deployment on 13 September (Figure 7), starting off on a nearly due west track and then turning back to a southeast trajectory. The nearshore drogues tended to track in a westerly (shoreward) direction at a rate of approximately 0.1–0.2 m/sec, which is comparable to model results. Drogues in Waimanalo Bay moved in a southerly direction during the two deployment periods.

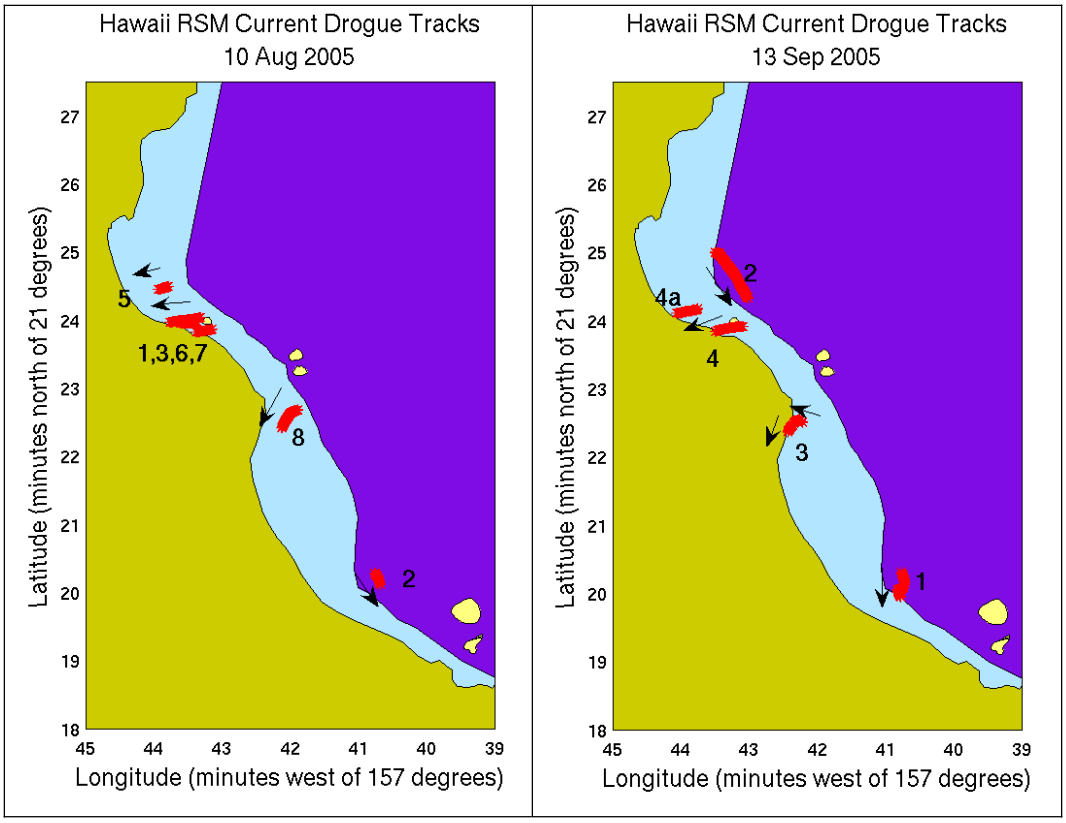

Figure 6. Drogue tracks with track numbers for 10 August (left) and 13 September (right).

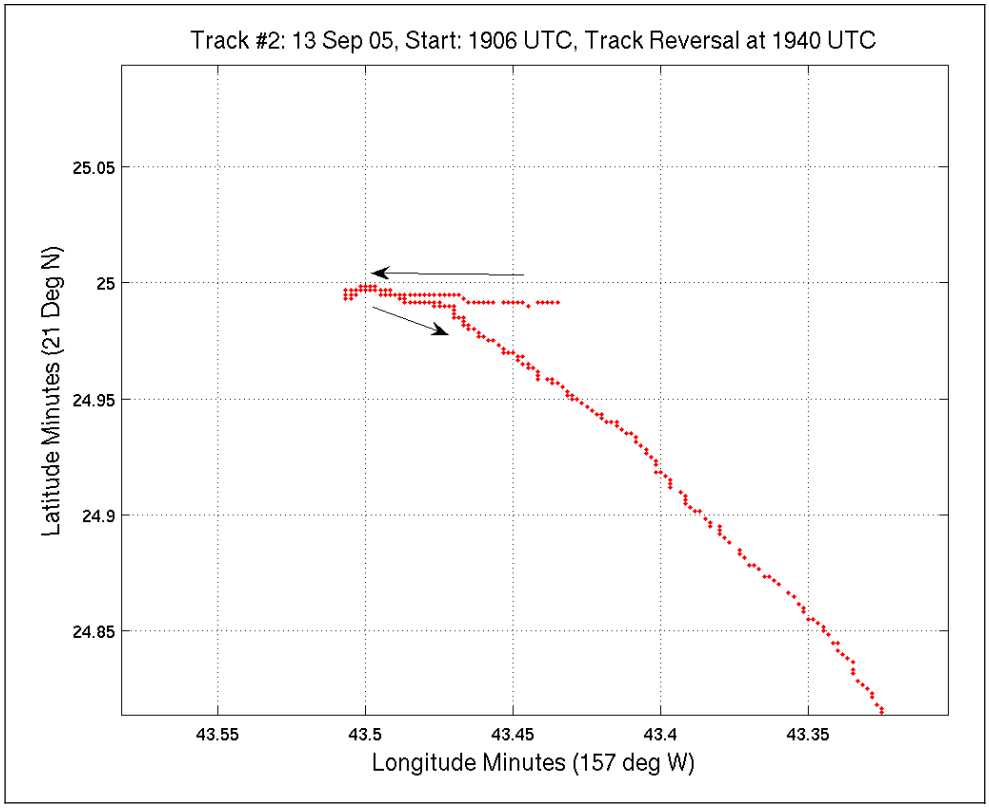

Figure 7. Drogue track reversal on 13 September.

3 Hydrodynamic Modeling

ADCIRC grid development

The ADCIRC (Luettich et al. 1992) numerical model, a regional two-dimensional (2-D) depth-integrated, finite-element hydrodynamic circulation model, was applied in this study to provide water level and depth-averaged current (circulation) information for SEO. The model solves the shallow-water equations in full nonlinear form and can be forced with tide, wind, waves, and flux boundary conditions. Two ADCIRC model grids were developed in the course of this modeling initiative. The first grid was a large circular grid centered on the SEO region and extended from the central point approximately 21 degrees latitude and longitude (2,300 km) in all directions. Initial attempts at validation were unsuccessful because of the existence of two tidal amphidromes that were close to the forcing boundary, shown in Figure 8. (An amphidrome is a location in the ocean where tidal amplitude is zero due to canceling of tidal waves.) To eliminate the problem introduced by the tidal amphidromes, the spatial extent of the ADCIRC model domain was reduced.

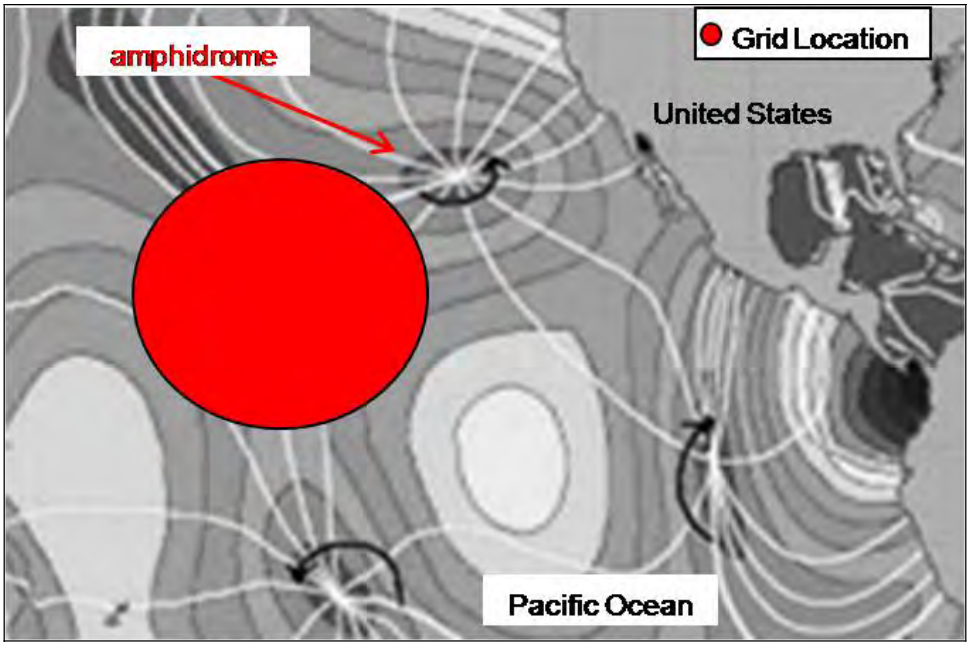

Figure 8. Approximate location of grid and amphidrome locations (background image from http://en.wikipedia.org/wiki/Image:M2_tidal_constituent.jpg).

The final ADCIRC mesh, shown in Figure 9, was a subdomain of the initial grid and is oblong in shape due to the orientation of the Hawaiian Islands. Depths on the mesh were referenced to mean tide level (mtl). The mesh contains 73,305 computational nodes and 140,849 elements. Individual element area ranges from a maximum of 462,500 km^2 in deep water to a minimum of 60 m^2 surrounding many of the island features. High resolution was added to the existing ADCIRC mesh in the study area around bathymetric features, such as islands, entrances, and reefs. The refined grid had many improvements over the initial grid:

1. The ADCIRC grid mesh is forced with the free surface position along the open-water boundary that surrounds the Hawaiian Islands. Since the extent of the grid domain for the final grid is smaller than the grid extent for the initial grid, the forcing boundary for the final grid is far away from the influence of the tidal amphidromes shown in Figure 8.
2. The area of Honolulu Harbor is better resolved in the final grid, which improves the comparison between calculated tides and gauge data in this area.

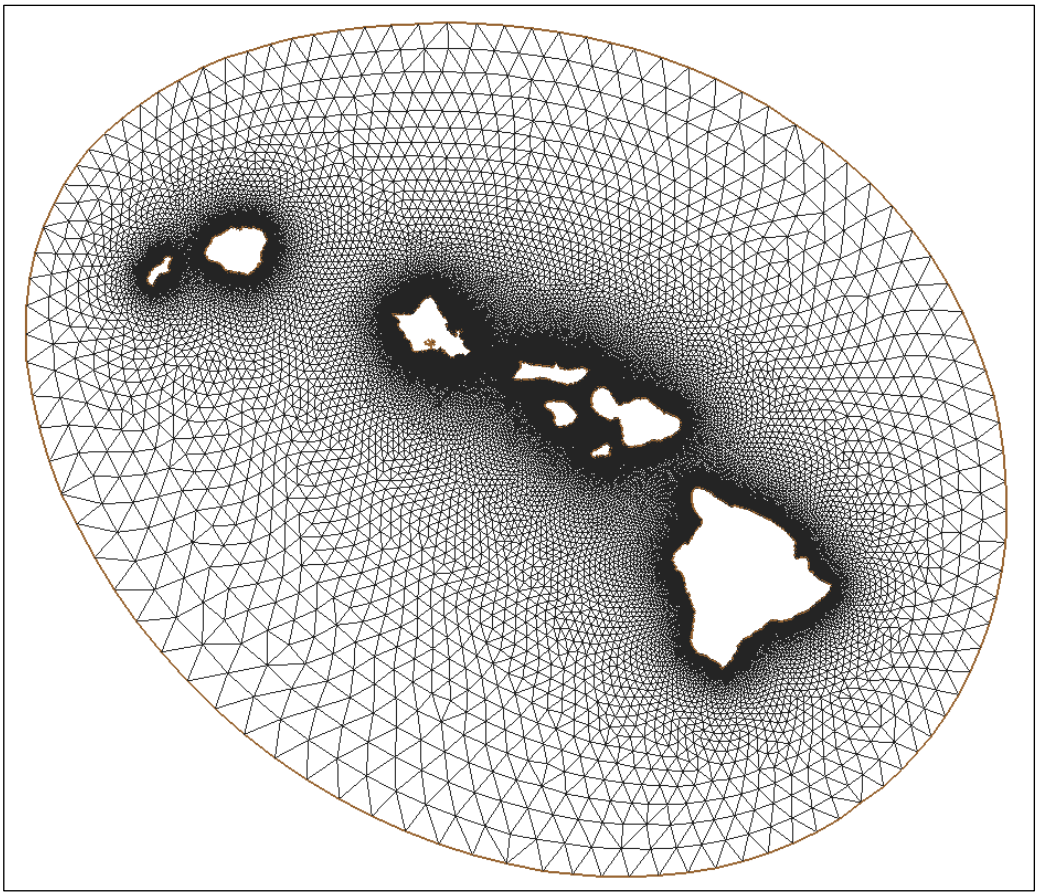

Figure 9. Final ADCIRC mesh domain.

3. Resolution around prominent features in the project reach was added, as well as topographic information for Rabbit and Turtle Islands located in the southern portion of the SEO region.

Wind sources

Three wind sources were investigated for potential application as a forcing condition in the ADCIRC model: National Oceanic and Atmospheric Administration (NOAA) National Data Buoy Center (NDBC) Buoy 51001, National Centers for Environmental Prediction (NCEP) hindcast, and Oceanweather, Inc. (OWI) hindcast wind data. The elevation of NCEP and OWI wind sources was 10 m. The NDBC buoy data were empirically transformed from the 5-m to 10-m elevation. A comparison of the observed (transformed) wind speed and direction at the NDBC Buoy 51001 and the nearest NCEP prediction point was performed for the months of January to June 2001 (Figure 10). Wind directions compared well; however, the NCEP wind speed consistently exceeded the buoy observations by 5 to 10 percent. These differences can be attributed to the buoy anemometer height being empirically transformed from the 5-m to 10-m elevation, whereas the NCEP surface level winds are predicted at an elevation of approximately 10 m. The comparisons suggest that long-term, historic NCEP winds can be applied in this project with a high degree of confidence for the initial validation time period.

NDBC Buoy 51001 winds were also compared to the predicted OWI basin level Pacific hindcast winds for the month of April 2001. A plot of this comparison is shown in Figure 11. Wind speed and directions compared well. These data suggest that OWI winds can also be applied to the project with a high degree of confidence. OWI winds were applied for the second validation (gauge deployment) time period.

ADCIRC model validation – wind and tide for initial validation time period

In the initial validation, the time period 10–24 April 2001 was selected for comparing model results to measured data because the OWI winds compared well with other wind sources for this time period. ADCIRC was forced along the open boundary with tidal information extracted from the OSU TOPEX/POSEIDON Crossover (TPXO) tidal database (Egbert et al. 1994). Wind speed and direction information were obtained from NDBC Buoy 51001. The ADCIRC hydrodynamic time-step was 0.4 sec and results

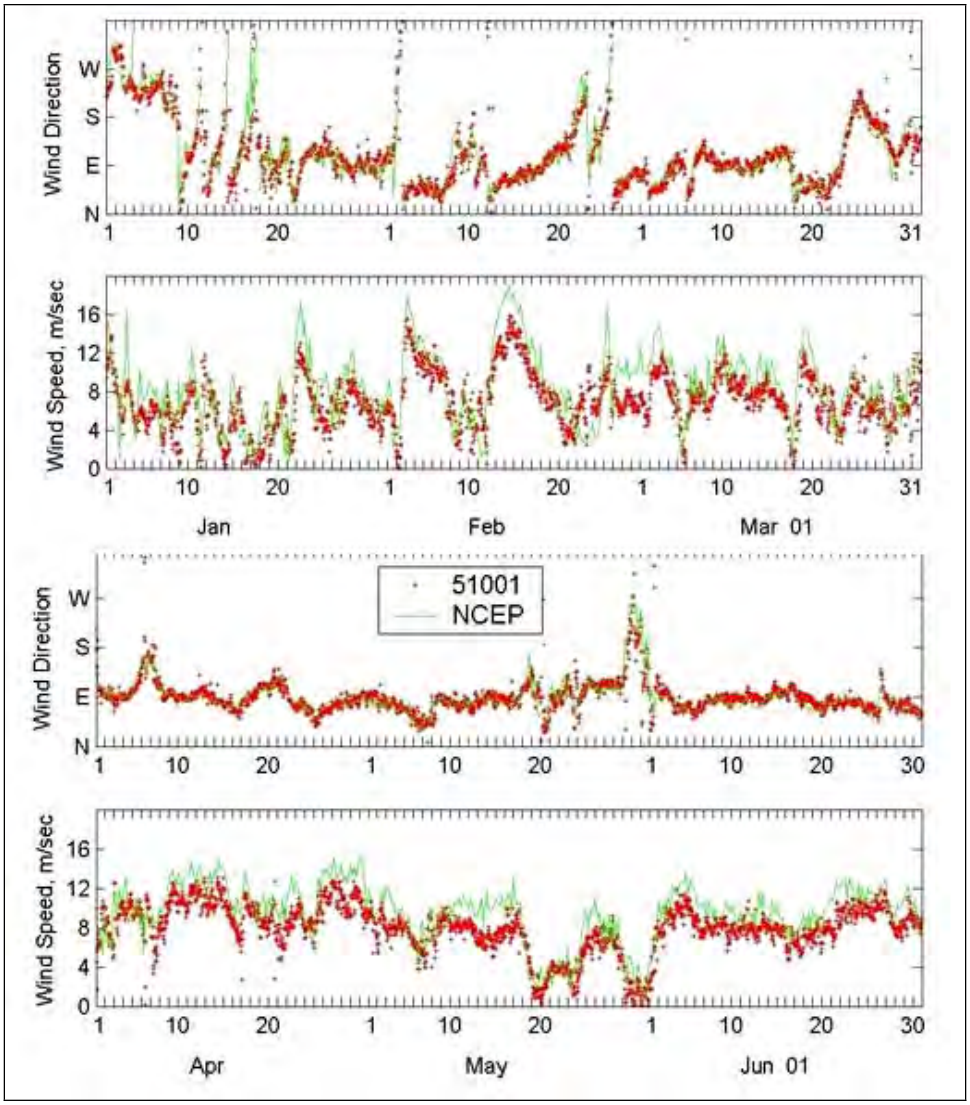

Figure 10. Comparison of observed (NDBC Buoy 51001) transformed to the 10-m elevation and predicted (NCEP) wind speed and direction.

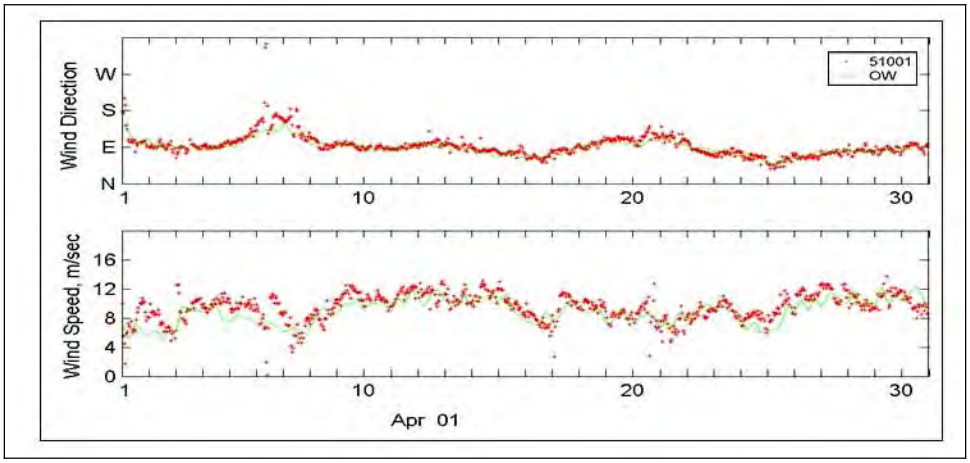

Figure 11. Comparison of observed (NDBC Buoy 51001) and predicted (OWI) wind speed and direction for April 2001.

were reported hourly. Simulations were performed on the U.S. Army Engineer Research and Development Center's (ERDC) High-Performance Computer (HPC) system in Vicksburg, MS, due to the large size of the ADCIRC domain.

For this initial model validation, ADCIRC results for water level were compared with the two NOAA tide gauges available on the southern and eastern portion of the island of Oahu. Figure 12 shows the locations of the two gauges (red circles) and their proximity to the project area (black box). The calculated water levels from the ADCIRC simulation of the April 2001 time period compared relatively well in range and phase with the NOAA gauge measurements, considering that the locations of the gauges were well outside the area of high resolution in the project area. Water level comparisons of the ADCIRC validations to the two NOAA gauges, Honolulu Harbor and Kaneohe Bay, are shown in Figures 13 and 14. Since these gauges were outside the project area and located in less resolved locations, it was determined that another validation would be made with the water level and current data received from ADV and ADCP gauges for the deployment period from 10–31 August 2005. Results of that validation are provided later in section entitled, "ADCIRC validation—wind, tide, and waves for gauge deployment time period."

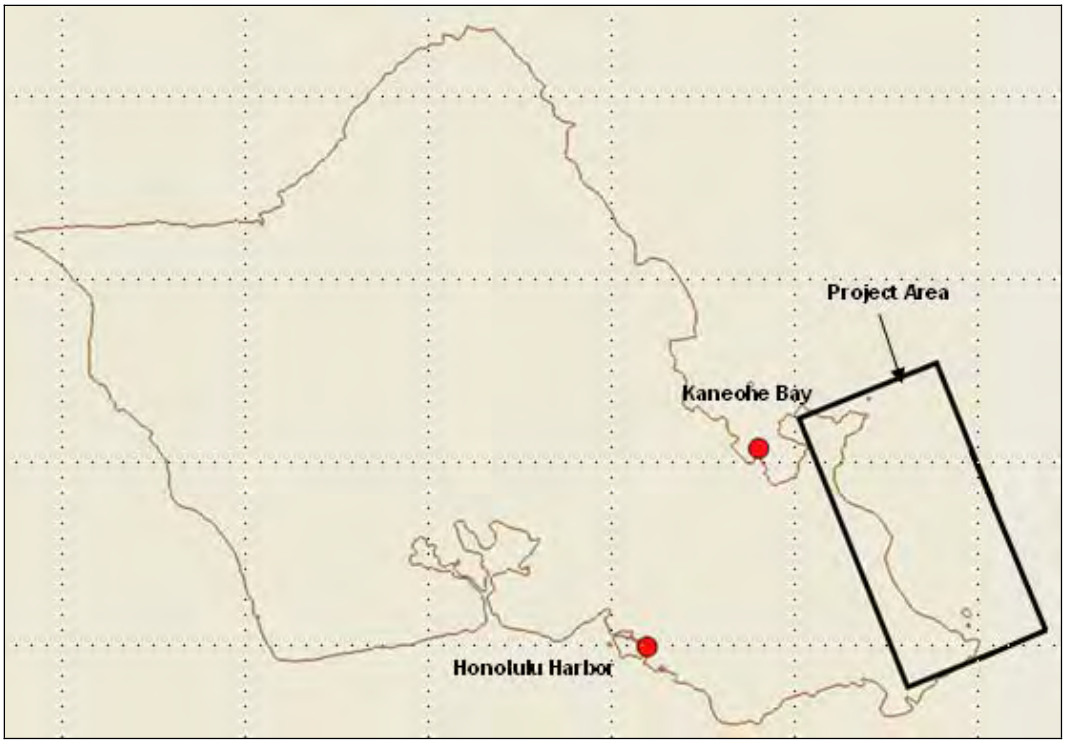

Figure 12. NOAA gauge locations for initial validation time period.

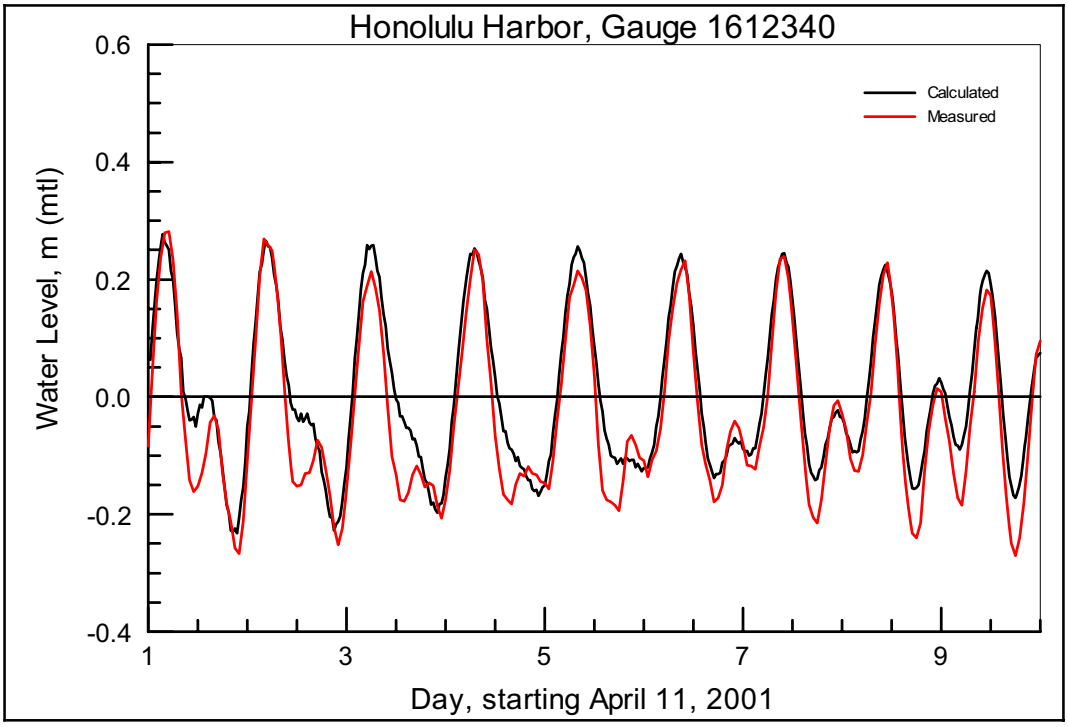

Figure 13. Comparison of calculated and measured water level at Honolulu Harbor gauge for initial validation period.

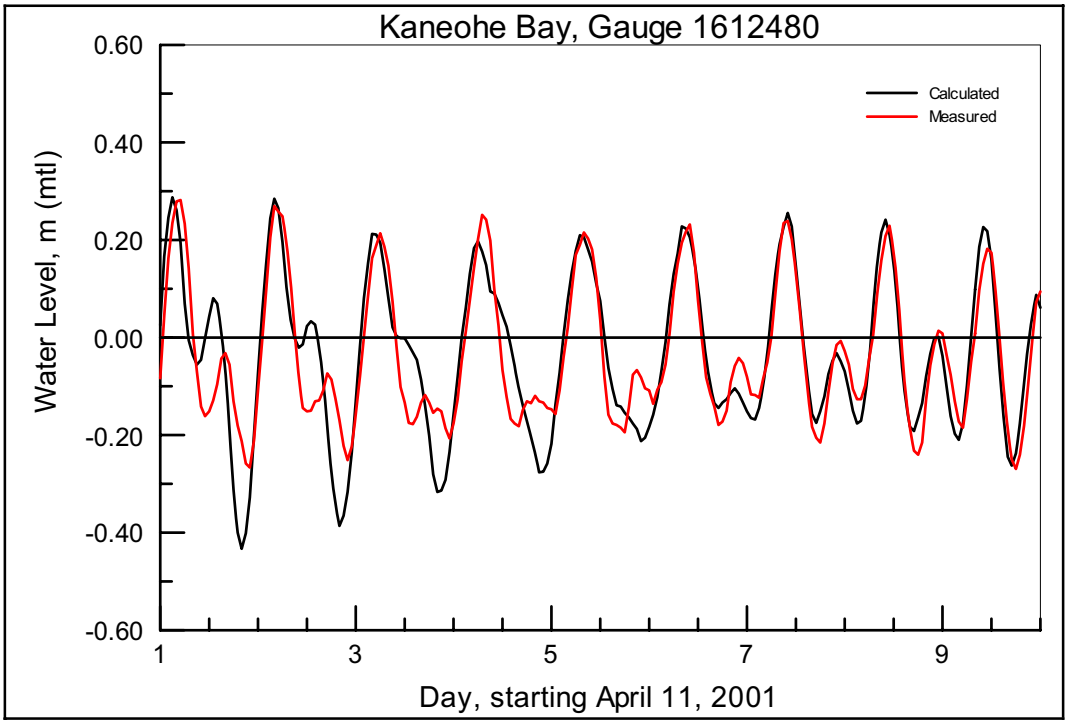

Figure 14. Comparison of calculated and measured water level at Kaneohe Bay gauge for initial validation period.

STWAVE

STWAVE is a steady-state, finite-difference model based on the wave action balance equation (Resio 1988; Smith et al. 2001). STWAVE simulates depth-induced wave refraction and shoaling, current-induced refraction and shoaling, depth- and steepness-induced wave breaking, diffraction, wind-wave growth, wave-wave interaction, and white-capping. The purpose of applying nearshore wave transformation models is to quantitatively describe the change in wave parameters between the offshore and the nearshore and, in this application, include simulating wave transformation over a reef. As previously mentioned, development of a spatially varying bottom friction capability in STWAVE was completed to enable application to the extensive reefs in the SEO study area.

Grid development

An STWAVE finite-difference grid was developed for the study area, with bathymetry interpolated from the ADCIRC grid mesh. The STWAVE grid resolution was 25 m × 25 m with a grid orientation of 210 deg counterclockwise from east. The original grid was 18 km (720 cells) in the alongshore direction by 6.2 km (248 cells) in the cross-shore direction and extended in the offshore to approximately the 100-m contour, with a maximum 344 m depth (Figure 15). After initial testing and consultation with the Honolulu District, it was determined that the lateral extent of the grid should be expanded around the headlands and the offshore boundary should be extended beyond the shallow water offshore from Mokapu Point and Makapu'u Point. The extended grid was 24.2 km (968 cells) in the alongshore direction by 7.8 km (310 cells) in the cross-shore direction and extended in the offshore to approximately the 300-m contour, with a maximum 480-m depth (Figure 15). The initial grid was applied for wave climate development and nearshore database generation. The extended grid was applied for comparison to field data and linkage to the ADCIRC model.

Wave climate -- model forcing conditions

Directional wave data were available at CDIP Station 098 (Mokapu Point) from August 2000 through 2004 (the study started in March 2005). Nondirectional wave data were available at Station 034 (Makapu'u) from 1981 to 1996. Directional wave data were available for Station 099 (Kailua Bay) for 2 months (November–December 2000). Station locations are shown in Figure 16.

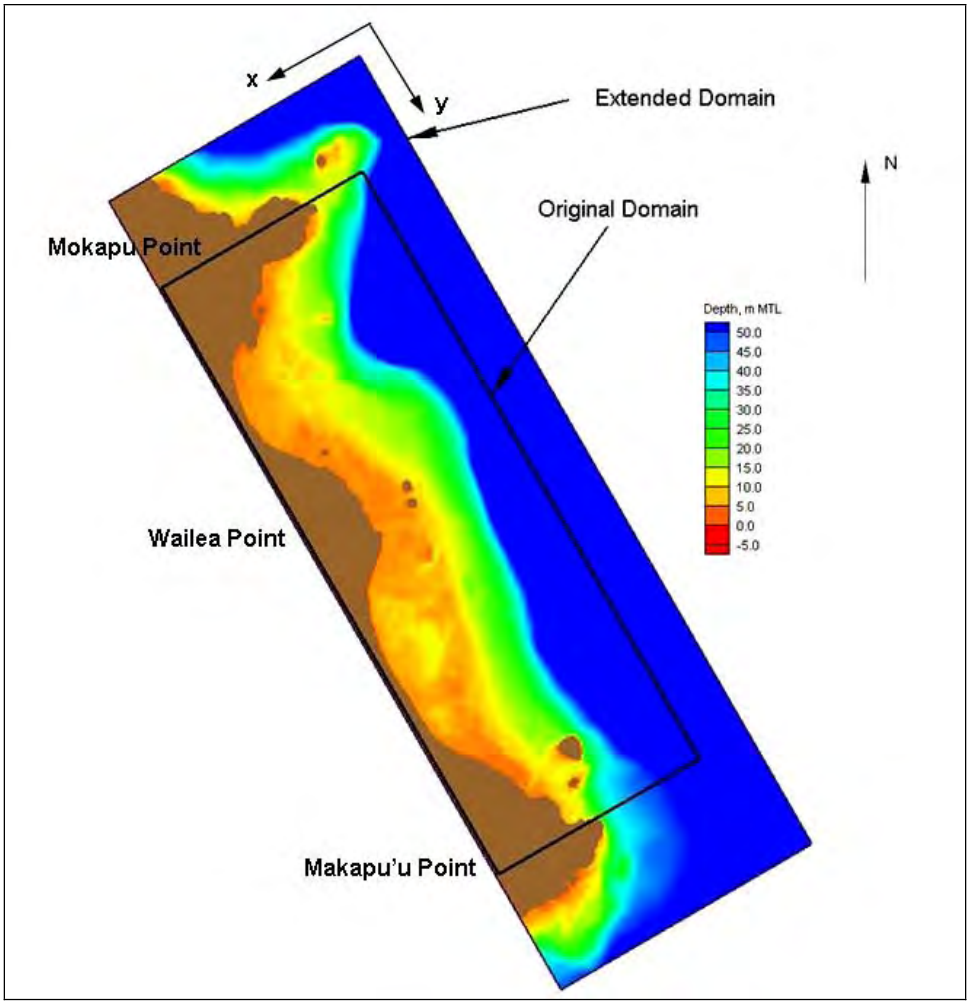

Figure 15. STWAVE grid domain.

For this study, the long-term data record (2000–2004) for Station 098 was analyzed with the Coastal Engineering and Data Analysis Software (CEDAS) 3.0 – Nearshore Evolution Modeling System (NEMOS) software. Since the purpose of this procedure was to determine all conditions that occurred at Station 098, the longest record possible, including the incomplete years 2000 and 2004, were included in the analysis. A 3-month gap in the data in 2004 and the small portion of 2005 data available at the time the study started (1 March 2005) were not included in the analysis.

Figure 16. CDIP buoy locations courtesy of CDIP web site (http://cdip.ucsd.edu).

Figures 17 and 18 show that waves are generally from the east-northeast quadrant and range in height from 0.5 to 6.0 m. Peak wave periods are generally 6 to 16 sec. From these tabulations, a set of discrete conditions was selected for simulation (Table 2). From the 216 possible height-period-direction combinations, 134 conditions occurred in the 2000–2004 time period. The wave height range was defined at 0.5-m intervals from 0.75 m to 2.75 m and at a 0.75-m interval to 3.5 m. The wave period range was 6 to 16 sec at a 2-sec interval. The wave directions were incremented every 22.5 deg from -22.5 deg to 90 deg, relative to True North. For each of the 134 selected wave conditions, Texel Marsden Arsloe (TMA) shallow-water spectra were generated by applying the SMS spectral wave generation software, and with those spectra applied at the model boundary; wave transformation was simulated by applying STWAVE over the project domain.

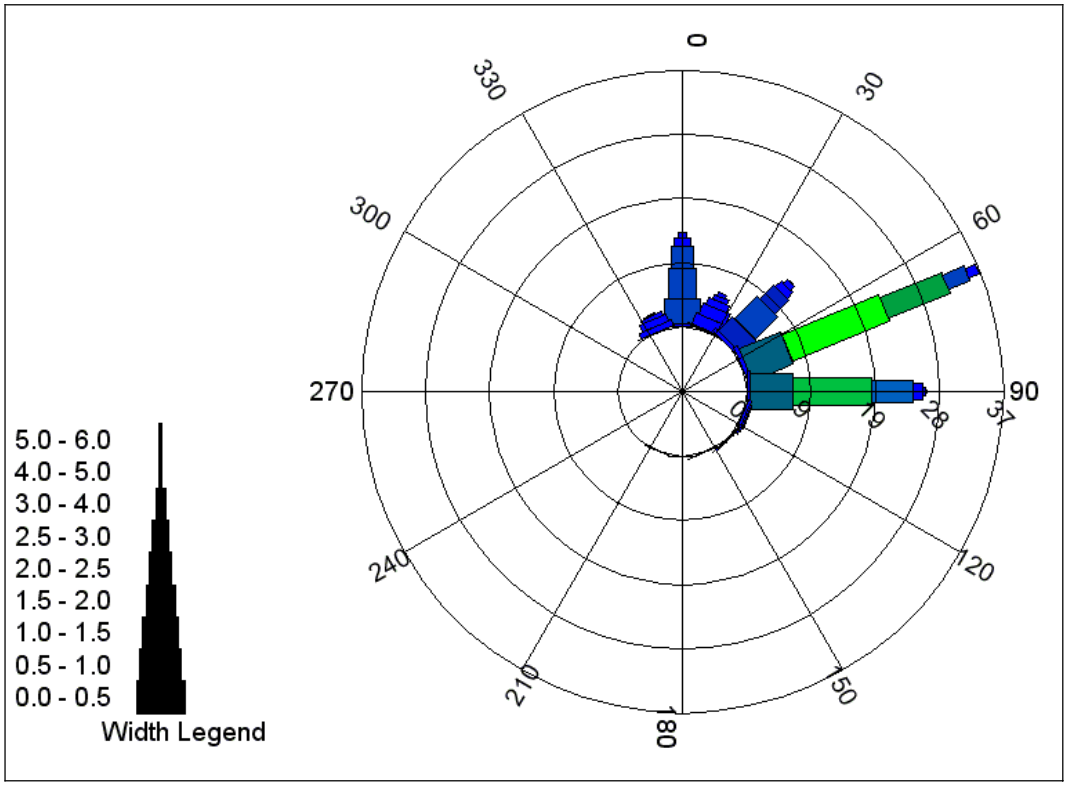

Figure 17. Wave height versus wave direction percent occurrence rose for CDIP Buoy 098 – Mokapu Point, HI (data from August 2000 through December 2004).

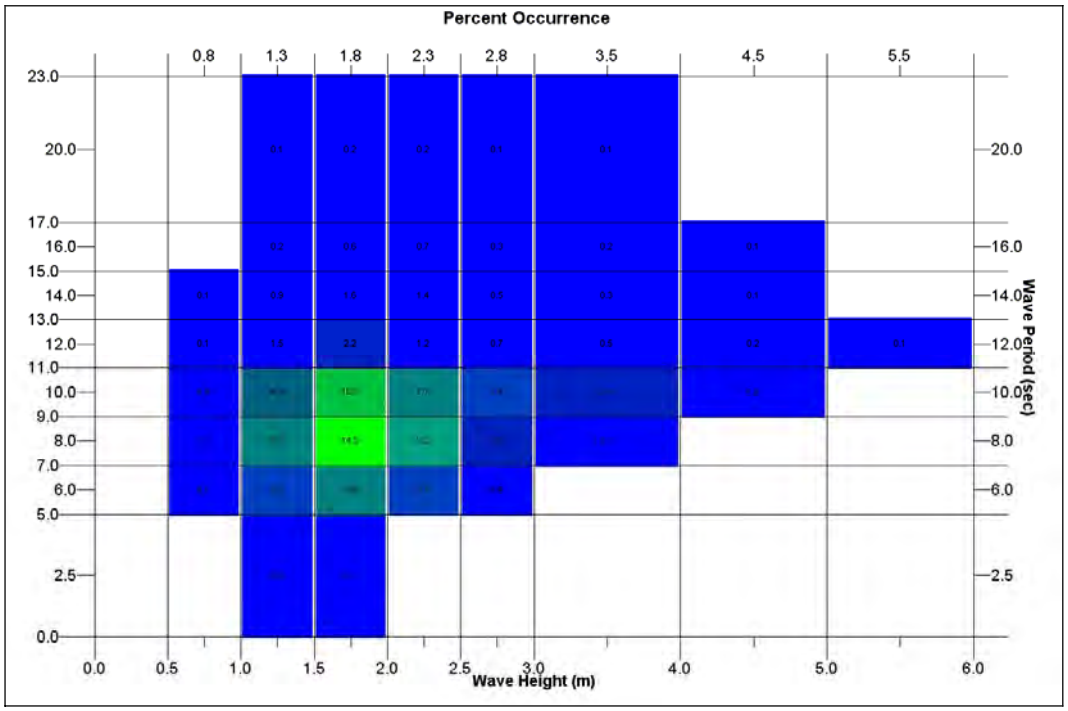

Figure 18. Block diagram of wave height versus wave period for CDIP Buoy 098 – Mokapu Point, HI (data from August 2000 through December 2004).

Table 2. Wave conditions.

Significant Wave Height, m	Wave Period sec	Wave Direction deg from North	Wave Direction deg from STWAVE axis
0.75	6	-22.5	82.5
1.25	8	0	60
1.75	10	22.5	37.5
2.25	12	45	15
2.75	14	67.5	-7.5
3.5	16	90	-30

Wave climate analysis

Nearshore conditions at a point in Waimanalo Bay [Figure 19, cell (229,506)] were extracted from the STWAVE model results for each of the 134 simulations. Since these simulations were to illustrate the technique for developing a wave climate, they did not include the detail of applying friction to the domain. A transformation correlation between the offshore

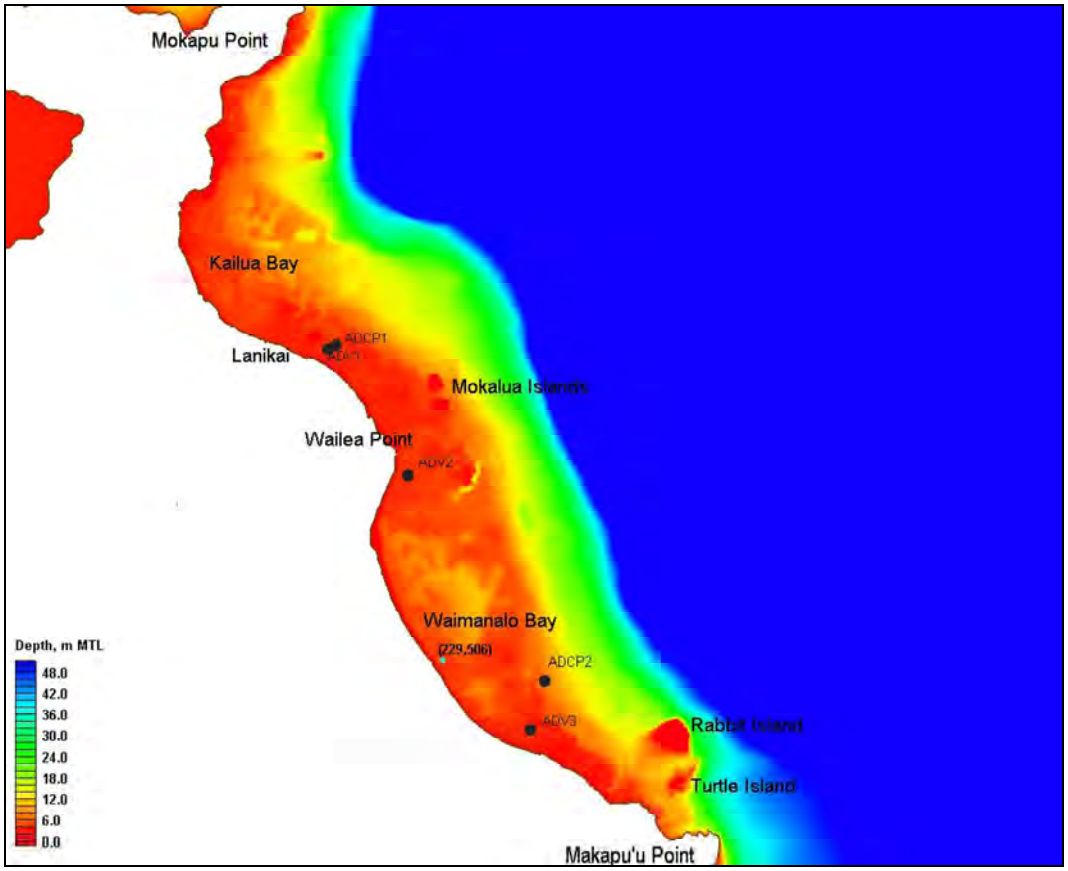

Figure 19. Location of extracted STWAVE model results (cell 229,506).

and nearshore conditions was then determined for each of the 134 simulations. By applying the appropriate transfer function to each wave condition in the 2000–2004 offshore time series at Station 098, a long-term (2000–2004) nearshore time series was generated (Figure 20). Note that the 3-month gap in the time series corresponds to 15 February to 19 May 2004 when the offshore CDIP Buoy 098 gauge was not operational. The nearshore time series demonstrates that there is a reduction in wave height from the offshore location to the nearshore location, landward of the extensive reef system due to depth-limited breaking and refraction. The time series, however, appears generally contained or banded between the 1.25 and 2.25 m wave height bins that were selected to represent the overall wave climate. Further analysis was required to determine if a more detailed representation of the offshore wave climate would better resolve the nearshore wave climate, and is discussed in the following.

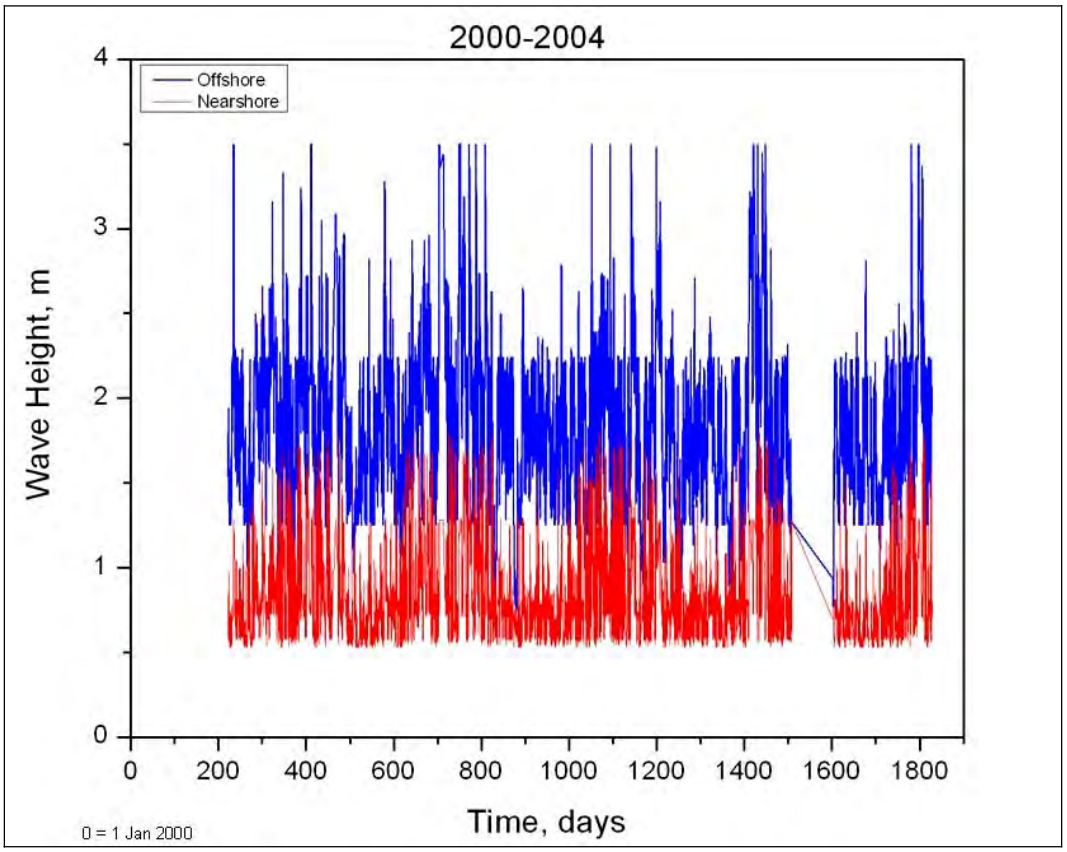

Figure 20. Nearshore time series (without friction) generated from offshore time series with 134 correlation conditions.

In order to capture the nearshore transformation time series more precisely and to include all wave conditions occurring in the time series, the range and refinement of the wave conditions simulated was expanded (Table 3). Wave heights ranged from 0.5 to 5.0 m with the finest increment being 0.25 m. Wave periods were expanded to include 20 sec. Wave angles were expanded to include waves from the east-southeasterly direction (representing waves 106–118 deg from True North) and were refined to 11.25 deg bands. For each of the 1274 selected wave conditions, TMA (shallow-water) spectra were generated by applying the SMS spectral wave generation software, and wave transformation was simulated by applying STWAVE over the project domain for each of the 1274 wave spectra. Again, nearshore conditions at cell (229,506) were extracted from the model results for each of the simulations. A transfer function between the offshore and nearshore conditions was then determined for each of the simulations. By applying the transfer function to each wave condition in the offshore time series at Station 098, a refined nearshore time series was generated (Figure 21), which shows a more realistic variation in the wave height. Note from the wave rose that wave directions converge to 35–73 deg relative to True North at the save point location shoreward of the reef and are predominantly directed shore-normal (60 deg). (In a follow-on study, the 1274 STWAVE simulations included bottom friction, and nearshore wave climates were developed for 10 nearshore locations.)

Table 3. Expanded (1274) wave conditions.

Significant Wave Height, m	Wave Period, sec	Wave Direction, deg from North	Wave Direction, deg from STWAVE axis
0.50	6	-22.5	82.5
0.75	8	-11.25	71.25
1.00	10	0	60
1.25	12	11.25	49.75
1.50	14	22.5	37.5
1.75	16	33.75	26.25
2.00	20	45	15
2.25		56.25	3.75
2.50		67.5	-7.5
2.75		78.75	-18.75
3.00		90	-30
3.50		101.25	-41.25
4.00		112.5	-52.5
5.00			

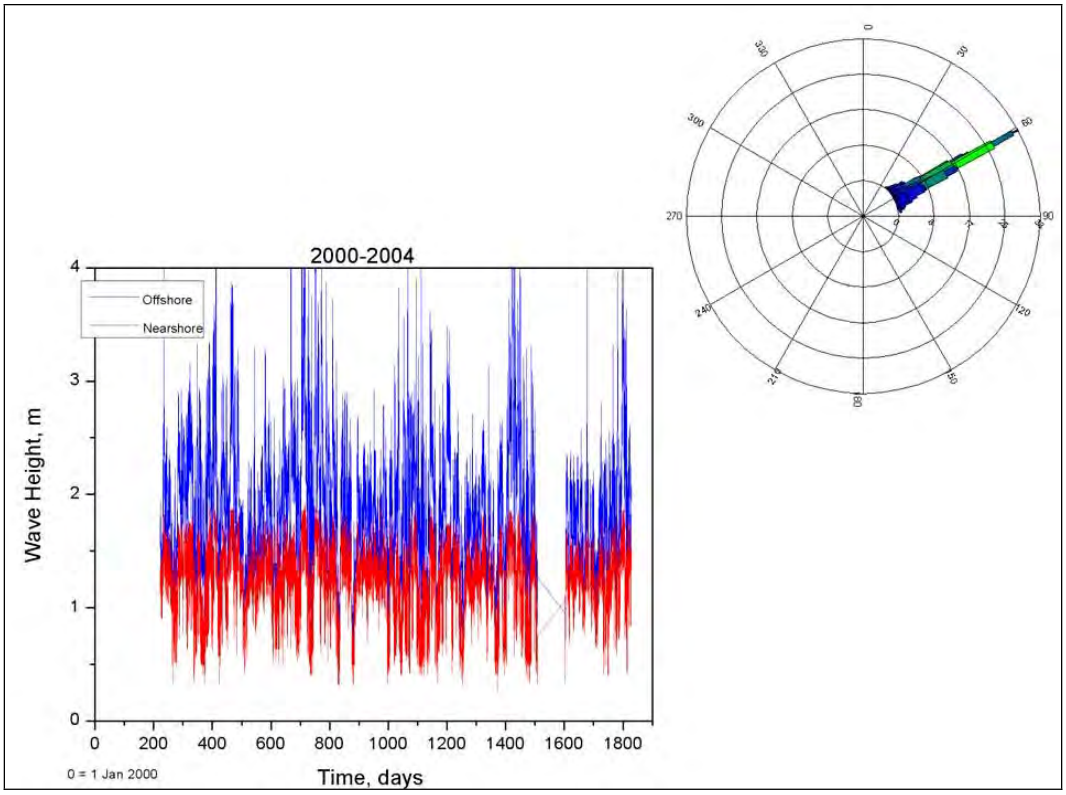

Figure 21. Nearshore time series (without friction) and wave rose generated from offshore time series with 1274 correlation conditions.

Bottom friction

Development of a bottom friction capability in STWAVE was completed for application to the extensive reefs in the SEO study area. STWAVE includes two formulations for bottom friction. The first is the JONSWAP formulation (Hasselmann et al. 1973; Padilla-Hernandez and Monbaliu 2001), where the spectral energy loss from bottom friction is formulated as a sink term, S_{bf}, in the energy balance equation,

$$S_{bf} = \frac{-1}{g} c_f \frac{\sigma^2}{\sinh^2 kd} E(f,\alpha) \tag{1}$$

where:

g = acceleration of gravity
c_f = bottom friction coefficient
σ = angular frequency
k = wave number
d = total water depth

E = spectral energy density divided by ($\rho_w g$), where ρ_w is density of water
f = wave frequency
α = wave direction.

The dissipation is summed over all frequencies and directions in the spectrum. A single friction coefficient, c_f, can be applied to the entire STWAVE domain, or a range of friction values can be applied on a cell-by-cell basis in a spatially varying manner. For the JONSWAP bottom friction formulation, c_f is specified as Γ/g, where the recommended values of Γ are in the range 0.038 to 0.067 m^2/sec^3 (or model input values of c_f = 0.004 to 0.007 m/sec) for sand beds based on the JONSWAP experiment and North Sea measurements (Hasselmann et al. 1973; Bouws and Komen 1983). Values of c_f applied for coral reefs range from 0.05 to 0.40 m/sec (Hardy 1993; Hearn 1999; Lowe et al. 2005). Equation 1 has a weak inverse dependence on water depth related to the increase in bottom wave orbital velocity as the relative depth, kd, decreases.

A Manning formulation is also available in STWAVE, based on Holthuijsen (2007),

$$S_{bf} = \frac{-1}{g}\left(\frac{gn^2}{d^{1/3}}\right)\frac{\sigma^2}{\sinh^2 kd}E(f,\alpha)u_{rms} \tag{2}$$

where the value of the Manning coefficient, n, is specified as input to STWAVE (either spatially constant or variable) and u_{rms} is the root-mean-square bottom velocity. With the Manning formulation, bottom friction dissipation has an additional inverse dependence on water depth. Estimates of Manning coefficients are available in most fluid mechanics reference books (e.g., 0.01 to 0.05 for smooth to rocky/weedy channels). Converting c_f values applied for coral reefs (0.05 to 0.40 m/sec) to Manning coefficients yields a range of 0.10 to 0.25. However, it is recommended that the specification of c_f or n be validated with field measurements. Application of this model capability to a specific site requires validation to field data.

A single friction value can be applied to the entire STWAVE domain or a range of friction values can be applied on a cell-by-cell basis. As an example, the 134 wave conditions first simulated were repeated with the revised STWAVE, applying a JONSWAP bottom friction coefficient typical for

reefs of c_f = 0.05 m/sec over the entire model domain. A comparison of nearshore waves at cell (229,506) was made (Figures 22 and 23). The offshore (blue) to nearshore without bottom friction (black) comparison shows a reduction in wave height of 38% (Figure 22). With bottom friction (red), the reduction in wave height is 84%. A comparison of the nearshore wave heights with and without bottom friction shows that, with the inclusion of bottom friction, wave heights range from 18–38% of the previous results that did not include bottom friction. On average, the wave height was 26% of the frictionless value at the selected location. Waves refract less with the inclusion of bottom friction, likely due to the reduction in energy at lower frequency (Figure 23).

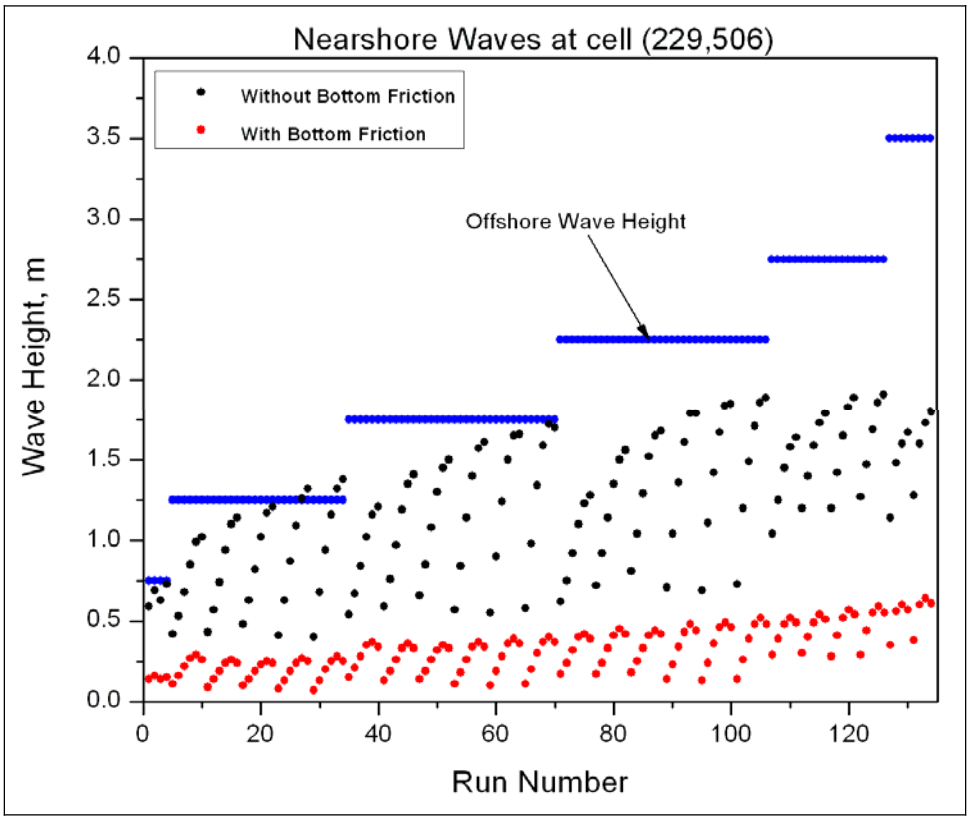

Figure 22. Comparison of predicted wave heights at cell (229,506) with and without the STWAVE bottom friction feature.

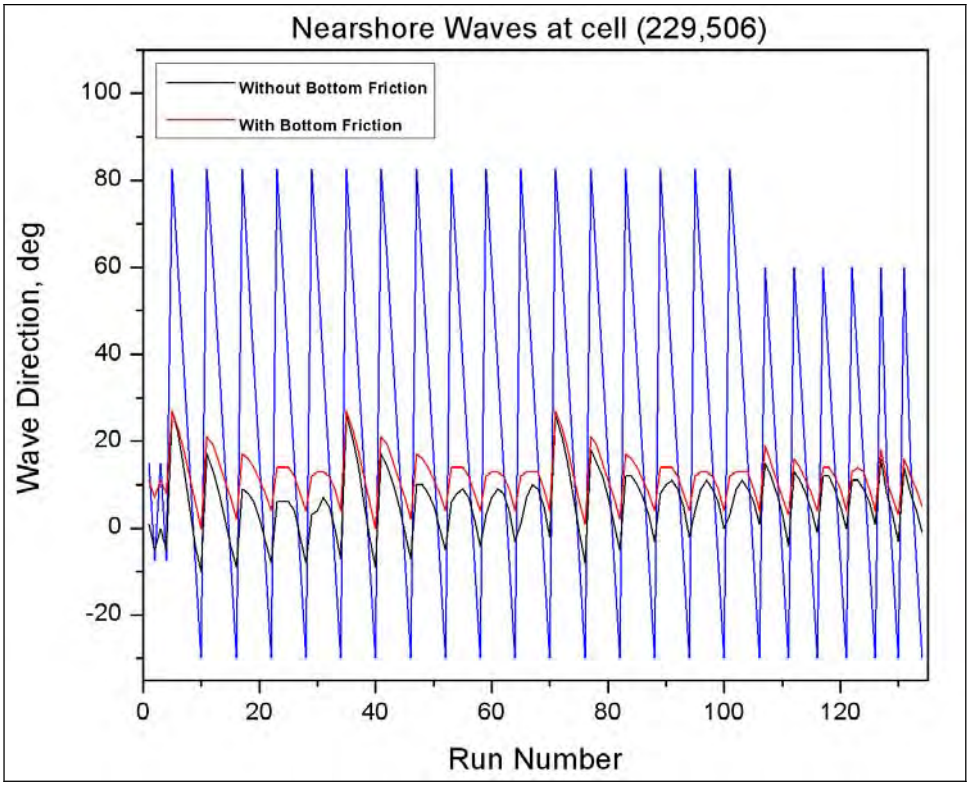

Figure 23. Comparison of predicted wave direction at cell (229,506) with and without the STWAVE bottom friction feature.

As another example, for each of the 1274 selected wave conditions simulated subsequently to achieve a more detailed wave climate, wave transformation *including spatially constant bottom friction* of 0.05 m/sec was simulated by applying STWAVE over the project domain for each of the 1274 wave spectra. Again, nearshore conditions at cell (229,506) were extracted from the model results for each of the simulations. A transfer function between the offshore and nearshore condition was then determined for each of the simulations. By applying the transfer function to each wave condition in the offshore time series at Station 098, a refined nearshore time series with bottom friction was generated (Figure 24). A comparison of Figures 21 and 24 shows that the constant 0.05 value for the JONSWAP bottom friction coefficient reduces nearshore wave heights by approximately 73%.

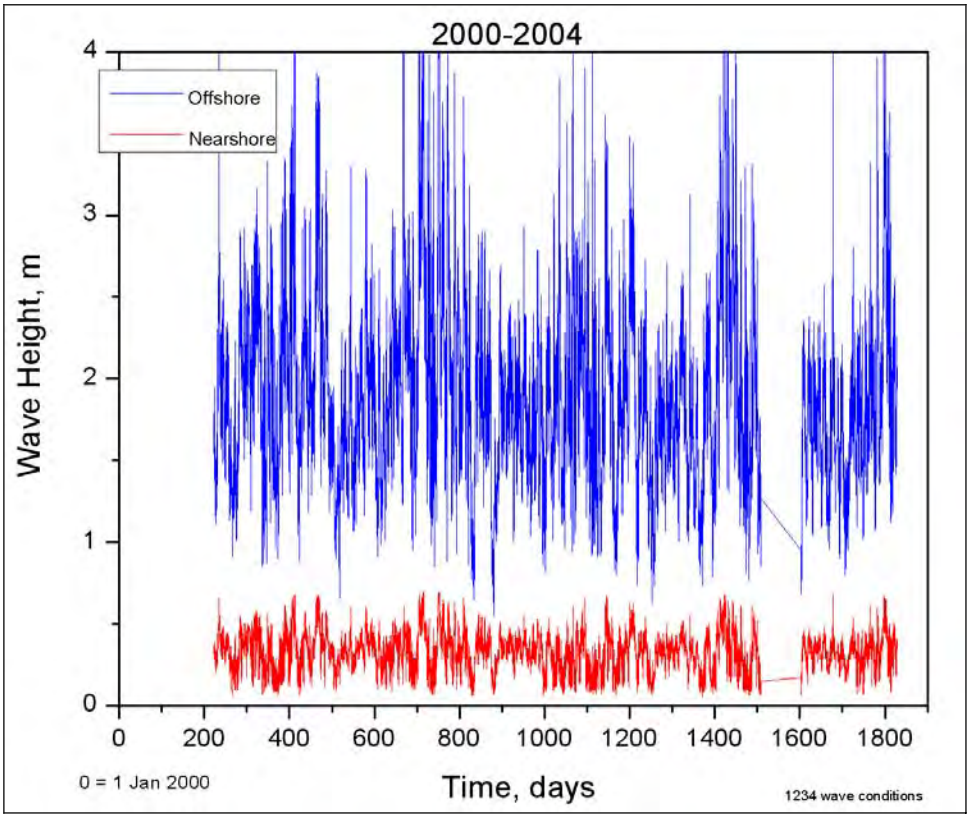

Figure 24. Nearshore time series (including spatially constant bottom friction) generated from offshore time series with 1274 correlation conditions.

Model validation

As previously discussed, the extended domain STWAVE grid was applied in the model validation process. The August 2005 model validation time period corresponded to a portion of the field data collection time period (9 August through 14 September 2005). CDIP Buoy data for August 2005 (Figure 25) were extracted from the CDIP website for every 3-hr interval of August 2005. For each of these measured wave conditions, TMA (shallow-water) spectra were generated by applying the SMS spectral wave generation software. These spectra were then applied to the offshore boundary of the model domain. Note that analysis was done to compare the waves at the 300-m depth STWAVE boundary and the 100-m depth gauge location by applying the University of Delaware Hydrodynamic Wave Calculator applet application (http://www.coastal.udel.edu/faculty/rad/wavetheory.html). It was found that the difference in wave height from the 300-m to 100-m depth is small (approximately 4% for periods <15 sec, which accounts for 98% of the waves) and the offshore gauge data were applied at the STWAVE boundary without back refracting to the 300-m water depth.

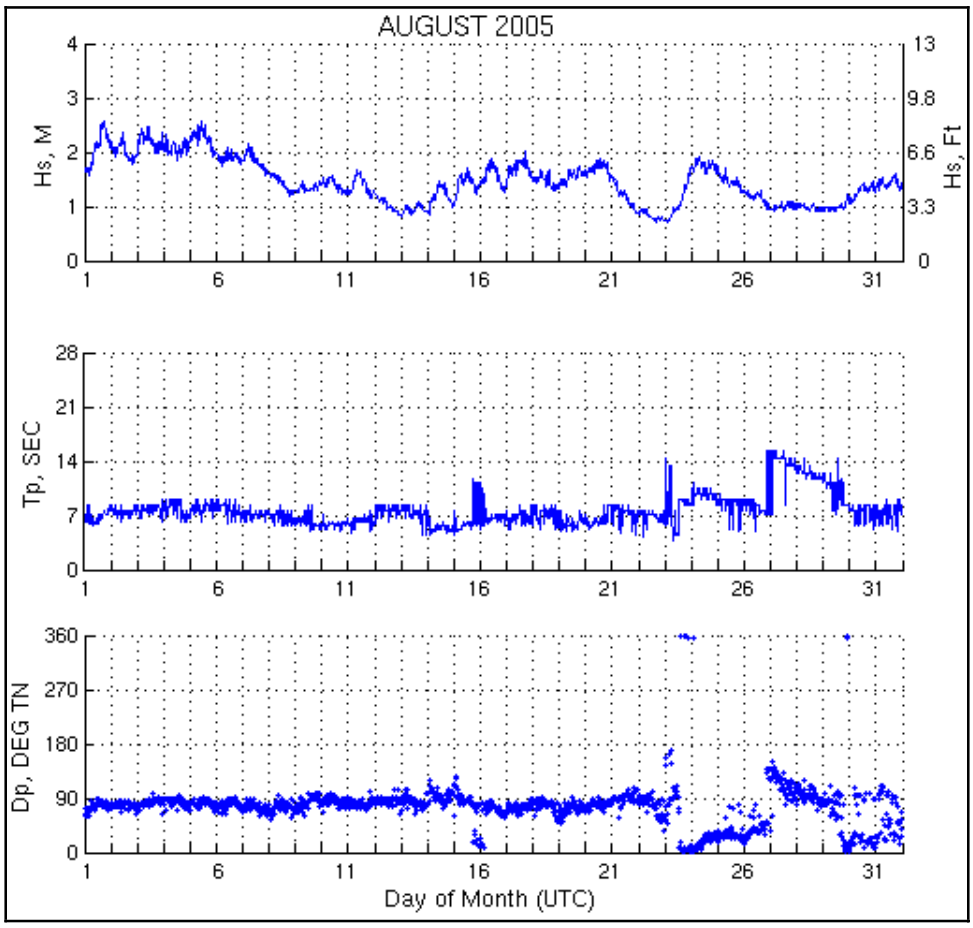

Figure 25. CDIP buoy data at station 098 (Mokapu Point, Hawaii) for August 2005.

Initially, a constant bottom friction value was applied to each cell of the STWAVE domain. Several simulations with different constant JONSWAP bottom friction values ranging from 0.04 to 0.12 m/sec were made to examine the range of response (wave height) at the gauge locations. Figure 26 shows the wave height time series generated by STWAVE at the location where ADV1 was placed, without bottom friction and for four simulations with bottom friction. These initial simulations indicated that, without bottom friction, wave heights at ADV1 are reduced on average by 21% relative to the offshore wave height due to depth-limited breaking. Bottom friction reduces wave height at ADV1's location by 64% for a JONSWAP bottom friction coefficient of 0.04 m/sec (wave height is 36% of the offshore wave height), by 71–76% for a bottom friction value of 0.05 m/sec (wave height is 24–29% of the offshore wave height), and by 93% for a bottom friction value of 0.12 m/sec (wave height is 7% of the offshore wave height). Applying a Manning friction coefficient of 0.15 to 0.25 to the reef resulted in average wave height reductions of 62–80%.

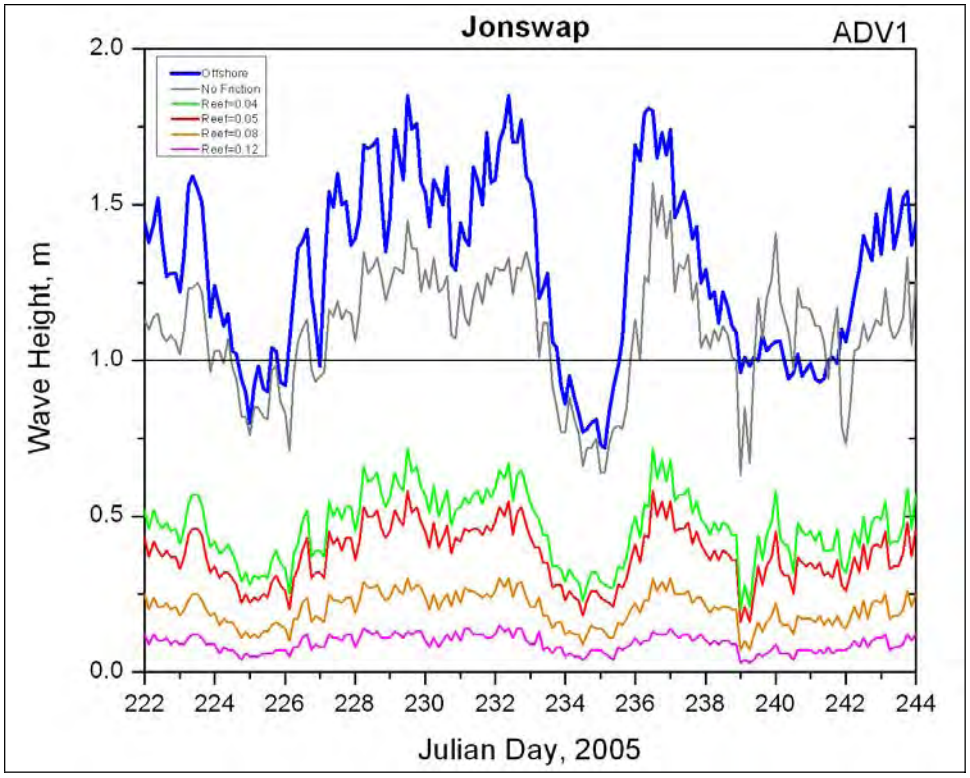

Figure 26. Simulated wave height time series at ADV1 with and without bottom friction.

The range of response indicates the importance of selecting the appropriate bottom friction value to represent the reefs in the study area. In addition, a variable friction field with a larger friction value applied only over the reef areas would be the most appropriate representation of the study area.

In the first set of validation simulations, a variable bottom friction field with JONSWAP friction coefficients of 0.05 m/sec applied to the reef region, 0.09 m/sec around the offshore islands (for compatibility/linkage to the ADCIRC model), and 0.006 m/sec in the offshore regions was utilized. A Manning validation simulation was also made with friction coefficients of 0.20 applied to the reef region (which is within the valid range of reef coefficients applied in the literature), 0.19 around the offshore islands, and 0.02 in the offshore regions. The simulations also included water level fluctuation due to tide. A comparison of field data collected at the three ADV locations (Figure 19) to the simulated wave heights was made. Figures 27–32 show the wave height time series generated by STWAVE at the gauge locations without bottom friction and for two simulations with bottom friction (with and without tide), along with the field measurements at these locations.

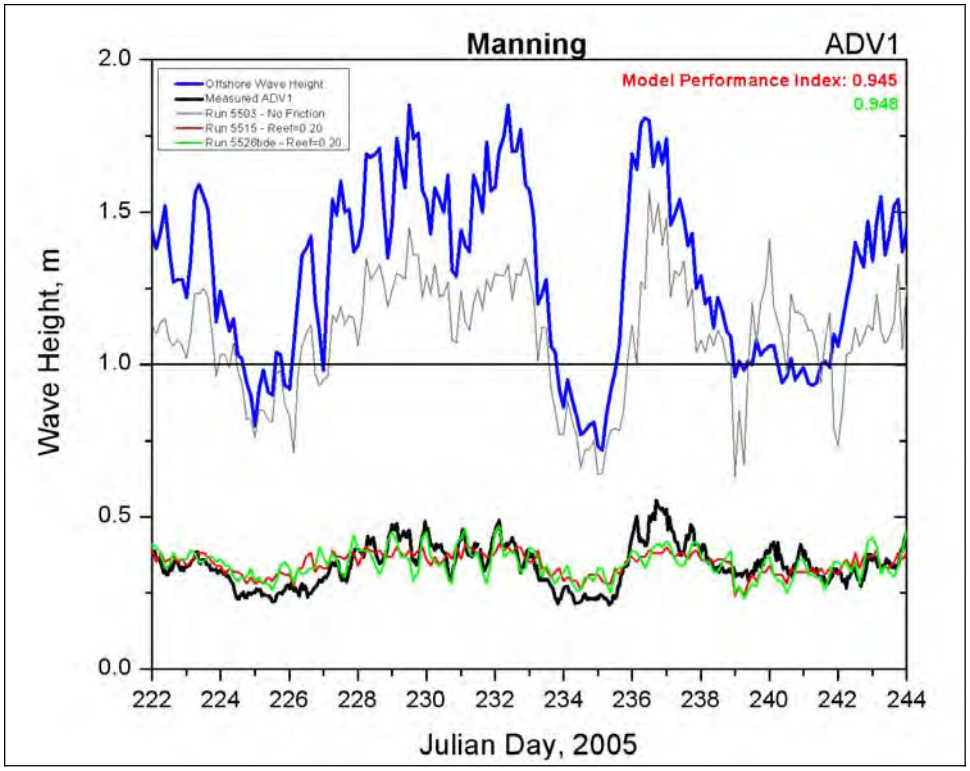

Figure 27. Comparison of measurements and STWAVE results at ADV1 with reef Manning bottom friction coefficient of 0.20.

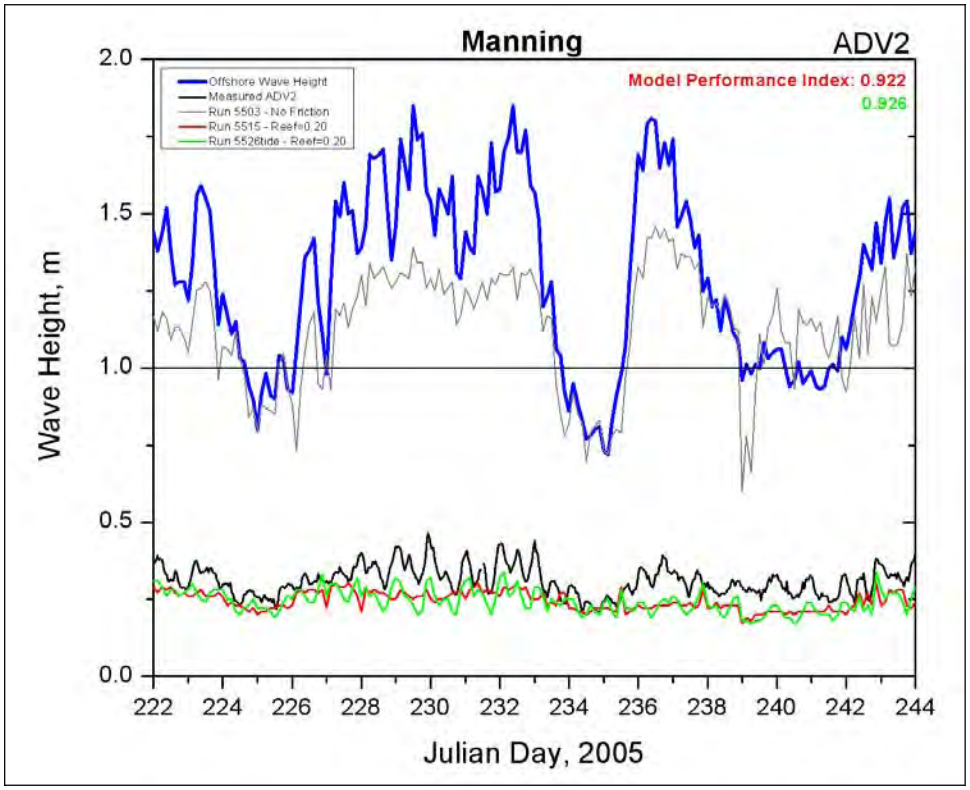

Figure 28. Comparison of measurements and STWAVE results at ADV2 with reef Manning bottom friction coefficient of 0.20.

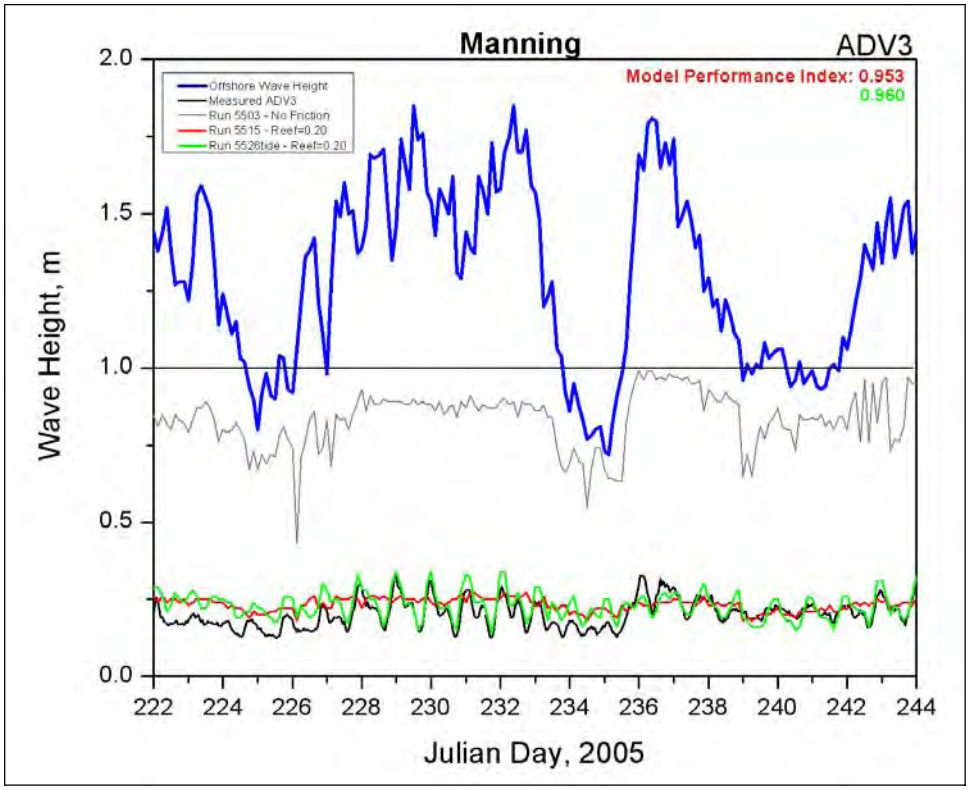

Figure 29. Comparison of measurements and STWAVE results at ADV3 with reef Manning bottom friction coefficient of 0.20.

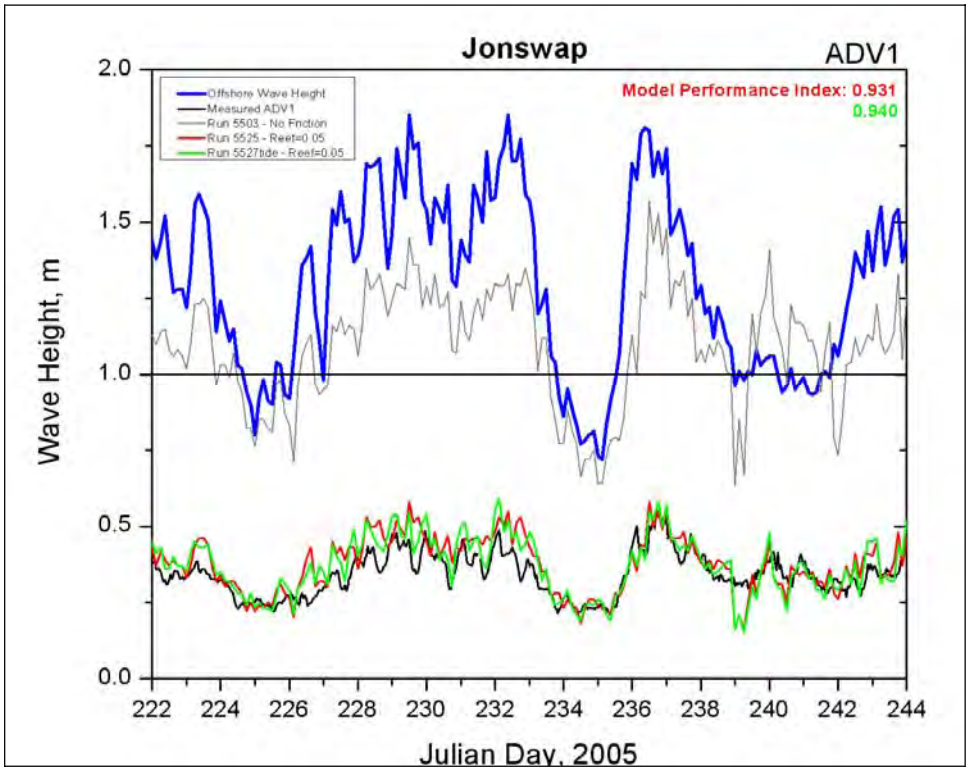

Figure 30. Comparison of measurements and STWAVE results at ADV1 f with reef JONSWAP bottom friction coefficient of 0.05.

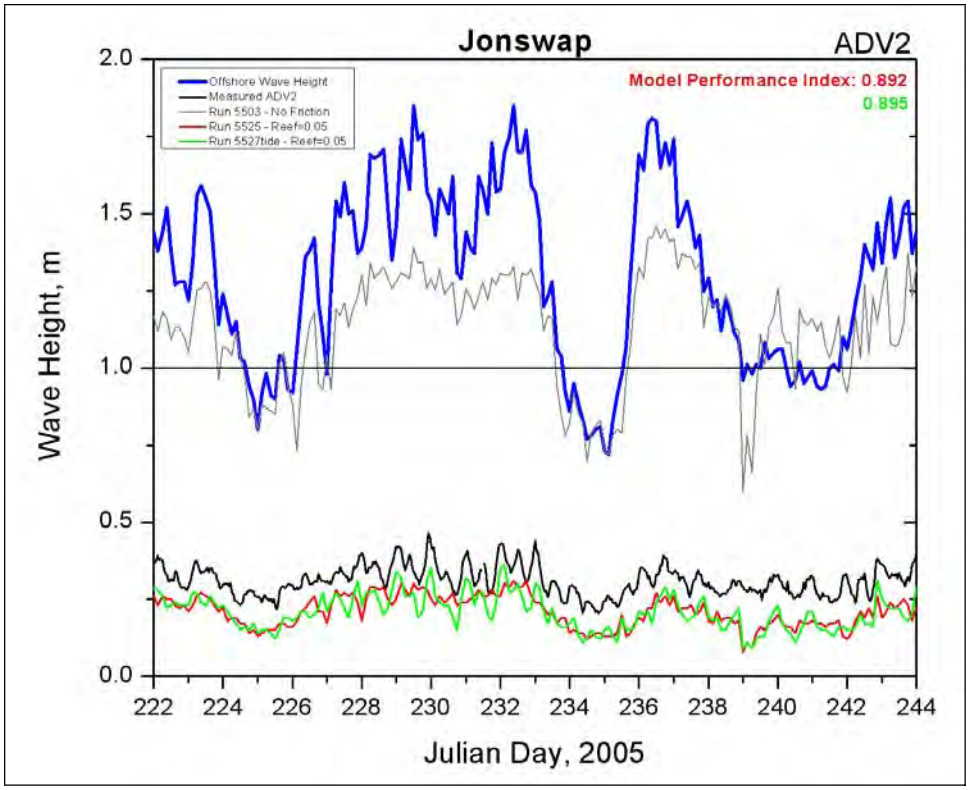

Figure 31. Comparison of measurements and STWAVE results at ADV2 with reef JONSWAP bottom friction coefficient of 0.05.

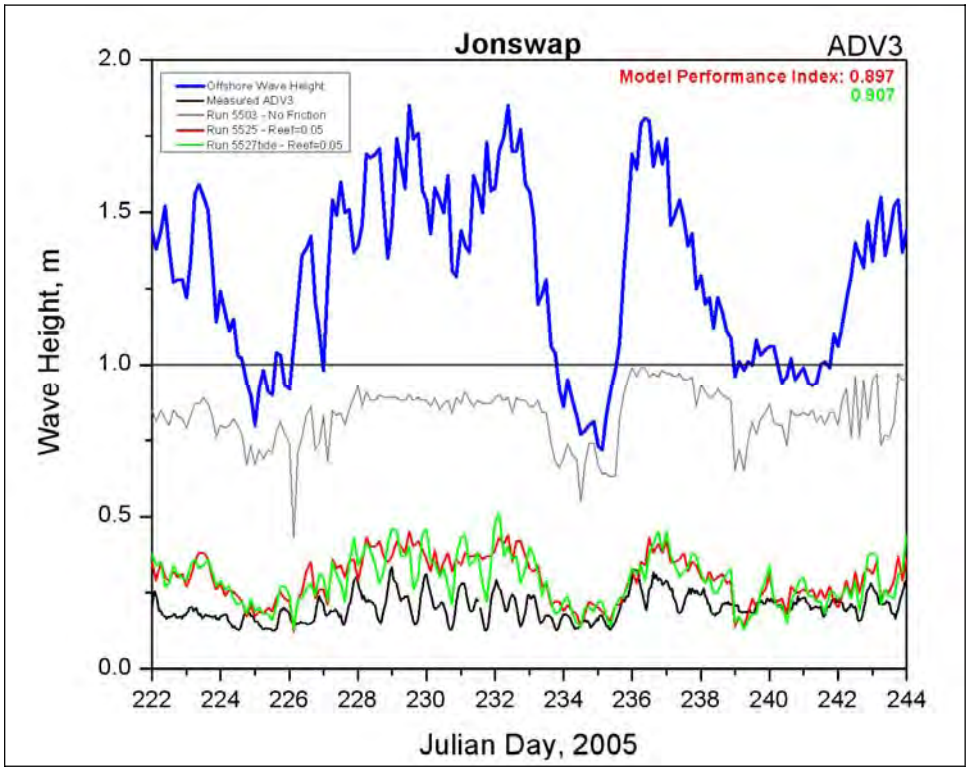

Figure 32. Comparison of measurements and STWAVE results at ADV3 with reef JONSWAP bottom friction coefficient of 0.05.

The field measurements range in wave height from 0.12 to 0.69 m for the data collection time period and the model results range from 0.08 to 0.59 m. The STWAVE model captures the large reduction in wave height from the offshore location to the three nearshore locations. The model results for the ADV1 location follow the magnitude and trend of the data well, particularly with the JONSWAP friction formulation. The inclusion of tidal fluctuation in the model improves the comparison to gauge data, particularly with the Manning friction formulation. Model results at the ADV2 location tend to underpredict the measured wave height with the selected validation friction coefficient. Model results at the ADV2 location show greater wave height variation with time, whereas the measurements show much less variability. Model results at ADV3 tend to over-predict the measured wave height when the offshore waves are greater than 1.3 m.

Another indicator of the model ability to estimate wave transformation over a reef is the Model Performance Index (MPI) (Smith 2000). The MPI is a measure of the models ability to capture the transformation from offshore to nearshore that is observed in the field data.

$$\text{MPI} = (1 - Error_{rms})/Changes_{rms} \quad (3)$$

where $Error_{rms}$ is the root-mean-square error of the model compared to the ADV gauge data and $Changes_{rms}$ is the root-mean-square change from the offshore data to the nearshore data. Values of the MPI near unity indicate good agreement. For the initial simulations with constant bottom friction applied to the reef, the MPI values are 0.92 to 0.96 for the Manning representation of bottom friction (n = 0.20) and 0.89 to 0.94 for the JONSWAP representation of bottom friction (c_f = 0.05).

Improvements to the results, particularly at ADV3, could be made by revising the friction coefficients to represent the spatial variability of the reef roughness. (The coral reefs in this region are described as “mushroom fields.” Some areas of the reef are more solid and some areas have gaps and holes in the reef.) Without detailed knowledge of the contiguous/noncontiguous areas of the reef, an educated attempt was made to represent the variations in the reef. The center section of the reef was given a smaller friction coefficient and the southern portion of the reef was given a larger coefficient (Figure 33). These adjusted values were selected based upon the under/overprediction of wave height at ADV2 and ADV3,

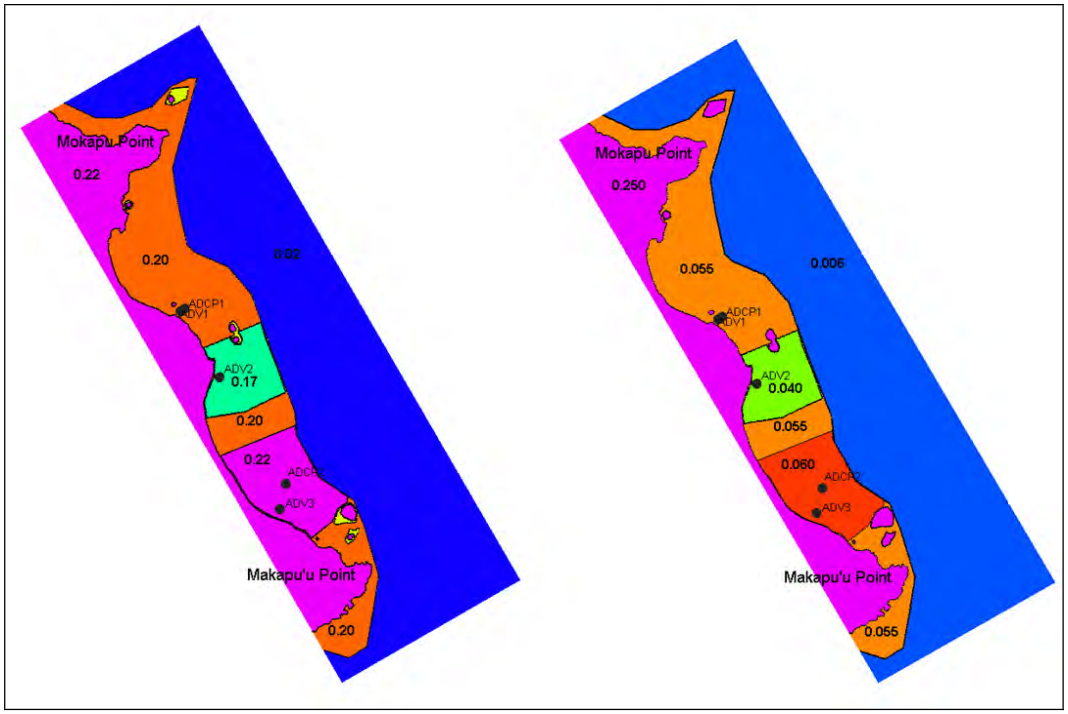

Figure 33. Variable Manning (left) and JONSWAP (right) friction fields.

respectively, in the previous simulation. The final validation simulation was made with JONSWAP friction coefficients of 0.04/0.055/0.06 variably applied to the reef region, 0.09 around the offshore islands (for compatibility/linkage to the ADCIRC model), and 0.006 in the offshore regions. A Manning validation simulation was also made with variable friction coefficients of 0.17/0.20/0.22 applied to the reef region, 0.19 around the offshore islands, and 0.02 in the offshore regions. Tidal fluctuation was included in these simulations.

As shown in Figures 34–39, with a variable bottom friction coefficient to represent variability in the reef structure, model results compare extremely well with the data at all three gauge locations with both the Manning and the JONSWAP friction formulations. The MPI values are 0.948 to 0.970 for the Manning simulations and 0.951 to 0.953 for the JONSWAP simulations. The magnitude and trend as well as the tidal fluctuation exhibited by the data are all captured by the model.

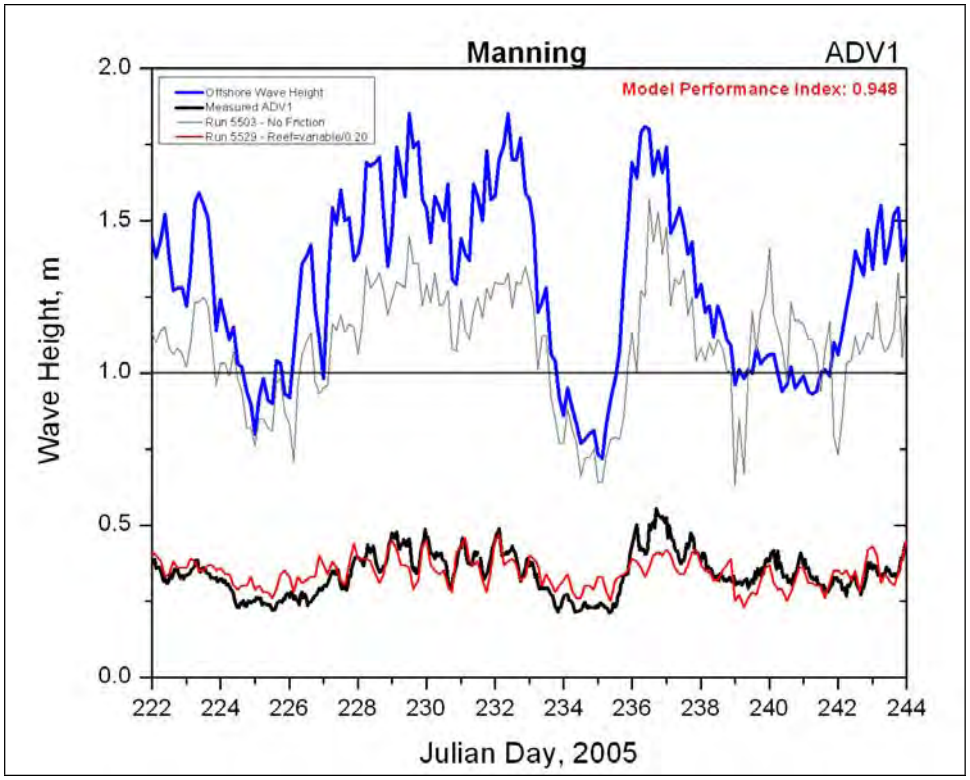

Figure 34. Comparison of measurements and STWAVE results at ADV1 for spatially varying Manning bottom friction.

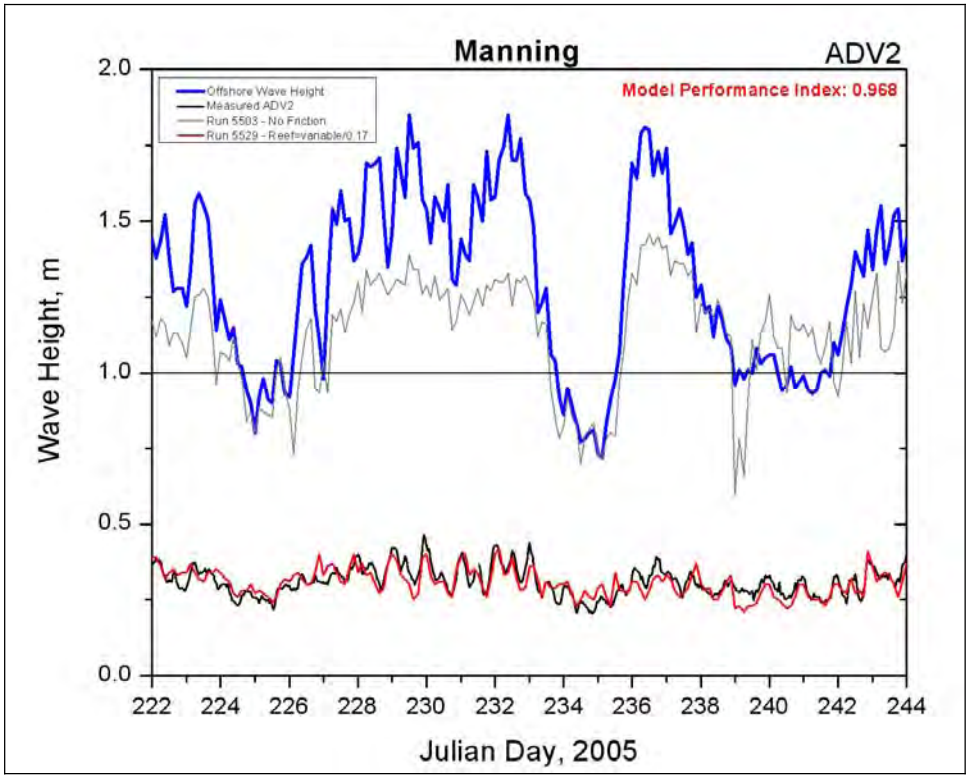

Figure 35. Comparison of measurements and STWAVE results at ADV2 for spatially varying Manning bottom friction.

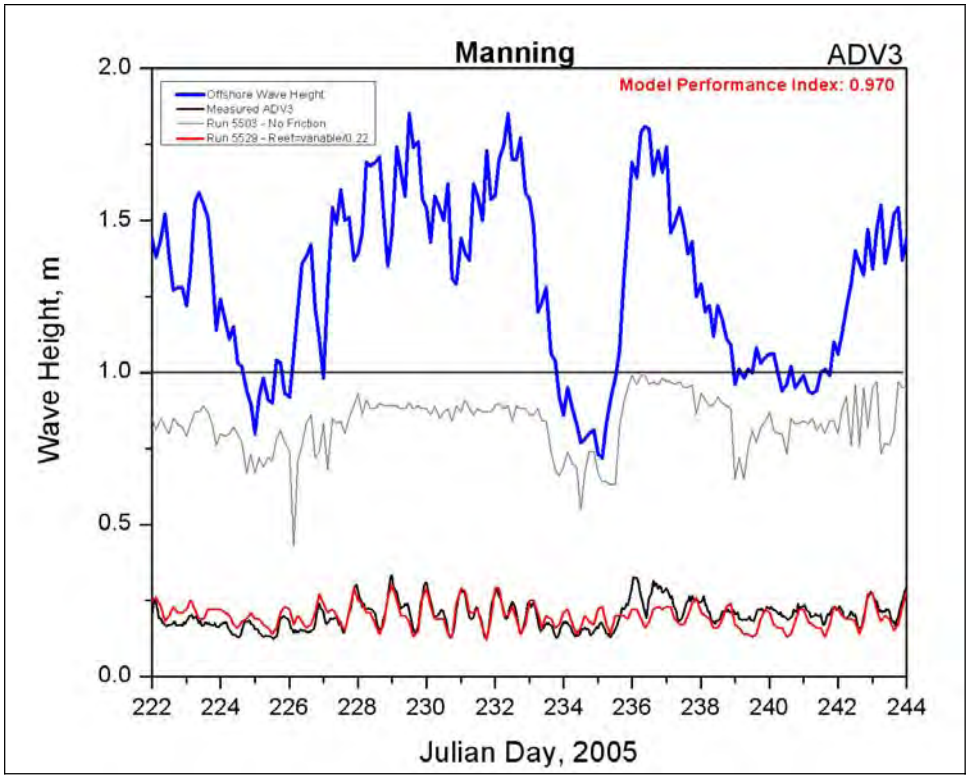

Figure 36. Comparison of measurements and STWAVE results at ADV3 for spatially varying Manning bottom friction.

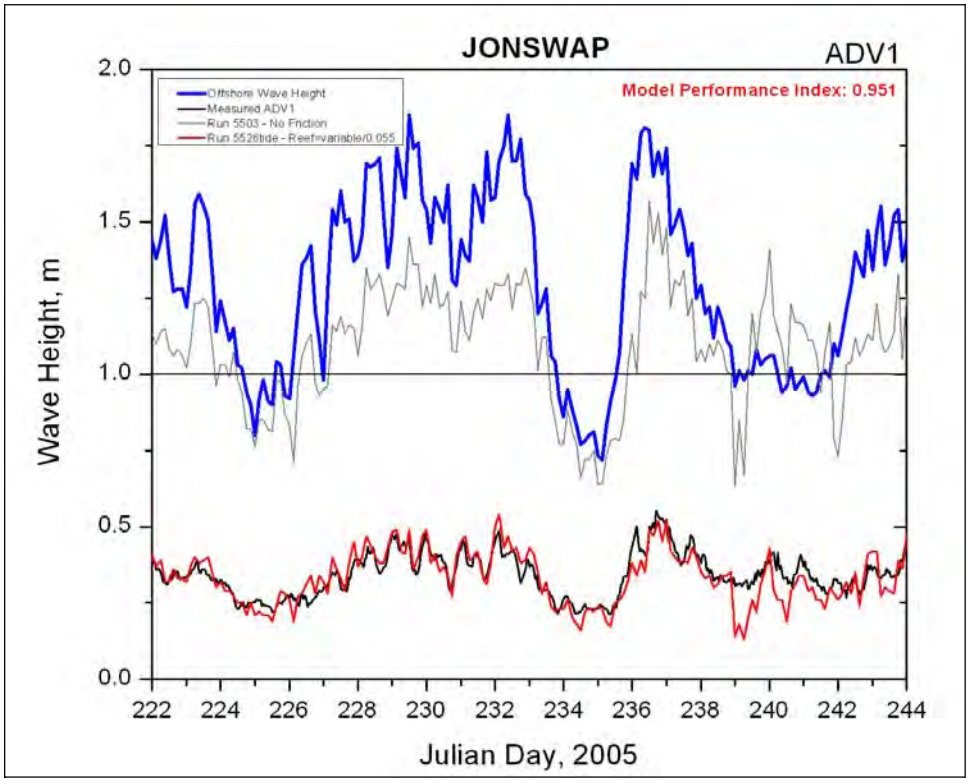

Figure 37. Comparison of measurements and STWAVE results at ADV1 for spatially varying JONSWAP bottom friction.

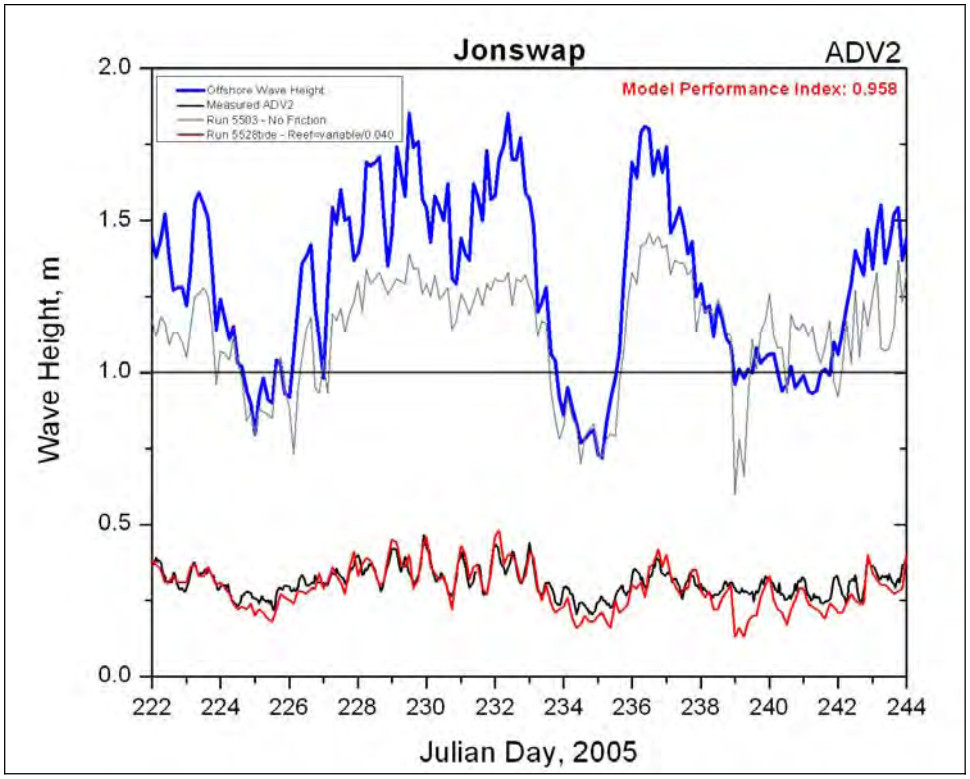

Figure 38. Comparison of measurements and STWAVE results at ADV2 for spatially varying JONSWAP bottom friction.

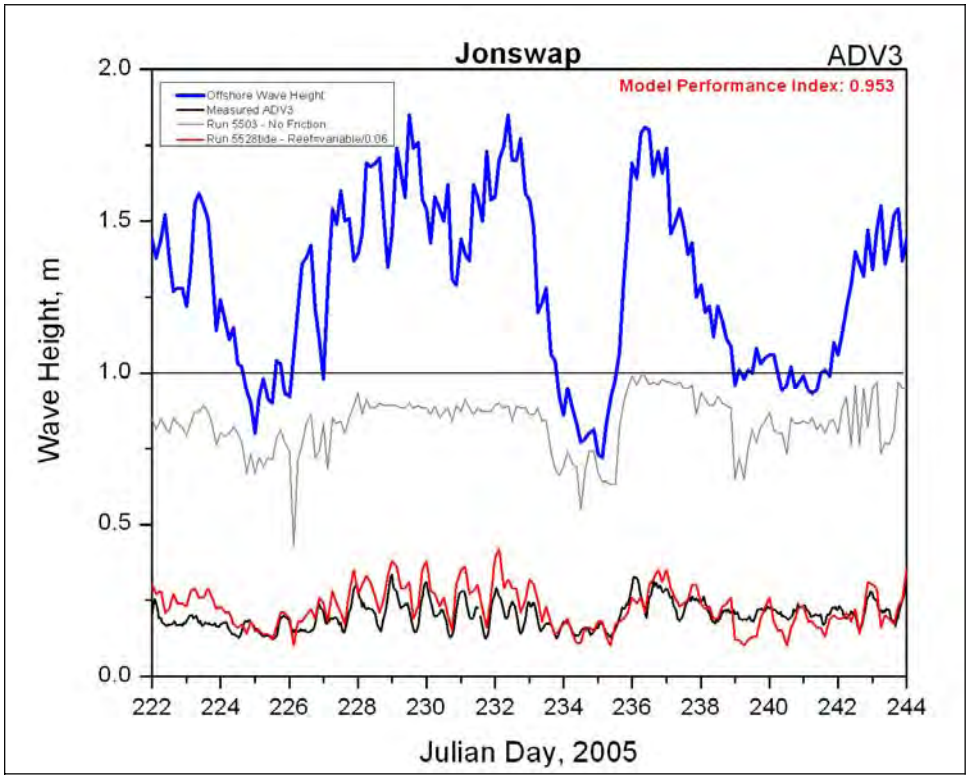

Figure 39. Comparison of measurements and STWAVE results at ADV3 for spatially varying JONSWAP bottom friction.

ADCIRC validation – wind, tide, and waves for gauge deployment time period

In the final validation, ADCIRC was applied to the study area for the August 2005 time period. This month overlapped the gauge deployment time period by approximately 2.5 weeks. ADCIRC was forced along the open boundary with tidal variation data extracted from the LeProvost tidal database. Wind speed and direction information were obtained from the OWI winds described in the wind sources section earlier in this document. Wave forcing information was provided from the STWAVE simulation driven by CDIP Buoy 098 data. A series of ADCIRC simulations were run for the selected month in the validation procedure. The ADCIRC simulations varied in the hydrodynamic parameters, bottom friction values, including with and without wind and wave forcing as part of this validation process. Some issues with the steep bathymetric gradients near the offshore island caused energetic wave breaking and created large radiation stress gradients, which led to ADCIRC model instability. This was overcome by applying a large bottom friction value (0.09) in STWAVE near the offshore islands and limiting radiation stress gradients to a maximum of 0.0001 m^2/sec^2. The final ADCIRC simulation applied a hybrid bottom friction formulation with a minimum c_f value of 0.003 m/sec (similar to the minimum value applied in the STWAVE validation — 0.006 m/sec), then increased in value in shallow depths (less than 1.0 m). The eddy viscosity was set to 4.0 m^2/sec, and the time step was 0.4 sec.

Simulation analysis

Currents and water levels were compared with field data obtained from the gauge deployment described earlier. Calculated water levels compared well in range and phase to measurements, but underestimated some lower peaks while overestimating some higher peaks. This may have been caused by localized interaction of the tides with the reefs surrounding the gauge locations. Water level comparisons with the three ADV gauges are shown in Figures 40–42. A harmonic analysis may prove useful in obtaining a better comparison to the tidal constituents. However, since the measured current velocities are so small, an improved tidal constituent forcing would not greatly influence the total range of water level and therefore would not increase the current velocities significantly. Therefore, no harmonic analysis was performed.

Current velocity data from the three ADV gauges (near-bottom point measurements) and two ADCP gauges (depth-averaged) were extremely small during the overlapping deployment time period—generally less than 10 cm/sec. (The near-bottom ADV measurements would be expected to be lower than depth-averaged values and therefore less than the ADCIRC-computed values.) Due to these small measured depth-averaged current magnitudes, depth-averaged current velocities calculated at these locations from the ADCIRC circulation model were not expected to compare well; however, the range of velocity model results (0.2–27.2 cm/sec) is well within one order of magnitude of the range of measurements (0.1–16.8 cm/sec) and generally very close to the measurements. Comparisons of ADCIRC circulation results to ADV and ADCP gauge measurements are shown in Figures 43–47. Note that this analysis indicates that tidal and wave-induced currents for this time period were not significant enough in this region to bring forward to sediment transport analysis. This reaffirms the typical conclusion that potential sediment transport mechanisms are more likely to be waves and storm-induced currents for the open coast. A follow-on study to examine the effects of waves and storm-induced currents on sediment transport is ongoing.

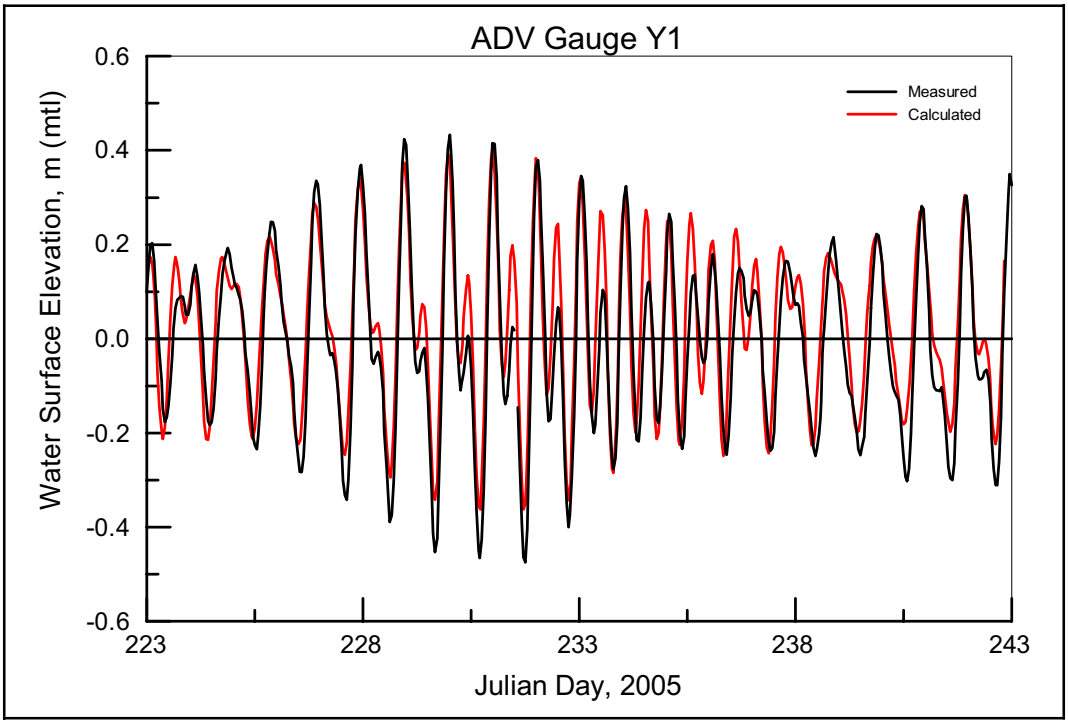

Figure 40. Water level comparison for ADV Gauge 1.

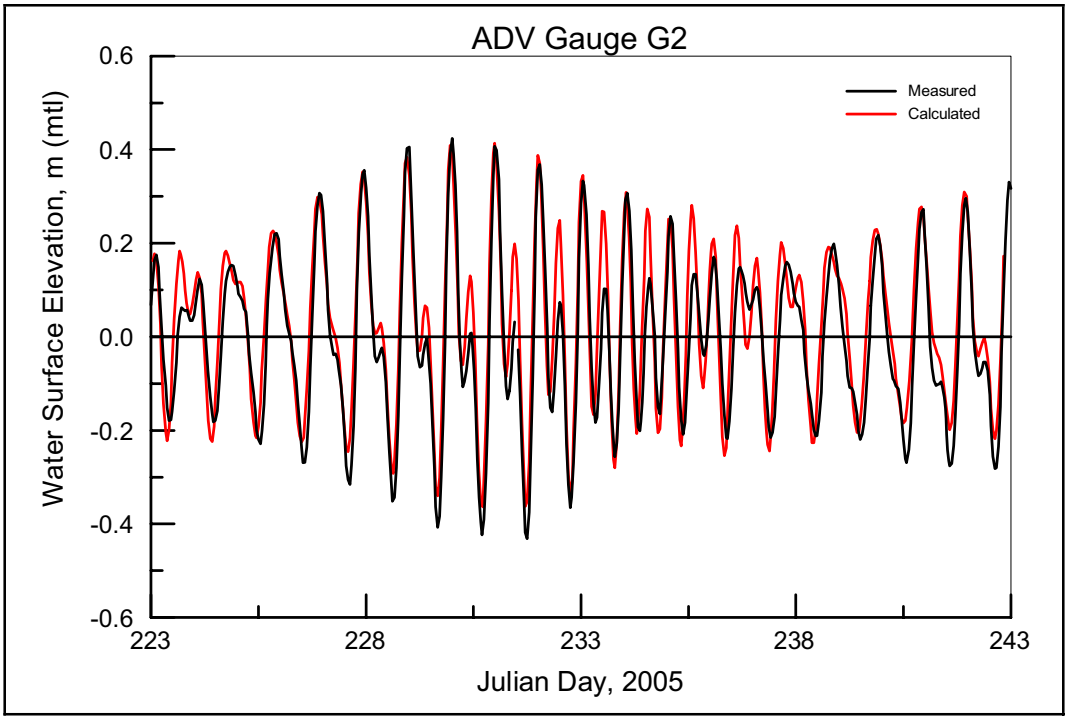

Figure 41. Water level comparison for ADV Gauge 2.

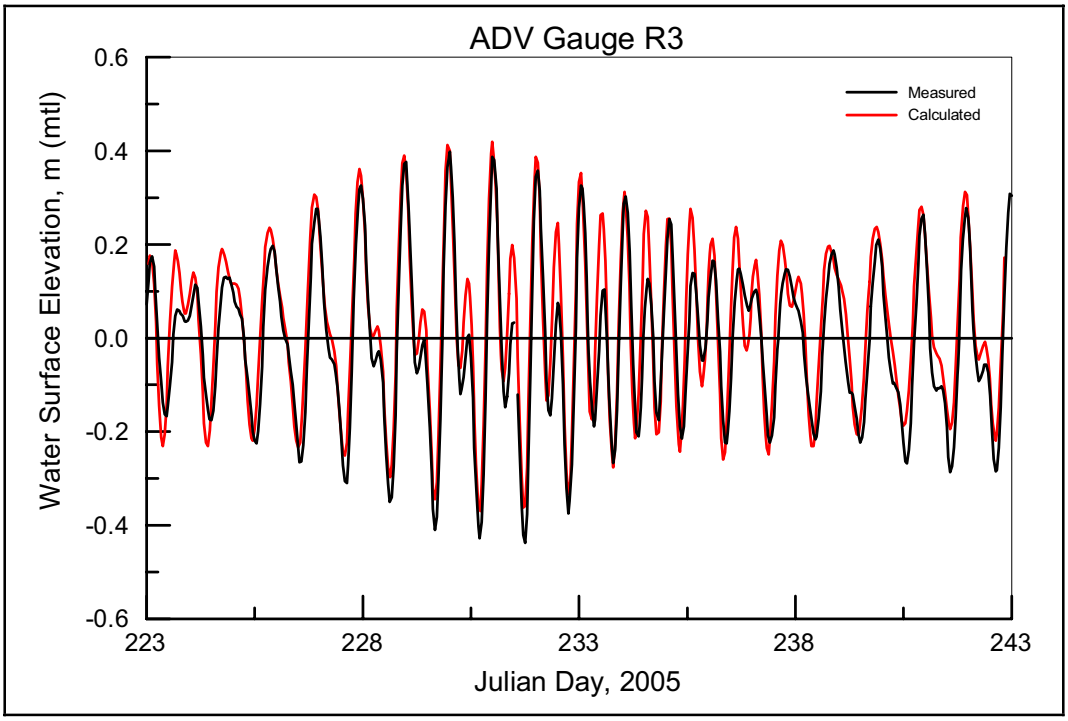

Figure 42. Water level comparison for ADV Gauge 3.

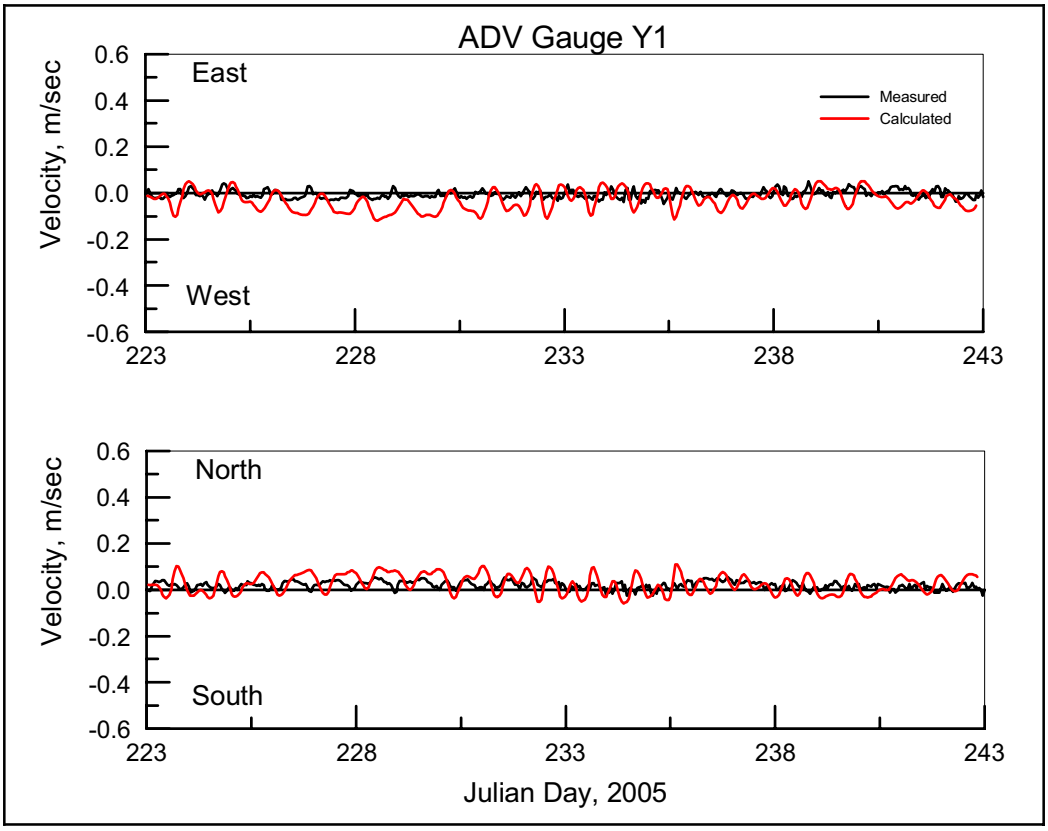

Figure 43. Velocity comparison for ADV Gauge 1.

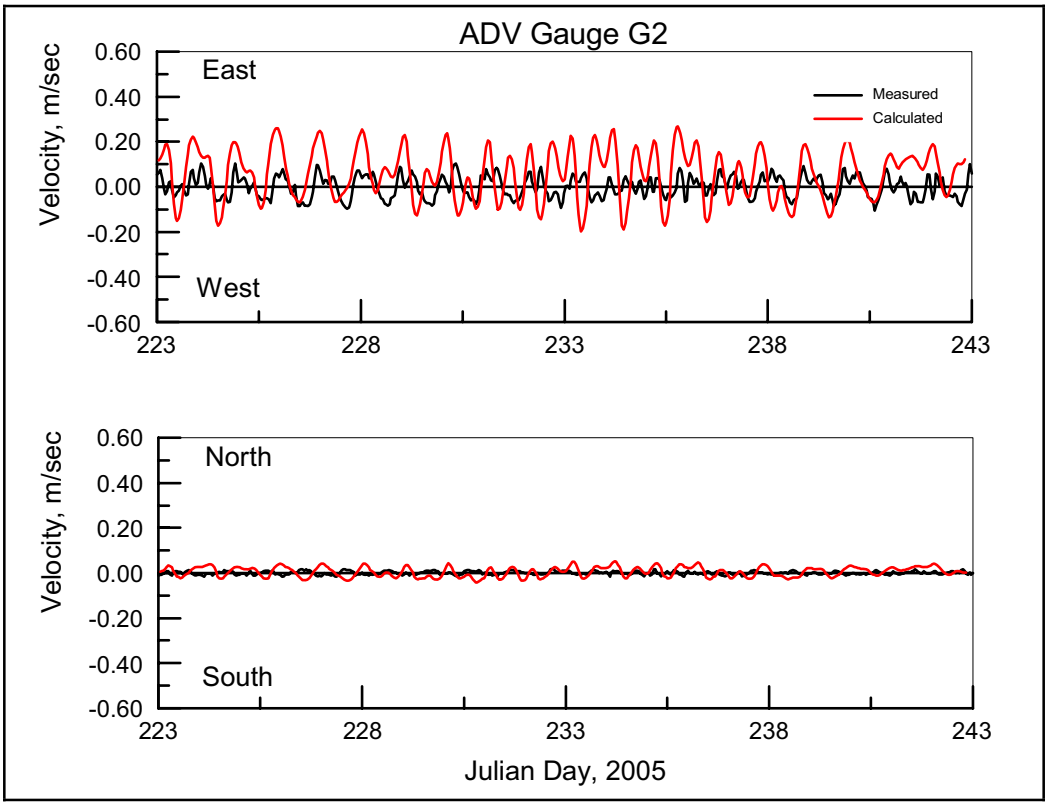

Figure 44. Velocity comparison for ADV Gauge 2.

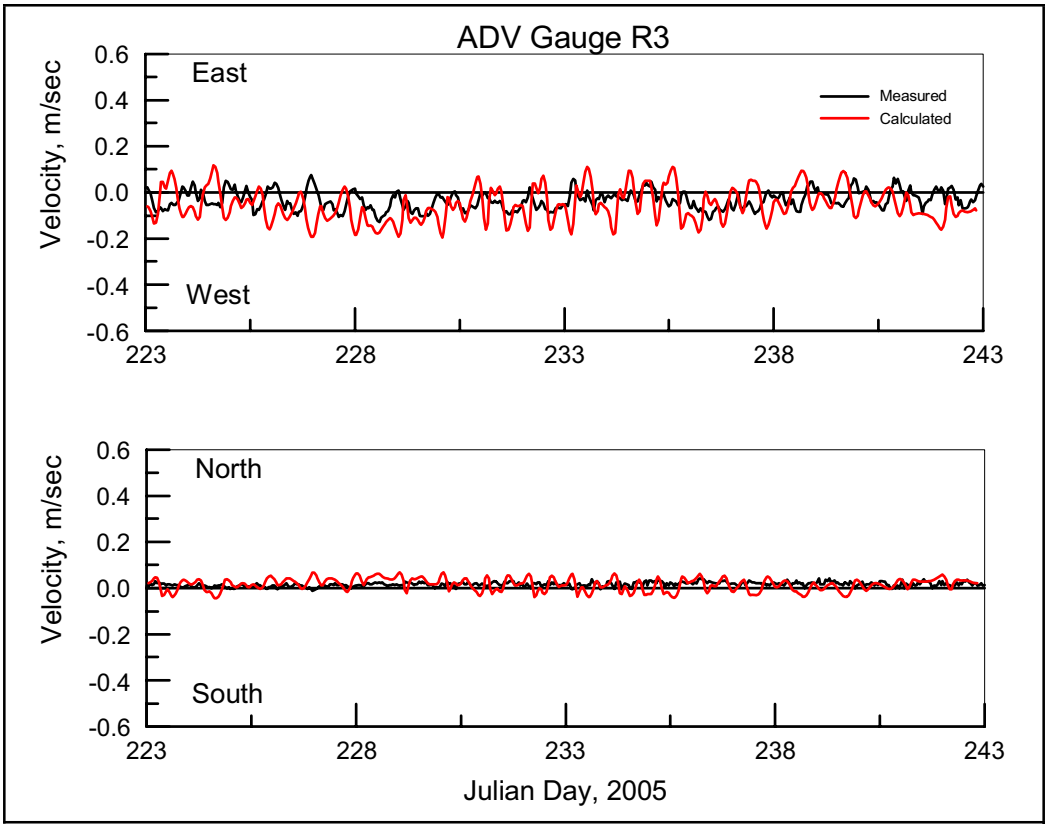

Figure 45. Velocity comparison for ADV Gauge 3.

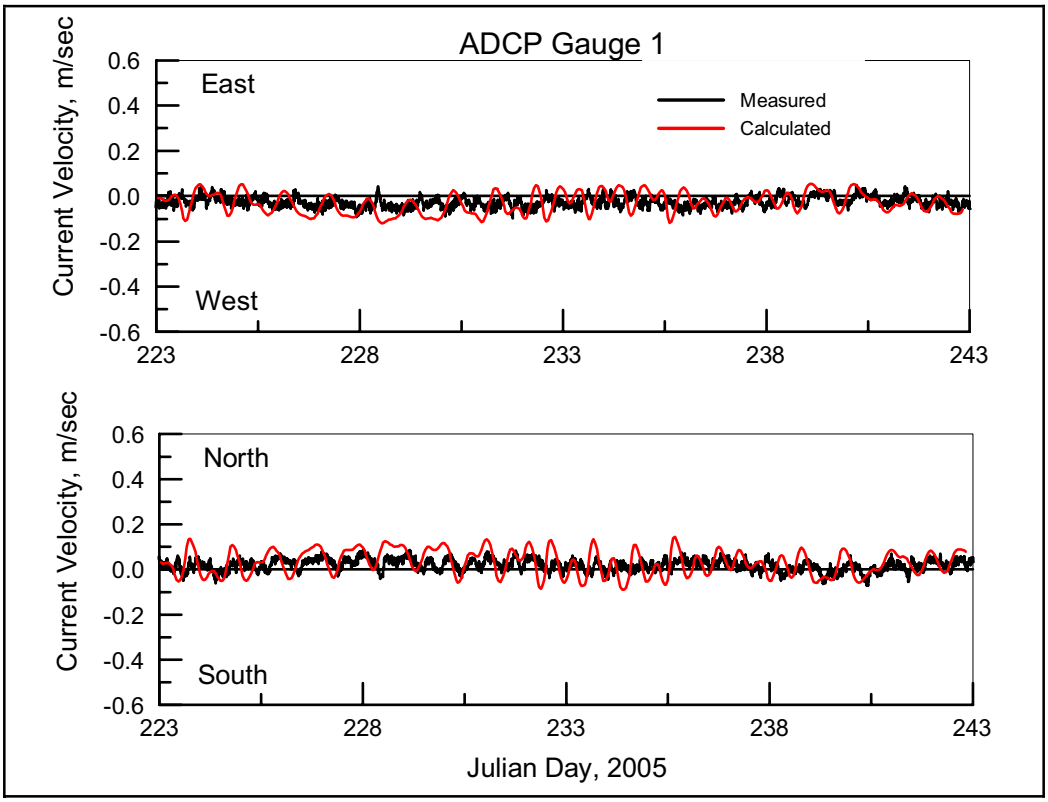

Figure 46. Velocity comparison for ADCP Gauge 1.

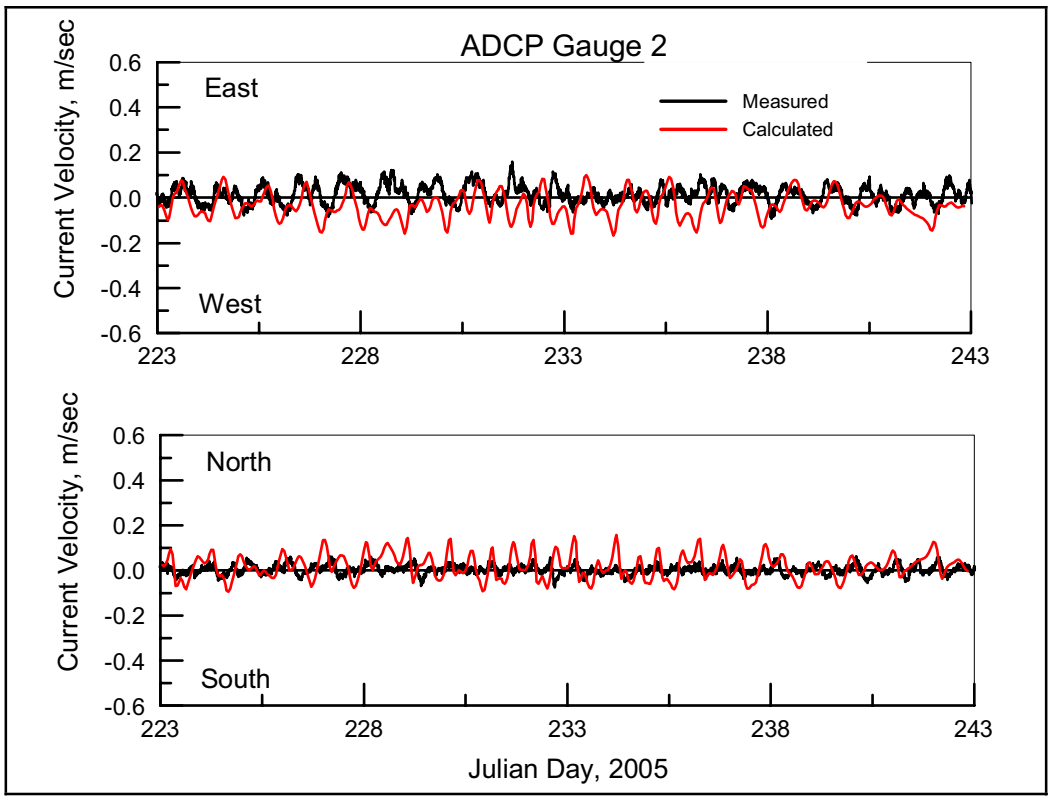

Figure 47. Velocity comparison for ADCP Gauge 2.

4 Summary

The purpose of the study was to provide POH with validated hydrodynamic and wave models for the project site. POH could then apply the models with various forcing conditions to develop a better understanding of nearshore circulation and sediment transport potential in the region and determine the likelihood of accretional and erosional areas within the model domain. The nearshore circulation study included six technical tasks: data collection/assessment, finite-element and finite-difference grid development, development of model forcing conditions, model validation, model simulations, and simulation analysis.

Wave, current, and water level data were collected in the field for a 1-month period with ADCP and ADV instruments. In addition, drogues were deployed on the 2 days that the ADCP/ADV were deployed and retrieved. Wave heights during the deployment period ranged from 0.12 to 0.69 m and were generally from the northeast direction, currents measured at the ADV and ADCP locations were small (generally less than 10 cm/sec), and water level ranged from +0.4 to -0.4 m, mtl. The drogue deployment provided general current trends for the two deployments.

A two-dimensional (depth-averaged) version of the hydrodynamic model (ADCIRC) was applied in this study. The ADCIRC modeling component for this study required grid development, validation of the bathymetric grid to known tidal constituents and wind forcing for April 2001, and comparison of the bathymetric grid forced with known tidal constituents, wind, and waves to measurements for the field data collection time period. The ADCIRC grid was developed as a circular mesh, encompassing the Hawaiian Islands, but was revised to an egg-shaped mesh to avoid tidal amphidromes in the Pacific Ocean.

For the initial model validation, ADCIRC results were compared with two NOAA gauges on the eastern half of the island of Oahu. The calculated water levels from the ADCIRC simulation of the April 2001 period compared relatively well in range and phase with the NOAA gauge measurements considering the locations of the gauges were well outside high-resolution sections of the grid in the project area. Since these gauges were outside the project area and in less resolved locations, another validation

was performed by simulating the field data collection time period and comparing model results to field data collected, specifically for this project, in the study area. Calculated water levels compared well in range and phase to measurements, but underestimated some lower peaks while overestimating some higher peaks. This may have been caused by localized interaction of the tides with the reefs surrounding the gauge locations. Current velocity data from the three ADV gauges and two ADCP gauges were extremely small during the overlapping deployment time period – generally less than 10 cm/sec. Velocities calculated at these locations from the ADCIRC circulation model were not expected to compare well to the measurements; however, the range of velocity model results is within one order of magnitude and generally very close. The application and validation of ADCIRC for the SEO study provides POH with the capability of simulating circulation in the study area for any required time period.

The purpose of applying nearshore wave transformation models such as STWAVE is to describe quantitatively the evolution of wave parameters from the offshore to the nearshore where nearshore wave information is required for the design of coastal engineering projects. STWAVE has been applied to numerous sites, and this project has the necessity of simulating wave transformation over a reef. Development of a bottom friction capability in STWAVE was completed for application to the extensive reefs in the SEO study area. Application of STWAVE for this project required development of a computational grid to simulate wave propagation, verification of calculated waves by comparison to measurements, and generation of a wave climate.

For demonstration of the wave climate development technique, nearshore conditions at a point in Waimanalo Bay were extracted from the STWAVE model results for each of the 134 simulations. A transformation correlation between the offshore and nearshore condition was then determined for each simulation. By applying the appropriate transfer function to each wave condition in the 2000–2004 offshore time series at Station 098, a long-term (2000–2004) nearshore time series was generated. The nearshore time series demonstrates that there is a reduction in wave height from the offshore location to the nearshore location, landward of the extensive reef system, as expected. The time series, however, appeared generally contained or banded between the 1.25 and 2.25 m wave height bins that were selected to represent the overall wave climate. In order to capture the nearshore transformation time series more precisely and to

include all wave conditions occurring in the time series, the range and refinement of the wave conditions simulated was expanded to 1274 wave conditions. The refined nearshore time series generated from analysis of these simulations shows a more realistic undulation in the nearshore wave height time series.

Development of a bottom friction capability in STWAVE was completed for application to the extensive reefs in the SEO study area. Based on existing literature, values of the JONSWAP bottom friction applied for coral reefs range from 0.04 to 0.12 m/sec. A single friction value can be applied to the entire STWAVE domain, or a range of friction values can be applied on a spatially varying basis. As an example, the 134 wave conditions simulated in the initial climate development were repeated with the revised STWAVE, applying a bottom friction coefficient typical for reefs of 0.05. With the inclusion of bottom friction, wave height at the nearshore location ranged from 18–38% of the previous results without bottom friction. On average, the wave height is 26% of the frictionless value at the selected location. The total wave spectrum refracts less with the inclusion of bottom friction, likely due to the dissipation of low-frequency energy. As another example, for each of the 1274 selected wave conditions simulated for the revised wave climate, wave transformation *including bottom friction* was simulated by applying STWAVE over the project domain for each of the 1274 wave spectra. The constant 0.05 value of bottom friction reduced nearshore wave heights by approximately 73% compared to wave heights without bottom friction.

The extended domain STWAVE grid was applied in the model validation process for the August 2005 model validation time period. Initially, a constant bottom friction value was applied to each cell of the STWAVE domain. Several simulations with different constant JONSWAP bottom friction values ranging from 0.04 to 0.12 were made to examine the range of response (wave height) at the gauge locations. Bottom friction reduced wave height at the ADV1 location by 64% for a bottom friction value of 0.04 (wave height is 36% of the offshore wave height), by 71–76% for a bottom friction value of 0.05 (wave height is 24–29% of the offshore wave height), and by 93% for a bottom friction value of 0.12 (wave height is 7% of the offshore wave height). The range of response indicates the importance of selecting the appropriate bottom friction value to represent the reefs in the study area.

In the validation simulation, a variable bottom friction field was utilized. Overall, all three measurement locations experience low wave energy relative to the offshore waves. The STWAVE model captures the large reduction in wave height from the offshore location to the three nearshore locations. The coral reefs in this region are described as "mushroom fields." Some areas of the reef are more solid and some areas have gaps and holes in the reef. Without detailed knowledge of the contiguous/noncontiguous areas of the reef, an educated attempt was made to represent the variations in the reef. The center section of the reef was given a smaller friction coefficient and the southern portion of the reef was given a larger coefficient. These adjusted values were selected based upon the under/overprediction of wave height at ADV2 and ADV3, respectively, in the simulation with a constant reef coefficient. Tidal fluctuation was also included in these simulations. With a variable bottom friction coefficient to represent variability in the reef structure, model results compare extremely well with the data at all three gauge locations with both the Manning and the JONSWAP friction formulations. The MPI values are 0.948 to 0.970 for the Manning simulations and 0.951 to 0.953 for the JONSWAP simulations. The magnitude and trend as well as the tidal fluctuation exhibited by the data were all captured by the model.

Lessons learned from this study include:

1. The technique of developing a nearshore wave climate by applying STWAVE for a large number (range) of offshore wave conditions provides a permanent "look up" table of nearshore wave conditions at any location in the computational domain and can be applied to any time period for which offshore data are available, provided that bathymetric conditions within the model domain remain similar. Note that the creation of a nearshore wave climate was applied to generate a nearshore time series for the 2000–2004 time period, and POH is applying the database-generated time series to develop sediment transport potential estimates in the project area. A follow-on study extended the time series through 2005 and expanded to 10 save point locations;
2. From the ADCIRC validation for the deployment time period and also from examination of the retrieved deployment data, it was concluded that the tidal and wave-induced currents in the project area are small and not sufficient to significantly transport sediment. A follow-on study is being conducted to examine simulation of higher energy (storm) conditions,

which may produce waves and currents that are strong enough to transport sediment; and

3. An improved model capability was developed for this study. Bottom friction was added to STWAVE to simulate wave transformation over reefs. It was shown that bottom friction is extremely important and has a pronounced effect on modeling transformation over reefs, decreasing wave heights from the without-friction condition by 71–76% for a constant JONSWAP bottom friction value of 0.05. Simulation of the transformation process over reefs could be improved further by including wave ponding, applying a more detailed breaking formulation such as Battjes and Janssen (1978), and implementing a coupling scheme between ADCIRC and STWAVE. In addition, field data collected for this project can be further analyzed to examine spectral energy dissipation from gauge location to gauge location and nonlinear interactions. These research topics may be examined in future STWAVE model development and application.

CHL assisted POH by documenting the methodologies and procedures used in this study and providing consultation in executing simulations and analyzing simulation results. STWAVE and ADCIRC working sessions have been conducted at POH and the completed modeling system was transferred to POH within the SMS framework.

5 References

Battjes, J. A., and J. P. F. M. Janssen. 1978. Energy loss and set-up due to breaking of random waves. *Proceedings, 16th International Conference on Coastal Engineering*. 569–587.

Bouws, E., and G. J. Komen. 1983. On the balance between growth and dissipation in extreme, depth limited wind-sea in the southern North Sea. *Journal of Physical Oceanography* 13:1653–1658.

Egbert, G., A. Bennett, and M. Foreman. 1994. TOPEX/Poseidon tides estimated using a global inverse model. *Journal of Geophysical Research* 99(C12): 24821–24852.

Guza, R. T., and E. B. Thornton. 1980. Local and shoaled comparisons of sea surface elevations, pressures, and velocities. *Journal of Geophysical Research* 85(C3):1524–1530.

Hardy, T. A. 1993. *The attenuation of spectral transformation of wind waves on a coral reef*. Townsville, Queensland, Australia: James Cook University of North Queensland.

Hasselmann, K., T. P. Barnett, E. Bouws, H. Carlson, D. E. Cartwright, K. Enke, J. A. Ewing, H. Gienapp, D. E. Hasselmann, P. Kruseman, A. Meerbrug, P. Muller, D. J. Olbers, K. Richter, W. Sell, and H. Walden. 1973. Measurements of wind-wave growth and swell decay during the Joint North Sea Wave Project (JONSWAP). *Dtsch. Hydrogr. Z.* A80(12), 95 pp.

Hearn, C. J. 1999. Wave-breaking hydrodynamics within coral reef systems and the effect of changing relative sea level. *Journal of Geophysical Research* 104(C12):30007–30019.

Holthuijsen, L. H. 2007. *Waves in ocean and coastal waters*. Cambridge: Cambridge University Press.

Kraus, N. C. 2006. *Mid-Bay Islands hydrodynamics and sedimentation modeling study, Chesapeake Bay*. ERDC/CHL TR-06-10. Vicksburg, MS: U.S. Army Engineer Research and Development Center.

Kraus, N. C., and H. T. Arden. 2003. *North jetty performance and entrance navigation channel maintenance, Grays Harbor, Washington; Vol 1: Main Text*. ERDC/CHL TR-03-12. Vicksburg, MS: U.S. Army Engineer Research and Development Center.

LeProvost, C. M., L. Genco, F. Lyard, P. Vincent, and P. Canceil. 1994. Spectroscopy of the world ocean tides from a finite element hydrodynamical model. *Journal of Geophysical Research* 99(C12):24777–24797.

Lowe, R. J., J. L. Falter, M. D. Bandet, G. Pawlak, M. J. Atkinson, S. G. Monismith, and J. R. Koseff. 2005. Spectral wave dissipation over a barrier reef. *Journal of Geophysical Research* 110(C04001).

Luettich, R. A., Jr., J. J. Westerink, and N. W. Scheffner. 1992. *ADCIRC: An advanced three-dimensional circulation model for shelves coasts and estuaries, report 1: theory and methodology of ADCIRC-2DDI and ADCIRC-3DL*. Dredging Research Program Technical Report DRP-92-6. Vicksburg, MS: U.S. Army Engineer Waterways Experiment Station.

Padilla-Hernández, R., and J. Monbaliu. 2001. Energy balance of wind waves as a function of the bottom friction formulation. *Coast. Eng*. 43(2):131–148.

Resio, D. T. 1988. A steady-state wave model for coastal applications. *Proceedings of the 21st Coastal Engineering Conference*, ASCE, 929–940.

Sea Engineering, Inc. 2008 (Draft). Lanikai Beach Restoration Study Conceptual Design Report. Prepared for: USACE, Honolulu District by Sea Engineering, Inc. and Group 70 International.

Smith, J. M. 2000. Benchmark tests of STWAVE. *Proceedings, 6th International Workshop on Wave Hindcasting and Forecasting*, 169–379.

Smith, J. M., A. R. Sherlock, and D. T. Resio. 2001. *STWAVE: Steady-state spectral wave model user's manual for STWAVE, Version 3.0*. ERDC/CHL SR-01-1. Vicksburg, MS: U.S. Army Engineer Research and Development Center.

U.S. Army Corps of Engineers (USACE). 2006. Louisiana Coastal Protection and Restoration (LACPR) Preliminary Technical Report to United States Congress.

U.S. Army Corps of Engineers (USACE), Mobile District. 2008. Mississippi Coastal Improvements Program (MSCIP) Comprehensive Plan and Integrated Programmatic Environmental Impact Statement. Draft peer review plan, 498 p. plus Appendixes.

Wozencraft, J. M., and J. L. Irish. 2000. Airborne lidar surveys and regional sediment management. *Proceedings, 2000 EARSeL: Lidar Remote Sensing of Land and Sea, EARSeL*. Dresden, Germany.

REPORT DOCUMENTATION PAGE

Form Approved
OMB No. 0704-0188

1. REPORT DATE *(DD-MM-YYYY)*	2. REPORT TYPE	3. DATES COVERED *(From - To)*
July 2008	Final report	

4. TITLE AND SUBTITLE

Southeast Oahu Coastal Hydrodynamic Modeling with ADCIRC and STWAVE

5a. CONTRACT NUMBER

5b. GRANT NUMBER

5c. PROGRAM ELEMENT NUMBER

6. AUTHOR(S)

Mary A. Cialone, Mitchell E. Brown, Jane M. Smith, and Kent K. Hathaway

5d. PROJECT NUMBER

5e. TASK NUMBER

5f. WORK UNIT NUMBER

7. PERFORMING ORGANIZATION NAME(S) AND ADDRESS(ES)

U.S. Army Engineer Research and Development Center
Coastal and Hydraulics Laboratory
3909 Halls Ferry Road
Vicksburg, MS 39180-6199

8. PERFORMING ORGANIZATION REPORT NUMBER

ERDC/CHL TR-08-9

9. SPONSORING / MONITORING AGENCY NAME(S) AND ADDRESS(ES)

U.S. Army Engineer District, Honolulu
Building 230
Fort Shafter, HI 96858-5440

10. SPONSOR/MONITOR'S ACRONYM(S)

11. SPONSOR/MONITOR'S REPORT NUMBER(S)

12. DISTRIBUTION / AVAILABILITY STATEMENT

Approved for public release; distribution is unlimited.

13. SUPPLEMENTARY NOTES

14. ABSTRACT

This study provides the Honolulu District (POH) with numerical modeling tools for understanding nearshore circulation and sediment transport for Southeast Oahu (SEO). Circulation and wave models are developed and validated for this region and can be applied to assess sediment transport potential for various forcing conditions and to determine the likelihood of accretional and erosional areas within the model domain.

Application of a wave model includes the generation of a wave climate. In the wave climate development technique, nearshore conditions are extracted from the wave model results for each simulation. A transformation correlation between the offshore and nearshore condition is then determined for each simulation. By applying the appropriate transfer function to each wave condition in the offshore time series, a long-term nearshore time series is generated. The nearshore time series demonstrates that there is a reduction in wave height from the offshore location to the nearshore location, landward of the extensive reef system as expected. The technique of developing a nearshore wave climate by applying the wave model for a range of offshore wave conditions provides a permanent "look up" table of nearshore wave conditions at any location in the

(Continued)

15. SUBJECT TERMS

ADCIRC
Circulation model
Hydrodynamic model
Oahu, HI
STWAVE
Two-dimensional model
Wave model

16. SECURITY CLASSIFICATION OF:			17. LIMITATION OF ABSTRACT	18. NUMBER OF PAGES	19a. NAME OF RESPONSIBLE PERSON
a. REPORT	b. ABSTRACT	c. THIS PAGE			19b. TELEPHONE NUMBER *(include area code)*
UNCLASSIFIED	UNCLASSIFIED	UNCLASSIFIED		60	

14. ABSTRACT (Concluded)

computational domain and can be applied to any time period for which offshore data are available, provided that bathymetric conditions within the model domain remain similar. POH is applying the database-generated time series to develop sediment transport potential estimates in the project area.

Development of a bottom friction capability in the wave model was completed for application to the extensive reefs in the SEO study area. It is shown that bottom friction is extremely important and has a pronounced effect on modeling transformation over reefs, decreasing wave heights from the without-friction condition by 71-76% for a constant JONSWAP bottom friction value of 0.05.

APPENDIX D

GEOTECHNICAL INVESTIGATIONS

SAND SAMPLE MAP
SAND FROM CRUSHED CORAL RUBBLE

Geotechnical Investigations

SOUTHEAST OAHU REGIONAL SEDIMENT MANAGEMENT DEMONSTRATION PROJECT SAND SAMPLE MAP

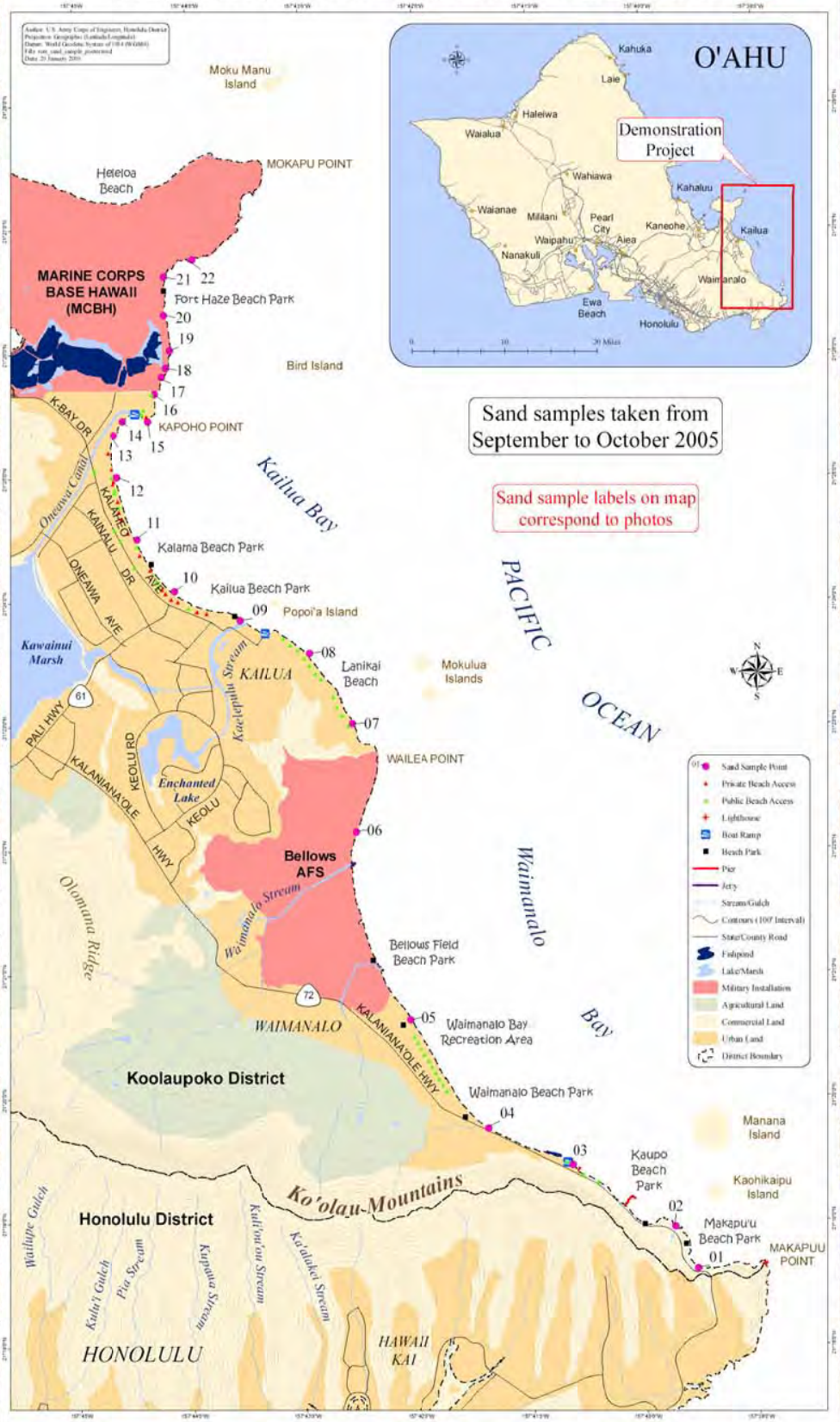

Sand samples taken from September to October 2005

Sand sample labels on map correspond to photos

SAND
from
CRUSHED CORAL RUBBLE

Beachrock Formation

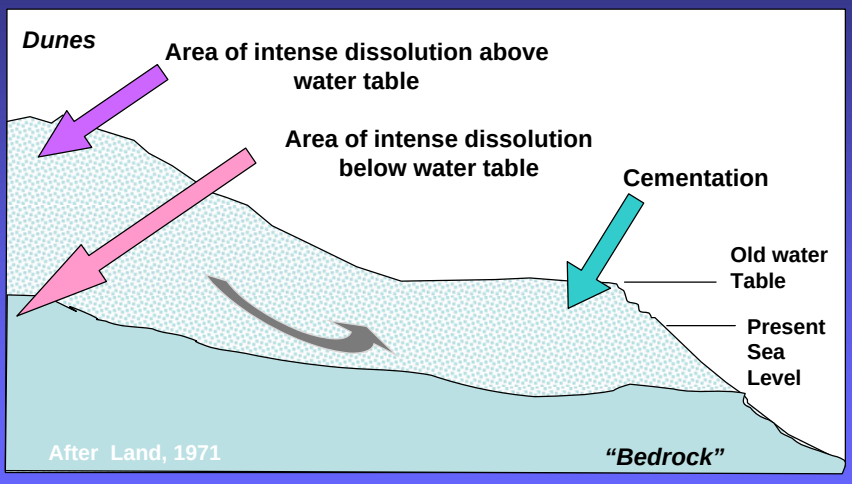

Washed Carbonate Sand Surface

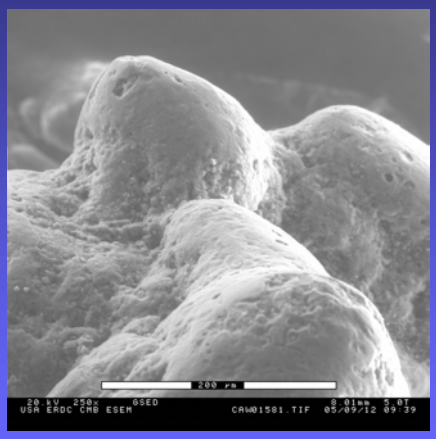

- **Carbonate sand grains were treated by washing in boiling hydrogen peroxide to remove microbial overgrowth**
- **Surface is polished**
- **Fractures show porous skeletal carbonate structure**

Overgrowth on Sand Surface

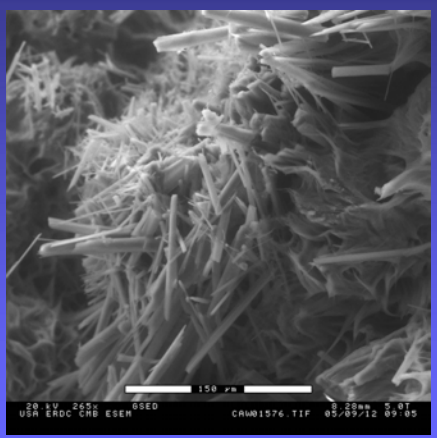

- **Sand grain treated by using carbonate and calcium solution to produce overgrowth of aragonite needles on surface**
- **Grains are cemented into beachrock by carbonate overgrowth**

Aragonite and Calcite Overgrowth

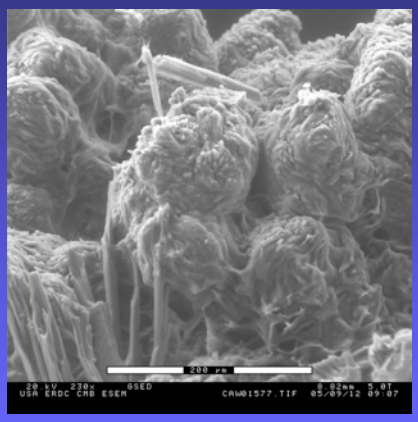

- Carbonate precipitation can produce calcite and aragonite overgrowth
- Aragonite is typically unstable and can redissolve and recrystalize as calcite
- Small crystals are less stable than large crystals and small crystals dissolve and large crystal grow larger (Ostwald crystal ripening).

Fatty Acids for Coating Materials

- Inexpensive, non-toxic
- Available in large quantities
- Available in all grades
- Slowly biodegradable
- React with and coat all carbonates
- End product is the calcium salt of the fatty acid (soap film)

What Loading Rate is Required?

- Assume the fine sediment is the source of the cement
- Three-micron diameter calcite fragments have a specific area of approx. 0.7 m^2/g
- Each molecule of stearic acid covers 20.5 sq. Å
- One gram of calcite has area of 7×10^{16} sq. Å
- Molecular wt of stearic acid = 284.5 (6×10^{23} molecules per mole)
- Approx. $6x10^{-9}$ moles stearic acid cover one gram
- Theoretically a metric ton of calcite requires less than 2 grams of stearic acid

Industrial Grade Fatty Acids

Commercial soaps are salts (typically sodium salts) of a mixture of fatty acids

Summary on Inhibiting Re-Cementing

- **Coatings can isolate the surface of carbonate grains to make solution of carbonates and overgrowth of cements slower**
- **Process of preserving the sand mimics natural processes that inhibit re-cementing of carbonates**
- **Fatty acid coatings can promote clustering of fine-grained carbonates reducing turbidity**
- **Coating process is inexpensive and can be integrated into manufacturing sand along with crushing and sieving steps**
- **A sieved, coated sand should provide a better beach than quarry-run crushings**

APPENDIX E

REGIONAL SEDIMENT MANAGEMENT
WEB-ENABLED GIS PLATFORM
e-GIS

GIS and the Internet

All of the RSM geospatial data is available over the Internet with new "Online Mapping" Tools

Data Layers

Layers on the site include:

- satellite imagery
- watershed boundaries
- land parcels
- roads
- soil types
- wetlands
- hydrography
- shoreline profiles
- historical shoreline change
- shoreline structures
- coastal habitat & reefs
- sediment deposit information
- revetments
- bathymetry
- wave gauges
- nautical charts
- and much more!

What Am I Looking At?

How Do I Turn a Layer On/Off?

1) Navigate to the Table of Contents , and click on the Layers tab (highlighted in red in the graphic to the right).

2) After you have activated the "Layers" tab, then just check (or uncheck) any of the square boxes (highlighted in purple in the graphic to the right). next to a layer to turn it on (off).

What Does the Standard Toolbar Do?

	Toggles the overview map on or off		Zoom-in on the map with user defined AOI		Zoom-out on the map with user defined AOI
	Zoom to the full extent of the map		Zoom to the extents of the active map layer		Zoom back to the previous extent of the map
	Pan the map in any direction		Retrieve attribute data by identifying a feature		Display standard query builder form
	Search the attributes of the specified layer		Measure linear distance on the map in specified units of measure.		Select map features and retrieve attribute data using a dynamically dragged window
	Select map features and retrieve attribute data by using a user defined polygon or line		Place a dynamic point on the map that is labeled with the point's coordinates		Calculate area of a user defined polygon in specified units of measure
	Add user defined text to the map where clicked		Place a user defined grid over the map with labeled rows and columns		Print the map
	Clears the map of any temporary selections.				

How Can I Calculate Acreage?

1) Zoom into the area on the map where you would like to calculate the area. This can be performed by using the "Zoom In" button , which is found on the Standard Toolbar.

2) After you have zoomed in to the area you would like to calculate, click on the "Calculate Area" button , which will activate the "Polygon Area" dialog box.

3) In the "Polygon Area" dialog box, set the Area Units you would like (acres, square feet, square meters, etc), as well as the fill color and transparency.

4) After you are happy with your settings, begin clicking on the map to designate the vertices of your area calculation. Before you reach your last vertex, click on the **Complete Polygon** button in the "Polygon Area" dialog box to auto complete the polygon.

5) The area information will appear on your map.

How Do I Print My Map?

1) Zoom into the area on the map where you would like to print. This can be performed by using the "Zoom In" button , which is found on the Standard Toolbar.

2) Add any coordinate labels, text, grids, etc that you want visible for printing.

3) After you have the map set just like you want, click on the "Print" button , which will activate the "Print Map" dialog box.

4) In the "Print Map" dialog box, type in your map title and any other comments you would like.

5) After you have your title and comments set, then select the paper size you want your map to print at.

6) After your paper size has been selected, click the **Generate Map** button.

7) Select File > Print to print the map out.

How Do I Save My Map?

1) Zoom into the area on the map where you would like to save. This can be performed by using the "Zoom In" button , which is found on the Standard Toolbar

2) Turn on/off any layers you would like visible/not visible.

3) Add any customized coordinate labels, text, grids, etc that you desire.

4) Right-click on the map, and select **Save Picture As…** from the context menu (highlighted in blue in the graphic to the right).

5) In the "Save Picture" dialog box, select where you would like the image saved, and then click the **Save** button.

6) Your image will be saved to your computer, and you can now insert it into e-mails, PowerPoint Presentations, project documents, etc.

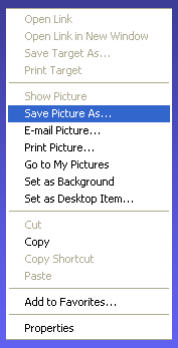

APPENDIX F

REGIONAL SEDIMENT PROCESSES

DEPARTMENT OF GEOLOGY AND GEOPHYSICS
UNIVERSITY OF HAWAII

A Reconnaissance of Reef Top Sediment Bodies in Windward Oahu, Hawaii

Draft (December 11, 2006)

by

Christopher Bochicchio
Charles Fletcher

Univeristy of Hawaii - Coastal Geology
Dept. of Geology and Geophysics
1680 East-West Rd.
POST 721a
Honolulu, HI 96822

Draft 06

INTRODUCTION

Fringing reefs in Hawaii display sand fields on their surfaces (Figure1) that potentially play a role in littoral sediment budgets, provide substrate for important components of reef ecology, and may serve as a resource for sand and gravel aggregate. These shallow sand fields may also potentially provide quantities of affordable sand for beach replenishment projects (Moberly et *al.*, 1975; Casciano and Palmer, 1969; Moberly and Chamberlain, 1964). However, the degree of sand storage they provide and their role in littoral sediment budgets has not been defined.

Past Studies: Several studies review offshore and onshore carbonate sand sources on the island of Oahu, Hawaii. Moberly et *al.* (1975) present a general survey of offshore sand resources surrounding Oahu in the 0 – 18 m depth zone. At three sites, Sand Island, North Shore, and Penguin Bank, sand thickness is measured using a sub-bottom seismic profiler and sand volumes are estimated. Ocean Innovators in conjunction with the US Army Corps of Engineers completed jet probe surveys and sediment sampling at a number of shallow and deep sand resource areas around Oahu (Ocean Innovators, 1977a – c, 1978a – b, 1979).

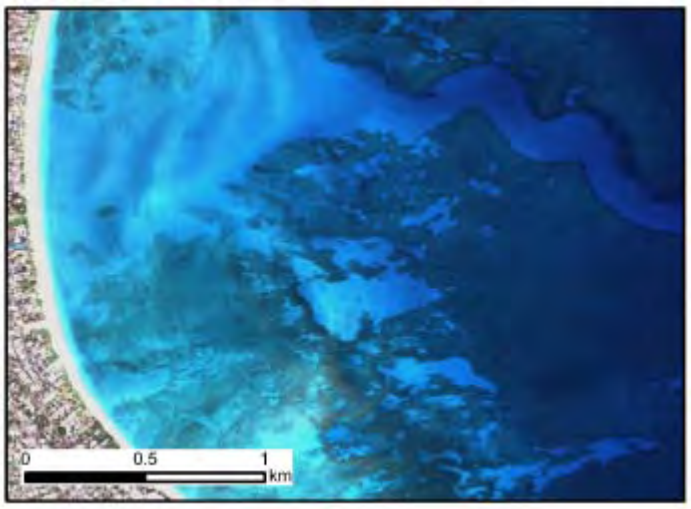

Figure 1. Bodies of sand fill depressions on the near-shore carbonate platform.

Coulbourn et *al.* (1988) perform detailed statistical analysis on sand samples taken by Ocean Innovators to identify grain size correlations to depth and depositional environment. Sea Engineering (1993) presents a summary of sand exploration studies performed around the island of Oahu as well as comparative ratings for exploitable deposits. Hampton et *al.* (2003) and Hampton et *al.* (2004) identify significant bodies of

sediment stored in the deep, 18 –100 m, fore-reef area at various Oahu locations using sub-bottom seismic imaging. Neither of Hampton's reports makes significant mention of sand bodies in water < 18 m.

The NOAA Benthic Habitat Mapping Program (Coyne et *al.* 2003) mapped sandy substrate from the shoreline to 30 m depth as part of a benthic habitat classification for the whole of Oahu. Conger et *al.* (2006) created detailed maps of sandy substrate to 20 m depth at sites around Oahu via supervised classification of multispectral satellite imagery, but these lack volume estimates.

Present Study: Past studies describe sand resources at sites around Oahu in varying degree of detail. The focus of this report pertains to three adjoining locations on the eastern Oahu shore: Kailua Bay, Lanikai, and Waimanalo Bay. Previous studies that provide detailed subsurface sampling within our area of interest include: Ocean Innovators (1978a), Coulbourn et *al.* (1988), Hampton et *al.* (2003), and Hampton et *al.* (2004). Sea Engineering (1993) provides a summary of data in Kailua Bay.

This study is an initial large-scope investigation of sediment volume within the study area. The intent of this study is to highlight areas of significant volume that could be the subject of more detailed measurement and study in the future. Here we report the results of 205 jet probe thickness measurements obtained from 54 distinct sand bodies in the 0 – 20 m depth zone across the reef platform of Kailua Bay, Lanikai, and Waimanalo Bay. Volume estimates and uncertainties are presented with discussion of sand body morphologies. The focus of this research is to quantify the volume geometry of reef-top sand bodies, improve our understanding of controls on variations in thickness of these sand resources, and infer the role of reef top sand bodies in littoral sediment processes.

STUDY AREA: KAILUA BAY, LANIKAI, AND WAIMANALO BAY

Wave Climate: Wave energy influences coastline stability, nearshore submarine sand transport, and mechanical abrasion on the reef. Hawaii's regional wave climate (Figure 2) is described in four components by Bodge and Sullivan (1999):

Figure 2. Components of Oahu's wave environment.

1) High-energy northeast Pacific swell created during the winter by storms north of Hawaii. Waves are incident on WNW to NNE shorelines; typical heights of 1.5 – 4.5 m and periods of 12 – 20 seconds.
2) Lower energy south Pacific swell between the months of April and October. Waves are incident on most south facing shorelines and have typical heights of 0.3 – 1.8 m and periods of 12 – 20 seconds.
3) Kona storms infrequently produce from the south and west wave heights of 3 – 4.5 m and periods of 6 – 10 seconds.
4) Trade wind waves consistently approach from the general northeast quadrant for 90% of the summer months and 55 – 65% of the winter months (Fletcher et *al.* 2002). Trade wind wave heights are 1.2 – 3 m with periods of 4 – 10 seconds.

Additionally, large but infrequent hurricane waves can have significant impact on the reef (Fletcher et. al, 2002). Rooney et *al.* (2004) discuss the occurrence of extraordinarily large winter swell associated with strong El Nino episodes. They conclude that these events exert control over fringing reef accumulation and have essentially terminated most shallow water accretion on north-exposed coasts in Hawaii since approximately 5,000 yrs B.P (before present).

The primary wave regime for our windward study area is governed by the consistent full strength of trade wind swell. This swell is modified by annual and decadal

North Pacific wave events that wrap around Mokapu Peninsula into the study area. Large south swell affects the study area to a lesser extent. Easterly storms may also impact the study with high winds and/or high waves approaching on an interannual basis from the northeast, east, or southeast. Calmest conditions in the study area occur during Kona wind conditions as trade winds diminish, frequently producing offshore air flow.

Shelf Origin: The underlying carbonate framework of the study area is the product of reef accretion over recent interglacial cycles. Specifically, the shallow shelf of Oahu is a fossil reef complex dating from Marine Isotope Stage (MIS) 7 (~190,000 – 210,000 yrs B.P., Sherman et *al.*, 1999; Grossman and Fletcher, 2004). The front of this shelf accreted separately during MIS 5a-d (ca. 80,000 – 110,000 yrs B.P.). Eolianites of late last interglacial age (ca. 80,000 yrs B.P., Fletcher et *al.*, 2005) are found on the nearshore and coastal plain regions of windward Oahu.

Modern Holocene reef accretion is limited to deeper environments on the front of the reef where wave energy is not destructive. Grossman and Fletcher (2004) and Conger et *al.* (2006) infer that rugosity in depths less than 10 m atop the fringing reef is the result of karstification of limestone during times of lower sea-level, most recently since the last interglacial. Modern wave scour has prevented accretion in this zone. In depths greater than 10 m the karst surface has largely been over grown by Holocene accretion (Conger et *al.*, 2005).

Coastal Plain: Harney and Fletcher (2003) provide a synthesis of drill cores and radiometric dating obtained in the Kailua coastal plain over the last 60 years. It is demonstrated that sediments underlying the town of Kailua and the Kawaianui Marsh reflect 5,000 years of coastal sedimentation during a sea-level highstand (+2 m) and subsequent declines in sea-level position (Grossman and Fletcher, 1988). A 3-10 m thick sandy accretion strand plain is deposited over lagoonal sediments (marine silt with shell and coral fragments) >40 m in thickness. Under modern Kawainui Marsh, cores penetrate 15 m of peat, terrestrial mud, and lagoonal sediments. The presence of lagoonal sediment is attributed to formation of a marine embayment ca. 3,500 yrs B.P. during the high-stand followed by formation of a terrestrial marsh following sea-level fall ca. 2,200 years B.P. (Kraft, 1982, 1984; Athens and Ward, 1991). The accretion strand

plain is lies between the marsh and the beach face of modern Kailua Bay and has an especially thick central portion attributed to shoreward expression of the offshore paleo-stream channel that has filled with sand (Harney and Fletcher, 2003). The strand plain formed by shoreline regression as sea-level fell to its modern position following the mid-Holocene highstand. Coastal plain deposits underlying Kawainui Marsh and the town of Kailua are found by Harney and Fetcher (2003) to contain 10,049 (+/- 1,809) x 10^3 m^3 of carbonate sand and silt of Holocene age.

General Sediment Characteristics: Moberly and Chamberlain (1964) characterize Kailua Bay, Lanikai, and Waimanalo Bay as having very poorly sorted highly calcareous beach sands and large but thin patches of offshore sand. Kailua and Lanikai sands are described as poorly sorted, with Kailua tending towards bimodality. Waimanalo sands are described as coarse- to medium- grained and vary from well sorted to poorly sorted with high *foraminifera* fractions. Landward of Kailua and Waimanalo beaches are modern vegetated dunes and older lithified eolianites, consisting of coarse well-sorted sand, in which *foraminifera* constitute the highest compositional fraction.

Sediment Production: Harney et *al.* (2000) completed a detailed study of beach, channel, and reef-top sand bodies in Kailua Bay. Harney determined >90% of sediments were biogenic carbonate, dominated by coralline (red) algal fragments. They identified two primary sources of sediment for Kailua Bay. The offshore reef platform is a primary source of framework sediments (coral and coralline algae) while nearshore hardgrounds and landward portions of the reef platform are sources of direct sediment production (*Halimeda*, mollusks, and benthic *foraminifera*).

Radiometric dating of sand grains indicate middle to late Holocene age for surficial sediment stored in Kailua Bay. Most surficial sediments were found to be older than 500 yrs, suggesting relatively long storage times in the immediate sediment budget. Harney et *al.* (2000) concluded that sand stored in Kailua Bay represents production under a higher sea-level stand (+ 2 m; Grossman and Fletcher, 1998) that retreated during the late Holocene.

Coralline algae, the primary compositional element of Kailua sands, are primary reef framework producers in high wave energy environments (Harney et *al*, 2000). High

coralline algae composition suggests that a strong wave environment is a major controlling factor on sediment production in Kailua Bay during the past 5000 yrs. Grossman (2001) and Rooney et *al.* (2004) analyzed drill cores from reef platforms exposed to strong modern north swell and concluded that positive fringing reef accretion was halted by an increase in wave energy ca. 5000 yr ago. Rooney et *al.* conclude the increase in northern swell ca. 5000 yr ago corresponds to amplification of El Nino/Southern Oscillation (ENSO), which is responsible for unusually large northern wave events in Hawaii during particularly strong El Nino episodes. It stands that sediment storage in Kailua Bay reflects a diminishing sediment production regime over the last 5000 years, brought on by stronger ENSO induced north swell and reduced accommodation space due to sea-level fall.

Benthic organism data collected at the Kailua sand channel by Harney (2003) shows a 50% decrease in living coral cover (57% to 7%) along the channel margin where depth decreases from 10 m to 3 m. This reduction in coral cover is the result of higher wave shear stress in shallower waters (Grossman, 2001) aided by higher suspended sediment concentrations. A combination of higher shear stress and less accommodation space likely led to reduced reef framework growth at shallow depths around windward Oahu (Grossman and Fletcher, 2004).

PREVIOUS SAND RESOURCE INVESTIGATIONS IN THE STUDY AREA

Onshore Resources: Inventory and mapping of sand resources in Kailua and Waimanalo began with Moberly and Chamberlain (1964). Kailua Bay, Lanikai, and Waimanalo Bay beach sands are described as very poorly sorted and highly calcareous. Offshore sand bodies are described as large but thin and patchy. Moberly et *al.* (1975) identify lithified eolianites in Kailua, Bellows, and Waimanalo as a potential source of beach sand. Moberly describes the deposits as the most extensive on windward Oahu, but adds that houses and beach parks cover a majority of these. As of 1975, island-wide deposits of lithified dune lacking development and available for mining were estimated at less than 2 x 10^6 m^3 (2.7 million yd^3). Existing modern vegetated dunes are mentioned, but considered a great deal more valuable intact than mined, as removed would yield

relatively small volumes of sand and have negative impacts on wildlife habitat and flood protection.

Pacific Rock & Concrete (PR&C) began crushing limestone mined in a Waimanalo quarry in the late 1960's. The intent of PR&C was to use the sand as material for beach replenishment (personal interview relayed by Casciano and Palmer, 1969).

Offshore Resources: Moberly et *al.* (1975) completed the first intensive survey of offshore sand resources around Oahu. Spatial extent of offshore sand fields was roughly mapped by aerial surveys. Major sand bodies from sea-level to 18 m depth were mapped for the Kailua and Waimanalo areas, however the survey of deeper sand bodies (18 m – 90 m) excluded the region between central Kailua and Koko Head. None of the areas selected for detailed thickness measurements were within the Kailua or Waimanalo regions.

Ocean Innovators (1978, 1979) completed a jet probe survey of the Kailua sand channel and an adjacent sand body for the U.S. Army Corps of Engineers in 1978. Jet probing was performed in a series of 13 transects perpendicular to the channel axis in depths of 5 to 24 m and 3 transects between 5 and 6 m in the adjacent sand body. Minimum volumes were estimated for the sand channel, 3.7×10^7 m^3 (4.84×10^7 yds^3), and the adjacent sand body, 2.08×10^6 m^3 (2.72×10^6 yds^3).

Surface and subsurface sampling in Kailua channel performed in the same locations revealed a variability in grain size, sorting and color with no discernable pattern. Median grain sizes of samples varied from fine to coarse sand (0.11 to 1.4 mm) with the percentage of samples finer than 0.15 mm varying between 1% and 81%. In only 7 out of 36 samples were less than 10% of the grains found to be finer than 0.15 mm. The average percentage of material finer than 0.15 mm was 38%. The color varied between slightly gray and yellow. Initial results indicated the sand channel contained very thick sand, in excess of 9 m in most instances and occasionally over 15 m. Sediment washed out by the jet probe initially appeared suitable for use in beach replenishment. However, subsurface samples analyzed by Casciano (US Army Corps of Engineers, 1978) concluded that the sand was highly stratified in terms of grain size and would ultimately be too fine for beach replenishment.

Sea Engineering (1993) conducted a beach nourishment viability study for the Hawaii Coastal Zone Management Program. The study synthesized all data taken on offshore sand resources around Oahu and scored each deposit based on site depth and wave exposure, interaction with adjacent littoral cells, deposit volume, and sediment grain size characteristics. Using these criteria it was concluded that the Kailua channel sand body was unsuitable for mining. The primary negative criteria were unsuitably fine grain sizes and the concern that reducing sediment volume in the channel posed a considerable risk to the stability of the immediate and adjacent littoral cells (Richmond, 2002).

Hampton et *al.* (2004) mapped sediment thickness in the Kailua sand channel using a tunable, swept-frequency (0.6 kHz to 3 kHz) acoustic profiler (see Barry et *al.* 1997 and Sea Engineering, 1993) supplemented by analysis of sediment recovered from 13 vibracores in 2000 and 14 vibracores in 1997. Thickness mapping in Kailua was performed in 60 -100 m of water. Sand deposits extend for about 4 km in an arc parallel to the Kailua reef front with a maximum thickness of 40 m, a mean thickness of 11 m, and is strongly skewed towards the smaller thickness. The total volume calculated for the deposit is 5.3×10^7 m^3 (6.9×10^7 yds^3). Grain size analysis of vibracored sediments revealed the sediment is finer than that which is usually used in beach replenishment. Compositional and abrasion analysis shows the sand has a low resistance to abrasion due to a high portion of *Halimeda* skeletal grains.

Conger et *al.* (in press) analyzes the surficial spatial distribution of benthic sand bodies across Oahu's insular shelf (to 20 m depth) at nine locations around Oahu, totaling 125 km^2 (39% of Oahu's shoreline). For each region, shallow benthic sand bodies are delineated, totaling 14,037 sand bodies for the study. Of the 125 km^2 of reef area studied 25 km^2 (~20%) was identified as sand, with a majority (64%) located in sand channels and fields. Sand bodies were classified in deposit shape classes by an automated classification algorithm accounting for a combination of individual shape characteristics such as area, orientation, and roundness. The resulting dataset of 14,037 sand body polygons was mapped to 2.4 m resolution, and each assigned a classification based on its shape.

A quantitative comparison of regional variations in sand bodies (number, shape, and size) to regional geomorphic setting (deep vs. wide reef) and wave climate (high,

medium, or low-energy) shows that the distribution of reef-top sediment is strongly influenced by reef geomorphology and, to a lesser extent, wave energy. Sand coverage is most extensive in two depth zones: <10 m depth zone (24% of total) and straddling the 10 m contour (72% of total). Conger et *al.* concludes that sand coverage is greatest in these regions because, the sub-10 m depth zone precludes the possibility of depressions being closed by modern reef growth due to high shear stress. Sand conduits crossing the 10 m depth contour provide both storage and transport between near and –offshore sand bodies. The 0-10 m depth range is also likely the zone of highest sediment production.

Reef types supporting the highest sand coverage are low wave-energy, have offshore sand bodies, and a wide shallow back reef. Least sand coverage is found in reefs with high wave-energy, no offshore sand bodies, and no wide shallow back reef. Study areas were categorized by sand coverage (highest to lowest): 1) Honolulu and Keehi Lagoon, 2) Lanikai and South of Laie Point, 3) Waianae, 4)Kailua, Kaneohe, Mokapu Point, and North of Laie Point. Lanikai is a medium-energy wide reef falling into the second highest category of sand coverage. Kailua is classified as a medium-energy deep reef falling into the lowest category of sand coverage.

Potential Effects of Sand Mining on Adjacent Beaches: The threat of increasing beach erosion through the mining of offshore sand bodies stems from the nature of a littoral cell as a naturally organized, interconnected, system of sand production, storage, and loss. An offshore sand body in Keauhou Bay, Hawaii was mined during 1977 as part of a two-month field test of a new sand mining and delivery system (Maragos et *al.*, 1977). A total of 10,000 m^3 of sand were mined from a sand body located 120 m offshore in 15 – 25 m of water. The sand body was 150 m wide by 300 m long and 6 m in thickness and surrounded by flourishing coral community. A detailed environmental survey was performed before, during, and after the mining operation, the results of which are presented in Maragos et *al.*, (1977). The study showed that mining sand had no immediate effect on nearby beaches at Kahaluu (1.5 km north) and Disappearing Sands (3.5 km north). It was noted that there exists no clear pathway between the sand deposit mined and either beach, suggesting that the mining of well-isolated and distant sand fields will not have an effect on nearby coastlines. Sea Engineering's 1993 sand resource viability study considered sand deposits offshore of a rocky shoreline and with low

proximity to a local beach littoral cell to be less hazardous mining objectives than deposits offshore of a sand beach near an active littoral sediment cell (Sea Engineering, 1993).

Moberly and Chamberlain (1964) state that sand channels potentially support circulation that delivers sand to adjacent beaches, seaward into deeper water, or a seasonal exchange between sand channels and the beach. Cacchione and Tate (1998) noted in a study of Kailua sand transport that fossil channels almost always connect to both nearshore and offshore sand fields and act as conduits for sand movement in both onshore and offshore directions. Cacchione and Tate showed sand ripples in the Kailua sand channel migrate shoreward at a rate of 0.5 m/day during trade wind conditions and seaward at a rate of 0.5 m/day during winter swell conditions. This is supported by common observations of sand ripples and well-sorted sediments fining in shoreward direction, both signs of active transport occurring between deep and shallow fields at the terminal ends of the channel. Special consideration should be taken with regard to removing sand from this type of sand body as sediment supply to a pre-existing shore face or littoral cell could be diminished (Cox, 1975; Dollar, 1979).

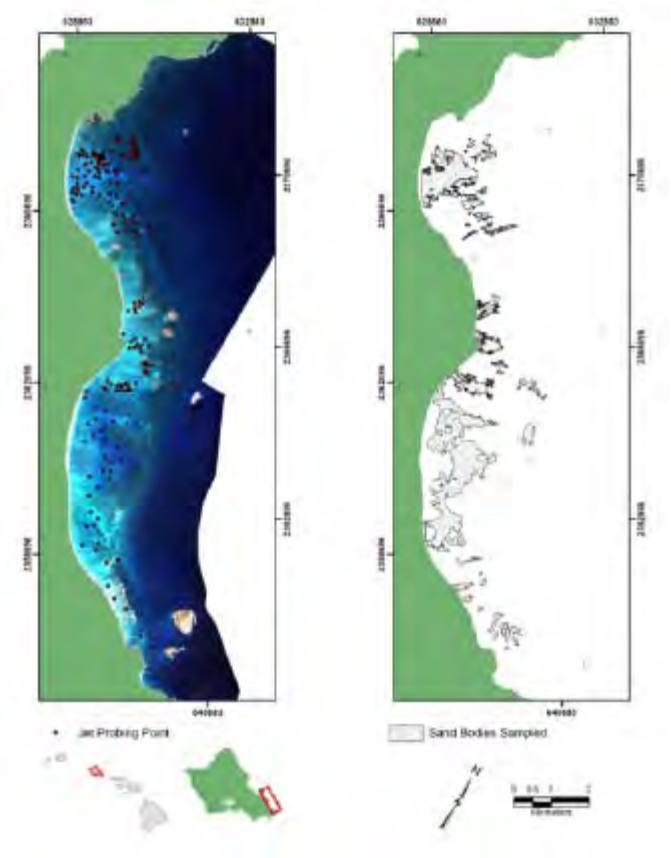

Figure 3. a) 205 jet probe measure were taken in the study area. b) 54 sand bodies are delineated for study.

MATERIALS AND METHODS

Boundaries of 54 sand bodies (Figure 3) in the study area were delineated for study using satellite imagery, LIDAR bathymetry, benthic slope maps (a product of LIDAR), NOAA benthic habitat maps, and sand classification maps produced by Conger et *al.*, 2005. Sand bodies were classified by morphology (Figure 4). Sampling with a jet probe (Figure 5) provided a total of 205 measurements of sand thickness. Thickness interpolation and griding of point data is accomplished using Kriging and Voronoi methods. Volumes estimates are calculated with for all sand bodies.

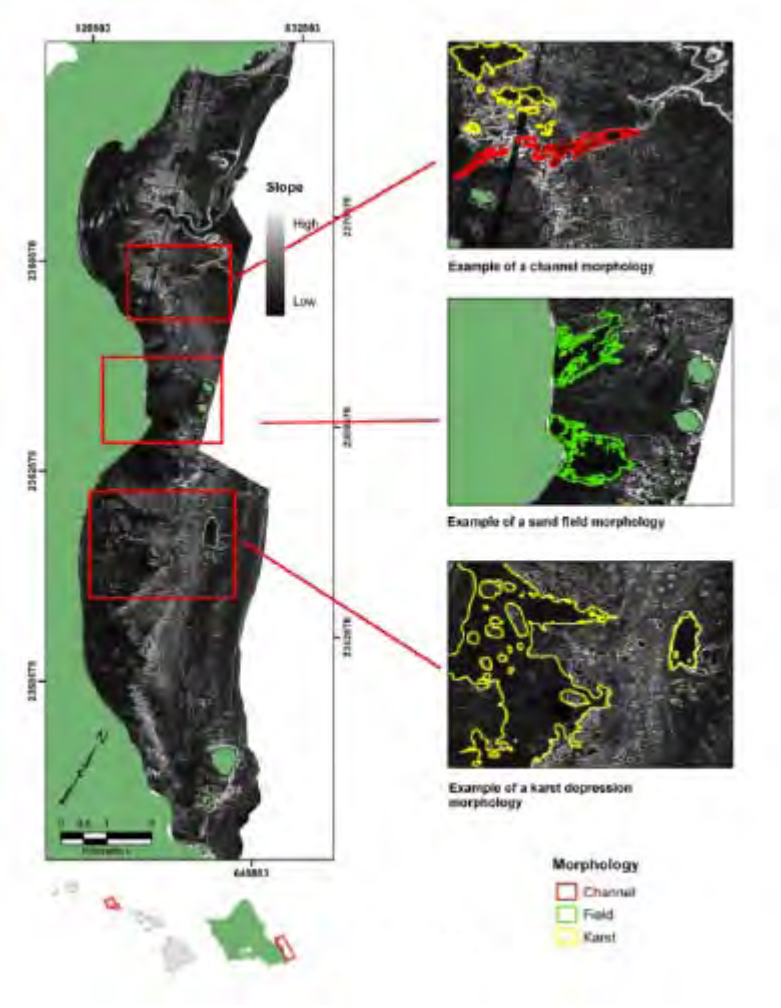

Figure 4. A slope map created from LIDAR bathymetry assists in classification of sand body morphology.

Morphology Classification:

Conger (2006) determined antecedent topography to be the primary control on morphology of reef top sand bodies. Karstification of the carbonate platform during periods of lower sea-level creates depressions which, once flooded, serve as basins that accumulate sand. Variations in relief, shape, and orientation of depressions are likely due to differing processes of karstification.

Following the work of Conger, a generalized morphology classification has been created for this study. Sand bodies sampled are classified as one of three morphologies: Sand Field, Fossil Channel, or Karst Depression. Variance in topographic relief, distribution of thickness, and generalized shape are used as major distinguishing factors used to classify sand body morphologies. Segregating sand bodies in this manner adds a

morphology component to the process of interpolating measured thicknesses and constructing a coverage map of estimated thickness, thereby increasing estimation confidence.

In addition to field observations, slope maps generated from LIDAR bathymetry were used to evaluate the topographic relief between the reef platform and the surface of the sand body. Figure 4 illustrates distinctions between morphologies by highlighting examples on a slope map of the study area. Table 1 summarizes sand body morphology classifications and location.

NUMBER of SAND BODIES	Fossil Channel	Karst Depression	Sand Field	Total
Kailua Bay	7	26	0	33
Lanikai	1	3	4	8
Waimanalo Bay	0	5	8	13
Total	8	34	12	54

Table 1. Number of sand bodies organized by morphology (columns) and region (rows).

Sand Fields: Sand fields are defined, in this study, as areas of continuous sand cover deposited over a broad topographic swale in the reef platform. Boundaries generally have little to no topographic relief and irregular borders. Sand fields are generally found near to shore in shallow (0 - 5.0 m) areas, have broad landward openings toward the beach face that separate and thin into separate fingers of sand that continue seaward and terminate on shallow reef locations. Of the 54 sampled sand bodies, a total of 13 were designated as sand fields.

Fossil Channel: Fossil channels are seaward extensions of watershed systems, incised into the carbonate shelf during low sea-level stands. The high topographic relief of the channel allows fossil channels to act as effective traps for littoral sediment. Channels in Kailua and Waimanalo are typically shore-normal in orientation and cross the –10 m isobath. Major channels, such as the Kailua sand channel, have steep walls of fossil reef and widen shoreward into large sand fields that lack significant bounding relief. Shoreward transition from bounding walls to a more gradual surface occurs in water shallower than 5 m, at which point sand is no longer confined to a channel and spreads

out into a sand field. Large sand channels can contain sediment over 9 m thick (Ocean Innovations, 1978) and remain thickest along the axis of the channel, thinning to 1.0 – 1.5 m at the margins and adjoining landward field. Of the 54 sampled sand bodies, a total of 7 were designated as fossil channels.

Karst Depression: Karst depressions are similar to fossil channels in that they are likely the result of subaerial exposure causing a sinkhole style karst incision. They differ from fossil channels in that they occupy smaller areas, have no dominant orientation, and do not serve as a connection between sand fields. Karst depressions have steep boundaries, generally dropping 1-3 m below the carbonate platform thus distinguishing them from sand fields. Of the 54 sampled sand bodies, a total of 34 were designated as karst depressions.

***Thickness Measurements*:** Sediment thickness measurements were obtained with a jet probe (Figure 5) deployed from a small boat, and operated by a researcher on SCUBA. The jet probe is built from a small diameter pipe connected to a shipboard water pump via fire hose. High-pressure water is pumped out of the pipe in order to displace sediment as the SCUBA diver pushes it into sandy substrate. The probe stops penetrating when it contacts a boundary with bedrock or an impenetrable layer of consolidated sediment. The depth of penetration provides a measure of unconsolidated sediment thickness. The probe length is 3.0 m. If the sand

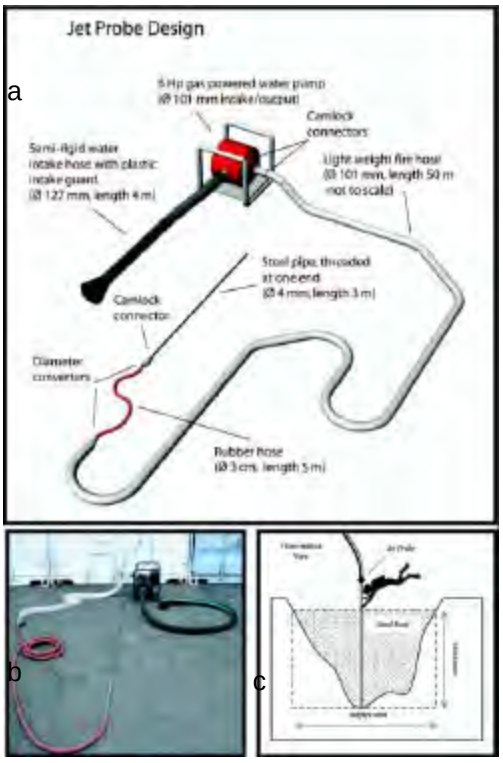

Figure 5. a) Jet probe schematic. b) Jet Probe. c) The jet probe is inserted into sand bodies until it ceases to penetrate. Thickness is measured in 10 cm increments off the probe.

body thickness exceeds 3.0 m, the value of 3.1 m is recorded. Appendix B contains tabulated jet probing results.

Sampling Locations: Using the jet probe, a total of 205 thickness measurements were obtained from 54 distinct sand bodies on the Kailua, Lanikai, and Waimanalo reef platforms. At each sample location 3 thickness measurements were taken within a 20 m radius of the anchored boat and the average thickness recorded for that site. Water depth at sample locations was recorded from a hull-mounted fathometer at an accuracy of +/- 0.5 m. Water depth varied from 1.5 m to 16.8 m, with an average of 5.2 m. General sediment characteristics were noted at each site. The probe was completely removed and inserted multiple times with each measurement to insure repeatable results. All sample locations were predetermined by examining aerial photos and bathymetry in conjunction with NOAA benthic habitat maps (Coyne et *al.*, 2002) and previous substrate studies in the region (Sea Engineering, 1997; Conger et *al.*, 2006). Survey points were located with a GPS receiver at an accuracy of +/- 5 m. Once anchored, drift of the boat was adjusted to match sample location so a diver could use the boat as a reference point for placing the jet probe. Figure 3 illustrates jet probe sample locations and sand body delineation.

Volume Calculations: Estimates of sand volume were obtained for each sand field by using one of two methodologies: 1) a Kriging method or 2) a Voronoi method with a volume correction factor. The selection of either methodology was based on the spatial density of available thickness measurements as well as the size and complexity of the given sand body. In instances of good data coverage a Kriging method was used. The Voronoi method was used for sand bodies with sparse coverage, where a single measurement must be representative of a large area, as it does not require a high data density. A total of 54 sand bodies are analyzed; Kriging was applied to a 9 sand bodies while the Voronoi model was applied the remaining 45 bodies. Table 2 summarizes sand body morphologies as applied to each methodology. Appendix C contains details on all volume estimations.

	MORHOLOGY			
METHOD	Channel	Field	Karst	Total

	Kriging	1	5	4	9
	Voronoi	6	8	30	45
	Total	7	13	34	54

Table 2. Summary of interpolation methods (column) applied to sand body morphologies classes.

Reporting of Volumes: In order to make volume estimates a more useful product, volume is not reported over the entire surface of every sand body sampled. In areas were the Kriging method could be used, volume was only calculated for the areas of greatest thickness (> 0.50 m). Similarly, volume results are given in a section-by-section basis for sand bodies using the Voronoi method. In many cases a single sand body, identified by a Sand Body ID, is broken into multiple sections, each reported as an Area ID. Volumes are reported for each Area ID individually. Table 3 summarizes volume estimations by region and Table 4 summarizes measured area of sand bodies. A series of maps and tables detailing thickness and volume estimations are included in Appendix A.

VOLUME (m^3)	Channel	Error	Karst	Error	Field	Error	Total	Error
Kailua Bay	825,115	75,056	150,715	15,244	0	0	975,830	90,300
Lanikai	23,616	5,432	43,703	9,719	129,987	3,089	197,306	18,240
Waimanalo Bay	0	0	504,396	47,999	20,136	1,660	524,532	49,659
Total	848,731	80,488	698,814	72,962	150,123	4,749	1,697,668	158,199

Table 3. Volume estimates with error in cubic meters presented as morphology class (column) and region (row).

AREA (m^2)	Fossil Channel	Karst Depression	Sand Field	Total
Kailua Bay	668,701	290,399	0	959,100
Lanikai	67,923	169,469	1,148,858	1,386,251
Waimanalo Bay	0	653,341	235,144	888,485
Total	736,624	1,113,209	1,384,002	3,233,836

Table 4. Sand body surface area presented as morphology class (column) and region (row).

***Kriging Method*:** The Kriging approach is a more statically robust method of estimation than the Voronoi method and was preferentially used whenever data density was suitable. Boundaries of sand bodies are assumed to be zero thickness and were represented by

points of zero thickness generated at 1 m spacing around each sand body. Modeling the variation between measurement points and the edges was accomplished with a semi-variogram. A semi-variogram model quantifies the relationship between variability of a native dataset and spatial location as an equation for a line. The equation for each semi-variogram model is used to model the rate of change between points where thickness is known, i.e. jet probe thickness measurements and edges (Webster and Oliver, 2001). In this usage, the changing slope of the semi-variogram line is analogous to the changing slope of the reef-top depression.

A separate variogram equation was produced for each sand body so that the thickness model would be individualized to the unique characteristics of each body. A spherical semi-variogram model was used in all cases. Points of zero thickness along the edge were included when producing semi-variogram. Rasterized thickness estimation maps were created at a resolution of 1 m. Volume calculations were made for areas of sediments estimated to be >0.50 m thick, each reported as a separate Area ID. Thickness and volume calculation results are presented in Appendix A.

Voronoi Method: The Voronoi method assumes that sand body thickness is perfectly uniform up to the edge of the sand body. See Figure 5 for an illustration of the method. This method is used when thickness data is too sparse for a Kriging approach to be useful. Perimeters of each sand body and thickness measurements were mapped and entered into ArcGIS. An ArcGIS Voronoi function was used to subset each sand body into series of smaller adjoining polygons or sub-polygons; each sub-polygon formed around a single thickness measurement. The Voronoi function draws sub-polygon boundaries so that any location within a given sub-polygon is closer to its associated measurement point than to the measurement point of any other sub-polygon (Webster and Oliver, 2001).

The sediment thickness within each sub-polygon is assumed to be the same as the thickness measurement it contains. Volume of sediment is calculated for each sub-polygon as the product of the area and thickness. The volumes for all sub-polygons within a single sand body are summed to calculate a total sediment volume for the entire sand field (see Appendix C). Afterwards, a correction is applied to account for over-

estimation of volume. Sub-polygons created by this process form the boundaries for the individual Area ID's.

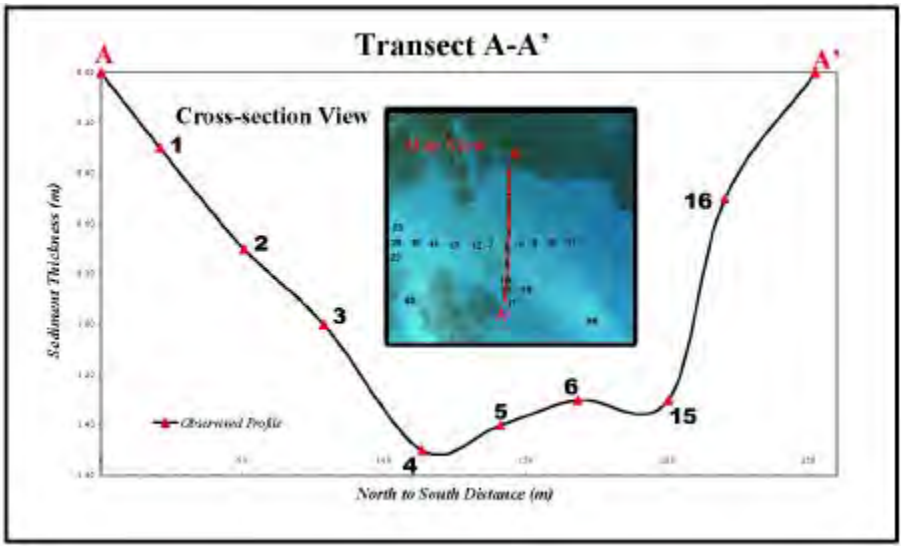

Figure 6. Kailua Bay. Thickness profile generated from a transect of point measurements. Note the thickness irregularity in sand bodies.

Voronoi Volume Correction: A major source of uncertainty with the Voronoi model is the assumption that the walls of reef top depressions are at right angles to the base of the depression. A transect of thickness measurements (transect A-A' in Figure 6) from Kailua Bay suggests that sand bodies are thickest in the center and gradually thin toward the edges.

Given the high range of variability in sand body thickness, failing to account for sand body morphology likely produces an over-estimate of sand volume. Correction of over-estimated sand volumes is accomplished by calculating an empirically derived reduction factor. Reduction factors are calculated as the average percent difference between Kriging and Voronoi estimations performed on the same set of sand bodies. Results from comparative volume estimations of 10 sand bodies are segregated by sand body morphology and averaged so as to calculate reduction factors that are morphology specific.

Of the 10 bodies used, 4 were classified as sand fields, while the remaining 6 were classified as karst fields. No bodies classified as channel morphology were used due to a lack of adequate examples, however the assumption is made that channel and karst morphologies share similar aspects of genesis, possess similar subsurface-

topography, and thus can utilize the same reduction factor. The reduction factor calculated for sand field morphologies is 88.25% ±8.25% (i.e. Voronoi estimations are reduced by 88.25% ±8.25%), while 64.67% ±23% is used for karst and channel morphologies. Uncertainty calculation is described below, in the section *Prediction Uncertainty.* These reduction factors cause dramatic decreases when applied to the Voronoi-based volume estimates, but provide a more informed and realistic estimate.

Prediction Uncertainty: Measurement uncertainties are ±5 cm vertical uncertainty associated with jet probe measurement and ±5 m of horizontal uncertainty associated with accuracy of the GPS receiver. These uncertainties are taken into account during the Kriging process as a nugget variable and thus are propagated through the interpolation process as a pixel-by-pixel error value. Therefore, every map of estimated volume created via Kriging also has a map of the pixel-by-pixel estimation uncertainty in meters. Areas defined for volume estimations are used with error maps to calculate the error in volume estimation for each area.

Percent difference between estimated volume and estimated error was calculated for each sand body. These percent differences were averaged simultaneously with values used for calculating the reduction factors, resulting in the uncertainty values reported for Voronoi estimates. The error results are presented as tables in the maps of estimated sediment volumes (Appendix A).

RESULTS AND DISCUSSION

Fossil Channel: Of the 54 sampled sand bodies, 8 were classified as fossil channels. Fossil channels are estimated to contain 848,731 +/-80,488 m^3 of sediment and cover an area of 736,624 m^2. The average volume-to-surface area ratio is 1.15 m^3/m^2, the highest ratio in the study area. Most sediment in this morphology class is contributed by the Kailua sand channel, of which only the shoreward section is being considered in this study. Previous jet probe studies in the deeper channel have shown sediment thickness to exceed 3.0 m. In southern Kailua, a group of smaller channels form the fragmented

remnants of what is most likely a channel closed by reef growth. Another smaller intact channel exists in Lanikai, but does not connect with a significant shoreward sand body.

Defining a specific morphology for the shoreward end of the Kailua sand channel is difficult as the channel widens landward, losses the high bounding topographic relief, and transitions into sand field type morphology. However, a linear trace of high thickness continues landward through the sand field along the central axis of the channel. This indicates that the shoreward portion of the channel has been filled and overtopped by sand, producing a sand body that qualifies as both a channel and a field. For the purpose of estimating sand volume the Kailua sand channel is considered a member of channel morphology class.

Sand deposits in fossil channels tend to be consistently thick and yellow to white coloration. Surface sediments in these channels appear medium- to coarse-grained, however subsurface sampling in the Kailua channel has shown significant amounts of fine-grained sediment (US Army Corps of Engineers, 1978). Channels likely serve as surge channels for waves breaking over the fringing reef. The focusing of wave energy through these channels would cause preferential grain sorting as grains transported, leaving a varied stratigraphy of fine and coarse sediments related to variations in transport energy.

Sand Field: Of the 54 sampled sand bodies, 12 were classified as sand fields. Sand fields are estimated to contain 150,123 +/-4,749 m^3 of sediment and cover an area of 1,384,002 m^2. The average volume-to-surface area ratio is 0.11 m^3/m^2, the lowest ratio in the study area.

Sediment thickness tends to grade from 0.5 m near to shore thickening to over 3.0 m near the seaward edge. Sediments are fine to medium sand with a mixture of sandy and gravelly substrata. Nearshore sand fields are generally connected to the adjacent beach where they potentially function as sediment storage and source locales participating is volume fluctuations on the beach.

Karst Depressions: Of the 54 sampled sand bodies, 34 are classified as karst depressions. Karst depressions are estimated to contain 695,814 +/-47,999 m^3 of sediment and cover

an area of 1,113,209 m^2. The average volume-to-surface area ratio is 0.63 m^3/m^2, the mid-range ratio in the study area.

Sediments in karst depressions are observed to contain one or both of two characteristic strata: 1) medium to coarse light-colored sand and 2) coral gravel varying between 5 cm fragments to hand-sized branches. Sediment bodies in karst depressions consist of either 1.0 – 2.0 m thick sand, 0.5 – 1.0 m sand overlaying coral rubble, or an absence of sand with coral rubble outcropping on the surface. Coral rubble deposits were not included in thickness and volume analysis. Sandy bodies without coral rubble tend to lie directly on fossilized reef platform.

Coral accretion on the perimeter of karst depressions suggests Holocene growth has shrunk the area of many depressions, possibly isolating one large depression into a number of smaller depressions. Sediment produced on the reef is thought to be transported to the beach in a series of steps between depressions (Moberly and Chamberlain, 1964) making karst depressions a potentially important component of shallow (3.0 – 5.0 m depth) sediment storage in the littoral system.

An expansive system of interconnected, sand-filled karst depressions dominates the topography of the central-south Waimanalo area. This feature resembles a sandy lagoon in that it runs shore-parallel between a fringing reef and outcropping back reef in 4-7 m of water. Sediment thickness is greatest in two isolated semi-circular areas. The lack of any linear zones of thickness exclude this feature from consideration as a channel feature.

CONCLUSIONS

Jet probing of shallow sand bodies allows volume estimates to be made for a total of 54 sand bodies. Sand channels appear to have the greatest overall volume-to surface area ratio (1.15 m^3/m^2), however if data from the Kailua sand channel is excluded, the ratio drops to 0.29 m^3/m^2, indicating that the volume of sediment infilling channels in the study area varies greatly. Most sand channels in the study area lack the size, continuality, and terminal sand fields of the Kailua sand channel. Absence of a major terminal sand body attached to either end of the smaller channels most likely indicates a lack of active transport, which could account for low volume relative to the larger Kailua sand channel.

Karst depressions have a volume-to surface area ratio of 0.63 m^3/m^2 and lack major anomalies such as the Kailua sand channel. The relative abundance of karst depressions in the study area suggests that karst depressions play a major role in reef-top sand storage. Sand fields have the lowest volume-to-surface area ratio (0.11 m^3/m^2). Given that a lack of significant confining topographic relief is the differentiating feature for sand fields, it is likely that topography is the foremost control in reef-top sand storage.

APPENDICES

A. Maps of Sediment Thickness and Volume Estimates

B. Tabulated Jet Probing Results

C. Tabulated Sediment Thickness and Volume Estimates

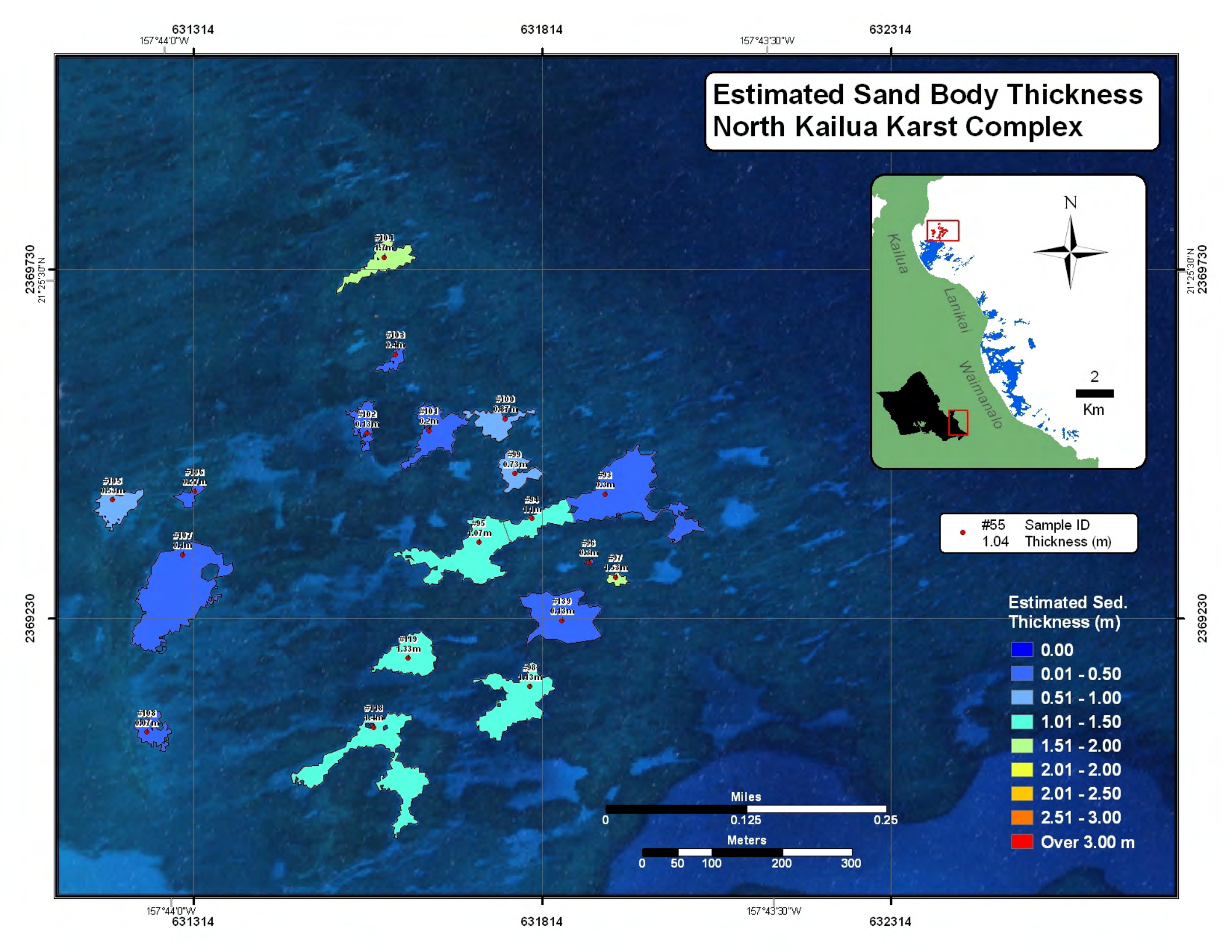
Estimated Sand Body Thickness
North Kailua Karst Complex
631314
631814
632314
157°44'0"W
157°43'30"W
2369730
2369230
21°25'30"N
N
Kailua
Lanikai
Waimanalo
2
Km
#55 Sample ID
1.04 Thickness (m)
Estimated Sed. Thickness (m)
0.00
0.01 - 0.50
0.51 - 1.00
1.01 - 1.50
1.51 - 2.00
2.01 - 2.00
2.01 - 2.50
2.51 - 3.00
Over 3.00 m
Miles
0 0.125 0.25
Meters
0 50 100 200 300

Estimated Sediment Volume
North Kailua Karst Complex

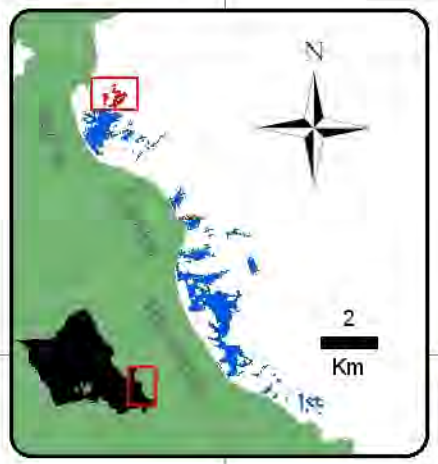

Area ID	Area m^2	Volume m^3	Error m^3	Vol/Area m^3/m^2	Method
4	2,602	1,716	± 395	0.66	Voronoi
5	710	110	± 25	0.15	Voronoi
6	1,996	674	± 155	0.34	Voronoi
7	1,450	73	± 17	0.05	Voronoi
8	3,483	270	± 62	0.08	Voronoi
9	1,917	543	± 125	0.28	Voronoi
10	653	68	± 16	0.10	Voronoi
11	2,141	440	± 101	0.21	Voronoi
12	2,597	1,108	± 255	0.43	Voronoi
13	9,328	1,086	± 250	0.12	Voronoi
14	79	9	± 2	0.11	Voronoi
15	7,123	2,957	± 680	0.42	Voronoi
16	399	237	± 55	0.59	Voronoi
17	6,206	313	± 72	0.05	Voronoi
18	11,958	464	± 107	0.04	Voronoi
19	3,575	1,845	± 424	0.52	Voronoi
20	6,003	2,632	± 605	0.44	Voronoi
21	1,601	43	± 10	0.03	Voronoi
22	8,221	4,466	± 1027	0.54	Voronoi

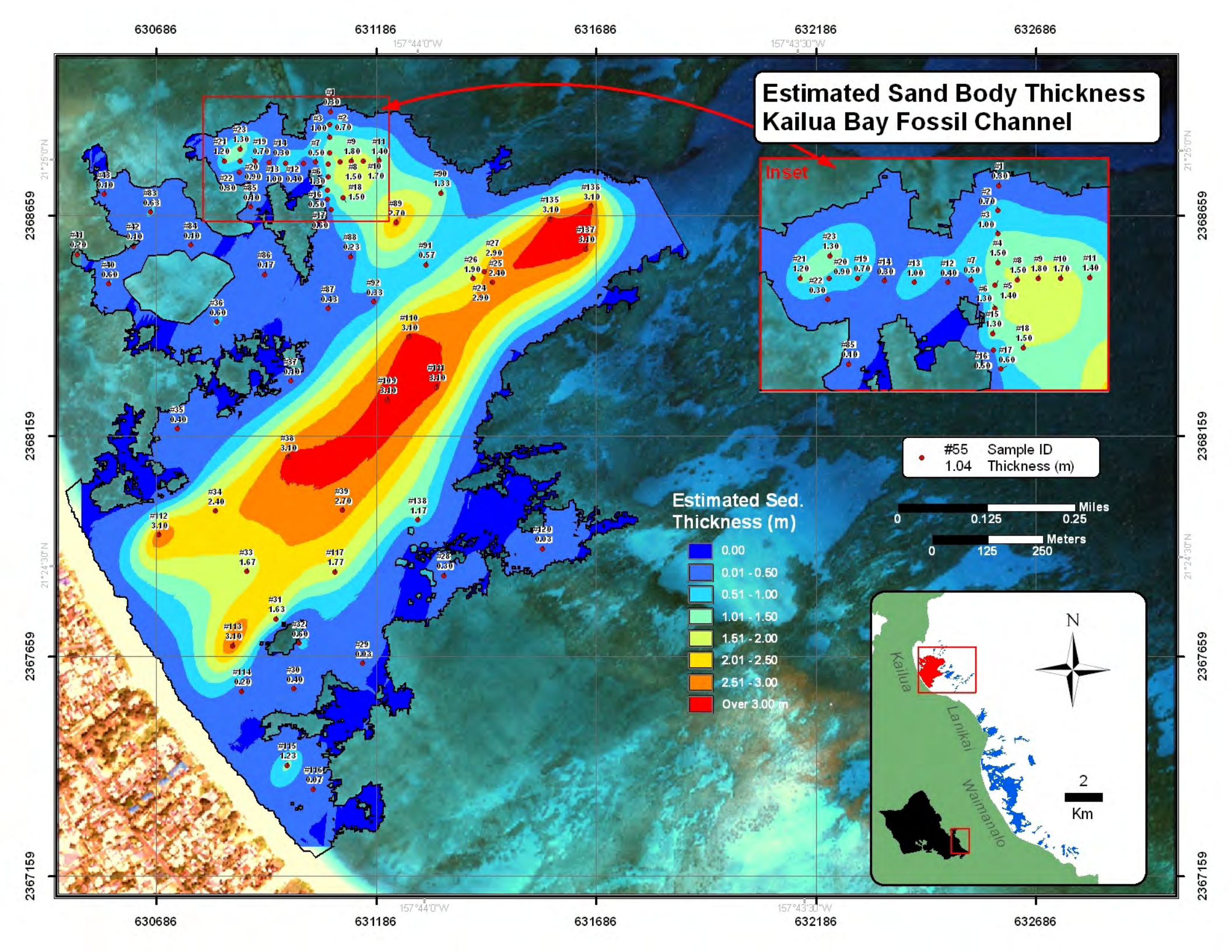
Estimated Sand Body Thickness
Kailua Bay Fossil Channel
Inset
630686
631186
631686
632186
632686
157°44'0"W
157°43'30"W
21°25'0"N
21°24'30"N
2368659
2368159
2367659
2367159
#55 Sample ID
1.04 Thickness (m)
Estimated Sed. Thickness (m)
0.00
0.01 - 0.50
0.51 - 1.00
1.01 - 1.50
1.51 - 2.00
2.01 - 2.50
2.51 - 3.00
Over 3.00 m
Miles
0 0.125 0.25
Meters
0 125 250
N
Kailua
Lanikai
Waimanalo
2
Km

Estimated Sediment Volume
Kailua Bay Fossil Channel

Area ID	Area m^2	Volume m^3	Error m^3	Vol/Area m^3/m^2	Method
1	586,831	801,695	+/- 70,484	1.37	Kriging
2	7,394	2,513	+/- 455	0.34	Kriging
3	4,572	1,027	+/- 350	0.22	Kriging

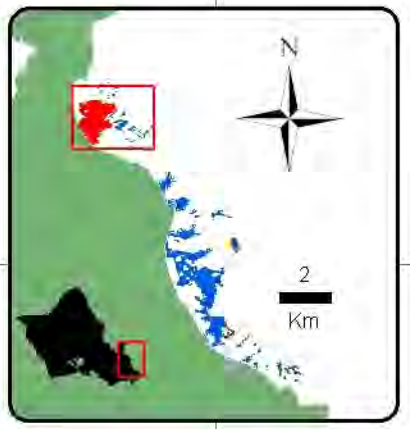

Estimated Sediment Volume (m^3)

- 0 - 1,000
- 1,001 - 10,000
- 10,001 - 30,000
- 30,001 - 50,000
- 50,001 - 100,000
- 100,001 - 200,000
- 200,001 - 500,000
- 500,001 - 900,000

Meters: 0 50 100 200 300 400 500

Miles: 0 0.125 0.25

630686 631186 631686 632186 632686

157°44'0"W 157°43'30"W

21°25'0"N 21°24'30"N

2368659 2368159 2367659 2367159

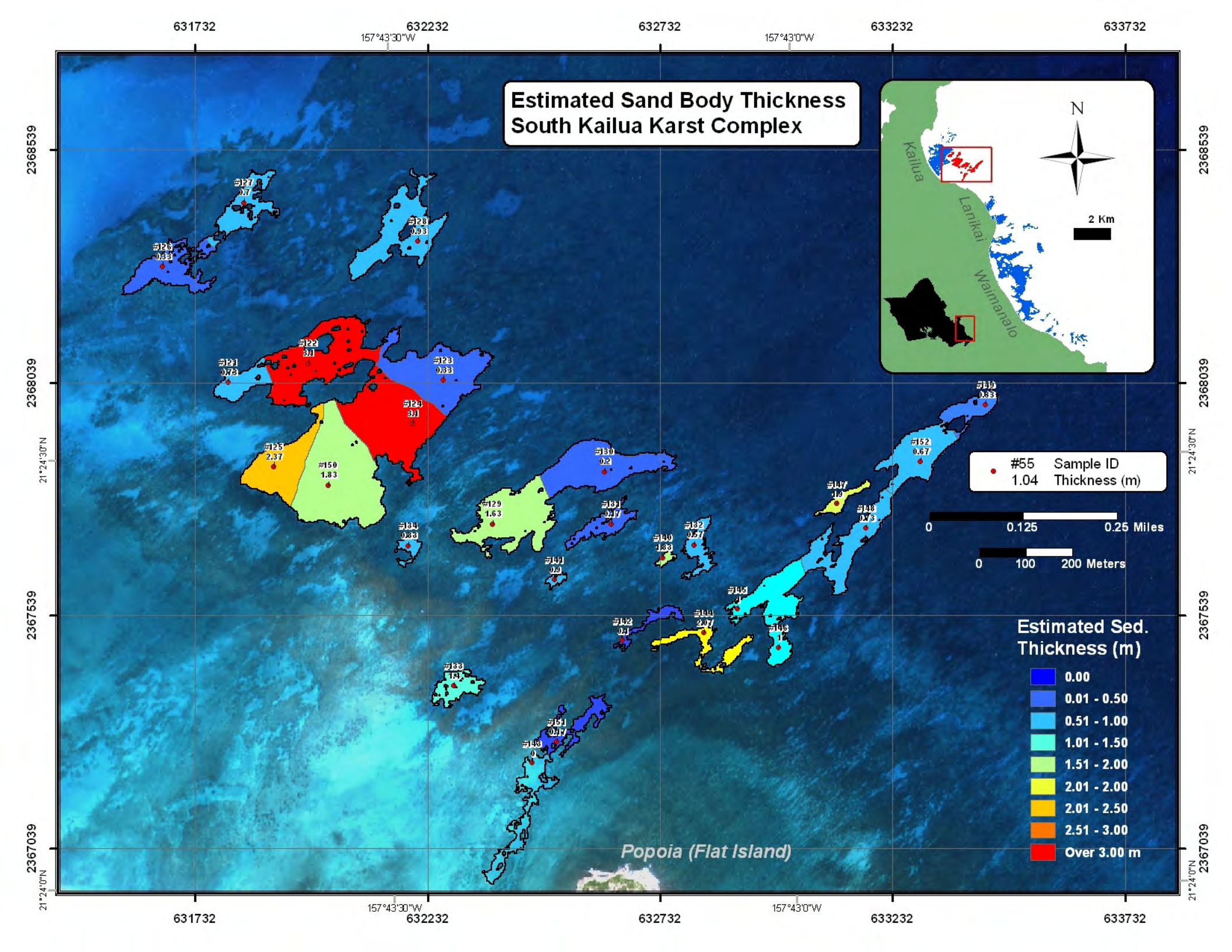
Estimated Sand Body Thickness
South Kailua Karst Complex
631732
632232
632732
633232
633732
157°43'30"W
157°43'0"W
2368539
2368039
2367539
2367039
21°24'30"N
21°24'0"N
N
Kailua
Lanikai
Waimanalo
2 Km
#55 Sample ID
1.04 Thickness (m)
0 0.125 0.25 Miles
0 100 200 Meters
Estimated Sed. Thickness (m)
0.00
0.01 - 0.50
0.51 - 1.00
1.01 - 1.50
1.51 - 2.00
2.01 - 2.00
2.01 - 2.50
2.51 - 3.00
Over 3.00 m
Popoia (Flat Island)

Estimated Sediment Volume
South Kailua Karst Complex

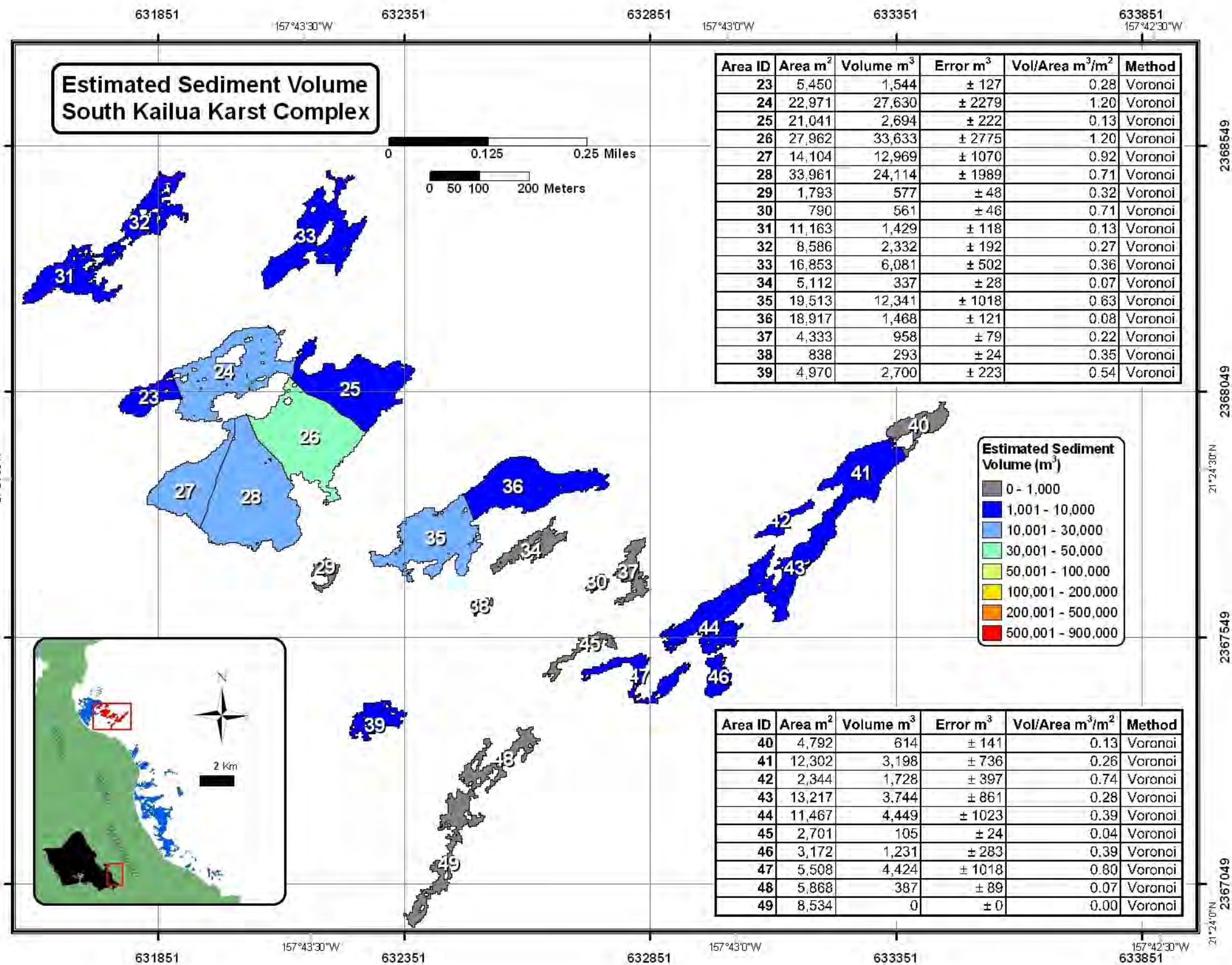

Area ID	Area m²	Volume m³	Error m³	Vol/Area m³/m²	Method
23	5,450	1,544	± 127	0.28	Voronoi
24	22,971	27,630	± 2279	1.20	Voronoi
25	21,041	2,694	± 222	0.13	Voronoi
26	27,962	33,633	± 2775	1.20	Voronoi
27	14,104	12,969	± 1070	0.92	Voronoi
28	33,961	24,114	± 1989	0.71	Voronoi
29	1,793	577	± 48	0.32	Voronoi
30	790	561	± 46	0.71	Voronoi
31	11,163	1,429	± 118	0.13	Voronoi
32	8,586	2,332	± 192	0.27	Voronoi
33	16,853	6,081	± 502	0.36	Voronoi
34	5,112	337	± 28	0.07	Voronoi
35	19,513	12,341	± 1018	0.63	Voronoi
36	18,917	1,468	± 121	0.08	Voronoi
37	4,333	958	± 79	0.22	Voronoi
38	838	293	± 24	0.35	Voronoi
39	4,970	2,700	± 223	0.54	Voronoi

Area ID	Area m²	Volume m³	Error m³	Vol/Area m³/m²	Method
40	4,792	614	± 141	0.13	Voronoi
41	12,302	3,198	± 736	0.26	Voronoi
42	2,344	1,728	± 397	0.74	Voronoi
43	13,217	3,744	± 861	0.28	Voronoi
44	11,467	4,449	± 1023	0.39	Voronoi
45	2,701	105	± 24	0.04	Voronoi
46	3,172	1,231	± 283	0.39	Voronoi
47	5,508	4,424	± 1018	0.80	Voronoi
48	5,868	387	± 89	0.07	Voronoi
49	8,534	0	± 0	0.00	Voronoi

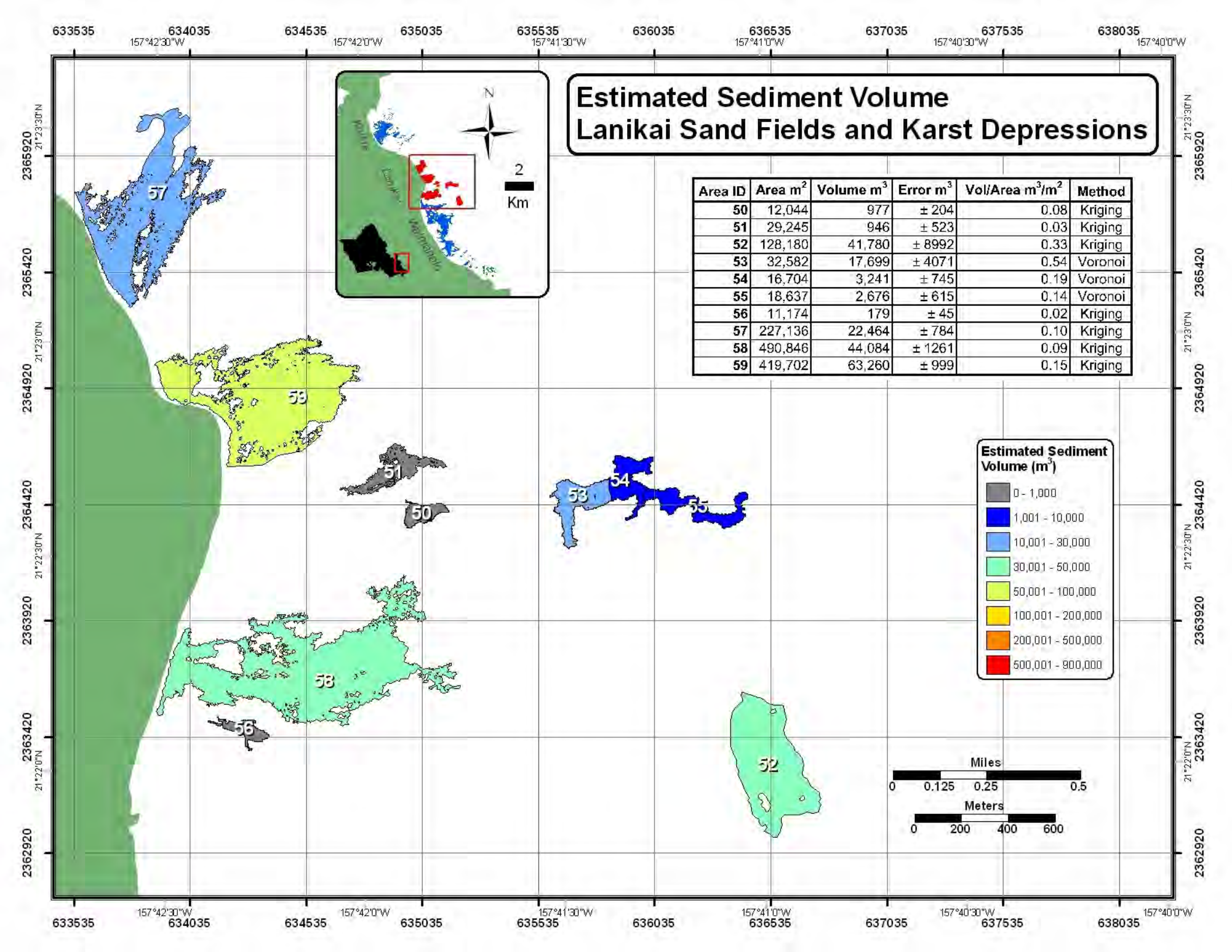

Area ID	Area m^2	Volume m^3	Error m^3	Vol/Area m^3/m^2	Method
50	12,044	977	± 204	0.08	Kriging
51	29,245	946	± 523	0.03	Kriging
52	128,180	41,780	± 8992	0.33	Kriging
53	32,582	17,699	± 4071	0.54	Voronoi
54	16,704	3,241	± 745	0.19	Voronoi
55	18,637	2,676	± 615	0.14	Voronoi
56	11,174	179	± 45	0.02	Kriging
57	227,136	22,464	± 784	0.10	Kriging
58	490,846	44,084	± 1261	0.09	Kriging
59	419,702	63,260	± 999	0.15	Kriging

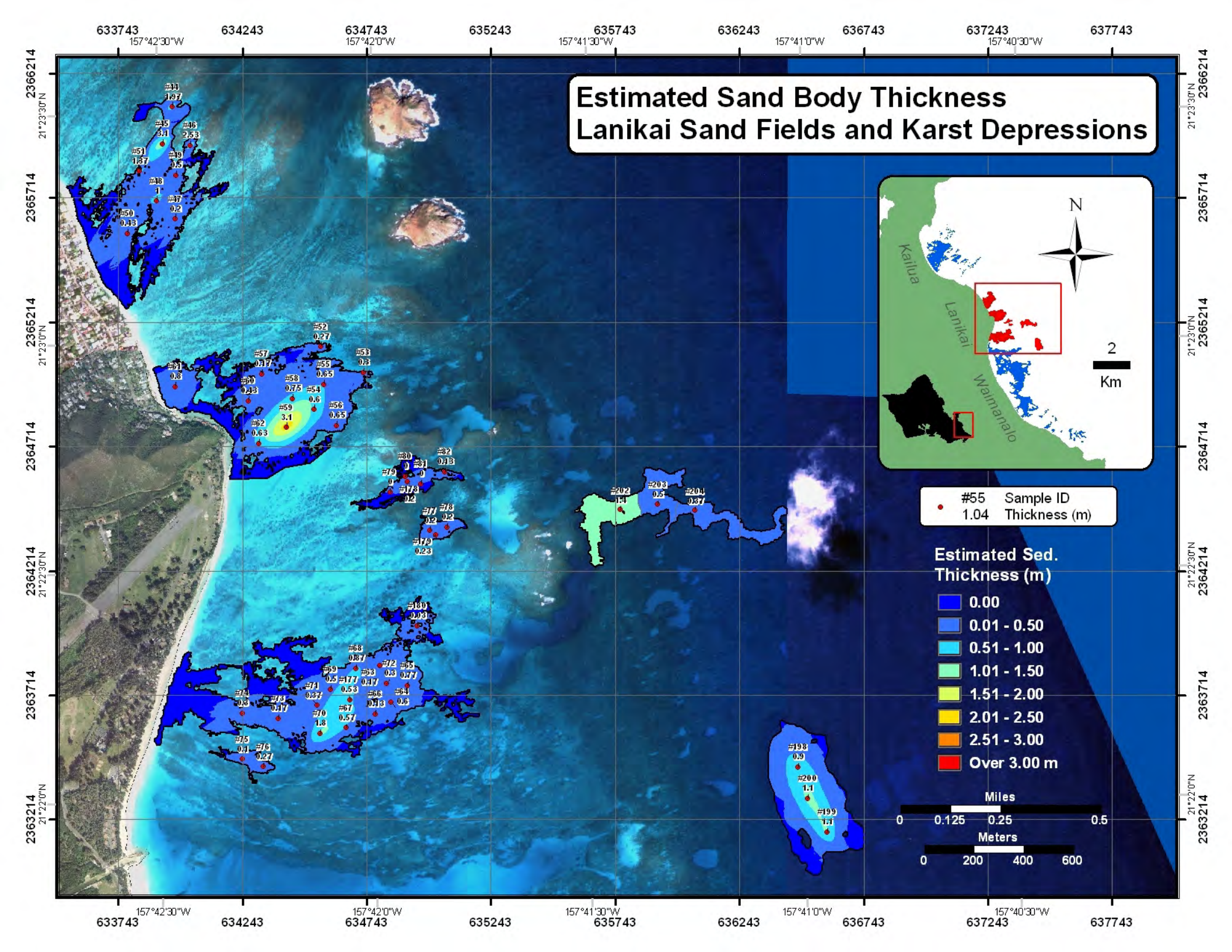
Estimated Sand Body Thickness
Lanikai Sand Fields and Karst Depressions
633743
634243
634743
635243
635743
636243
636743
637243
637743
157°42'30"W
157°42'0"W
157°41'30"W
157°41'0"W
157°40'30"W
2366214
2365714
2365214
2364714
2364214
2363714
2363214
21°23'30"N
21°23'0"N
21°22'30"N
21°22'0"N
N
Kailua
Lanikai
Waimanalo
2
Km
#55 Sample ID
1.04 Thickness (m)
Estimated Sed. Thickness (m)
0.00
0.01 - 0.50
0.51 - 1.00
1.01 - 1.50
1.51 - 2.00
2.01 - 2.50
2.51 - 3.00
Over 3.00 m
Miles
0 0.125 0.25 0.5
Meters
0 200 400 600

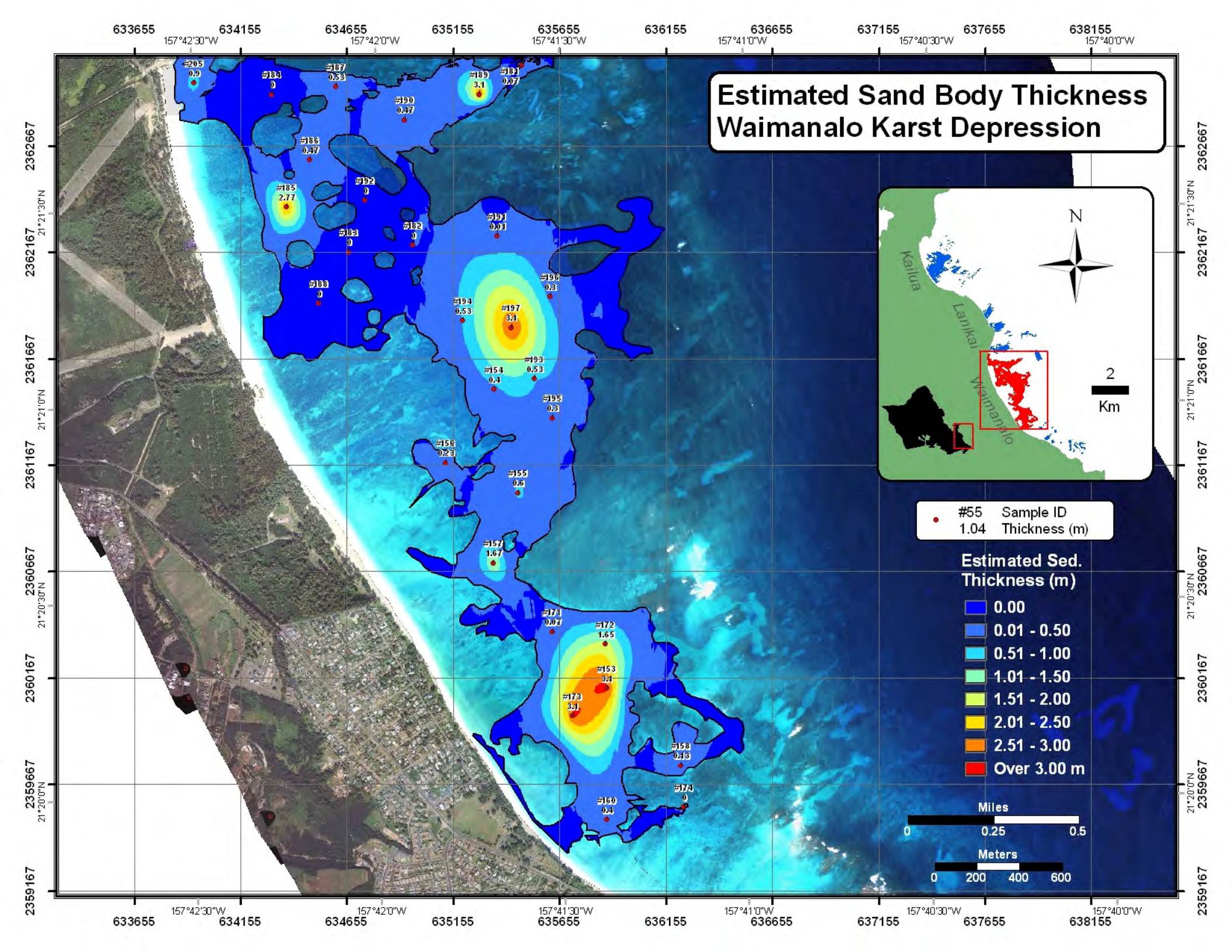
Estimated Sand Body Thickness
Waimanalo Karst Depression
633655
634155
634655
635155
635655
636155
636655
637155
637655
638155
157°42'30"W
157°42'0"W
157°41'30"W
157°41'0"W
157°40'30"W
157°40'0"W
2362667
2362167
2361667
2361167
2360667
2360167
2359667
2359167
21°21'30"N
21°21'0"N
21°20'30"N
21°20'0"N
#205 0.9
#184 0
#187 0.53
#189 3.1
#181 0.07
#190 0.47
#186 0.47
#185 2.77
#192 0
#191 0.01
#183 0
#182 0
#188 0
#196 0.3
#194 0.53
#197 3.1
#193 0.53
#154 0.4
#195 0.3
#156 0.23
#155 0.6
#157 1.67
#171 0.07
#172 1.65
#153 3.1
#173 3.1
#158 0.43
#174 0
#160 0.4
N
Kailua
Lanikai
Waimanalo
2
Km
#55 Sample ID
1.04 Thickness (m)
Estimated Sed. Thickness (m)
0.00
0.01 - 0.50
0.51 - 1.00
1.01 - 1.50
1.51 - 2.00
2.01 - 2.50
2.51 - 3.00
Over 3.00 m
Miles
0 0.25 0.5
Meters
0 200 400 600

Estimated Sediment Volume
Waimanalo Karst Depression

Area ID	Area m^2	Volume m^3	Error m^2	Vol/Area m^3/m^2	Method
73	221,114	243,220	± 15266	1.10	Kriging
74	17,195	5,860	± 802	0.34	Kriging
75	240,583	173,502	± 18808	0.72	Kriging
76	37,555	23,946	± 1957	0.64	Kriging
77	21,496	13,672	± 1000	0.64	Kriging

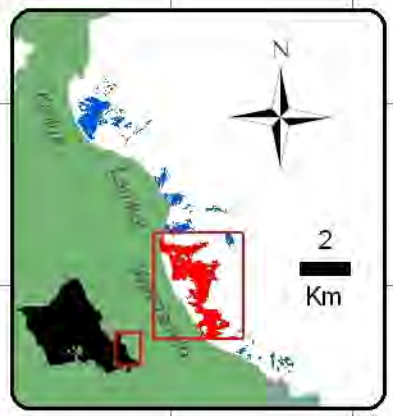

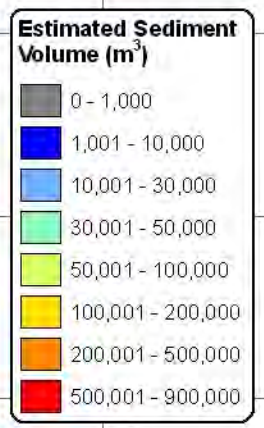

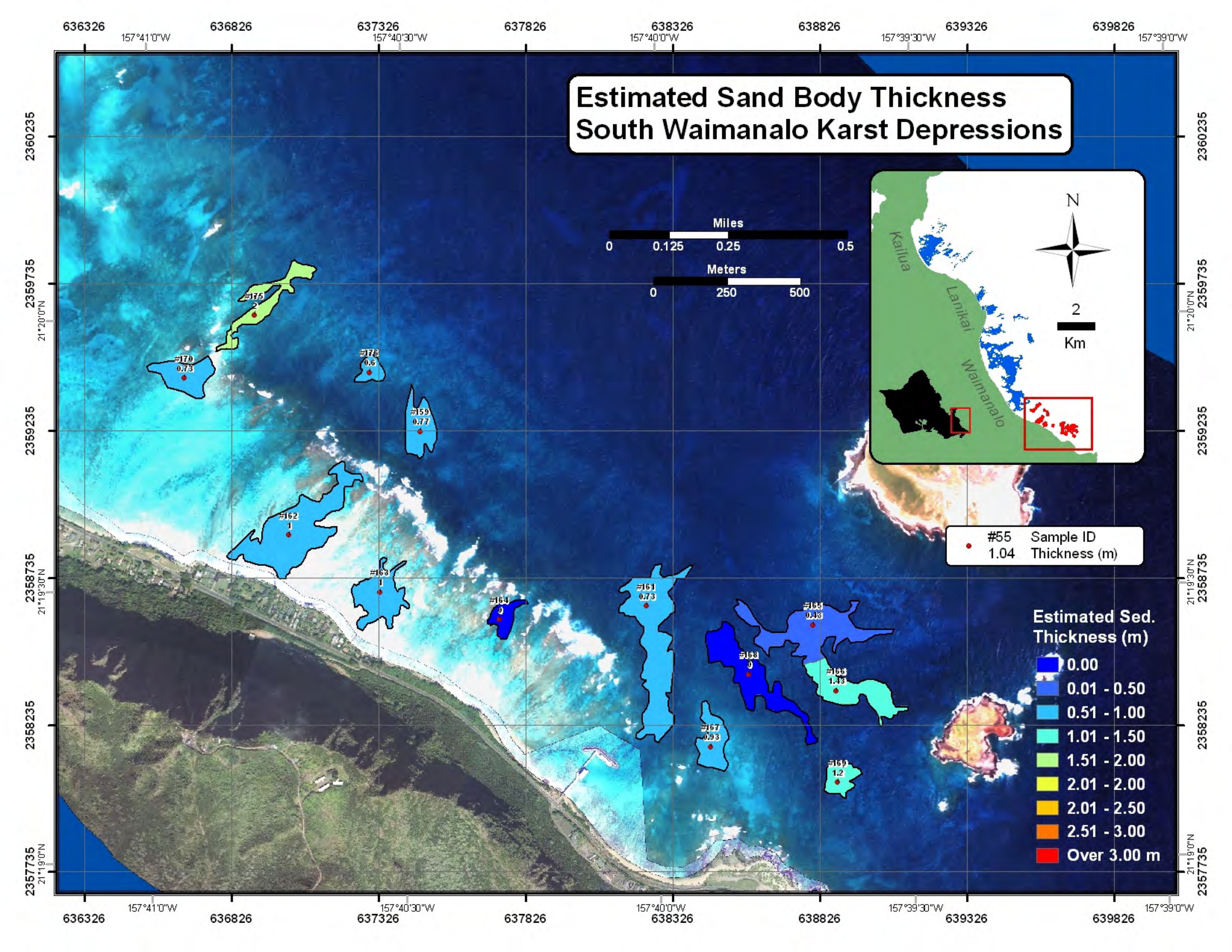
Estimated Sand Body Thickness
South Waimanalo Karst Depressions
636326
636826
637326
637826
638326
638826
639326
639826
157°41'0"W
157°40'30"W
157°40'0"W
157°39'30"W
157°39'0"W
2360235
2359735
2359235
2358735
2358235
2357735
21°20'0"N
21°19'30"N
21°19'0"N
Miles
0
0.125
0.25
0.5
Meters
0
250
500
N
2
Km
Kailua
Lanikai
Waimanalo
#55 Sample ID
1.04 Thickness (m)
Estimated Sed. Thickness (m)
0.00
0.01 - 0.50
0.51 - 1.00
1.01 - 1.50
1.51 - 2.00
2.01 - 2.00
2.01 - 2.50
2.51 - 3.00
Over 3.00 m
#175
2
#170
0.73
#176
0.6
#159
0.77
#162
1
#163
1
#164
0
#161
0.73
#165
0.43
#168
0
#166
1.43
#167
0.93
#169
1.2

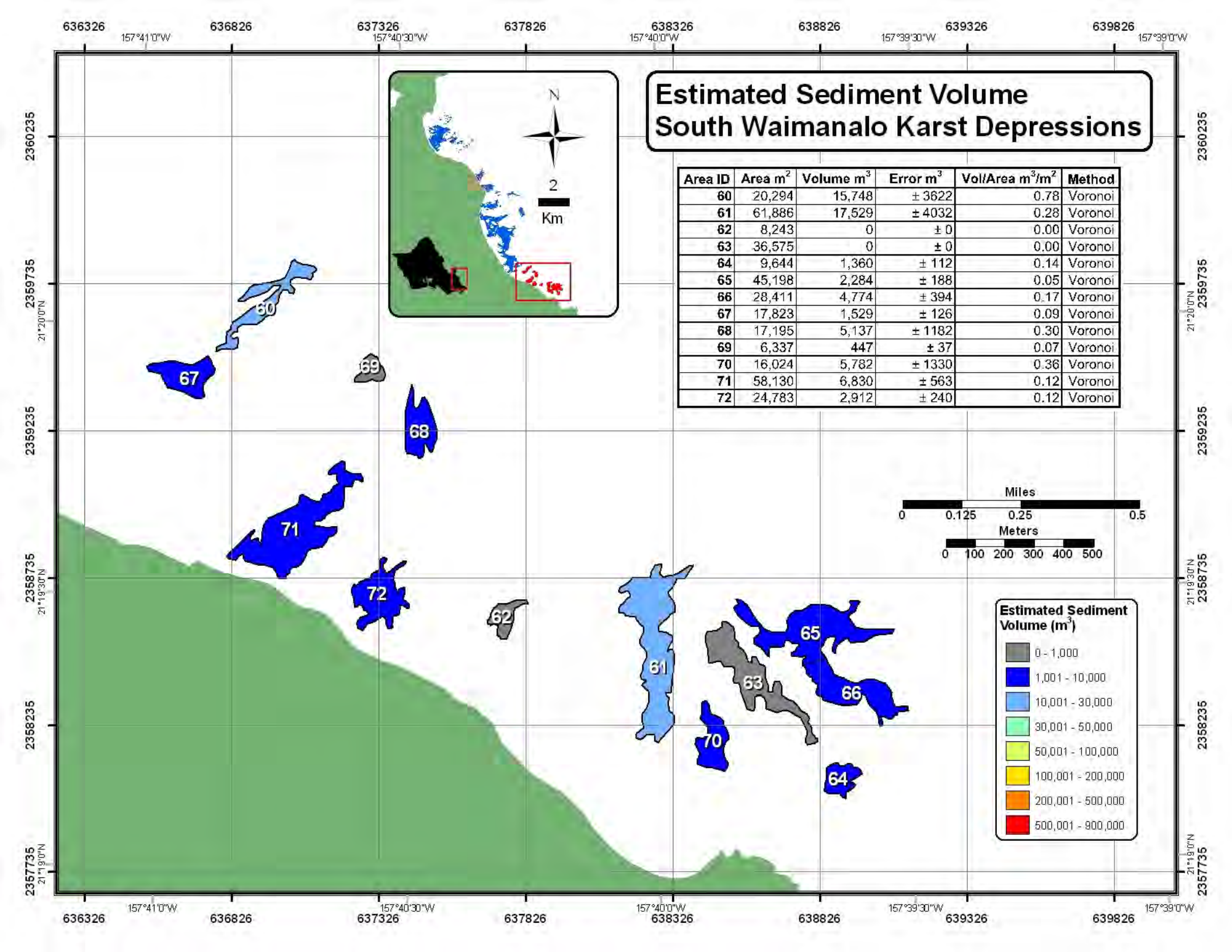

Area ID	Area m^2	Volume m^3	Error m^3	Vol/Area m^3/m^2	Method
60	20,294	15,748	± 3622	0.78	Voronoi
61	61,886	17,529	± 4032	0.28	Voronoi
62	8,243	0	± 0	0.00	Voronoi
63	36,575	0	± 0	0.00	Voronoi
64	9,644	1,360	± 112	0.14	Voronoi
65	45,198	2,284	± 188	0.05	Voronoi
66	28,411	4,774	± 394	0.17	Voronoi
67	17,823	1,529	± 126	0.09	Voronoi
68	17,195	5,137	± 1182	0.30	Voronoi
69	6,337	447	± 37	0.07	Voronoi
70	16,024	5,782	± 1330	0.36	Voronoi
71	58,130	6,830	± 563	0.12	Voronoi
72	24,783	2,912	± 240	0.12	Voronoi

Appendix B
Thickness
Measurement Data

POINT LOCATION *MORPHOLOGY*	MEASUREMENT POINT ID	WATER DEPTH (m, MSL)	SEDIMENT THICKNESS (m)	OBSERVATIONS
Kailua Bay				
Fossil Channel				
	1	-5.5	0.30	Sand overlaying hardbottom
	2	-5.0	0.70	Sand overlaying hardbottom
	3	-5.0	1.00	Sand overlaying hardbottom
	4	-4.5	1.50	Sand overlaying hardbottom
	5	-4.0	1.40	Sand overlaying hardbottom
	6	-3.6	1.30	Sand overlaying hardbottom
	7	-4.0	0.50	Sand overlaying hardbottom
	8	-4.5	1.50	Sand overlaying hardbottom
	9	-4.5	1.80	Sand overlaying hardbottom
	10	-5.0	1.70	Sand overlaying hardbottom
	11	-5.7	1.40	Sand overlaying hardbottom
	12	-3.6	0.40	Sand overlaying hardbottom
	13	-3.8	1.00	Sand overlaying hardbottom
	14	-3.7	0.30	Sand overlaying hardbottom
	15	-3.6	1.30	Sand overlaying hardbottom
	16	-3.2	0.50	Sand overlaying hardbottom
	17	-3.0	0.60	Sand overlaying hardbottom
	18	-3.5	1.50	Sand overlaying hardbottom
	19	-3.6	0.70	Sand overlaying hardbottom
	20	-3.7	0.90	Sand overlaying hardbottom
	21	-3.8	1.20	Sand overlaying hardbottom
	22	-3.6	0.30	Sand overlaying hardbottom
	23	-4.0	1.30	Sand overlaying hardbottom
	24	-4.6	2.90	Sand overlaying hardbottom
	25	-4.6	2.40	Sand overlaying hardbottom
	26	-4.3	1.90	Sand overlaying hardbottom
	27	-5.1	2.90	Sand overlaying hardbottom
	28	-4.0	0.30	Sand overlaying hardbottom
	29	-3.7	0.03	Limestone outcroping in thin sand
	30	-3.8	0.40	Sand overlaying hardbottom
	31	-4.0	1.63	Sand overlaying hardbottom
	32	-4.1	0.60	Sand overlaying hardbottom
	33	-4.1	1.67	Sand overlaying hardbottom
	34	-3.7	2.40	Sand overlaying hardbottom
	35	-3.5	0.40	Sand overlaying hardbottom
	36	-3.4	0.60	Sand overlaying hardbottom
	37	-3.0	0.10	Limestone outcroping in thin sand
	38	-3.5	3.10	Sand beyond probing thickness (>3.0 m)

Appendix B

LOCATION	MEASUREMENT	WATER DEPTH	SEDIMENT THICKNESS	
MORPHOLOGY	POINT ID	(m, MSL)	(m)	OBSERVATIONS
Kailua Bay				
Fossil Channel				
	43	-3.2	0.10	Limestone outcroping in thin sand supporting algea
	83	-2.7	0.63	Sand overlaying hardbottom
	84	-3.7	0.10	Limestone outcroping in thin sand
	85	-3.0	0.10	Limestone outcroping in thin sand supporting algea
	86	-3.7	0.17	Limestone outcroping in thin sand
	87	-3.7	0.43	Sand overlaying hardbottom
	88	-3.7	0.23	Sand overlaying hardbottom
	89	-3.0	2.70	Sand overlaying hardbottom
	90	-5.5	1.33	Sand overlaying hardbottom
	91	-4.0	0.57	Sand overlaying hardbottom
	92	-3.7	0.33	Sand overlaying hardbottom
	109	-4.3	3.10	Sand beyond probing thickness (>3.0 m)
	110	-3.7	3.10	Sand beyond probing thickness (>3.0 m)
	111	-4.3	3.10	Sand beyond probing thickness (>3.0 m)
	112	-3.7	3.10	Sand beyond probing thickness (>3.0 m)
	113	-3.7	3.10	Sand beyond probing thickness (>3.0 m)
	114	-3.7	0.20	Sand overlaying hardbottom
	115	-2.7	1.23	Sand overlaying hardbottom
	116	-3.0	0.07	Limestone outcroping in thin sand supporting algea
	117	-3.4	1.77	Sand overlaying hardbottom
	120	-4.6	0.03	Limestone outcroping in thin sand
	135	-5.5	3.10	Sand gravel mixture beyond probing thickness (>3.0 m)
	136	-8.2	3.10	Sand gravel mixture beyond probing thickness (>3.0 m)
	137	-7.0	3.10	Sand gravel mixture beyond probing thickness (>3.0 m)
	138	-4.9	1.17	Sand overlaying limestone, grey sands observed
	142	-6.1	0.10	Gravel and rubble with little sand
	143	-3.0	0.00	Gravel and rubble
	144	-5.5	2.07	Sand overlaying hardbottom
	145	-6.4	1.00	1.0 m of sand overlaying resistant layer of shell and coral rubble
	146	-7.3	1.00	1.0 m of sand overlaying resistant layer of coral rubble
	147	-10.4	1.90	Sand overlaying hardbottom
	148	-10.4	0.73	0.73 m sand overlaying resistant layer of coral rubble
	149	-13.7	0.33	Sand overlaying hardbottom
	151	-3.0	0.17	Gravel and rubble with little sand
	152	-12.2	0.67	Sand overlaying hardbottom

Appendix B

LOCATION *MORPHOLOGY*	MEASUREMENT POINT ID	WATER DEPTH (m, MSL)	SEDIMENT THICKNESS (m)	OBSERVATIONS
Kailua Bay				
Karst Depression				
	95	-7.3	1.07	Sand overlaying hardbottom
	96	-5.2	0.30	Sand overlaying hardbottom
	97	-6.7	1.53	Sand with a thin resistive layer at -1.0 m
	98	-9.1	1.13	Sand and carbonate discs 5 - 40 cm in diameter
	99	-7.6	0.73	Sand overlaying hardbottom
	100	-6.1	0.87	Sand overlaying hardbottom
	101	-7.6	0.20	Sand overlaying hardbottom
	102	-7.9	0.13	Sand overlaying hardbottom
	103	-6.4	0.40	Sand overlaying hardbottom
	104	-7.3	1.70	Sand overlaying hardbottom
	105	-6.4	0.53	Sand overlaying hardbottom
	106	-6.4	0.27	Sand overlaying hardbottom
	107	-7.6	0.10	Gravel and rubble with little sand
	108	-6.7	0.07	Limestone outcroping in thin sand
	118	-7.9	1.40	Sand overlaying hardbottom
	119	-8.5	1.33	1.33 m of sand overlaying resistant layer of shell and coral rubble
	139	-8.2	0.13	Gravel and rubble with little sand
	121	-6.7	0.73	Sand overlaying hardbottom
	122	-6.1	3.10	Sand beyond probing thickness (>3.0 m), resistive layer at -0.3 m
	123	-8.2	0.33	0.4 m of sand overlaying resistant layer of shell and coral rubble
	124	-6.1	3.10	Sand beyond probing thickness (>3.0 m), resistive layer at -0.6 m
	125	-3.0	2.37	Sand overlaying hardbottom
	126	-6.1	0.33	Limestone outcroping in thin sand
	127	-7.6	0.70	Sand overlaying hardbottom
	128	-7.6	0.93	Sand overlaying hardbottom
	129	-4.9	1.63	Sand overlaying hardbottom
	130	-7.6	0.20	Sand overlaying hardbottom
	131	-6.1	0.17	Limestone outcroping in thin sand
	132	-4.6	0.57	Sand overlaying hardbottom
	133	-5.5	1.40	Very fine sand overlaying hardbottom
	134	-4.9	0.83	Sand overlaying hardbottom
	140	-6.1	1.83	Sand overlaying hardbottom
	141	-4.3	0.90	Sand overlaying hardbottom
	150	-2.4	1.83	Sand overlaying hardbottom
	63	-3.1	0.17	Thin sand over hard bottom
	64	-3.3	0.60	Sand over hard bottom
	65	-3.1	0.77	Sand over hard bottom
	66	-3.8	0.13	Limestone outcroping in thin sand
	67	-3.8	0.57	Sand overlaying hardbottom
	68	-3.7	0.87	0.87 m of sand overlaying resistant layer of shell and coral rubble

Appendix B

LOCATION *MORPHOLOGY*	MEASUREMENT POINT ID	WATER DEPTH (m, MSL)	SEDIMENT THICKNESS (m)	OBSERVATIONS
Kailua Bay				
Karst Depression				
	73	-3.5	0.17	Limestone outcroping in thin sand
	74	-3.0	0.30	Limestone outcroping in thin sand
	75	-3.9	0.10	Limestone outcroping in thin sand
	76	-4.5	0.27	Limestone outcroping in thin sand
	177	-3.4	0.53	0.53 m of sand overlaying resistant layer of shell and coral rubble
	180	-3.7	0.03	Thin sand over hard bottom
	202	-9.1	1.40	Sand overlaying hardbottom
	203	-10.7	0.50	Sand overlaying hardbottom
	204	-11.3	0.37	Sand overlaying hardbottom
Lanikai				
Sand Field				
	44	-2.4	1.97	0.5 m of sand overlaying resistant layer of shell and coral rubble
	45	-2.4	3.10	Sand beyond probing thickness (>3.0 m)
	46	-2.4	2.53	2.53 m of sand overlaying resistant layer of shell and coral rubble
	47	-2.4	0.20	Sand overlaying hardbottom
	48	-2.4	1.00	Sand overlaying hardbottom
	49	-2.1	0.50	0.5 m of sand overlaying resistant layer of shell and coral rubble
	50	-2.1	0.43	Sand overlaying hardbottom
	51	-2.4	1.37	0.5 m of sand overlaying resistant layer of shell and coral rubble
	52	-4.0	0.27	0.27 m of sand overlaying resistant layer of shell and coral rubble
	53	-4.6	0.30	Sand overlaying hardbottom
	54	-3.4	0.60	0.6 m of sand overlaying resistant layer of shell and coral rubble
	55	-4.0	0.65	0.65 m of sand overlaying resistant layer of shell and coral rubble
	56	-3.7	0.65	0.65 m of sand overlaying resistant layer of shell and coral rubble
	57	-3.7	0.17	Thin sand overlaying hardbottom
	58	-3.4	0.75	0.75 m of sand overlaying resistant layer of shell and coral rubble
	59	-3.4	3.10	Sand beyond probing thickness (>3.0 m)
	60	-3.4	0.43	Sand overlaying hardbottom
	61	-2.4	0.80	Sand overlaying hardbottom
	62	-3.4	0.63	0.63 m of sand overlaying resistant layer of shell and coral rubble

Appendix B

LOCATION *MORPHOLOGY*	MEASUREMENT POINT ID	WATER DEPTH (m, MSL)	SEDIMENT THICKNESS (m)	OBSERVATIONS
Lanikai				
Karst Depression				
	77	-4.9	0.20	0.20 m of sand overlaying resistant layer of shell and coral rubble
	78	-4.6	0.20	0.20 m of sand overlaying resistant layer of shell and coral rubble
	79	-3.7	0.00	Gravel and rubble with little fine sand
	80	-3.4	0.00	Gravel and rubble with little fine sand
	81	-4.0	0.00	Gravel and rubble with little fine sand
	82	-4.3	0.13	Gravel and rubble with little sand
	178	-3.4	0.20	Sand overlaying hardbottom
	179	-4.3	0.23	Sand overlaying hardbottom
	198	-16.8	0.90	Coarse sand with sparse carbonate rubble throughout
	199	-16.8	1.10	Coarse sand with sparse carbonate rubble throughout
	200	-16.8	1.10	Coarse sand with sparse carbonate rubble throughout
Waimanalo Bay				
Fossil Channel				
	181	-7.3	0.07	Gravel and rubble with little sand
	184	-6.4	0.00	Halimeda rich gravel with partially hardened surface
	187	-6.4	0.53	Sand overlaying hardbottom
	189	-5.5	3.10	Sand beyond probing thickness (>3.0 m)
	190	-6.4	0.47	Sand overlaying hardbottom
	201	-4.3	0.90	0.9 m of fine sand overlaying halimeda rich gravel
	205	-4.6	0.90	0.9 m of fine sand overlaying halimeda rich gravel
Waimanalo Bay				
Sand Field				
	162	-1.5	1.00	Sand overlaying hardbottom
	163	-1.5	1.00	Sand overlaying hardbottom
	164	-3.4	0.00	Gravel and rubble
	170	-1.5	0.73	Sand overlaying hardbottom
Waimanalo Bay				
Karst Depression				
	153	-5.5	3.10	Coarse gravely sand beyond probing thickness (>3.0 m)
	154	-7.9	0.40	Reddish sand overlaying hardbottom
	155	-7.6	0.60	0.6 m of fine sand overlaying halimeda rich gravel
	156	-6.1	0.23	0.23 m of fine sand overlaying halimeda rich gravel
	157	-4.9	1.67	Sand overlaying hardbottom
	160	-4.6	0.40	Fine sand overlaying hardbottom
	171	-3.4	0.07	Limestone outcroping in thin sand
	172	-3.7	1.65	Gravely sand overlaying hardbottom
	173	-7.0	3.10	Coarse sand beyond probing thickness (>3.0 m)

Appendix B

LOCATION *MORPHOLOGY*	MEASUREMENT POINT ID	WATER DEPTH (m, MSL)	SEDIMENT THICKNESS (m)	OBSERVATIONS
Waimanalo Bay				
Karst Depression				
	188	-6.4	0.00	Gravel and rubble
	191	-9.1	0.01	thin sand overlaying halimeda rich gravel
	192	-6.7	0.00	Halimeda rich gravel
	193	-9.1	0.53	0.53 m of fine sand overlaying halimeda rich gravel
	194	-7.9	0.53	Sand overlaying hardbottom
	195	-9.1	0.30	0.30 m of sand overlaying halimeda/coral gravel
	196	-9.8	0.30	0.30 m of sand overlaying halimeda/coral gravel
	197	-8.8	3.10	Sand beyond probing thickness (>3.0 m)
	158	-4.6	0.13	Limestone outcroping in thin sand
	159	-6.7	0.77	Sand overlaying hardbottom
	161	-7.9	0.73	Very fine sand overlaying hardbottom
	165	-8.2	0.43	Sand with fossil reef and coral rubble outcroping
	166	-8.8	1.43	Gravely sand with fossil reef outcroping
	167	-3.4	0.93	Coarse sand overlaying hard bottom
	168	-7.6	0.00	Limestone supporting algea
	169	-7.9	1.20	1.20 m of sand overlaying coral gravel
	174	-3.4	0.00	Limestone surface with no sand
	175	-4.6	2.00	Sand overlaying hardbottom
	176	-5.2	0.60	Spur and groove reef with sand infill

Appendix C
Volume Estimates

LOCATION *MORPHOLOGY*	SAND BODY ID	AREA ID	AREA (m^2)	VOLUME (m^3)	ERROR (m^3)	VOL/AREA (m^3/m^2)	METHOD
Kailua Bay							
Fossil Channel							
	26	1	586,831	801,695	± 70,484	1.37	Kriging
	26	2	7,394	2,513	± 455	0.34	Kriging
	26	3	4,572	1,027	± 350	0.22	Kriging
	46	40	4,792	614	± 141	0.13	Voronoi
	46	41	12,302	3,198	± 736	0.26	Voronoi
	53	42	2,344	1,728	± 397	0.74	Voronoi
	46	43	13,217	3,744	± 861	0.28	Voronoi
	46	44	11,467	4,449	± 1023	0.39	Voronoi
	54	45	2,701	105	± 24	0.04	Voronoi
	15	46	3,172	1,231	± 283	0.39	Voronoi
	47	47	5,508	4,424	± 1018	0.80	Voronoi
	25	48	5,868	387	± 89	0.07	Voronoi
	25	49	8,534	0	± 0	0.00	Voronoi
Karst Depression							
	1	23	5,450	1,544	± 127	0.28	Voronoi
	1	24	22,971	27,630	± 2279	1.20	Voronoi
	1	25	21,041	2,694	± 222	0.13	Voronoi
	1	26	27,962	33,633	± 2775	1.20	Voronoi
	1	27	14,104	12,969	± 1070	0.92	Voronoi
	1	28	33,961	24,114	± 1989	0.71	Voronoi
	13	29	1,793	577	± 48	0.32	Voronoi
	14	30	790	561	± 46	0.71	Voronoi
	24	31	11,163	1,429	± 118	0.13	Voronoi
	24	32	8,586	2,332	± 192	0.27	Voronoi
	41	33	16,853	6,081	± 502	0.36	Voronoi
	42	34	5,112	337	± 28	0.07	Voronoi
	43	35	19,513	12,341	± 1018	0.63	Voronoi
	43	36	18,917	1,468	± 121	0.08	Voronoi
	44	37	4,333	958	± 79	0.22	Voronoi
	45	38	838	293	± 24	0.35	Voronoi
	48	39	4,970	2,700	± 223	0.54	Voronoi
	3	4	2,602	1,716	± 395	0.66	Voronoi
	4	5	710	110	± 25	0.15	Voronoi
	38	6	1,996	674	± 155	0.34	Voronoi
	5	7	1,450	73	± 17	0.05	Voronoi
	38	8	3,483	270	± 62	0.08	Voronoi
	6	9	1,917	543	± 125	0.28	Voronoi
	7	10	653	68	± 16	0.10	Voronoi
	8	11	2,141	440	± 101	0.21	Voronoi

Appendix C

LOCATION *MORPHOLOGY*	SAND BODY ID	AREA ID	AREA (m^2)	VOLUME (m^3)	ERROR (m^3)	VOL/AREA (m^3/m^2)	METHOD
Kailua Bay							
Karst Depression							
	10	17	6,206	313	± 72	0.05	Voronoi
	51	18	11,958	464	± 107	0.04	Voronoi
	11	19	3,575	1,845	± 424	0.52	Voronoi
	39	20	6,003	2,632	± 605	0.44	Voronoi
	12	21	1,601	43	± 10	0.03	Voronoi
	40	22	8,221	4,466	± 1027	0.54	Voronoi
Lanikai							
Karst Depression							
	49	50	12,044	977	± 204	0.08	Kriging
	28	51	29,245	946	± 523	0.03	Kriging
	37	52	128,180	41,780	± 8992	0.33	Kriging
Fossil Channel							
	29	53	32,582	17,699	± 4071	0.54	Voronoi
	29	54	16,704	3,241	± 745	0.19	Voronoi
	29	55	18,637	2,676	± 615	0.14	Voronoi
Sand Field							
	50	56	11,174	179	± 45	0.02	Kriging
	27	57	227,136	22,464	± 784	0.10	Kriging
	29	58	490,846	44,084	± 1261	0.09	Kriging
	28	59	419,702	63,260	± 999	0.15	Kriging
Waimanalo Bay							
Karst Depression							
	2	60	20,294	15,748	± 3622	0.78	Voronoi
	20	61	61,886	17,529	± 4032	0.28	Voronoi
	34	68	17,195	5,137	± 1182	0.30	Voronoi
	36	70	16,024	5,782	± 1330	0.36	Voronoi
Sand Field							
	22	62	8,243	0	± 0	0.00	Voronoi
	30	63	36,575	0	± 0	0.00	Voronoi
	31	64	9,644	1,360	± 112	0.14	Voronoi
	32	65	45,198	2,284	± 188	0.05	Voronoi
	32	66	28,411	4,774	± 394	0.17	Voronoi
	33	67	17,823	1,529	± 126	0.09	Voronoi
	35	69	6,337	447	± 37	0.07	Voronoi
	21	71	58,130	6,830	± 563	0.12	Voronoi
	17	72	24,783	2,912	± 240	0.12	Voronoi

BIBLIOGRAPHY

Athens, J. S., and Ward, J. V., 1991, Paleoenvironmental and Archaeological Investigations, Kawainui Marsh Flood Control Project, Oahu Island, Hawaii.: International Archaeological research Institute, Inc. Honolulu Hawaii Prepared for U.S. Army Engineering Division, Pacific Ocean. Contract No. DACW83-90-C-0050.

Barry, J., Schock, S., and Ericksen, M., 1997, A New Broad Band Frequency Modulated Subbottom Profiling Developed for Hawaii: Seventh Annual International Offshore and Polar Engineering Conference p. 120-128.

Bodge, K., and Sullivan, S., 1999, Hawaii Pilot Beach Restoration Project: Coastal Engineering Investigaton: State of Hawaii Department of Land and Natural Resources, Honolulu.

Cacchione, D., and Tate, G., 1998, Bottom Currents, Waves and Sand Transport in Reef Channel off Kailua, Hawaii: Proc. Sea grant Coastal Erosion Mgmt, Conf., Maui, Hawaii.

Casciano, F., and Palmer, R., 1969, Potential of Offshore Sand as an Exploitable Resource in Hawaii: Sea Grant Program: Univ. of Hawaii: #69-4.

Conger, C. L., Fletcher, C., Hochberg, E., Frazer, N., and Rooney, J., In Review, Patterns of Sand Distribution Across the Insular Shelf, Oahu, Hawaii.

Conger, C. L., Hochberg, E., Fletcher, C. H., and Atkinson, M., 2006, Decorrelating Remote Sensing Color Bands From Bathymetry in Optically Shallow Waters: IEEE Transactions on Geoscience and Remote Sensing, v. 44.

Conger, C. L. F., C.H., and Barbee, M., 2005, Artificial neural network classification of sand in all visible submarine and subaerail regions of a digital image: Journal of Coastal Research, v. 21, p. 1173-1177.

Coulbourn, W., Campbell, J., Anderson, M., Daugherty, V., Greenberb, S., Izuka, R., Lauritzen, B., Tsutsui, B., and Yan, C., 1988, Sand deposits offshore Oahu, Hawaii: Pacific Science, v. 42, p. 267-299.

Cox, D., 1978, Notes on Hawaiian Sand Beach Management, Hawaii Coastal Zone Management Program, Honolulu, University of Hawaii.

Coyne, M., Battista, T., Anderson, M., Waddell, J., Smith, W., Jokiel, P., Kendall, M., and Monaco, M., 2003, Benthic Habitats of the Main Hawaiian Islands: NOAA Technical Memorandum NOS NCCOS CCMA 152, URL: http://biogeo.nos.noaa.gov/projects/mapping/pacific.

Dollar, S., 1979, Sand Mining in Hawaii: Research, Restrictions, and Choices for the Future: UNIHI-SEAGRANT-TP-79-01. Seagrant College Program, Univ. of Hawaii.

Fletcher, C. H., Grossman, E., Richmond, B. M., and Gibbs, A., 2002, Atlas of Natural of Natural Hazards on the Hawaiian Coasts: Denver, CO, U.S. Geological Survey, Geologic Investigations Series I-2761, 182 p.

Fletcher, C. H., Murrat-Wallace, C. G., C., Popp, B., and Sherman, C. E., 2005, Age and Origin of Late Quaternary Eolinanite, Kaiehu Point (Moomomi), Hawaii: Journal of Coastal Research, v. SI 42, p. 92-112.

Grossman, E., and Fletcher, C., 1998, Sea level higher than present 3500 years ago on the northern main Hawaiian Islands: Geology, v. 26.

—, 2004, Holocene Reef Development Where Wave Energy Reduces Accmmodation Space. Kailua Bay, Winward Oahu, Hawaii, USA: Journal of Sedimentary Research, v. 74, p. 49-63.

Grossman, E. E., 2001, Holocene sea-level history and reef development in Hawaii and the central Pacific Ocean, University of Hawaii, Manoa 257 p.

Hampton, M. A., Blay, C. T., and Murray, C., 2004, Carbonate Sediment Depositis on the Reef Front Around Oahu, Hawaii: Marine Georesources and Geotechnology, v. 22, p. 65-102.

Hampton, M. A., Blay, C. T., Murray, C., Torresan, L., Frazee, C., Richmond, B. M., and Fletcher, C., 2003, Data Report, Geology of Reef-Front Carbonate Sediment Deposits Around Oahu, Hawaii: U.S. Geological Survey Open-File Report 03-441.

Harney, J. N., and Fletcher, C. H., 2003, A budget of Caronate Framework and Sediment Production, Kailua Bay, Oahu, Hawaii: Journal of Sedimentary Research, v. 73, p. 856-868.

Harney, J. N., Grossman, E. E., Richmond, B. R., and Fletcher, C. H., 2000, Age and composition of carbonate shoreface sediments, Kailua Bay, Oahu, Hawaii: Coral Reefs, v. 19, p. 141-154.

Kraft, J., 1982, Terrigenous and Carbonate Clastic Facies in a Transgressive Sequence Over Volcanic Terrain: American Association of Petroleum Geologists Bulletin, v. 66, p. 589.

—, 1984, Local relative sea level changes and the evolution of coastal environments, windward Oahu, Hawaii: IGCP Proj. No. 061. Sea-Level 5:5-6.

Maragos, J., Roach, J., Bowers, R., Hemmes, D., Self, F., Macneil, J., Ells, K., Omeara, P., Vansant, J., Sato, A., Jones, J., and Kam, D., 1977, Enviromental Surveys Before, During, after Offshore Marine Sand Mining Operatations at Keauhou Bay, Hawaii: Sea Grant Program: Univ. of Hawaii, v. Working Paper No. 28.

Moberly, R., Campbell, J., and Coulbourn, W., 1975, Offshore and Other Sand resources for Oahu, Hawaii.

Moberly, R., and Chamberlain, T., 1964, Hawaiian Beach Systems: Univ. of Hawaii. Prepared for Habors Divions, Hawaii DOT. Contract 6496.

Ocean Innovators Inc, 1977a, Offshore Sand Deposit Data Collection, Kualoa regional Park Beach Erosion Project, Kaneohe Bay, Oahu.: Prepared for U.S. Army Engineer Div., Pacific Ocean.
—, 1977b, Offshore Sand Sample Data, South and West Shores, Oahu.: Prepared for Marine Affairs Coordinator, Task Order No. 120.
—, 1977c, Sand Deposit Investigation Offshore of Nanakuli, Oahu.: Prepared for the U.S. Army Engineer Div., Pacific Ocean.
—, 1978a, Kailua Bay Offshore Sand Survey: Prepared for U.S. Army Engineer Div., Pacific Ocean.
—, 1978b, North Kaneohe bay offshore Sand Reconnaissance and Sampling: Prepared for the U.S. Army Engineer Div., Pacific Ocean.
—, 1979, Offshore Sand Sampling North and Winward Shores, Oahu.: Under contract to Marine Affairs Coordinator, Office of Governer, State of Hawaii, Order No. 163.

Richmond, B. M., Cacchione, D., Howd, P., and D'Orio, M., 2002, Sand transport within a reef channel off Kailua, Oahu, Hawaii: Ocean Science meeting, American Geopyhical Union.

Rooney, J., Fletcher, C., Grossman, E., Engels, M., and Field, M., 2004, El Nino Influence on Holocene Reef Accretion in Hawaii: Pacific Science, v. 58, p. 305-324.

Sea Engineering Inc, 1993, Beach Nourishment Viablity Study: Prepared for Hawaii Coastal Zone Management Program

Sherman, C. E., Fletcher, C. H., and Rubin, K. H., 1999, Marine and Meteoric Diagenesis of Pleistocene Carbonates from a Nearshore Submarine Terrace, Oahu, Hawaii: Journal of Sedimentary Research, v. 69.

U.S. Army Engineer District, 1978, Detailed Project report and Final Environmental Statement, Kailua Beach Park Erosion Control, Kailua, Oahu, Hawaii.

Webster, R., and Oliver, M., 2001, Geostatistics for Environmental Scientists: Statistic in Pratice: West Sussex, Wiley &Sons.

Sediment Transport Study—Lanikai and Bellows Beaches

Chris Bochicchio, University of Hawaii Coastal Geology Group, February 2009

1. INTRODUCTION

Beach loss poses a serious hazard to the economy, ecology, and safety of many coastal regions. Over the latter part of the 20th century nearly 70% of the world's beaches have experienced net erosion (Bird, 1985). Much of this is attributed to the combined affect on coastal sediment budgets of rising sea level and increasing shoreline development (NRC, 1995). On the island of Oahu, Hawaii, historical analysis of beach length shows 24% of all beaches have either narrowed or disappeared over a ~60 year interval (Fletcher et al, 1997; Coyne et al., 1999). The impact of this beach loss is particularly profound in Hawaii as sandy beaches drive a multi-billion dollar tourism industry that accounts for 60% the jobs in the state and represents an important element of cultural identity.

Beach volume and shoreline position are largely governed by locally unique trends in longshore and cross-shore sediment transport. These are difficult to observe and predict over the long time scales needed in order to develop sustainable coastal management plans. Hence, where historical observations are available, it is important to investigate the processes driving shoreline change on poorly understood beaches.

Lanikai Beach on windward (east-facing) Oahu is a developed shoreline threatened by long-term and enigmatic beach erosion. Lanikai has experienced a series of decadal-scale erosion and accretion events producing > 50 m changes in beach width over a 60-year period. The net trend has been erosional and the total beach length has decreased from 2.3 km to 800 m over the period from 1950 to 2007. Discussion regarding appropriate management of Lanikai Beach has continued for over 30-years without resolution. Central to this debate is the source and fate of beach sand, and specifically whether sediment is exchanged around a rocky headland marking the southern littoral cell boundary of Lanikai Beach with Bellows Beach (Figure 1).

In this study, we test the hypothesis that littoral sediment transport occurring between Bellows and Lanikai beaches controls historical shoreline change at Lanikai. We examine the direction of this exchange and assess factors that have potentially altered sand transport over time. We integrate grain-size trend analysis and hydrodynamical modeling (Delft 3D) and compare the results with a detailed review of historical shoreline change (derived from aerial photographs) to evaluate littoral sediment transport across the Lanikai-Bellows boundary and along the greater shoreline. We expand our analysis to include historical shifts in wind direction as a driving factor in shoreline change. Results indicate a significant southeast to northwest trend in net sand transport that governs shoreline behavior.

We conclude that sediment transport does occur around Wailea Point linking Bellows and Lanikai Beach and hardening of the Bellows shoreline has starved Lanikai Beach by impounding its sediment supply. We also find strong evidence that wind direction has had a strong influence on sediment transport in this area. These results also indicate that future integration of sediment grain-trend analysis into shoreline change studies could be beneficial to coastal authorities tasked with managing poorly understood shorelines. This study is the first major reconstruction of shoreline dynamics along the Lanikai-Bellows Beach and represents the first application of sediment grain-size trend analysis (GSTA) to studying shoreline change.

2. STUDY SITE

The Lanikai-Bellows region encompasses roughly 4.3 km of coastline along a broad, embayed headland marking the boundary between Kailua and Waimanalo Bays on the southeastern or windward coast of Oahu, Hawaii. The northern reach of the study area terminates at Alala Point, while the southern terminus is defined by the mouth of Waimanalo Stream in Waimanalo Bay. The center of the study area is Wailea Point, which marks the boundary between northeast facing Lanikai Beach and southeast facing Bellows Beach. Wind conditions are dominated by northeast trade winds with an average speed of 10-20 kn over 90% of the summer season (April-September) and 50-80% of the winter season (October-March) (Harney, 2000). Trade wind waves dominate during summer months, with average deepwater significant wave heights of 1-3 m and periods of 6-9 s. During the winter, refracted deepwater swell from the North Pacific occasionally reach significant wave heights of 4 m with periods of 10-20 s. Wave heights reaching the beach are substantially lower (less than 0.5 m) as a shallow reef crest and the twin Mokulua Islands dissipate most incoming swell energy. Typical tidal range in Hawaii is less than 1 m.

The coastal plain at Lanikai ends abruptly at Ka'iwa Ridge, creating a narrower coastal zone at Lanikai than at Bellows, exacerbating the effect of shoreline erosion on the crowded properties. Landward of the shoreline in both areas are unconsolidated carbonate marine and dune sediments (Grossman and Fletcher, 1998; Harney and Fletcher, 2003). An expansive reef flat fronts the majority of the site with widths between 0.5 and 1.0 km in water generally 2.0 to 3.5 m deep. Three large sand fields extend from the beach face to near the reef crest, containing a total of 130×10^3 m^3 of sediment with average thicknesses of 0.7-1.3 m (Bochicchio et al., 2009). Thin, isolated veneers of sediment, occasionally observed with ripple marks, are found over the reef flat. The reef flat shallows quickly seaward as it transitions to an irregular 100 m wide reef crest, parts of which are exposed during low tide. The twin volcanic Mokulua Islands stand among the reef crest, seaward of these islands the fore-reef slopes to >20 m depth.

Beaches at Lanikai and Bellows are generally narrow with gentle slopes and are made up of poorly sorted medium to fine-grained calcareous sand (Noda, 1989). Changes in beach volume along this coast tend to be related to chronic fluctuations in alongshore sand transport and sediment deficiencies, rather than event-based erosion because the offshore reef platform diminishes incoming swell (Fletcher et al., 1997). Currently, the northern and southern regions of Lanikai as well as northern Bellows Beach are without a beach and protected by seawalls.

Sediment transport on Hawaiian beaches occurs within littoral cells that span less than several kilometers of shoreline and cross-shore transport for nearshore sediment bodies often plays an important role in the sediment budget (Gerritsen, 1978). Noda (1989) investigated transport processes at Lanikai and stated that longshore transport is responsible for substantial historical shoreline change at Lanikai Beach despite a relatively mild wave climate. Noda found no evidence of sediment transport occurring around Alala Pt. to the north, indicating that the Kailua-Lanikai cell boundary is closed. A series of profiles extending from the southern Lanikai shoreline shows two sandbars at 15 and 30 m from the seawall, which corresponds with the node and anti-node of the mean incoming wave (Lipp, 1995). This indicates strong wave reflection off the Lanikai seawalls is, to some degree, preventing the accretion of a beach.

3. METHODS

To test our hypothesis that sand transport between Bellows and Lanikai cells controls shoreline change at Lanikai, we use grain-size trend analysis, hydrodynamic modeling, and historical shoreline change analysis.

3.1 Sediment grain-size trend analysis

3.1.1 Sample collection and analysis

A total of 214 sediment samples were collected on a grid surrounding Wailea Point (Figure 2). Spacing between sample sites varied from 37.5 m near Wailea Point, to 75 m within sand fields, and 150 m between sand fields. Samples were recovered from the ocean bottom using a sediment dredge, which removed between 10 and 30 cm of the surface sediment. Between 1000 and 2000 g of sediment were recovered in each sample. The upper 5 cm layer of sample within the dredge was discarded to reduce error caused by fine sediment potentially billowing out of the dredge mouth as it was pulled to the surface. A Global Positioning System (GPS) receiver with Wide Area Augmentation System (WAAS) correction was used to locate sample positions within 4 m. Grain-size distributions were based on the weight percent of each size fraction determined from standard sieve analysis method ASTM C 136 (ASTM, 2006) using sieve openings ranging between -2 and 5 Ø at 0.5 Ø intervals. The statistics mean size, sorting, and skewness were calculated from each distribution for use as parameters in the trend analysis.

3.1.2 General background on method

Spatial trends in the grain-size of surficial sediments are a direct result of natural sediment transport processes (Russell, 1939; McCave, 1978; Swift et al., 1972; Harris et al., 1990). The development of these trends is primarily the effect of transport processes selectively sorting and abrading sediment by grain-size according to the direction of transport (McLaren, 1985; Gao and Collins, 1992; Le Roux and Rojas, 2007). Using the parameters mean size, sorting, and skewness, four trends have been found to be reliable indicators of transport direction (McLaren and Bowles, 1985; Gao and Collins, 1992; Gao et al., 1994; Le Roux 1994b). Accordingly, transport pathways can be identified if a series of sediment samples follows one of the trends listed below (using Ø units after Folk and Ward, 1957):

Trend 1: finer, better sorted, and more negatively skewed
Trend 2: coarser, better sorted, and more positively skewed
Trend 3: coarser, better sorted, and more negatively skewed
Trend 4: finer, better sorted, and more positively skewed

Type 2 and 3 trends show a distinctive coarsening of grain size along the direction of transport that at first appears counterintuitive. These trends are interpreted as indicators of more rapid transport processes in which a majority of the surficial fine-grained material is removed creating a thin coarse-grained lag deposit that “shields” underlying fine-grained material. This coarse upper layer is mixed with underlying fine sediments during sampling, which results in an overall finer-grained texture upstream of the transport direction (McLaren and Bowles, 1985).

GSTA encompasses a range of techniques for recovering net transport direction from naturally sorted seafloor sediments by identifying the above grain-size trends in a series of discrete sediment samples collected around an area of interest. McLaren and Bowles (1985) first proposed a one-dimensional methodology to accomplish this task, which was followed by a number of two-dimensional approaches (e.g., Gao and Collins, 1992; Le Roux, 1994b,c; Asselman, 1999; Rojas et al., 2000; Rojas, 2003). These methods have been used to characterize sediment transport in a range of aquatic settings for a variety of engineering, environmental, and sedimentological investigations.

In this study we apply two separate methods put forth by Gao and Collins (1992) and Le Roux (1994) to a dataset collected offshore of Lanikai and Bellows beaches. These two methodologies use significantly different mathematical approaches for locating trends in the data, yet are shown to detect sediment transport at similar spatial scales (Rios et al., 2002). This study utilizes two methods to confirm that similar conclusions can be reached through two different means and to provide a comprehensive view of the regional transport processes. An overview of each method is provided below to highlight the methodological differences, provide an instructive reference, and aid in discussion of the results. Likewise, the respective authors of each method provide full descriptions in Gao and Collins (1992) and Le Roux (1994b). The Gao-Collins method is described in more detail using practical

examples (Appendix A), because current publications on this method are limited to theoretical application.

3.1.3 Gao-Collins and Le Roux methodologies

The method put forth in Gao and Collins (1992) determines sediment transport direction by comparing grain-size parameters among a group of sampling sites. Parameters at each site are compared with those of neighboring sites within a predefined characteristic distance. The characteristic distance is defined as the spatial scale over which transport is expected to occur in the study area, generally given as the maximum interval between any two adjacent sampling sites. This study uses a characteristic distance of 200 m, which reflects the spatial scale of transport processes anticipated for this region and maximum distance between potentially related sites. In every case where either Trend 1 or Trend 2 is identified, component vectors with the unit length (i.e. equal to 1) are drawn in the direction of the neighboring site (Figure 3A). Summing all component vectors at each site produces a single vector referred to as a transport vector (large arrow in Figure 3A and 3B). Component vectors are relevant only in terms of direction. Their lengths do not reflect differences in grain-size parameters or distance between points. As all component vector lengths are equal, the number and direction of neighboring sites showing a positive transport trend determine both the direction and length of the resulting transport vector. Determining transport vectors for every point produces a field of transport vectors (Figure 3B), which can be filtered to reduce noise and reveal the dominant trends, by averaging the vector at each site with surrounding transport vectors (Figure 3C). Details of the steps and calculations used in Figure 3 are included in Appendix A.

The method of Le Roux (1994b) functions by comparing grain-size parameters of a central site with the closest four neighboring sites in all cardinal directions (i.e. one site is selected from the North, East, South, and West quadrants) (Figure 4A). The Le Roux method searches for all four trend types individually, producing a vector field of transport for each trend.

Trend determination begins with the normalization of all three grain-size parameters between all five sites. These values are combined into a single value (*E*) representing the strength of transport along that axis. The process of normalizing and combining the parameters is modified in a manner depending on the trend type. For example, Equation 1 is used in the case of Trend 3, where all parameters are expected to decrease along the direction of transport.

In this process, sites with the smallest values receive the highest score (*E*) indicating stronger transport potential in the direction of that site. Conversely, to achieve the same effect with Trend 1, Equation 1 must be modified so that increasing mean grain-size results in a lower value of *E*. This is done simply by subtracting 33.33 from the normalized mean size parameter (Equation 2).

$$E = \frac{33.33}{\mathrm{mn}_{\max} - \mathrm{mn}_{\min}}\left(\mathrm{mn} - \mathrm{mn}_{\min}\right) + \frac{33.33}{\mathrm{var}_{\max} - \mathrm{var}_{\min}}\left(\mathrm{var} - \mathrm{var}_{\min}\right) + \frac{33.33}{\mathrm{sk}_{\max} - \mathrm{sk}_{\min}}\left(\mathrm{sk} - \mathrm{sk}_{\min}\right) \quad \text{Equation (1)}$$

$$E = \left(33.33 - \left[\frac{33.33}{\mathrm{mn}_{\max} - \mathrm{mn}_{\min}}\left(\mathrm{mn} - \mathrm{mn}_{\min}\right)\right]\right) + \frac{33.33}{\mathrm{var}_{\max} - \mathrm{var}_{\min}}\left(\mathrm{var} - \mathrm{var}_{\min}\right) + \frac{33.33}{\mathrm{sk}_{\max} - \mathrm{sk}_{\min}}\left(\mathrm{sk} - \mathrm{sk}_{\min}\right) \quad \text{Equation (2)}$$

Similar adjustments are made to the normalized skewness parameter for Trend 2 and the normalized variance parameter for Trend 4 to so that increasing values on these parameters result in higher values of *E*.

Values (*E*) are defined for every site (Figure 4B) then the value of the central site is subtracted from each adjacent site and the relative difference between sites is used to define the length of component vectors, which are summed to produce a final transport vector (Figure 4C). This process is repeated at every site to produce a field of transport vectors for each trend type. Trend 1 results are shown in Figure 4D. Commonly, the strongest vectors from each trend type are incorporated into a final vector field. The Watson (1966) non-parametric test is used to ensure that the final transport vectors are sufficiently non-random before smoothing the data to reduce noise (Le Roux et al., 2002).

The Gao-Collins and Le Roux methods both determine transport direction by searching for predefined trends between a single site and adjacent sites, but Gao-Collins uses only Trends 1 and 2, while Le Roux checks for all four trends. The Gao-Collins method checks a variable number of sites (all those that fall within the characteristic distance), while Le Roux only uses a central site and four adjacent sites. With Gao-Collins, direction of transport is determined by relative position of all neighboring sites showing a trend to the central site, with transport occurring in the direction of the most trend positive sites. In contrast, using Le Roux, transport direction and strength is determined from the calculated difference between the actual grain-size parameters of all five sites. Both methods have been shown to give comparable and informative results (Rios et al, 2002).

3.3 Computer hydrodynamic model (DELFT 3D)

The Delft3D-FLOW module (v. 3.24.03 used here) solves the unsteady shallow-water equations with the hydrostatic and Boussinesq assumptions. In 2D mode the model solves two horizontal momentum equations (see Eq. 3-4), a continuity equation (Eq. 5) and a transport (advection-diffusion) equation (Eq. 6) shown below:

$$\frac{\partial u}{\partial t}+u\frac{\partial u}{\partial x}+v\frac{\partial u}{\partial y}+g\frac{\partial \eta}{\partial x}-fv+\frac{\tau_{bx}}{\rho_w(h+\eta)}-\frac{F_x}{\rho_w(h+\eta)}-\nu_e\left(\frac{\partial^2 u}{\partial x^2}+\frac{\partial^2 u}{\partial y^2}\right)=0 \quad (3)$$

$$\frac{\partial v}{\partial t}+u\frac{\partial v}{\partial x}+v\frac{\partial v}{\partial y}+g\frac{\partial \eta}{\partial y}-fu+\frac{\tau_{by}}{\rho_w(h+\eta)}-\frac{F_y}{\rho_w(h+\eta)}-\nu_e\left(\frac{\partial^2 v}{\partial x^2}+\frac{\partial^2 v}{\partial y^2}\right)=0 \quad (4)$$

$$\frac{\partial \eta}{\partial t}+u\frac{\partial[(h+\eta)u]}{\partial x}+v\frac{\partial[(h+\eta)v]}{\partial y}=0 \quad (5)$$

$$\frac{\partial[hc]}{\partial t}+\frac{\partial[huc]}{\partial x}+\frac{\partial[hvc]}{\partial y}=h\left[\frac{\partial}{\partial x}\left(D_H\frac{\partial c}{\partial x}\right)+\frac{\partial}{\partial y}\left(D_H\frac{\partial c}{\partial y}\right)\right] \quad (6)$$

where *u* and *v* = the horizontal velocities in the *x* and *y* directions respectively; *t* = time; *g* = gravity; η = free surface height; *h* = water depth; *f* = coriolis force; ρ_w = density of water; τ_b = bed friction; *F* = external forces due to wind and waves, ν_e = horizontal eddy viscosity; D_H = horizontal eddy diffusivity; and *c* = concentration of suspended sediment. The equations are solved on a staggered finite difference grid using the Alternating Direction Implicit (ADI) method after Stelling (1984).

In this study the Delft 3D model is employed to examine the potential for different transport regimes developing under changing forcing conditions. This element of the study focuses on trade winds, as it is the most persistent type of forcing on Oahu's windward shore and most likely to determine equilibrium shoreline conditions.

Figure 5 shows a 58-year time series of trade wind direction recorded at Kaneohe Marine Corps, located on the coastline approximately 9 kilometers north of the study area. These data show periodic shifts in trade wind direction that persist over decadal-scale time periods and are in some cases rapid (e.g. 1964, 1974, and 1987). These changes in trade wind direction were first documented by Wentworth (1949) and implicated as a possible factor in shoreline change in Lanikai in a report by Noda (1988). This study is the first to extend the directional dataset presented by Wentworth (1949). The exact cause of these directional shifts is not currently understood. Using the range of observed wind directions, this study uses Delft 3D to model the potential influence that changing wind direction could have on sediment transport in the Lanikai region.

The model was calibrated using current and sea-level data collected by two acoustic doppler velocimeters deployed from August 10th to September, 12th 2005 on the southern and northern bounds of the study area. The model parameters included wind driven currents, tidal forcing, open ocean waves, and wave-driven currents. Ocean swell direction and height was simulated using a representative dataset from a deepwater directional wave buoy located 2 km north-east of the study area in

Kailua Bay (National Data Buoy Center number 51001). Tidal forces were modeled using standard harmonic components. Separate model runs used directional extremes from the historical dataset to simulate time periods when north-east (51°), east-north-east (71°), and east (85°) wind conditions dominated.

3.2. Shoreline change analysis

Analysis of shoreline change in this study draws from a portion of data collected in a separate study of the entire southern coastline of Oahu by Romine et al. (in press). Historical shoreline positions were hand digitized from survey quality aerial photos and T-sheets of the study area acquired during the following years: 1911, 1928, 1949, 1951, 1959, 1963, 1967, 1971, 1975, 1982, 1988, 1989, 1996, and 2005. Distortion errors from scanning the photos were corrected (Thieler and Danforth, 1994). Following the methodology of Fletcher et al. (2003), all photos were orthorectified and mosaicked using software from PCI Geomatics, Inc. Seaward and landward boundaries of the beach were defined as the position of mean lower low water (MLLW) (Bauer and Allen, 1995) and the vegetation line. Horizontal error in shoreline position was calculated to be ± 4.49 – 10.78 m. The position of MLLW and observations of seawall construction were used to create a timeline of shoreline change and armoring activity for the study area. In the case of a hardened shoreline where no beach currently exists, the vegetation and MLLW lines are the same.

4. RESULTS

4.1. Textural and transport trend analyses

Sediment texture over much of the study area is characterized by distinct, isolated zones of varying size. As a whole, sediments offshore of Lanikai tend to be coarser (Fig. 7), more poorly sorted (Fig. 8), and positively skewed (Fig. 9) than those at Bellows. While sediment textures directly adjacent to shore tend to be finer and more negatively skewed along the entire sample area. Offshore of Wailea Point, in the central portion of the study area, sediments are generally finer, better sorted, and more negatively skewed towards the tip of the point. However, closer examination of the entire study area shows a close juxtaposition of alternating sediment textures indicative of lag and lead deposits. In order to aid the description of textural and trend analysis results common regions, referred to in the text, are defined on both gridded textual data (Figures 7, 8, 9) and grain-size trend analysis results (Figure 10 and 11).

Results of the Gao-Collins (Figure 10) and Le Roux (Figure 11) methods indicate the direction and relative probability of sediment transport. A fundamental difference between the two methodologies is well illustrated by the smooth appearance of the Gao-Collins results and the noisier appearance of the Le Roux results. As described in the methodology, the Le Roux method is more sensitive to small differences in grain-size and to small-scale, isolated trends than the Gao-Collins method. Results of the two methodologies generally agree, with the only major exception being Region A in the southern part of the study area, where results differ considerably. In

this area the Gao-Collins results (Figure 10) show primarily north-to-northeast trends, while the Le Roux results (Figure 11) show an opposing southeast trend converging with a north-to-northwest trend.

Directly offshore of Bellows Beach (within 100 m), sediment textures alternate between coarse-positively skewed and fine-negatively skewed with all sediments becoming better sorted to the north (Region B). Results from the Le Roux method show a majority of transport to the north and Gao-Collins also shows a consistent northern trend adjacent to Bellows Beach.

Offshore sediment immediately south of Wailea Point (Region C) becomes finer, better-sorted, and more negatively skewed toward the north, which is the signature of a type 1 transport trend. Gao-Collins transport vectors along this section of coastline indicate uniform northern transport of sediment from the Bellows nearshore area towards Wailea Point. Similarly, Le Roux results show northwesterly transport toward Wailea Point where it meets an opposing transport trend. This trend is mirrored to the north in Region D, where sediment becomes finer, better-sorted, and more negatively skewed toward the south. Resulting transport vectors in Region D from both Le Roux and Gao-Collins methods are southeasterly and directly oppose transport in Region B.

Near the northern slightly embayed portion of Wailea Point (Region E), sediment within 250 m of southern Lanikai Beach shows two distinct textures. Nearshore sediments are finer, better-sorted, and more negatively skewed than sediment farther offshore. This contrast in sediment texture produces onshore and southeasterly transport vectors in the both Gao-Collins and Le Roux methodologies. To the north, both sets of results show an opposite northwesterly trend in Region F along Lanikai Beach. Sediment in the northern sample area tends to be relatively coarser, more poorly sorted, and positively skewed than the southern part of the sample area. In general, transport trends in areas F and E show divergence between northerly and southerly transport. Similar divergence occurs between Regions A and B, while both result show convergence near Wailea Point between Region C and D. Le Roux transport vectors seem to indicate a gyre-like circulation pattern across Regions C and D.

4.2. Shoreline change analysis

Changes in shoreline position are visible in historical aerial photographic sets of the Lanikai-Bellows study area (e.g. Fletcher et al., 1997, Romine et al., in review). A subset of vectorized historical shoreline positions that represent major fluctuations are overlain on a modern (2005) aerial photograph in Figures 12 and 13. Plots show relative shoreline position over time along transects (transects A through G) centered on sites with the greatest shoreline movement.

Lanikai Beach (Figure 12) shows multi-decadal historical trends of either accretion or erosion. These trends are indicated on transects B, C, and D. Shoreline position is relatively stable across the entire length of the beach from the beginning of the

record in 1912 through to the 1949 shoreline. This could be the effect of little data during this time period causing features to be missed in analysis. In southern Lanikai from 1949 and 1967 the shoreline accreted significantly, adding a maximum of approximately 60 m of new coastal land (transect D). During this period, central and northern Lanikai (transects C, B, and A) show little change.

After 1967, the accretion trend in southern Lanikai reversed until seawalls halted the erosion by 1990. Farther north, central and northern Lanikai (transects C and B) began accreting significantly during this period. Central Lanikai added approximately 30 m of coastal land by 1987, after which an erosional trend developed that has persisted through 2008. No erosional trend is evident at transect B, but an erosional trend has migrated southward from transect A since the 1975 shoreline.

Figure 13 summarizes a generally erosive trend on the Bellows shoreline south of Wailea Point. Shoreline positions at transect E indicate an erosional trend was present at the beginning of the dataset, between 1916 and 1928. Farther to the south, transect F indicates an accretionary trend between 1916 and 1928, followed by erosion between 1928 and 1961, resulting in the loss of approximately 40 m of coastal land. At transect G, shorelines remain stable until a general erosional trend developed during the 1961 to 1962 time period that continued until halted by seawalls in 1998. Erosional trends at transects E and F were also halted by seawall emplacement.

4.3. Hydrodynamic modeling results

A hydrodynamic model is useful for envisioning near shore currents that can develop under different forcing conditions. Our results show substantially different near shore current configurations in the Lanikai region when north-east (51°), east-north-east (71°), and east (90°) winds are used to force the model. Figures 14, 15, and 16 show the resulting mean current field for each wind condition. The most noticeable effect of changing wind direction is the shifting of the locations where longshore currents converge and diverge. Eastern winds induce northward transport along the entire study area (Figure 14). East-North-East winds create a divergence point in longshore currents near transect 40 along the Bellows shoreline and induced circulation similar to a gyre on the northern flank of Wailea Point (Figure 15). Under North East winds the divergence point shifts north along the Bellows coast to transect 20 and divergence develops in southern Lanikai near transect 95 (Figure 16). In general, southern transport becomes more common along both shorelines as the northern component of wind direction becomes more prominent, which is reasonable considering the geometry of the shoreline.

5. DISCUSSION

5.1. Historical Transport Patterns

What follows is a timeline of shoreline change in the Lanikai Bellows region. This discussion of historical transport will center on Figure 17, which shows an interpolated grid created from all available shoreline position data for the study area over time. Grid cell color indicates the rate of change (gradient in meters-per-year) in the shoreline during that time period (horizontal axis) and for a particular length of beach (vertical axis). As described earlier, the Lanikai-Bellows shoreline has been subject to considerable accretion and erosion. Viewing shoreline position data in as a running average of accretion or erosion rates allows these trends to be more readily apparent. For ease of discussion, the historical data is divided into eight time periods (I through VIII) that show common trends of localized accretions and erosion. Littoral sub-cell boundaries and the associated longshore transport patterns can both be inferred from this presentation of the data. Vertical and horizontal arrows indicate the direction of longshore transport over a time period as it is implied by shoreline change. This timeline of inferred littoral transport trends forms empirical control that the results of hydrodynamic modeling and sediment grain-size trends can be compared to.

I. 1910 – 1928

The relative scarcity and wide distribution of shoreline position data during this era makes only a basic analysis of shoreline movement feasible. Lower Lanikai eroded over the first half of this period (1911 to 1928), while the remainder of Lanikai and Bellows both accreted. Sand that eroded from this area either moved north, contributing to accretion in Upper Lanikai or to the south, where Bellows experienced a general accretion trend.

II. 1928 – 1953

The major feature of this period is a switch from accretion to erosion over the entirety of Bellows Beach, with the worst erosion seen on Upper Bellows. Sections of Upper and Central Lanikai began to erode, but the majority of the beach is either stable or accreting slightly. The strongest accretion is in southern Lower Lanikai that shifts northward by the end of this period. Timing of this accretion suggests Bellows Beach is providing the material for this accretion.

III. 1953 – 1964

The erosion trend along Bellows beach continues and intensifies near Wailea Point. During this time period the first sizable revetments appear at in aerial photographs along the region of Bellows Beach with the highest erosion rates. Accretion that began in northern Lower Lanikai during period II continues along a 400 meter section of beach. This trend added approximately 60 meters of new coastal land in this area and reached its maximum accretion rate during this period of time. Coincident with this accretion, both Southern Lower Lanikai and Central Lanikai

switch to an erosive trend. This suggests that the source material for the large Lanikai accretion is from both Bellows Beach and Central Lanikai. It is possible that two opposing longshore currents converge at Lower Lanikai maintaining a bulge in the shoreline between transects 80 and 100.

A similar point of convergence might have occurred to the north in Upper Lanikai between transects 10 and 30. The northern reach of Upper Lanikai began eroding almost simultaneously with Central Lanikai and the southerly propagation of the trend suggests southern longshore drift. There is, however, no major accretion between this erosion center and the erosion in Central Lanikai to support a converging center here. This divergence point could still exist if the relatively low erosion rate in Upper Lanikai was not providing a great deal of sand and the majority of the sand released in Central Lanikai was moved south.

IV. 1964 – 1972

During this period the large accretion in Lower Lanikai becomes an erosive trend that continues throughout the rest of the dataset until the mid-1990's when there is no appreciable beach remaining and seawalls have halted the erosion. During this period the area that was previously eroding in southern Lower Lanikai (transect 100 to 116) and Central Lanikai (transect 30 to 70) began accreting again. To the north, Central Lanikai begins accreting over a broad section of beach while erosion intensifies in Upper Lanikai. Further south, the erosion rate in Upper Bellows (transects 20 – 30) drops sharply, but is preceded by short-lived accretion to the north (transects 0 to 15) and the beginning of a longer accretion trend in Lower and Central Bellows (transects 45 to 85).

The onset of erosion in Lower Lanikai indicates a reduction in sediment supply to that section of coastline. Likewise, the previous current structure had allowed for sand accretion, but no northward drift. During this shift currents were restructured to allow northward movement of the already accreted sand toward Central Lanikai. It is possible to then that the new accretion in Lower Bellows is the result of Upper Lanikai sediments being transported south instead of north. The erosion in Lower Lanikai could be due changes in the nearshore current structure that lead to the rerouting of its sand supply and a simultaneous increase in northward transport along the Lanikai coastline. Another factor to consider is the further expansion of revetments along the Upper Bellows shoreline in response to decades of chronic erosion. Revetments along this reach of shoreline would effectively lockup the sand supply that fueled accretion in Lower Lanikai. If eroded material from Upper Bellows was driving shoreline expansion in this region, this introduction of revetments could explain the lack of large accretion events in the dataset for the Bellows shoreline.

V. 1972 – 1984

Central Lanikai accretes significantly over this time period, accompanied by peak erosion rates in both Lower and Upper Lanikai. Given the timing of erosion in Lower Lanikai, longshore transport is likely moving north from Lower Lanikai to Central

Lanikai during this time period. As with the previous accretion event in Lower Lanikai, the shoreline accretes consistently over one section of beach for 14 years with only a slight northward drift. This is further evidence convergent longshore currents effectively "holding" the sediment in one location and allowing a significant amount of new shoreline to form. If this process is occurring then it can be assumed that the northern component of longshore convergence is transporting eroded material from Upper Lanikai southward.

Upper Bellows shows isolated accretion (transect 15 to 30) that wanes to erosion by the end of the period. Accretion continues in Lower Bellows during the first half of this time period, but later transitions to erosion in all but the most southern region of Lower Bellows. The accretion pattern in Upper Bellows can again be interpreted as local convergence of longshore currents. The southward shift in accretion in Lower Bellows indicates a dominant southern longshore current direction. By this point in time, two jetties are in place at the southern boundary of the Bellows study area. Accretion occurring along the northern boundary of these jetties is likely a farther indicator of southern littoral transport.

VI. 1984 – 1987

Unlike the other periods defined in this section, this period does not reflect a system-wide change in transport patterns. The most notable feature during this period is the gradual expansion and decline of accreting shoreline along the most southern boundary of Lanikai Beach (transects 105 – 116). The rapid switch to erosion along this small reach of shore is an indication that conditions which had allowed accretion changed suddenly. It is necessary to single out this feature as it is important in the next section for the discussion of wind direction. This period also marks the beginning of a northward drift in the accretion and erosion trends in Lanikai.

VII. 1987 – 1995

This period is characterized by a sharp return to erosion across the entirety of the Bellows shoreline and the continued northward drift of the pre-existing accretion and erosion pattern in Lanikai. Central Lanikai begins to experience erosion as the accreting area shifts toward Upper Lanikai.

VIII. 1995 – 2008

The northward shift of accretion observed in Lanikai during the previous two periods continues until all of Upper Lanikai is accreting. Interestingly, the southern boundary of this accretion remains fixed until the most recent shoreline. As erosion in Central and Lower Lanikai continues there is effectively no beach left along the southern coast of Lanikai. The erosion appears to begin near transect 90 in Lower Lanikai and radiate north and south from there. This is a possible indication that nearshore currents are diverging near this point in Lower Lanikai, creating a relatively faster rate of erosion than at the southern edge of Lanikai.

Erosion continues in Upper Bellows until no beach remains. The shape of this erosion trend suggests it is migrating to the south. The reappearance of accretion against the jetty on the southern boundary of Bellows Beach is farther evidence of southern transport occurring during this time.

5.3. Influence of wind direction and sediment supply

Wind direction is identified in the hydrodynamic simulations as having strong possible control littoral sediment transport direction. Figure 18 overlays the time periods defined in Figure 17 on the record of wind direction. The close degree of fit between shoreline movement and changes in wind direction indicates wind is a likely driving force behind the fluxuation in transport direction along the Lanikai-Bellows shoreline.

These results show that the material accreted in Lanikai during the 1950s through to the 1970s was eroded from the Bellows shoreline. While wind direction seems to play an important role in transport on this coastline, the influence of coastal hardening must also be considered. The north Bellows shoreline is currently hardened by coastal revetments. These revetments were constructed in Bellows to halt the erosion of the shoreline that has occurred over much of the 20th century. Given the sediment exchange between Bellows and Lanikai documented in this study, it is likely that the source of accretion in Lanikai was cut off by revetment construction.

The effect of Bellows revetments can be seen in periods III, IV, and V in Figure 17. Wind direction in period III was inducing transport from Bellows to Lanikai. This transport was shutdown by more northerly winds during period IV (Figure 18) and during this time Bellows began seeing isolated sediment accretion along reaches of beach that could remain stable under that wind direction. In period V winds once again became more easterly, which reestablished the northern Bellows-to-Lanikai transport pathway, but much sediment was impounded within the Bellows shoreline by the revetments. This resulted in little sediment entering Lower Lanikai to replace the sand that migrated north to Central Lanikai, which eventually lead to a major sediment deficit in Lower Lanikai. This presents a situation in which erosion is caused by a lack of sand supply not a lack of a mechanism to move the sand. Understanding the interplay between wind direction, littoral transport, and sediment supply gives coastal managers of this area, and potentially any other windward shoreline, a strong foundation on which to build a remediation plan to control coastal erosion.

5.2 Evaluation of methods

5.2.1 Hydrodynamic modeling

While it is changes in wind direction can be correlated with changes in erosion/accretion patterns, understanding the exact physical mechanism for driving these changes is more difficult. Tradewind direction has been near perpendicular to

Lanikai-Bellows shoreline. It stands to reason then that small changes in wind directions could produce relatively large changes in littoral current configuration. We use a hydrodynamic model to predict these possible littoral current patterns and understand beach change in context of dominant wind direction.

Results of the hydrodynamic model (Figures 14, 15, and 16) show a relationship between the increasing northern component of trade winds and the existance of southerly littoral currents and more complex flow patterns. Littoral convergence and divergence creates an overall more dynamic shoreline over time. For example, period II is characterized by consistent erosion of Bellows and accretion in Lanikai under easterly winds, which the model shows will create mostly northern littoral currents (Figure 16). During period III winds become more northerly, introducing a more complex littoral currents (Figure 15) which lead to more discrete areas of accretion and erosion. During this time the concentration of sediment in Lower Lanikai is at the presumed expense of Central Lanikai. Period IV shifts the winds further north, which is accompanied by a shut down of accumulation and possible reversal of transport direction in Lanikai. This period of more northerly wind, during which north transport seems weaker and less uniform, could be the cause of stabilization and accretion on the Bellows shoreline.

Winds return to a more eastern bearing in Period V. This shift is accompanied by a renewal of northern transport in Lanikai, but an accumulation in Central Lanikai as apposed to Lower Lanikai. This illustrates the potentially high degree of sensitivity this system has to wind direction, as the actual different between winds in period III and V is slight (period V is more eastern by approximately 5 degrees). Not seen in the hydrodynamic model is a southerly longshore current in Upper Lanikai. A possible reason for this discrepancy is that the model does not perform as well in close proximity to the model boundary. This missing southerly trend could be the result of an accounted for influence from neighboring Kailua Bay.

Period VI shows a rapid and short lived spike in wind direction toward the northeast. During this period, a small area on the southern boundary of Lanikai accretes as through a mini-convergence zone has developed on Wailea Point. This convergence near the Point is predicted to happen in northeasterly winds by the hydrodynamic model (Figure 16). As the wind shifts to a more easterly bearing, this small accretion area also disappears, further indicating the relevance of the modeled predictions.

5.2.2 Grain-size trend analysis in coastal change studies

The combined results of the historical shoreline and hydrodynamic modeling provide both an empirical record of change and process information. The GSTA results further support the transport pathways established by these other two methods. Figure 19 shows a combined interpretation of both GSTA methods. The points of divergence or convergence on Figure 19 are approximately transects 10 and 30 in Bellows and transects 110, 90, 70 in, transect 90 in Lanikai. It is important to note

many of these points of littoral transport divergence and convergence are similar between all three datasets.

An interesting secondary observation is a chance to evaluate how GSTA integrates the signal of multiple overlapping and sometimes opposite transport trends into a single transport pattern. The question of what time frame GSTA results represent can be addressed in this study by comparing the result to the historical shoreline change record. Comparing Figures 17 and 19, it is evident that the GSTA results of the Lanikai-Bellows shoreline retains an integration of all major littoral processes from approximately 1964 (Period IV) to present (Period VIII). The beginning of erosion in Lower Lanikai (Period IV, transect 90) is recorded as a diverging trend over the same area in Figure 19. The northern edge of the GSTA sample area shows convergence in Central Lanikai in the same location that accretion has been observed in the historical record (Periods IV, V, VI; transect 70). Sediment accumulation on either side of Wailea Point, two-way transport around the Wailea Point, and the offshore gyre observed in modeling results in northeast winds (Figure 14) are also represented in the GSTA results. In Upper Bellows, diverging littoral transport is shown in the GSTA results at transect 30. This area of shoreline shows a diverging trend during Periods IV and VIII in the historical results. In the offshore a general northward trend exists, most likely reflecting the dominate mode of northward wind driven transport in this region.

The results of this study indicate that grain-size trend analysis can be a useful component of a coastal sediment budget if nearshore transport vectors are used as indicators of dominant longshore transport direction. The transport vectors obtained from GSTA of the benthic sediment shows that grain-size transport signatures persist even after the original transport process has stopped. This would need to be accounted for when interpreting GSTA results in sediment systems that have experienced multiple transport patterns through time. GSTA serves a valuable role as “ground truthing” transport pathways that can be hypothesized from models and historical results. It can also be used to identify possible littoral cell boundaries and test for the possibility of transport between littoral cells.

The Lanikai-Bellows shoreline has experienced a number of transport patterns in recent decades. The GSTA results contain many of the transport patterns known to have existed at the Lanikai-Bellows. It is possible that shorelines which have undergone a number of different transport patterns will all encounter trend that are no longer active. Over all GSTA proved valuable for defining major areas of transport activity, evaluating the complexity of transport in a region, and validating the results of the hydrodynamic model.

5.3 Directional changes in the wind record

The cause of the decadal directional shift in trade winds is not fully understood. A potential explanation for the directional shifts might lie in small shifts in the North Pacific High pressure system, north of the Hawaii islands. This system already controls the occurrence of Kona storms in Hawaii. It is possible that influence of a

decadal scale cycle, such of Pacific Decadal Oscillation could be effecting the North Pacific High and resulting in the directional shifts seen in the data.

6. CONCLUSIONS

This study integrates sedimentological data, hydrodynamic computer modeling, historical shoreline change analysis to investigate the dynamics controlling enigmatic and large coastal change on Lanikai-Bellows shoreline. The results of the study show wind direction to be a major controlling factor in the patterns of shoreline movement. Most major accretion and erosion events can be linked to periodic shifts in the dominate tradewind direction. Revealing this aspect of the Lanikai-Bellows beach system represents a major step in the creation of a regional sediment budget and allows an excellent opportunity to practice integration of multiple analysis techniques. We reveal the hypothesis of sediment transfer across Wailea Point to be true, indicating Bellows Beach and Lanikai Beach are dynamically linked.

The availability of historical shoreline records allows for a powerful empirical comparison point to evaluate and intemperate the results of GSTA. In general, GSTA results reveal in select elements of a 40-year period of shoreline change and identified most the major transport trends also seen in the historical and hydrodynamic results. This study also represents the first use of sediment trend analysis to study coastline change and has revealed the underlying processes that form the resulting trends using by the analysis.

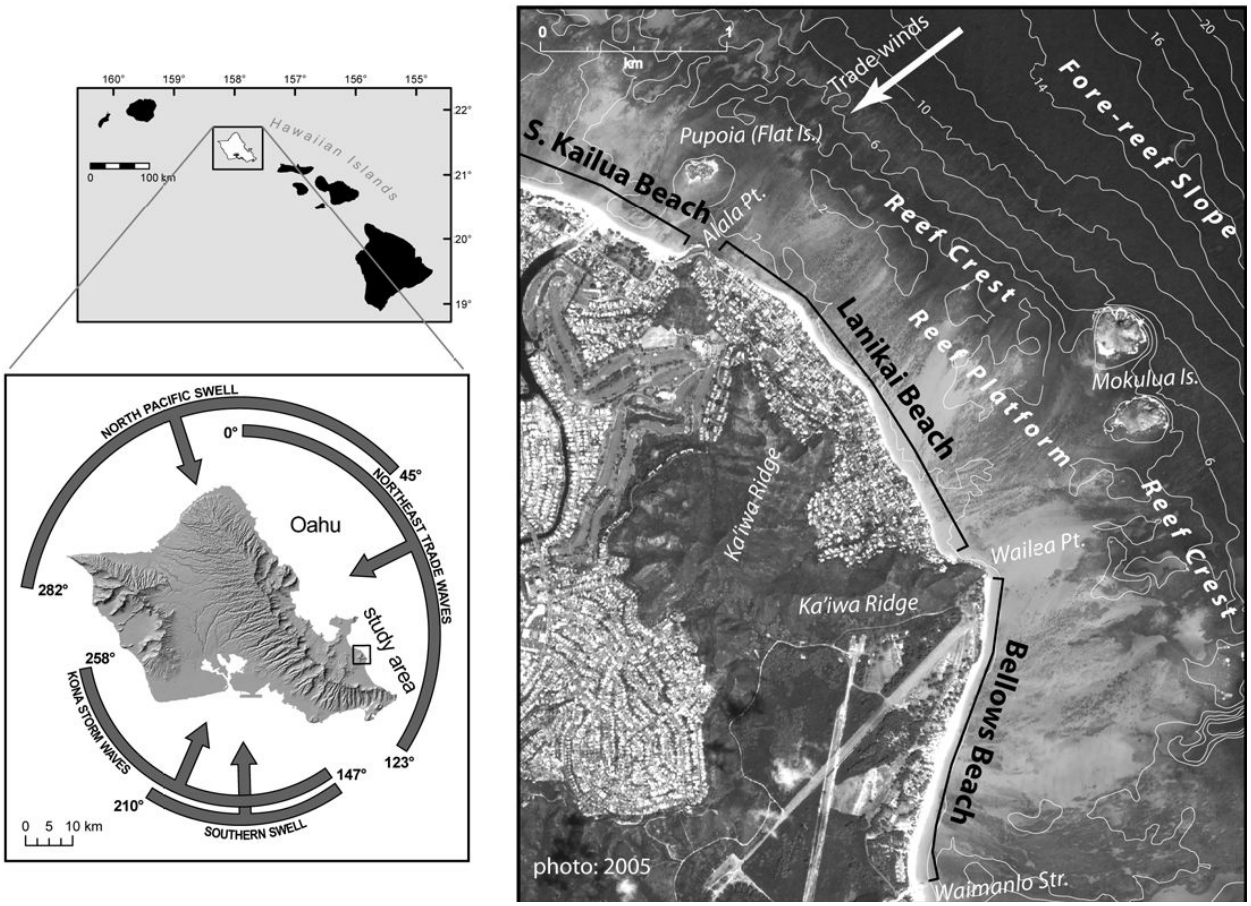

Figure 1. Study area. Bathymetric contours are in meters.

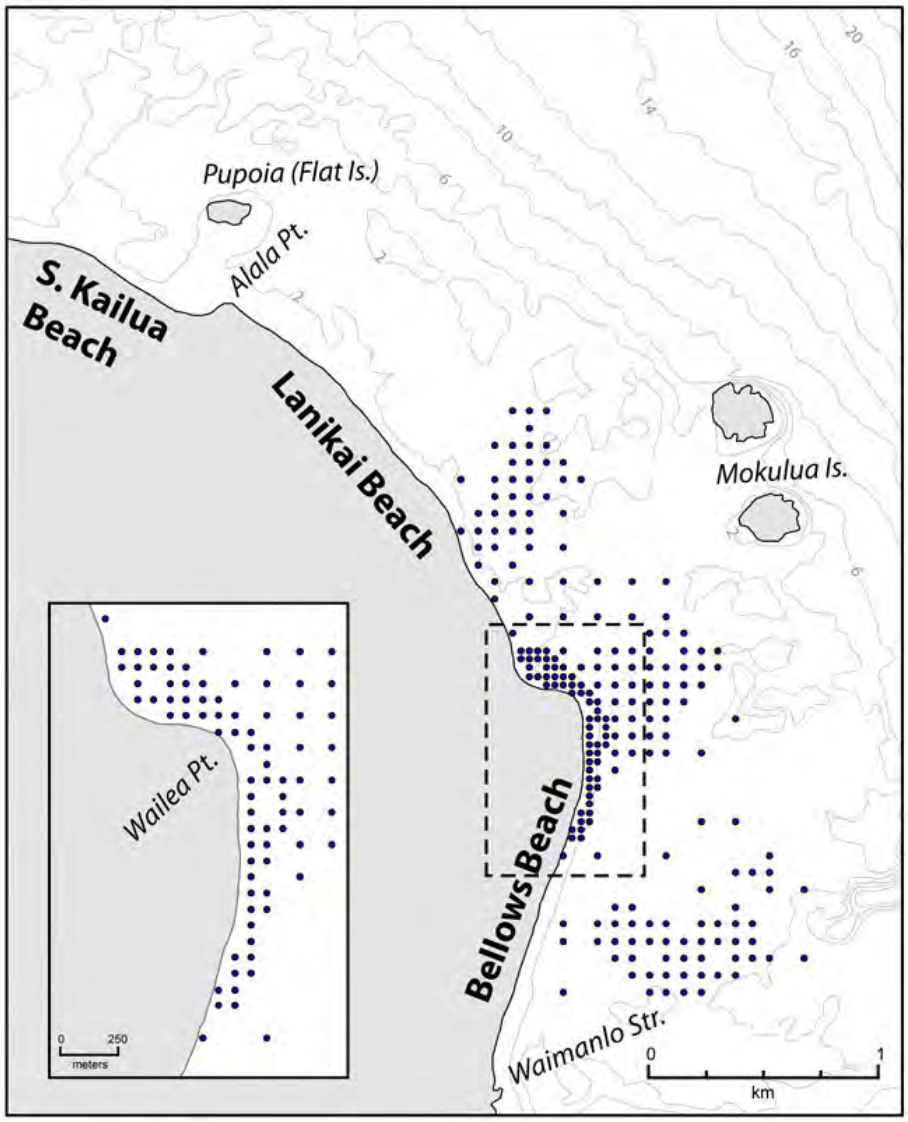

Figure 2. Location of surficial sediment sampling sites for sediment grain size trend analysis. Inset: samples in the vicinity of Wailea Pt.

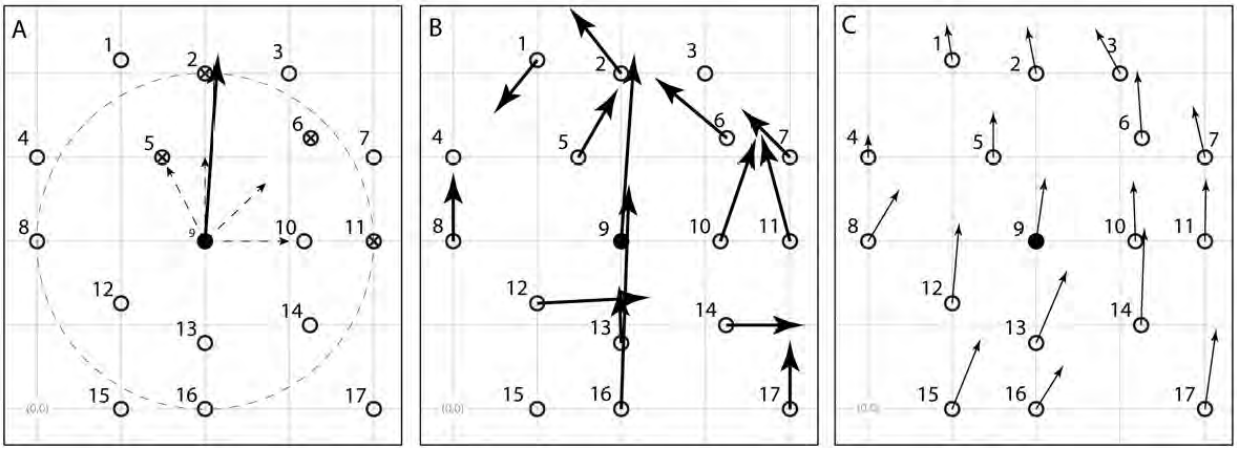

Figure 3. Gao-Collins method for determining sediment transport. See Appendix A for data and calculations used in figure. A) Illustration of transport determination at site 9 with characteristic distance equal to 2 (dashed circle). Circles represent sampling sites; those containing "x" show either a trend 1 or trend 2 relationship in grain size parameter with site 9. Dashed arrows indicate component unit vectors (length = 1) drawn in the direction of each trend positive site, while the bold arrow is the summation of the component vectors. B) The process is repeated at each site producing a transport vector field, which is filtered (C) by averaging adjacent vectors.

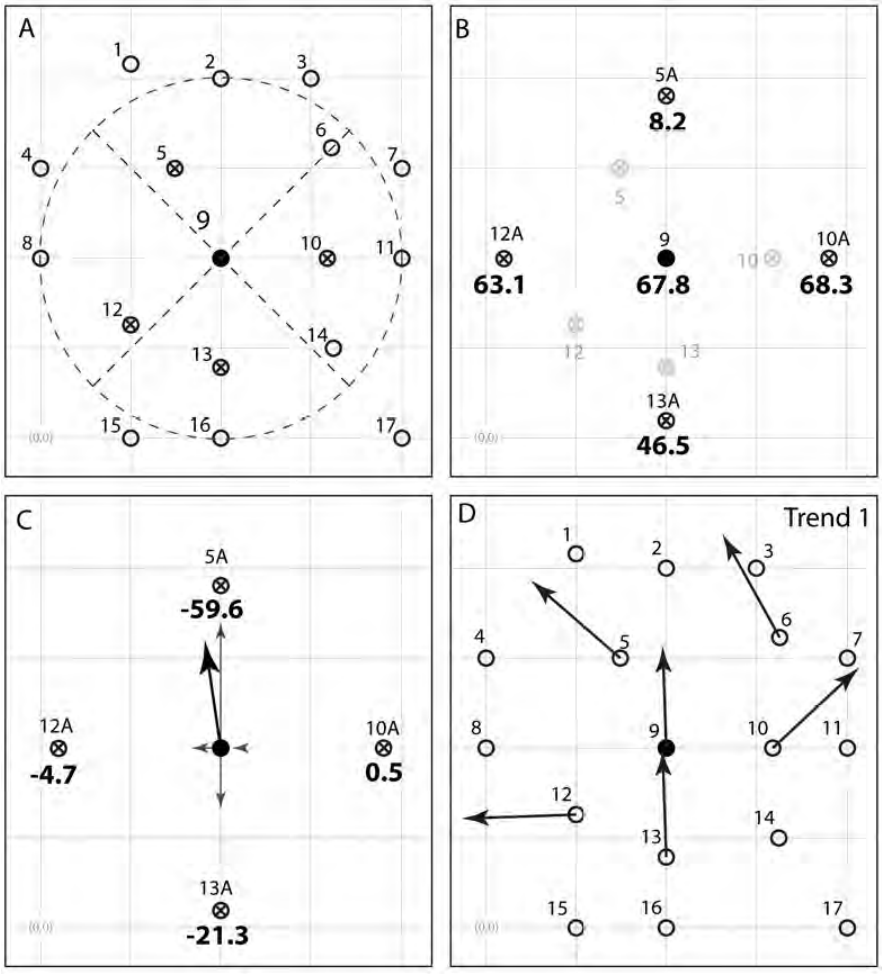

Figure 4. Le Roux method for determining sediment transport. Grain size parameters are identical to those of Figure 3. This method considers each trend type separately, only Trend 1 is considered in this example. A) The closest site in the Northern, Eastern, Southern, and Western quadrants is selected for used; dotted lines illustrate quadrants and "x" on a site indicates selection. B) All sites are transformed to lie at an equal distance of the central site on the cardinal radials; site 5 is at the position of site 5A, 10 is moved to 10A, etc. Grain size parameters are modified to reflect the new positions and summed using the appropriate form of equation (1) for the trend type being investigated. C) The value of the central site is subtracted from all sites. The resulting values indicate transport magnitude in each direction, with negative values indicating transport away from the central site and positive values towards the central point. Summation of component vectors determines the final transport vector. D) The process is repeated at every site with available adjacent sites to produce a vector field for that trend type.

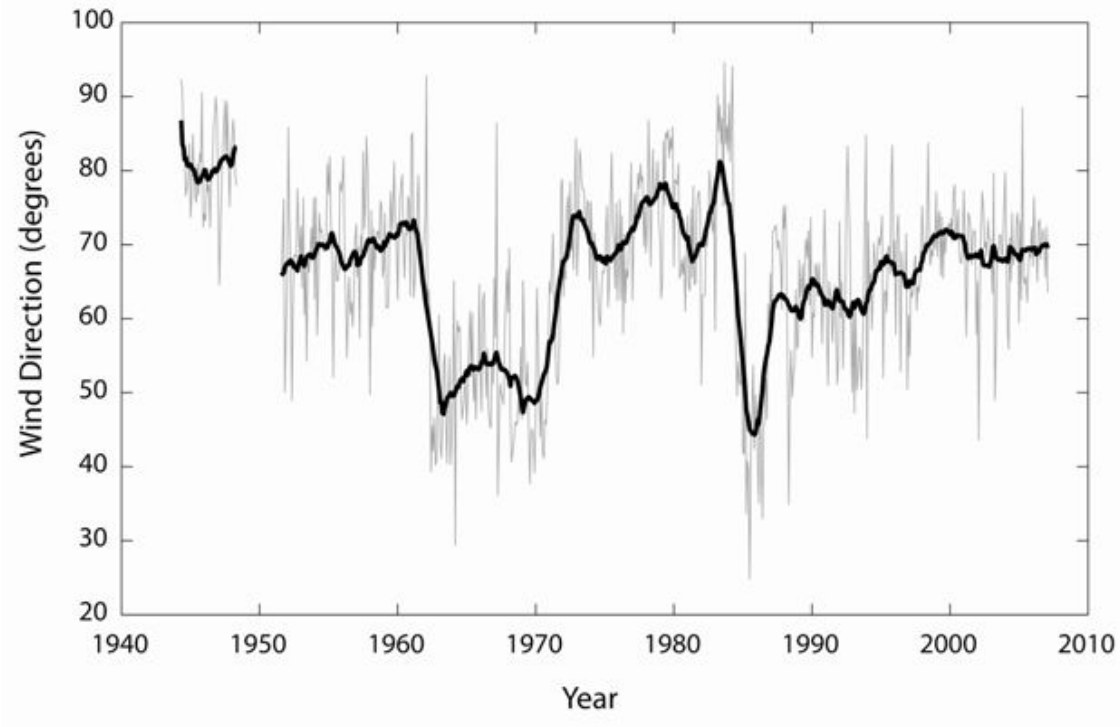

Figure 5. Directional wind data from Kaneohe Marine Corps. Air Base. Values range between 1 and 135 degrees.

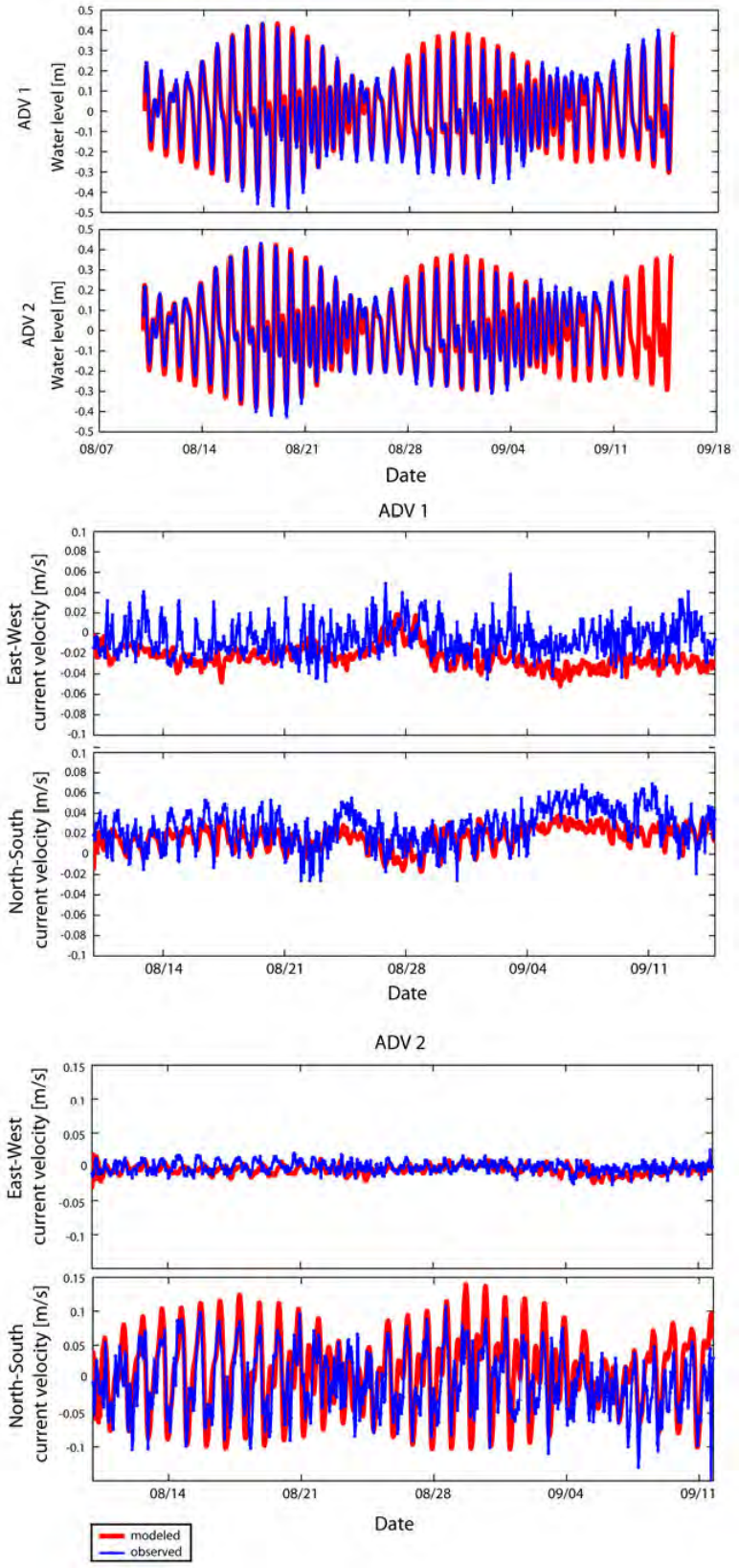

Figure 6. Sea level and wave energy calibration for ADVs.

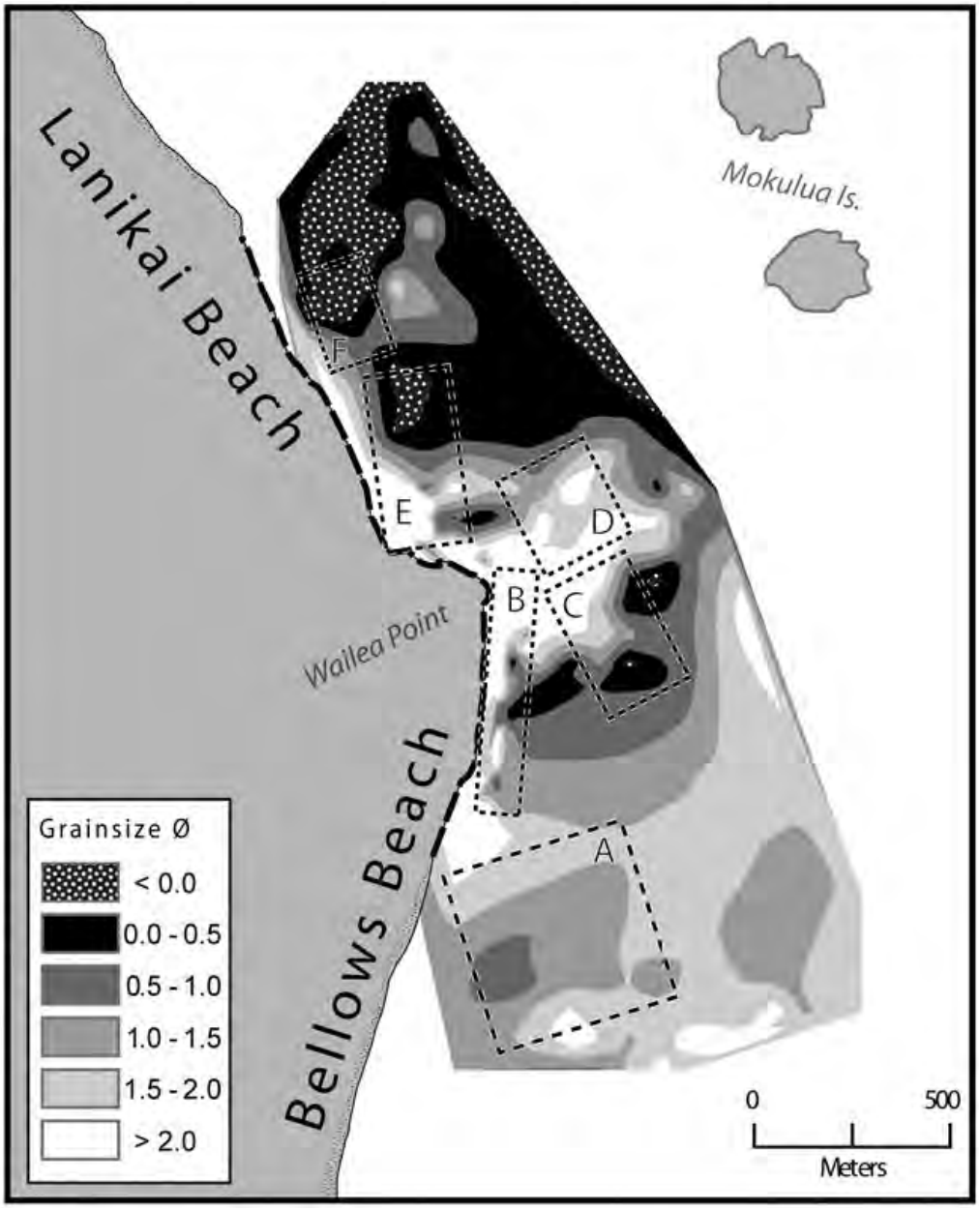

Figure 7. Mean size, sorting, and skewness interpolated from seafloor sediment samples.

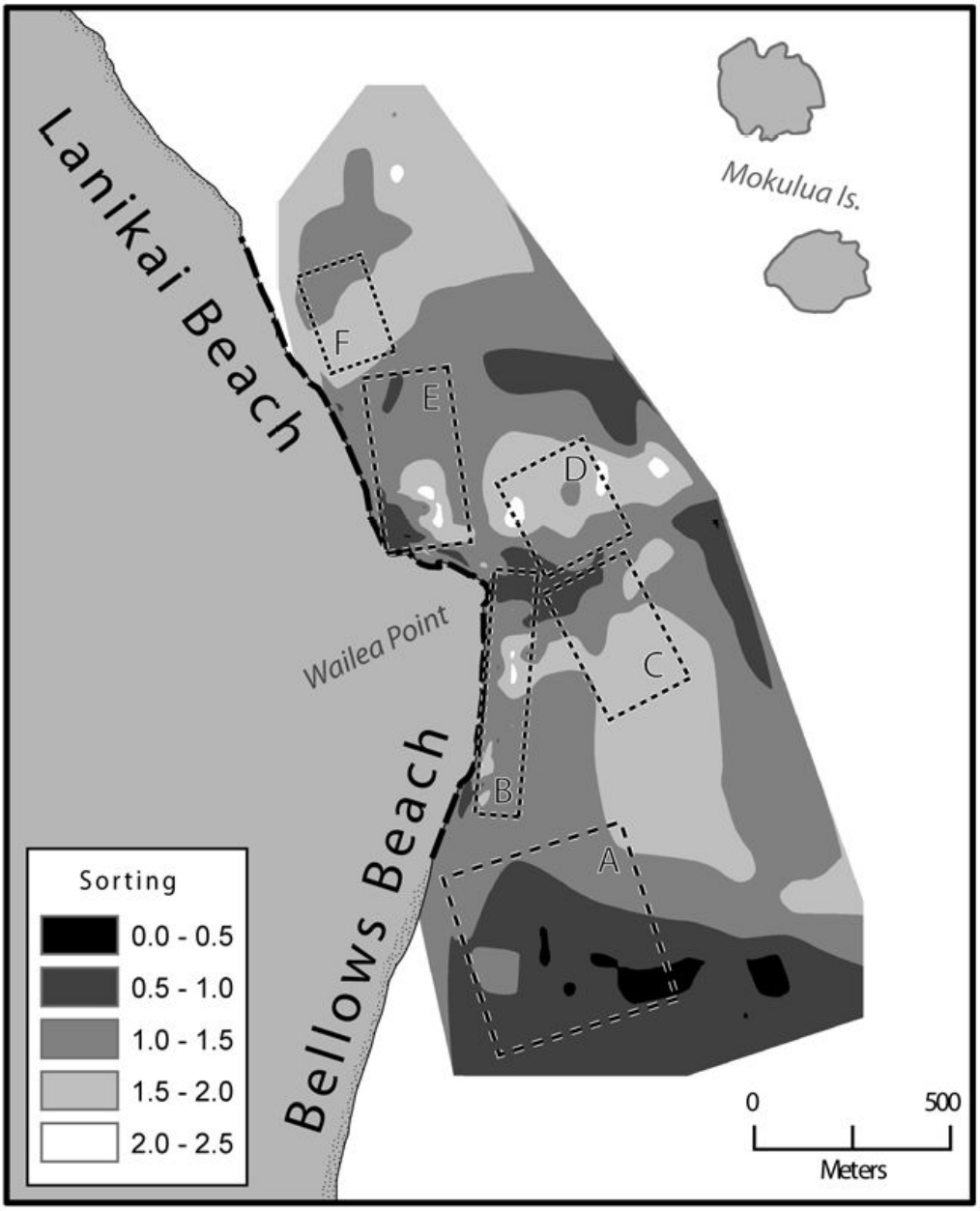

Figure 8. Results of Gao-Collins method for sediment grain trend analysis.

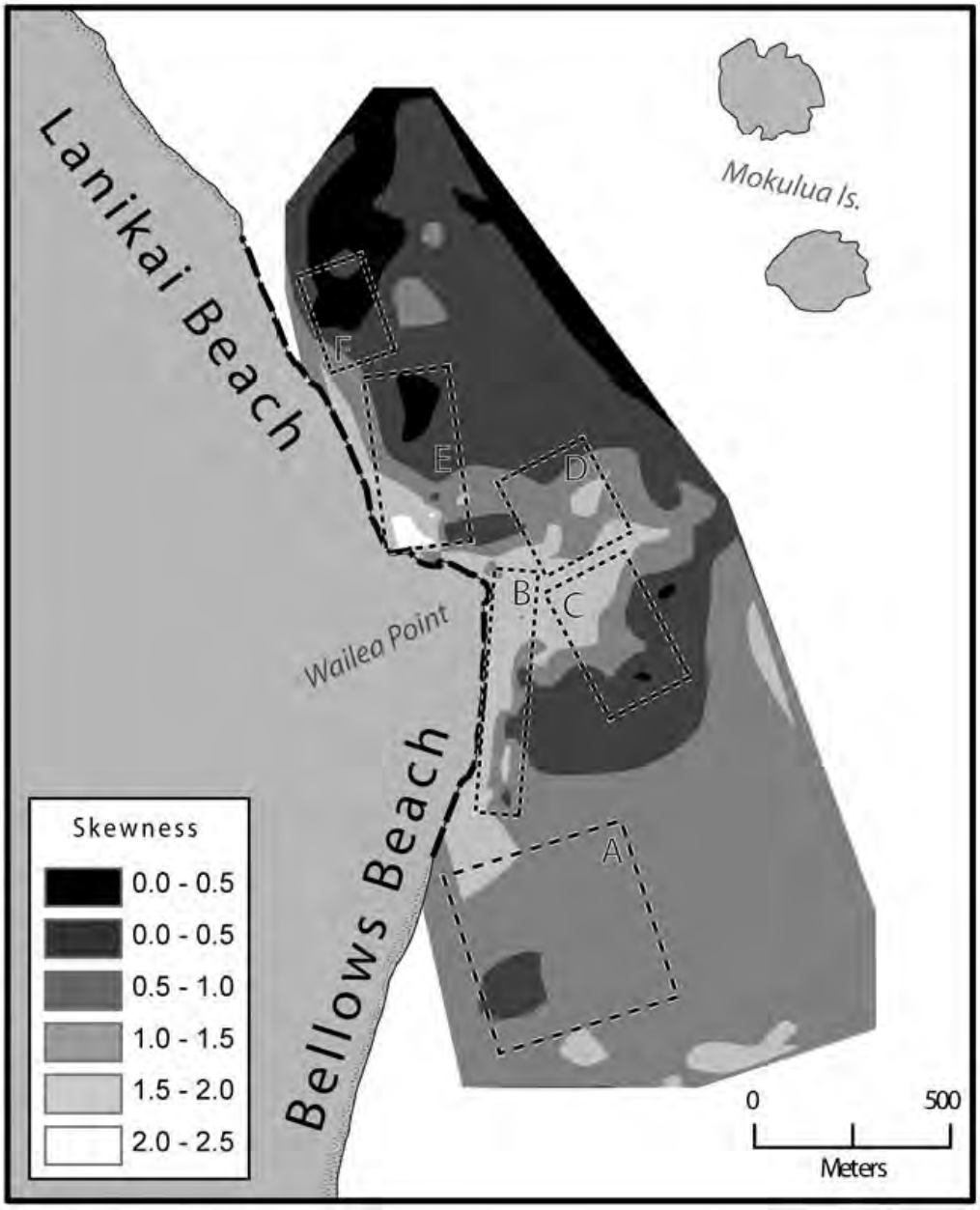

Figure 9. Results of Roux method for sediment grain size trend analysis.

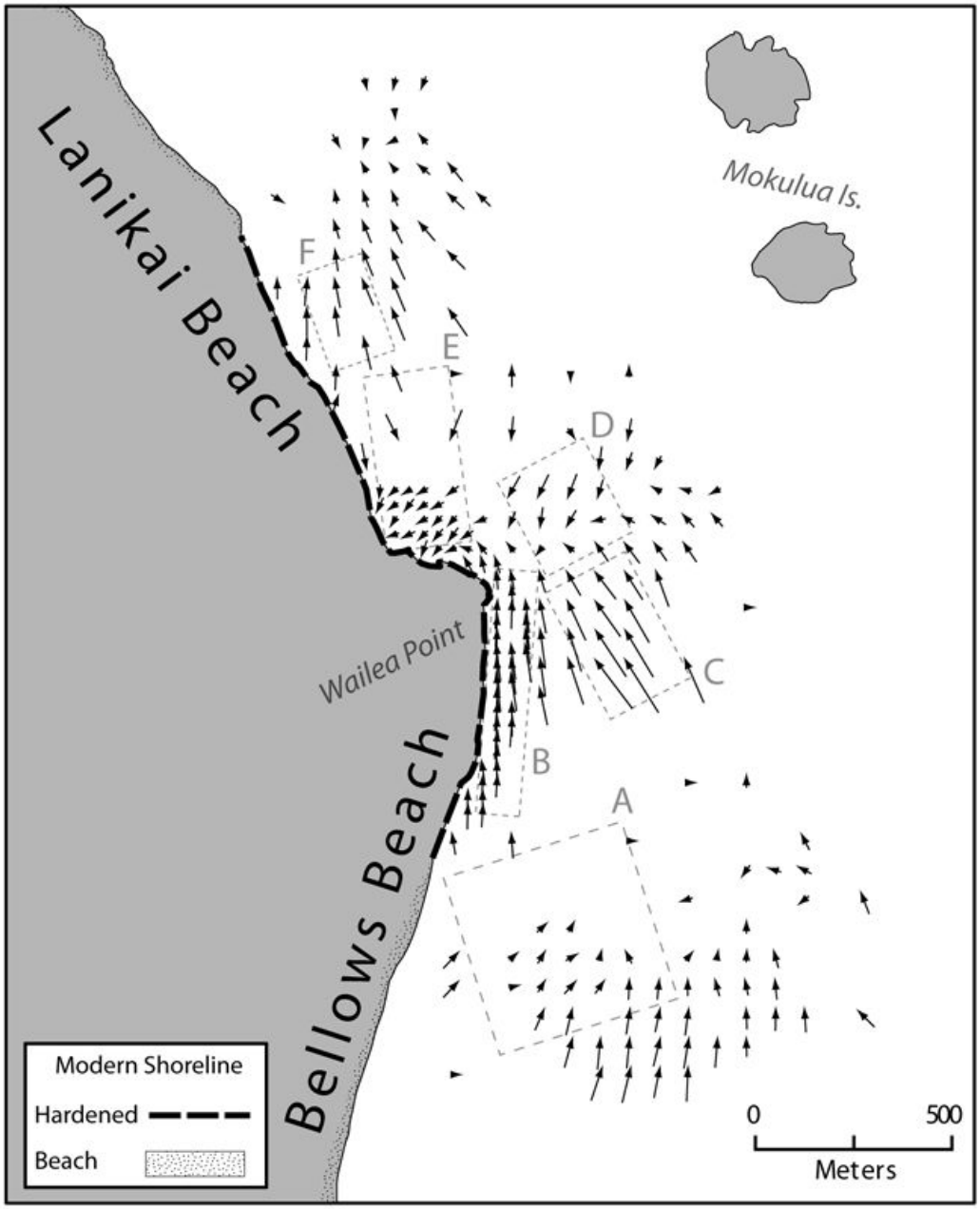

Figure 10. Gao-Collins sediment grain-size analysis results.

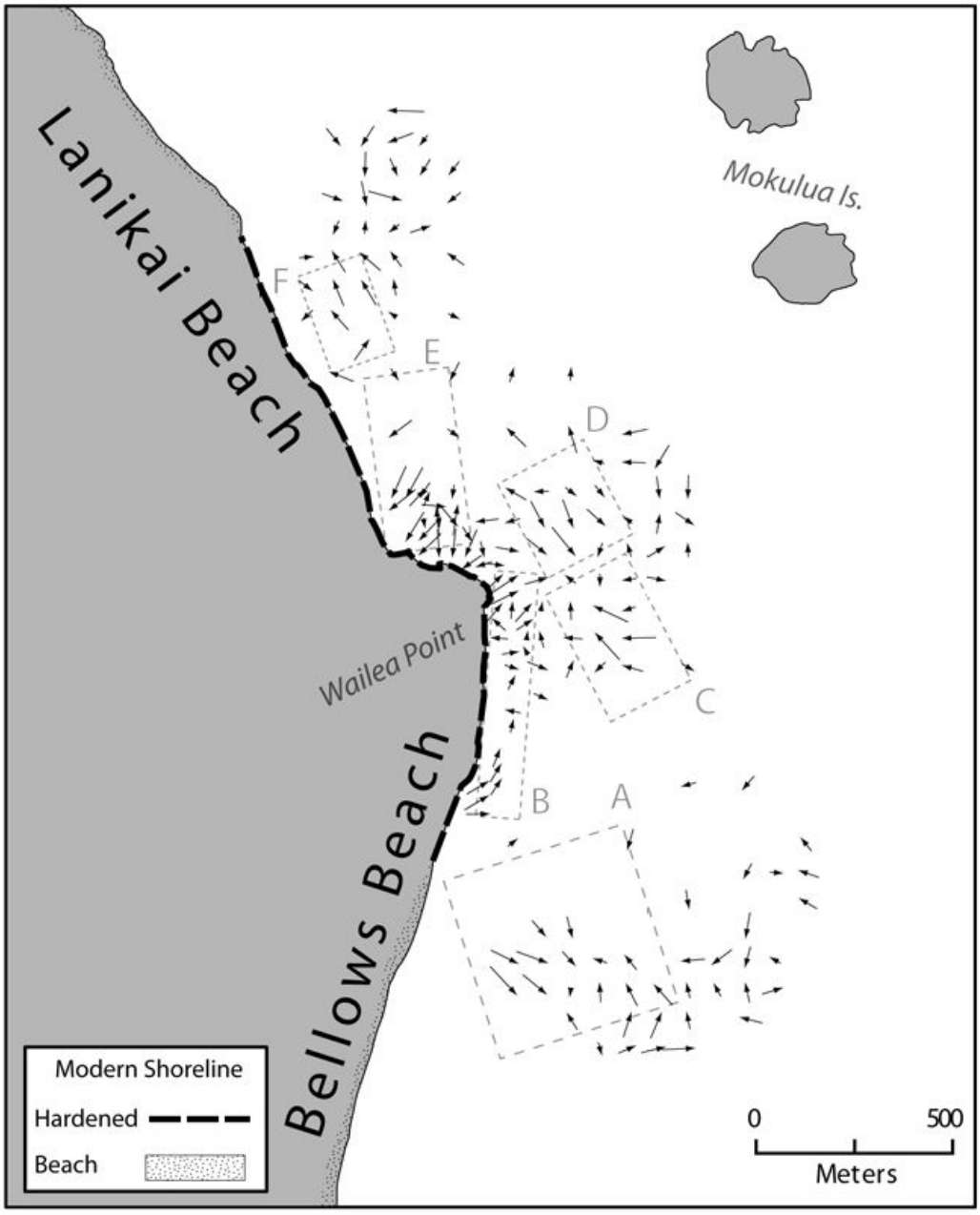

Figure 11. Le Roux sediment grain-size analysis results.

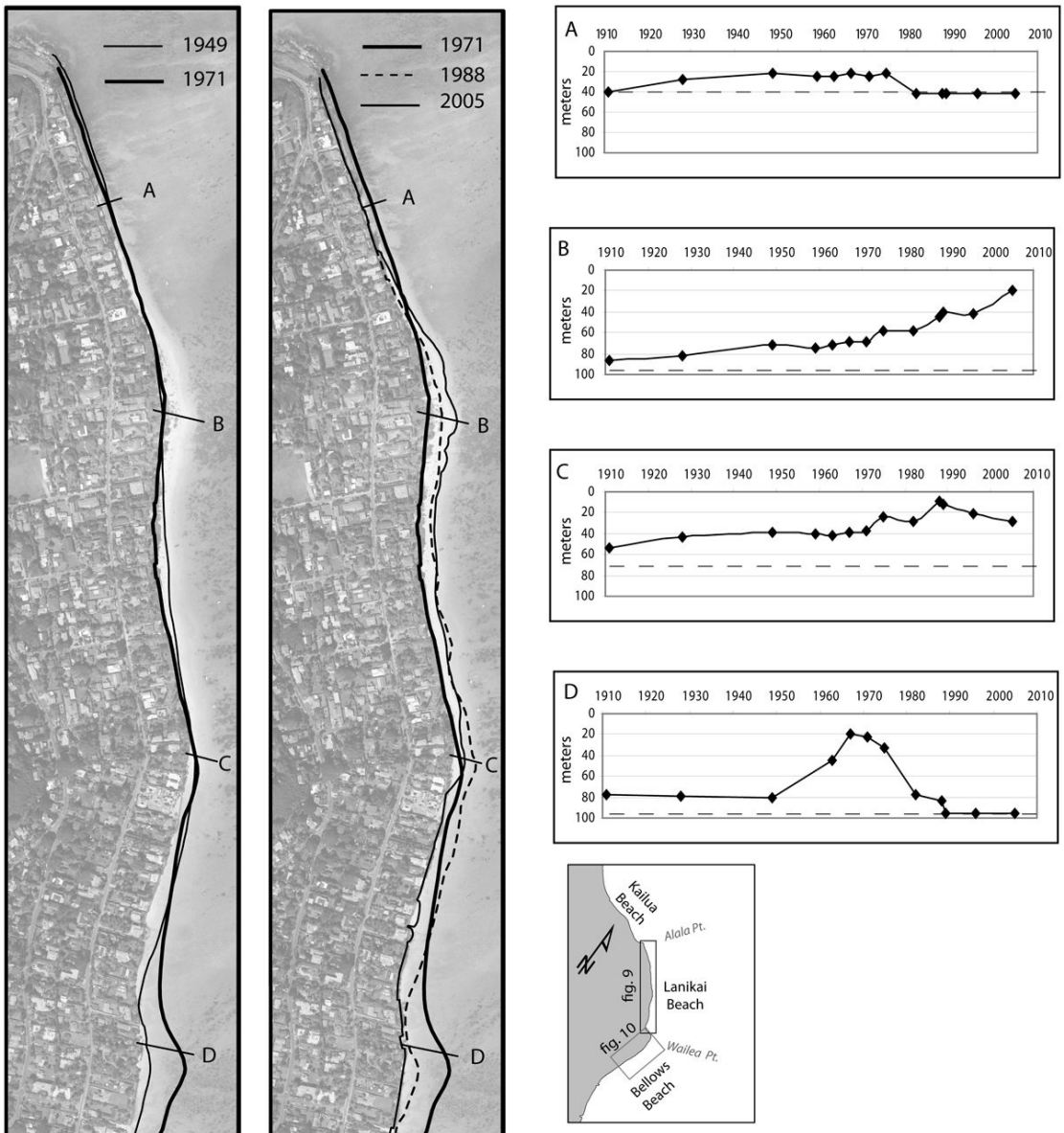

Figure 12

Figure 12. Summary of historical shoreline position at Lanikai Beach. Graphs A, B, C, and D show representative datasets for each corresponding transect location. Positions are given as meters from an offshore baseline, thus positive shifts indicate accretion and negative shifts erosion. Gray boxes track the development of a sudden accretion trend. Left map shows a period of accretion in Southern Lanikai (1949 – 1971). Right map shows erosion trend in the South Lanikai and subsequent accretion at central Lanikai.

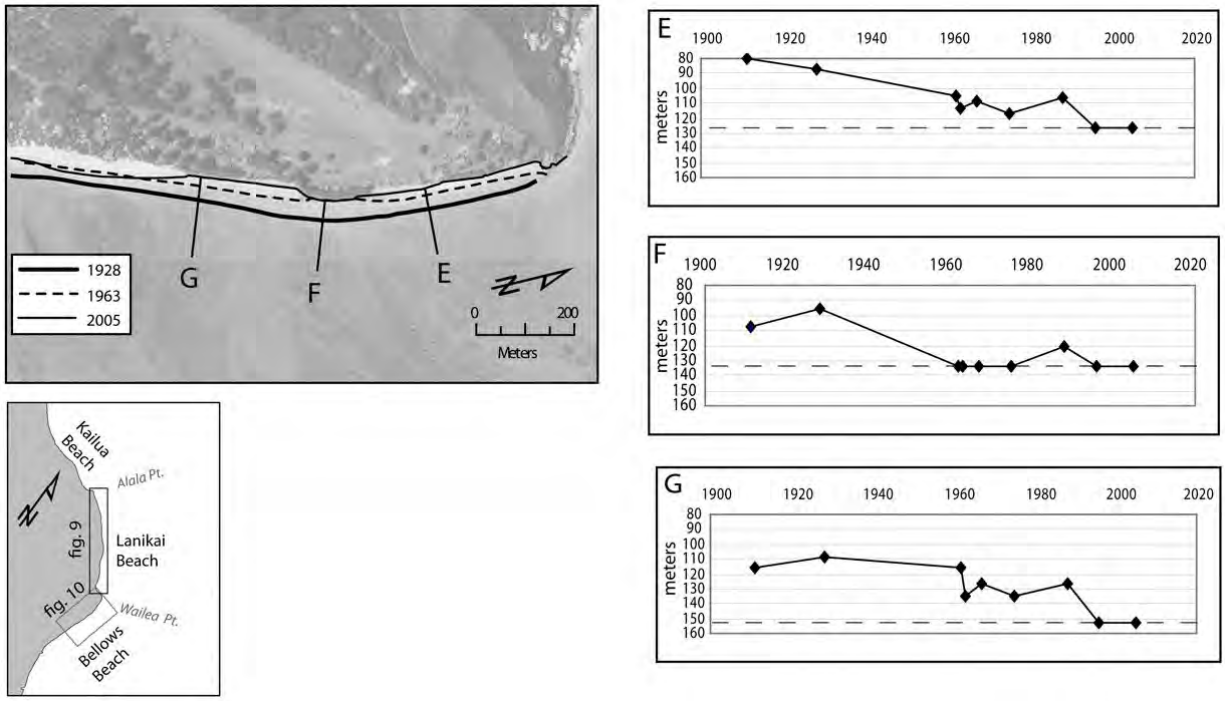

Figure 13. Summary of historical shoreline position at North Bellows Beach. Graphs A, B, and C show representative datasets for each corresponding transect location. Positions are given as meters from an offshore baseline, thus positive shifts indicate accretion and negative shifts erosion. Map shows persistent erosion across region. Arrows mark beginning of seawall construction in response to erosion.

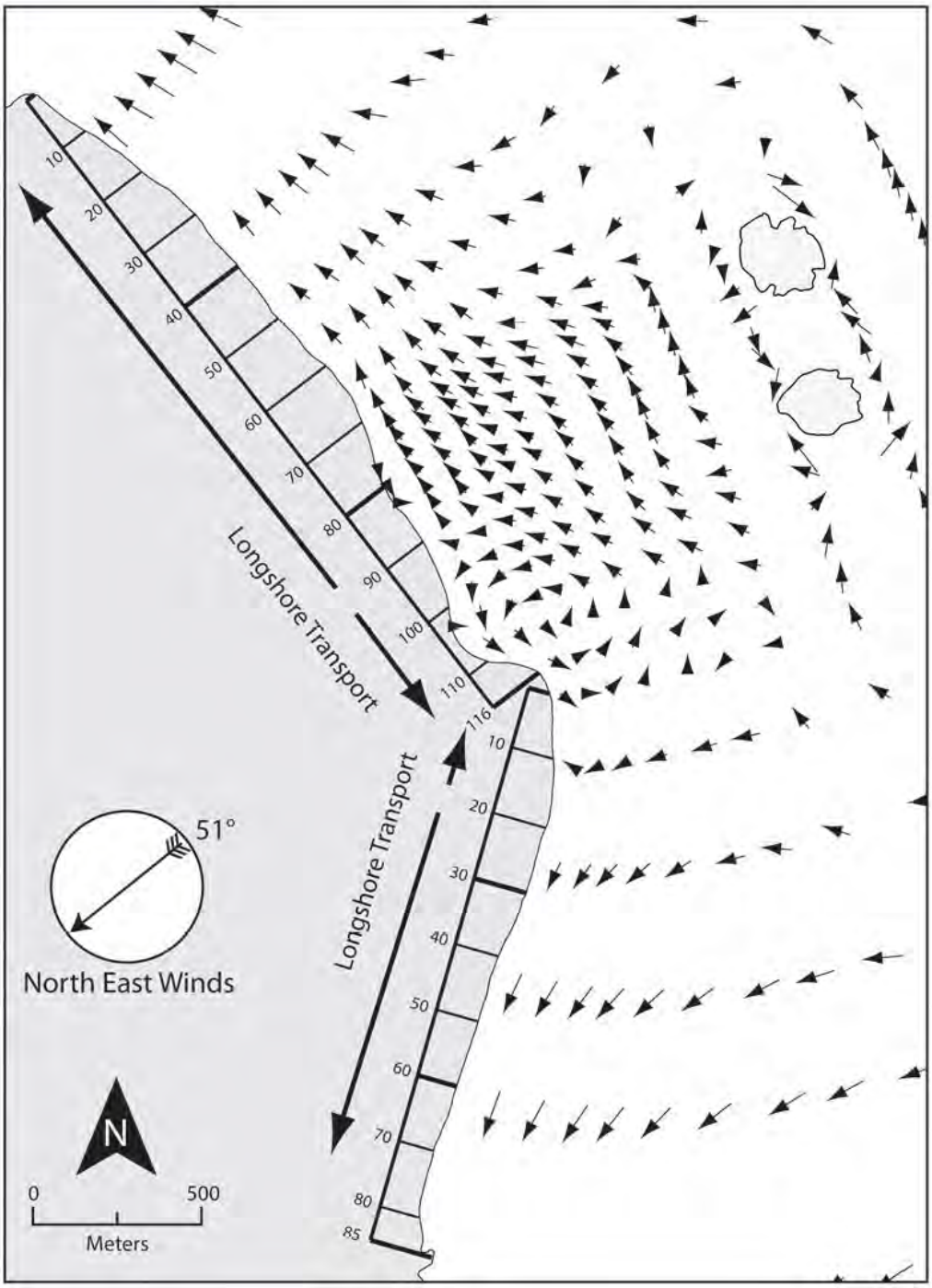

Figure 14. Hydrodynamic model result for 51 degree winds.

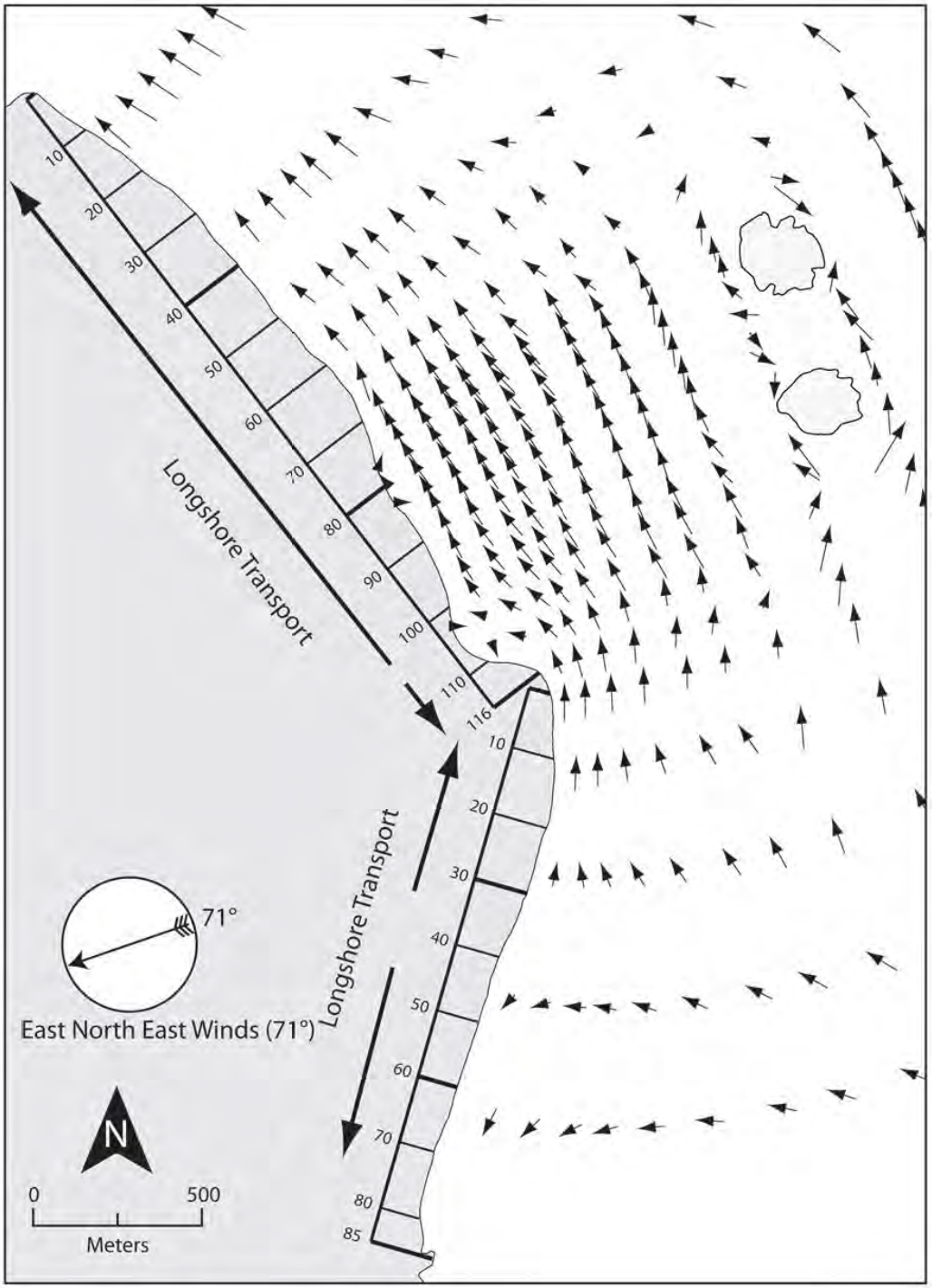

Figure 15. Hydrodynamic model result for 71 degree winds.

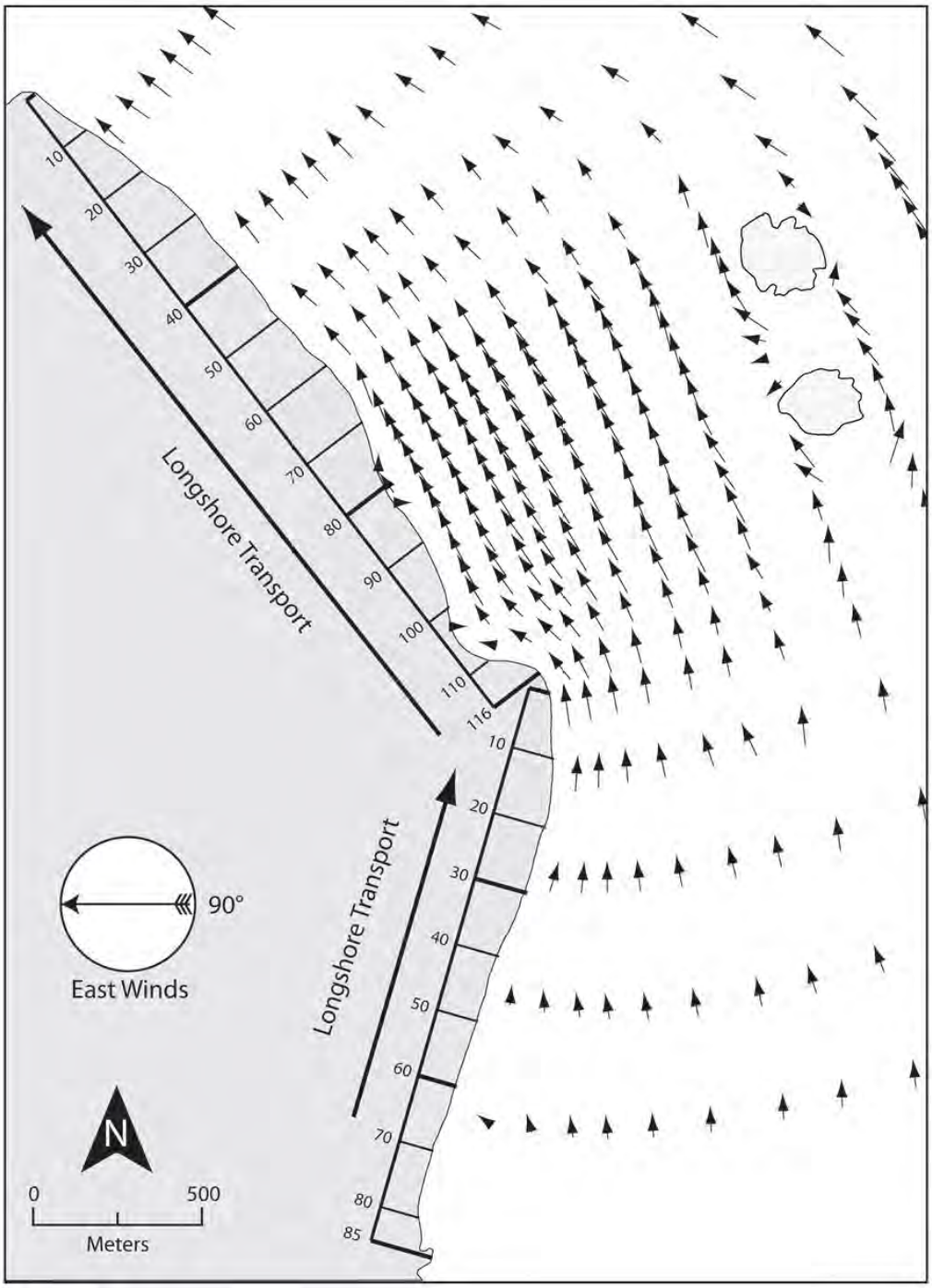

Figure 16. Hydrodynamic model result for 90 degree winds.

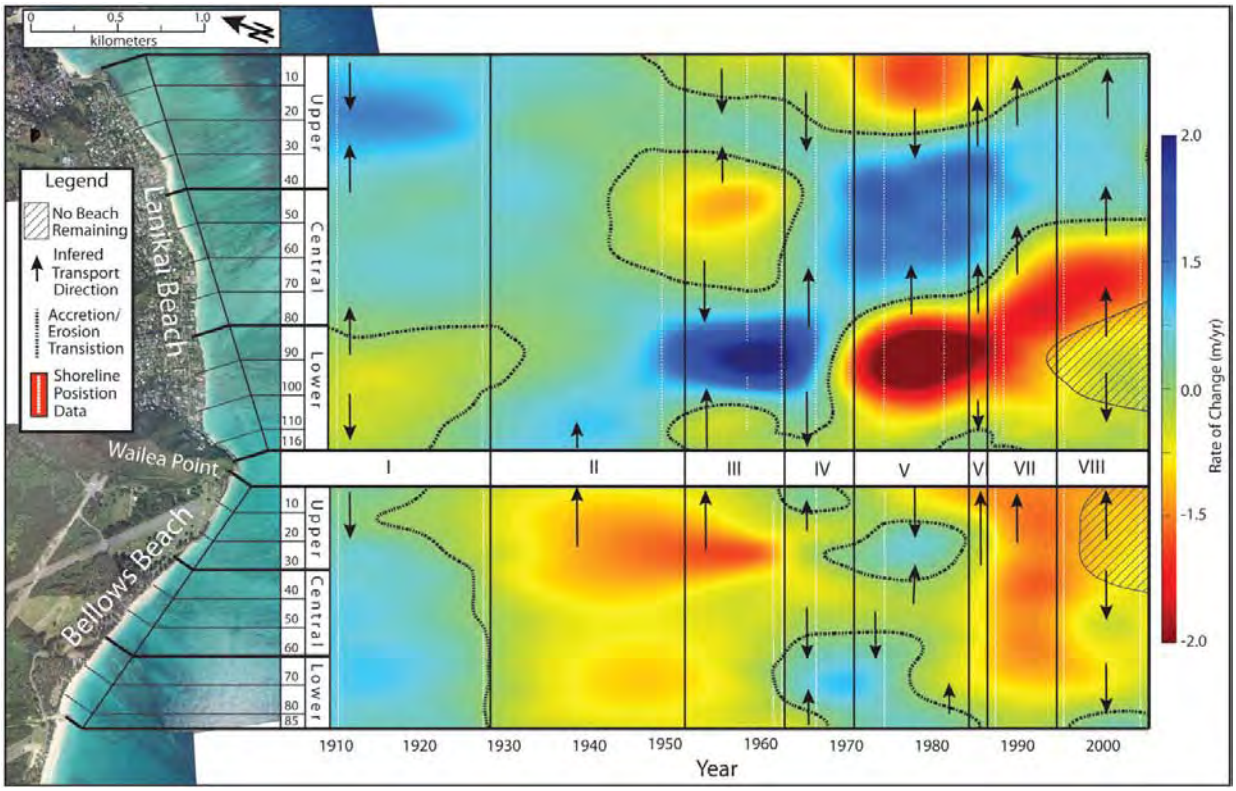

Figure 17. Historical Shoreline record for Lanikai-Bellows beach. Red indicates erosion rate, blue indicates accretion rate.

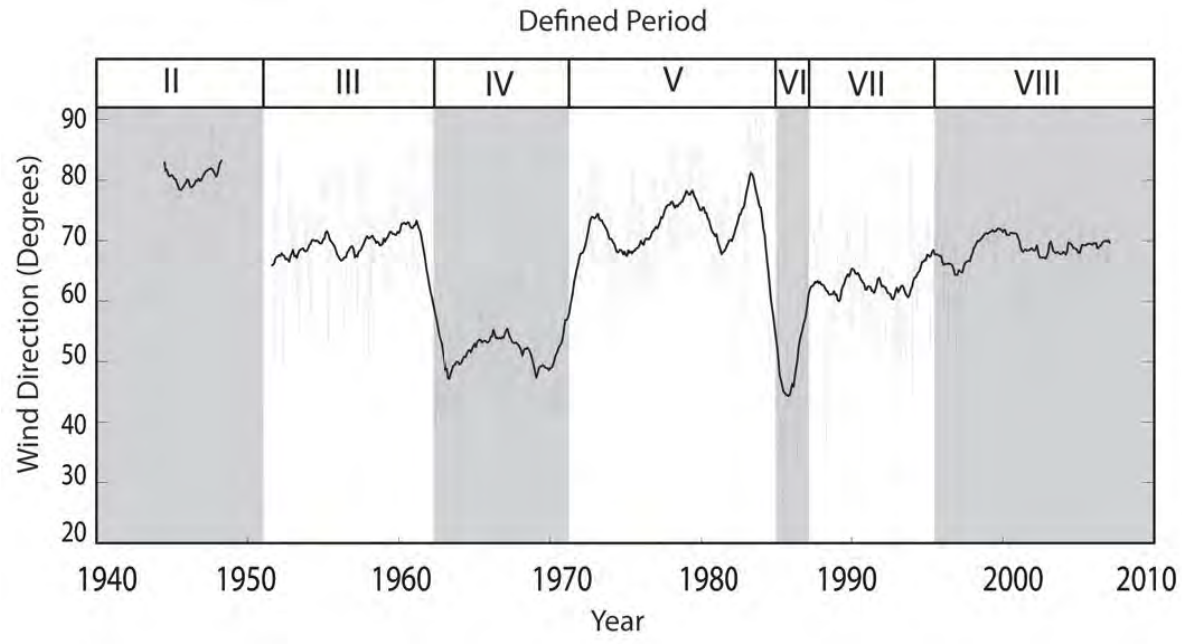

Figure 18. The wind record showing divisions used to separate period of like sediment transport.

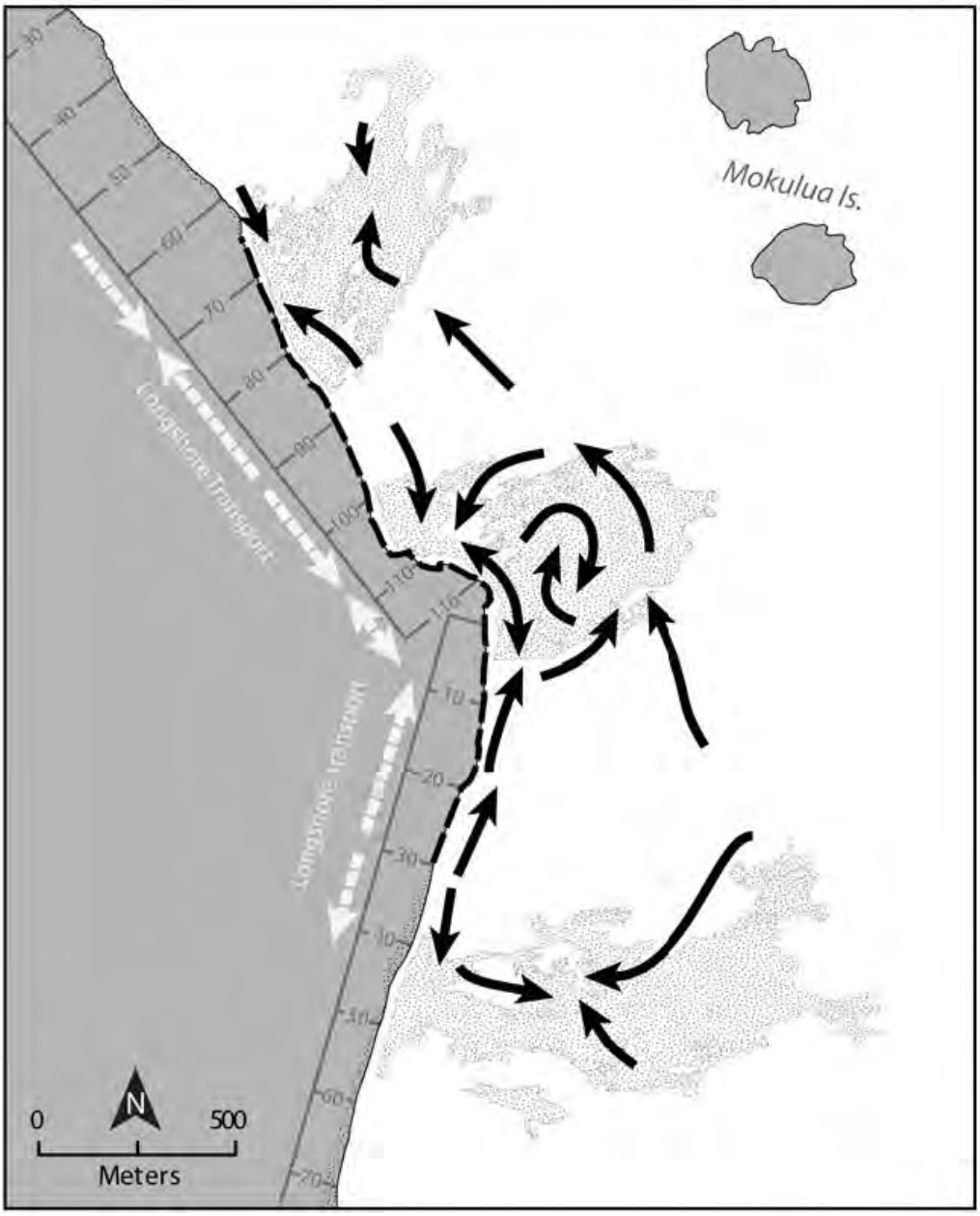

Figure 19. Combined interpretation of results from Le Roux and Gao-Collins methods.

APPENDIX A

Figure 8 illustrates the Gao-Collins method. This appendix details the application of the Gao-Collins method to a synthetic dataset. Calculations associated with site 9 are included.

Table 1. Coordinates and grain-size data for the calculations used in Figure 7.

Site			mean	sorting	skewness	Trend Type*	Component Vector*	
I	X_i	Y_i	μ	σ	Sk		$r(x)_i$	$r(y)_i$
1	1	4.25	-0.5	1	1.2	-	-	-
2	2	4	0.3	1	0.8	1	0	1
3	3	4	-1	0.8	1.5	-	-	-
4	0	3	0.2	0.3	0.7	-	-	-
5	1.5	3	1	0.8	0.9	1	-0.45	0.89
6	3.25	3.25	-0.7	1.1	1.3	2	0.71	0.71
7	4	3	-1.2	0.9	1.8	-	-	-
8	0	2	-0.1	0.5	1.5	-	-	-
9*	2	2	-0.3	1.4	1.1	-	-	-
10	3.2	2	-0.9	1.6	0.7	-	-	-
11	4	2	-0.9	1.3	1.4	2	1	0
12	1	1.25	-0.8	1.8	1.3	-	-	-
13	2	0.75	-0.7	1.3	0.5	-	-	-
14	3.25	1	-0.4	1.7	0.9	-	-	-
15	1	0	-0.5	1	1	-	-	-
16	2	0	1	1.7	0.8	-	-	-
17	4	0	-0.7	1.4	1	-	-	-

*Trend type and component vectors calculated in table for site 9 only.

Step 1. Determine which sites are within the characteristic distance from the site of consideration (site 9). In the example, the characteristic distance is equal to two, which encompasses ten sites: 2, 5, 6, 8, 10, 11, 12, 13, 14, and 16.

Step 2. Check for the existence of trends 1 or 2 between the central site (site 9) and the proximal sites listed above. Trend 1: sites 2 and 5. Trend 2: sites 6 and 11.

Step 3. Define component vectors $r(x,y)_i$ between the central site and those showing a transport trend. All component vector magnitudes are assumed to be equal (i.e. value = 1). When a trend is found the vectors is assigned to the site with the highest sorting coefficient. As an example, calculations to determine the component vector from site 9 to site 5 are below:

$$r(x)_5 = \frac{(X_5 - X_9)}{d} = \frac{(1.5 - 2)}{1.118} = -0.45$$

$$r(y)_5 = \frac{(Y_5 - Y_9)}{d} = \frac{(3-2)}{1.118} = 0.89$$

where *d* is the distance between site 2 and the central site 0, given as:

$$d = \sqrt{(X_5 - X_9)^2 + (Y_5 - Y_9)^2} = \sqrt{1^2 + 0.5^2} = 1.118$$

Step 4. Sum all component vectors $r(x,y)_i$ to make a sum vector $R(x,y)$:

$$R(x,y)_9 = \sum_{i=1}^{17} r(x,y)_i = [0.26 \;\; 3.60]$$

Step 5. Repeat steps 1 – 4 on every site in the data set to define sum vectors at every site. Results of this step are presented in Table 2.

Table 2.

Site	Sum Vector		Average Vector		Azimuth Direction*	Vector Length*
i	$R(x)_i$	$R(y)_i$	$R_{Av}(x)_i$	$R_{Av}(y)_i$	Θ	*VL*
1	0.72	-1.95	-0.24	0.83	322	0.39
2	-0.97	1.24	-0.18	0.48	333	0.39
3	-0.83	-0.55	-0.58	0.3	316	0.83
4	0	0	0.18	0.85	143	0.3
5	0	0	0.05	1.05	6	0.48
6	-1.22	1.01	-0.35	0.82	340	1.05
7	-0.71	0.71	-0.53	1.12	322	0.85
8	0	1	0.57	0.85	44	0.82
9	0.26	3.6	0.09	0.39	7	0.78
10	-0.07	1.06	-0.22	0.98	345	0.85
11	-0.51	1.86	-0.19	1.18	349	0.98
12	2.59	-0.67	0.15	1.59	7	1.18
13	0	0	0.57	0.67	30	1.15
14	0.42	-0.62	0.07	1.15	2	1.59
15	0	0	0.84	1.23	49	1.12
16	0.78	3.62	0.47	0.39	45	0.67
17	0	1	0.17	1.21	8	1.23

*Result of the average vector.

Step 6. Remove noise by averaging each sum vector with the neighboring sum vectors determined to be within the characteristic distance (i.e. sites identified in

Step 1). This effectively serves as a low-pass filter with a search radius of 2. For site 9 this processes is expressed as:

$$R_{av}(x,y)_9 = \frac{1}{(k+1)}\left[R(x,y)_9 + \sum R(x,y)_q\right] = \frac{1}{(10+1)}\left(\begin{bmatrix}0.26 & 3.6\end{bmatrix} + \begin{bmatrix}1.03 & 8.50\end{bmatrix}\right)$$

$$= \begin{bmatrix}0.09 & 0.77\end{bmatrix}$$

where *q* is a list of all sites within the characteristic distance of site 0:

q = $\begin{bmatrix}2 & 5 & 6 & 8 & 10 & 11 & 12 & 13 & 14 & 16\end{bmatrix}$

and k is the total number of such sites:

k = 10

Thus, the final averaged transport vector at site 0 has an x-component of 0.09 and a y-component of 0.77.

Step 7. Convert average vector into azimuth direction Θ (exact formula will vary) and vector length *VL*:

$$\Theta = 90 - \arctan\left(\frac{0.77}{0.09}\right) \approx 7 \text{ degrees}$$

$$VL = \sqrt{\left(R_{av}(x)_i\right)^2 + \left(R_{av}(y)_i\right)^2} = \sqrt{(0.77)^2 + (0.09)^2} = .78$$

Journal of Coastal Research	00	0	000–000	West Palm Beach, Florida	Month 0000

Historical Shoreline Change, Southeast Oahu, Hawaii; Applying Polynomial Models to Calculate Shoreline Change Rates

Bradley M. Romine, Charles H. Fletcher, L. Neil Frazer, Ayesha S. Genz, Matthew M. Barbee, and Siang-Chyn Lim

Department of Geology and Geophysics
School of Ocean and Earth Science and Technology
University of Hawaii
1680 East West Road
Honolulu, HI 96822, U.S.A
romine@hawaii.edu

ABSTRACT

ROMINE, B.M.; FLETCHER, C.H.; FRAZER, L.N.; GENZ, A.S.; BARBEE, M.M., and LIM, S.-C.; 2009. Historical shoreline change, southeast Oahu, Hawaii; applying polynomial models to calculate shoreline change rates. *Journal of Coastal Research,* 00(0), 000–000. West Palm Beach (Florida), ISSN 0749-0208.

Here we present shoreline change rates for the beaches of southeast Oahu, Hawaii, calculated using recently developed polynomial methods to assist coastal managers in planning for erosion hazards and to provide an example for interpreting results from these new rate calculation methods. The polynomial methods use data from all transects (shoreline measurement locations) on a beach to calculate a rate at any one location along the beach. These methods utilize a polynomial to model alongshore variation in the rates. Models that are linear in time best characterize the trend of the entire time series of historical shorelines. Models that include acceleration (both increasing and decreasing) in their rates provide additional information about shoreline trends and indicate how rates vary with time. The ability to detect accelerating shoreline change is an important advance because beaches may not erode or accrete in a constant (linear) manner. Because they use all the data from a beach, polynomial models calculate rates with reduced uncertainty compared with the previously used single-transect method. An information criterion, a type of model optimization equation, identifies the best shoreline change model for a beach. Polynomial models that use eigenvectors as their basis functions are most often identified as the best shoreline change models. Polynomial models with linear fit in time indicate chronic erosion along 36% of the length of southeast Oahu beaches. Polynomial models including acceleration indicate recent increasing rates of erosion along 33% of the length of the study area.

ADDITIONAL INDEX WORDS: *Coastal erosion, shoreline change, erosion rate, polynomial, PX, PXT, EX, EXT, ST, single-transect, information criterion, Hawaii.*

INTRODUCTION

Tourism is Hawaii's leading employer and its largest source of revenue. Island beaches are a primary attraction for visitors, and some of the most valuable property in the world occurs on island shores. Beaches are also central to the culture and recreation of the local population. During recent decades many beaches on the island of Oahu, Hawaii, have narrowed or been completely lost to erosion (Fletcher *et al.,* 1997; Hwang, 1981; Sea Engineering, 1988), threatening business, property, and the island's unique lifestyle.

Results from a Maui Shoreline Study (Fletcher *et al.,* 2003) resulted in the first erosion rate-based coastal building setback law in the state of Hawaii (Norcross-Nu'u and Abbott, 2005). Concerns about the condition of Oahu's beaches prompted federal, state, and county government agencies to sponsor a similar study of shoreline change for the island of Oahu. The primary goals of the Oahu Shoreline Study are to analyze trends of historical shoreline change, identify future coastal erosion hazards, and report results to the scientific and management community.

It is vital that coastal scientists produce reliable, *i.e.,* statistically significant and defensible, erosion rates and hazard predictions if results from shoreline change studies are to continue to influence public policy. To further this goal, Frazer *et al.* (2009) and Genz *et al.* (2009) have developed polynomial methods for calculating shoreline change rates. The new methods may calculate rates that are constant in time or rates that vary with time (acceleration, both increasing and decreasing). The polynomial models without rate acceleration are generally referred to as PX models (for polynomials in the alongshore dimension, X) and the models with rate acceleration are PXT (polynomials in X and time). The PX methods, with a linear fit in time, best characterize the trend of the whole time series of historical shorelines and, therefore, describe the long-term change at a beach. The PXT methods may provide additional information about recent change at a beach and can show how rates may have varied with time. These methods are shown here and in the Frazer *et al.* and Genz *et al.* papers (2009) to produce statistically

DOI: 10.2112/08-1070.1 received 1 May 2008; accepted in revision 27 October 2008.

significant shoreline change rates more often than the commonly used single-transect (ST) method using the same data. Here we employ the polynomial methods to calculate shoreline change rates for the beaches of southeast Oahu.

PHYSICAL SETTING

The study area consists of the northeast-facing beaches along the southeast coast of Oahu, Hawaii. The area is bounded to the north and south, respectively, by basalt Mokapu and Makapuu points (Figure 1). This shoreline is fronted by a broad fringing reef platform extending 1 to 3.5 km from the shoreline except in the far south. The reef crest shallows to −5 to 0 m depth, 0.3 to 1.0 km from shore, along 70% of the study area. This fringing reef protects most beaches from the full energy of open-ocean waves (Bochicchio *et al.,* 2009).

The beaches in the study area face predominantly toward the northeast. The study area is exposed to trade wind swell from the northeast (typically 1–3 m with 6- to 8-second period) throughout the year (Bodge and Sullivan, 1999). Trade winds are most common during the summer (April to September, 80% of the time) and are less persistent, though still dominant, in winter. Moderately high to very high energy refracted long period swells from the north (typically 1–5 m with 12- to 20-second period) impinge in winter. Significant offshore wave heights of 8 m (average of largest one-third of wave heights) recur annually (Vitousek and Fletcher, 2008). The fraction of open-ocean wave energy reaching the inner reef and shoreline varies throughout the study area and is controlled by refraction and shoaling of waves on the complex bathymetry of the fringing reef.

The study area contains four beach study sections, which are additionally subdivided into 14 beach study segments by natural and anthropogenic barriers to sediment transport and/or gaps in reliable shoreline data.

Kailua Beach

Kailua Beach is a 3.5-km crescent-shaped beach bounded to the north by limestone Kapoho Point and to the south by basalt Alala Point. Between Mokapu Point and Kapoho Point is primarily hard limestone and basalt shoreline (no beach). A sinuous 200 m wide sand-floored channel bisects the reef platform. The channel widens toward the shore into a broad sand field at the center of Kailua Beach. The inner shelf and shoreline are protected from large, long period swell by the fringing reef. Wave heights become progressively smaller toward the southern end of Kailua Beach because shallow reef crest and Popoia Island refract and dissipate more of the open ocean swell.

The residential area of Kailua is built on a broad plain of Holocene-age carbonate dune ridges and terrestrial lagoon deposits (Harney and Fletcher, 2003). Low vegetated dunes front many of the homes on Kailua Beach. Kaelepulu Stream empties at Kailua Beach Park at the southern end of Kailua Beach.

For shoreline change analysis, Kailua Beach is divided into two study segments with a boundary at the Kaelepulu stream mouth. The boundary is required because of a gap in reliable shoreline data at the stream mouth. Shoreline positions from the stream mouth are not considered reliable because they are prone to high variability related to stream flow, and this is not accounted for in our uncertainty analysis.

Lanikai Beach

The Lanikai shoreline is a slightly embayed 2 km wide headland between the basalt outcrops of Alala Point and Wailea Point. Lanikai Beach is a narrow 800 m long stretch of sand in the north-central portion of the Lanikai shoreline. The remainder of Lanikai has no beach at high tide, except for a small pocket of sand stabilized by a jetty in the far south. Waves break against seawalls in areas without beach.

The fringing reef fronting Lanikai is shallower than the reef fronting the adjacent areas of Kailua and Waimanalo. The shallow reef platform extends 2 km offshore to the Mokulua Islands. Wave heights along the Lanikai shoreline are typically small (<1 m) because of refraction and breaking of open-ocean waves on the shallow fringing reef and shores of the offshore Mokulua Islands. The community of Lanikai is built on the foot of the basalt Keolu Hills and on a narrow coastal plain composed of carbonate sands and terrigenous alluvium (Sherrod *et al.,* 2007).

Bellows and Waimanalo Beach

Bellows and Waimanalo Beach is a nearly continuous 6.5 km long beach extending from near Wailea Point to southern Waimanalo. In the northern end of the Bellows shoreline (from Wailea Point 700 m to the south), waves break against stone revetments at high tide. The beach was lost to erosion in the northern portion by 1996. The beach is partially interrupted at two other locations by stone jetties at Waimanalo Stream and remains of a similar structure at Inaole Stream.

A broad reef platform extends to a shallow reef crest 1.5–0.5 km offshore. Paleochannels, karst features, and several large depressions on the reef platform contain significant sand deposits and likely play an important role in storage and movement of beach sand (Bochicchio *et al.,* 2009). Bellows Field and the town of Waimanalo are built on a broad plain of carbonate and alluvial sediments.

Bellows and Waimanalo Beach are divided into three study segments for analysis with boundaries at the Waimanalo and Inaole stream mouth jetties. These boundaries are needed because of gaps in reliable shoreline data at the stream mouths, though sand is undoubtedly transported around the jetties.

Kaupo and Makapuu Beaches

Between Southern Waimanalo and Makapuu beaches are a series of narrow pocket beaches separated by natural and anthropogenic hard shoreline, which divide this study section into eight beach segments for shoreline change analysis. The broad carbonate coastal plain found to the north is absent from most of this section. The steep basalt Koolau cliffs rise within a few hundred meters behind the shoreline. Beaches in the northern two-thirds of the study section are generally narrow (5–20 m). Seawalls front homes along the northern

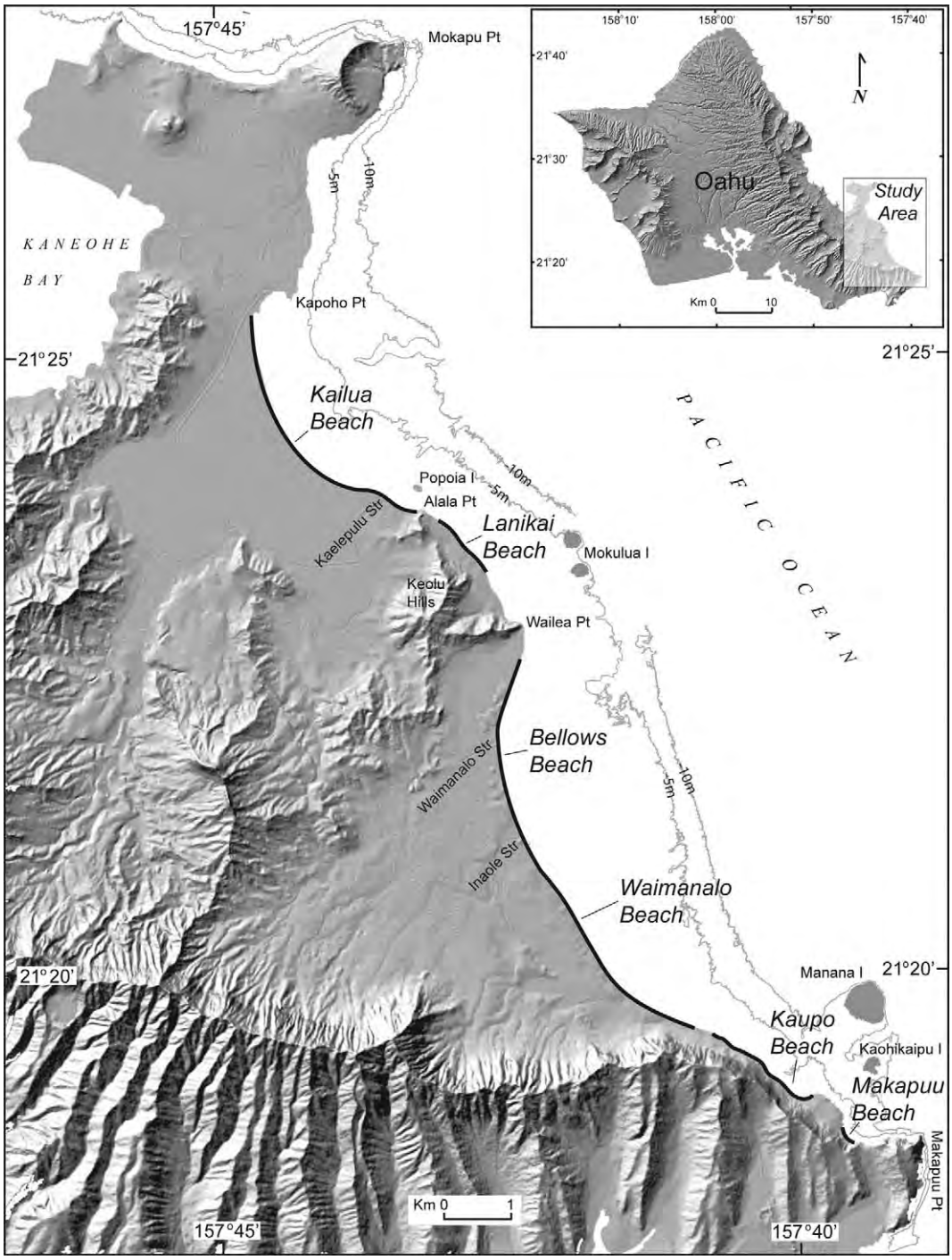

Figure 1. Southeast Oahu study area and beaches. The −5- and −10-m bathymetry contours mark the approximate seaward edge of the nearshore reef platform.

portion of Kaupo Beach. To the south the beaches are backed by a low rock scarp (1–2 m) or by man-made revetments.

Along Kaupo Beach the shallow fringing reef blocks most wave energy. The fringing reef disappears offshore of Makapuu Beach allowing the full brunt of easterly trade wind waves and refracted northerly swells to reach the shoreline there. Makapuu Beach, popular with bodysurfers, is well known for its large shore-breaking waves. Makapuu Beach is wide (50 m) and sediment-rich compared with beaches to the north. The back-beach area is characterized by vegetated

dunes sloping against the base of the Koolau cliffs. A sand-filled channel extends offshore.

PREVIOUS WORK

Hwang (1981) was the first to compile historical shoreline change for beaches of Oahu. His study utilized a vegetation line and a waterline as the shoreline proxies. Historical shoreline positions were measured from aerial photographs along shore-perpendicular transects roughly every 1000 ft (328 m). His study reported position changes of the vegetation line from one aerial photo to another and from these the net change in the vegetation line and waterline through the time span of the study. Annual rates were not calculated from the data. Movement of the vegetation line at Kailua Beach indicated long-term (net) accretion along the whole length of the beach. Historical shorelines at Kailua Beach Park indicated erosion between 1971 and 1978. Long-term accretion was found at most transects at Lanikai Beach, except at the north and south ends. Erosion was also noted at north and south Lanikai for the more recent years of historical shorelines (the beach has since disappeared in these areas). Most transects at Bellows and Waimanalo beaches indicated erosion over the long term. Hwang reports the beach was effectively lost (submerged at high tide) at north Bellows Beach by 1980.

Sea Engineering (1988) produced an update to the Hwang (1981) study with a more recent aerial photo set, while using the same methods and transects. More recent aerial photographs (1988) indicated that long-term accretion continued at all transects at Kailua Beach. Erosion slowed or turned to accretion at Kailua Beach Park from 1980 to 1988. Their study reported extensive areas of erosion and beach loss at north and south Lanikai between 1980 and 1988. However, this erosion was not apparent in their shoreline change measurements because the vegetation line was effectively fixed at the seawalls now fronting homes along the eroded portions of the Lanikai shoreline.

Norcross, Fletcher, and Merrifield (2002) calculated annual shoreline change rates and interannual beach volume change at Kailua Beach. They used orthorectified aerial photographs and NOAA topographic maps (T-sheets) to map a low water mark as a shoreline proxy. Annual shoreline change rates were calculated using the single-transect (ST) method. Interannual beach volume changes were calculated using data from beach profile surveys. The study concluded that Kailua Beach experienced annual shoreline accretion from 1926–1996 and recent (prior to 1996) net increase in beach sand volume.

Our study provides an important update and comparison to the results of previous studies. We aim to improve on all of the previous studies by utilizing improved photogrammetric methods for measuring historical shoreline positions and statistical methods for calculating shoreline change rates. In addition, a modern aerial photograph set (2005) provides more recent shoreline positions for our study beaches.

METHODS

Mapping Historical Shorelines

For this study we adhere closely to the methods of Fletcher *et al.* (2003) for mapping historical shorelines on Maui, Hawaii. Historical shorelines are digitized from NOAA NOS topographic maps (T-sheets) and 0.5-m spatial resolution (pixel) orthorectified aerial photo mosaics. Only large-scale (typically <0.5 m scanned pixel resolution, media-dependent), vertical, survey-quality air photos with sufficient tonal and color contrast to delineate a high-resolution shoreline proxy were chosen for this study. Orthorectification and mosaicking was performed using PCI Geomatics' Geomatica Orthoengine software (2007) to reduce displacements caused by lens distortion, Earth curvature, refraction, camera tilt, radial distortion, and terrain relief. The orthorectification process typically resulted in root mean square (RMS) positional errors of <2 m based on the misfit of the orthorectification model to a master orthorectified image and a digital elevation model (DEM).

New aerial photography of study beaches was acquired in late 2005. Aircraft position (global positioning system locations) and orientation data (*e.g.,* altitude, pitch, roll, and yawl) were recorded in an on-board positional orientation system (POS). The recent images are orthorectified and mosaicked in PCI using polynomial models incorporating POS data and high-resolution (5-m horizontal, submeter vertical) DEMs. The orthorectified 2005 photo mosaics serve as master images for the orthorectification of older aerial photographs.

T-sheets are georeferenced using polynomial mathematical models in PCI with RMS errors <4 m. Rectification of T-sheets is also verified by overlaying them on orthophoto mosaics to examine their fit to rocky shorelines and other unchanged geological features also visible in the modern photography. T-sheet shorelines may be discarded if a satisfactory fit to a hard shoreline cannot be achieved and/or if the RMS error grossly understates the misfit. Previous workers have addressed the accuracy of T-sheets (Crowell, Leatherman, and Buckley, 1991; Daniels and Huxford, 2001; Shalowitz, 1964), finding that they meet national map accuracy standards (Ellis, 1978) and recommending them for use in shoreline change studies as a valuable source for extending the time series of historical shoreline position (National Academy of Sciences, 1990).

The beach toe, or base of the foreshore, is digitized from orthophoto mosaics and is a geomorphic proxy for the low water mark (LWM). The LWM is what we define as the shoreline for our change analysis. Removing or quantifying sources of uncertainty related to short-term (interannual to hourly) changes in shoreline position is necessary to achieve our goal of identifying chronic long-term trends in shoreline behavior. A LWM offers several advantages as a shoreline proxy on Hawaiian carbonate beaches, toward the goal of limiting our uncertainty. Studies from beach profile surveys have shown that a LWM is less prone to spurious position changes typical of other shoreline proxies (*e.g.,* wet–dry line, high water mark) (Norcross, Fletcher, and Merrifield, 2002). The bright white carbonate sands typical of Hawaii beaches often hinder interpretation of water line proxies in aerial photographs—especially in older black and white images with reduced contrast and resolution. The vegetation line was used as the shoreline proxy in some previous Oahu studies (Hwang, 1981; Sea Engineering, 1988). However, on most Oahu beaches the vegetation line is cultivated and therefore often does not track the natural movement of the shoreline. Nonetheless, we create a vector of the vegetation line so that

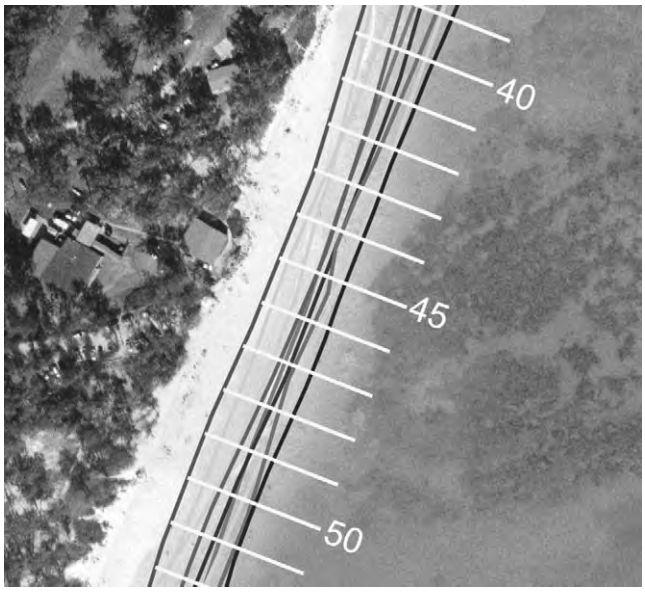

Figure 2. Historical shorelines and shore-perpendicular transects (measurement locations, 20-m spacing) displayed on a portion of a recent aerial photograph.

it is available to track historical changes in beach width between the vegetation line and the LWM.

Surveyors working on T-sheets mapped the high water mark (HWM) as a shoreline proxy. To include the T-sheet shorelines in the time series of historical LWM shorelines, the HWM is migrated to a LWM using an offset calculated from measurements in beach profile surveys. HWM and LWM positions have been measured in beach profile surveys collected at nine locations in the study area in summer and winter for 8 years. The offset used to migrate the T-sheet HWM to a LWM is the median distance between HWM and LWM positions measured in the profiles at a beach or a nearby beach with similar littoral characteristics (*e.g.,* wave exposure, beach morphology).

Six to thirteen historical orthomosaics and T-sheets comprise our time series between 1911 and 2005. To determine patterns of movement, relative distances of the historical shorelines are measured from an offshore baseline along shore-perpendicular transects spaced 20 m apart (Figure 2).

Uncertainties in Shoreline Position

Shoreline position is highly variable on short time scales (interannual to hourly) because of tides, storms, and other natural fluctuations. Procedures for mapping historical shorelines introduce additional uncertainties. It is vital that these uncertainties be identified, rigorously calculated, and included in shoreline change models to ensure that the shoreline change rates reflect a long-term trend and are not biased because of short-term variability (noise). Building on Fletcher *et al.* (2003), Genz *et al.* (2007), and Rooney *et al.* (2003), we calculate seven different sources of error in digitizing historical shoreline position from aerial photographs and T-sheets.

Table 1. *Shoreline uncertainties: southeast, Oahu, Hawaii.*

Uncertainty Source	± Uncertainty Range (m)
E_d, digitizing error	0.5–5.7
E_p, pixel error, air photos	0.5
E_p, pixel error, T-sheets	3.0
E_s, seasonal error	3.6–6.2
E_r, rectification error	0.6–3.0
E_{td}, tidal error	2.5–3.4
E_{ts}, T-sheet plotting error	5.1
E_{tc}, T-sheet conversion error	3.4–5.7
E_t, total positional error (see text)	4.5–10.8

C1

Identifying the probability distribution (*e.g.,* normal, uniform) for each error process (*e.g.,* tidal fluctuation, seasonal variance) provides the tools to calculate the individual error uncertainty. The total positional uncertainty, E_t, is the root sum of squares of the individual uncertainties. We assume E_t follows a normal distribution because the Central Limits Theorem states that the sum of many sources of uncertainty tends toward a normal distribution (Draper and Smith, 1998). E_t is applied as a weight for each shoreline position when calculating shoreline change models using weighted regression methods. Total positional uncertainties for southeast Oahu historical shorelines are between ±4.5 and ±10.8 m (Table 1). Please note: This is the range of actual uncertainties. No historical shoreline had the highest values for all individual uncertainty sources.

??1

Digitizing Error, E_d. Only one analyst provides the final digitized shorelines from all orthomosaics and T-sheets to ensure consistency in the criteria used to locate each shoreline. Uncertainties in interpreting the shoreline position in aerial photographs are calculated by measuring variability in shoreline position when digitized by several experienced analysts working on a sample portion of shoreline. The digitizing error is the standard deviation of differences in shoreline position from a group of experienced operators. If an E_d value has not been calculated for a particular orthomosaic, a value from a mosaic with similar attributes (*e.g.,* resolution, photo year) is used. E_d values range from ±0.5 to ±5.7 m.

Pixel Error, E_p. The resolution (pixel size) of our orthomosaics limits our ability to resolve the position of a feature (*e.g.,* LWM) finer than 0.5 m. Therefore, E_p equals ±0.5 m. T-sheets are digitally scanned at a lower resolution than aerial photographs. E_p for T-sheets is ±3 m.

Table 2. *Average shoreline change rates and ± uncertainties for southeast Oahu beaches.*

C2

Beach	ST Avg Rate (m/y)	PX Avg Rate (m/y)	PXT Avg Rate (m/y)
Kailua	0.4 ± 0.2	0.4 ± 0.0	0.1 ± 0.1
Lanikai	0.3 ± 0.2	0.3 ± 0.1	0.5 ± 0.1
Bellows and Waimanalo	0.0 ± 0.3	0.0 ± 0.1	0.0 ± 0.1
Kaupo (all)	−0.1 ± 0.1	−0.1 ± 0.1	0.1 ± 0.1
Makapuu	0.0 ± 0.0	0.0 ± n/a	0.0 ± n/a
Southeast Oahu, all	0.2 ± 0.2	0.1 ± 0.1	0.1 ± 0.1

Rate and uncertainty of all transects averaged along the length of the beach.
Negative = erosion; positive = accretion.
n/a = not applicable.

Seasonal Error, E_s. We do not attempt to identify and remove storm shorelines based on *a priori* knowledge of major storm and wave events for two reasons. One, our study (and most shoreline studies) have limited historical shoreline data (*e.g.,* aerial photography years) and removing one or more shorelines comes at the cost of reducing an already limited data set. Two, storms tend to affect shoreline position in a nonuniform manner in an island setting. Instead, we calculate an uncertainty in shoreline position due to seasonal changes (waves and storms). To measure seasonal variability, we surveyed beach profiles summer and winter for 8 years at 33 beaches on Oahu. The seasonal change is the difference between shoreline (LWM) positions along a survey transect between summer and winter. A randomly generated uniform distribution (>10,000 points) is calculated incorporating the standard deviation of the measured seasonal changes. A uniform distribution is an adequate approximation of the annual probability of shoreline positions resulting from seasonal fluctuations because an aerial photo has equal probability of being taken at any time of year. The seasonal error, E_s, is the standard deviation of this randomly generated distribution. For beaches without profile data, an E_s value from a nearby beach with similar littoral characteristics is used. E_s values range from ±3.6 to ±6.2 m.

Rectification Error, E_r. Aerial photographs are orthorectified to reduce displacements caused by lens distortion, Earth curvature, camera tilt, and terrain relief using PCI Orthoengine software. The software calculates an RMS error from the misfit of the orthorectification model to the master orthorectified image and DEM. E_r values range from ±0.6 to ±3.0 m for orthophoto mosaics. T-sheets are georeferenced in PCI Orthoengine using polynomial models. E_r for T-sheets ranges from ±1.4 to ±2.9 m.

Tidal Fluctuation Error, E_{td} (aerial photographs, only). Aerial photographs are obtained without regard to tidal cycles, and the time of day each photo is collected is typically unknown, resulting in inaccuracies in digitized shoreline position from tidal fluctuations. Rather than attempting to correct the shoreline position, the possible fluctuations due to tides are included as an uncertainty. Hawaii is situated in a microtidal zone of the Pacific Ocean with maximum tidal fluctuations of 1 m. Therefore, tides have less of an effect on shoreline position at Hawaii beaches than at most beaches on the continental United States, where tides typically vary by several meters. Surveys of the horizontal movement of LWMs (beach toe) between a spring low and high tide at three beaches in the study area found that the beach toe migrated horizontally landward 8 to 12 m from low to high tide. The probability of an aerial photograph being taken at low or high tide is assumed to be equal. Thus, a uniform distribution is a conservative estimate of the probability distribution of LWM positions due to tidal fluctuation in an aerial photograph. E_{td} is the standard deviation of a randomly generated uniform distribution derived from the standard deviation of the surveyed tidal fluctuations. E_{td} values range from ±2.5 to ±3.4 m for this study.

T-Sheet Plotting Error, E_{ts} (T-sheets only). Surveyors working on T-sheets mapped the high water mark (HWM) as a proxy for shoreline position. The T-sheet plotting error is based on Shalowitz's (1964) analysis of topographic surveys. He identifies three major errors in the accuracy of these surveys: (1) measuring distances, ±1 m; (2) plane table position, ±3 m; and (3) delineation of the high water line, ±4 m. The total plotting error, E_{ts}, for all T-sheets is the root sum of squares of the three distinct errors, ±5.1 m.

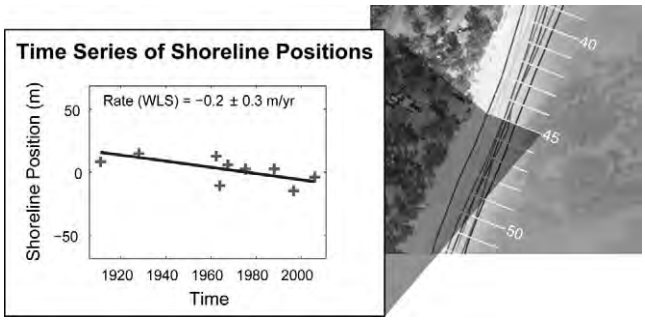

Figure 3. Calculating shoreline change rate using the single-transect (ST) method (weighted least squares regression, WLS). The slope of the line is the annual shoreline change rate.

Conversion Error for T-Sheets, E_{tc} (T-sheets only). To compare historical shorelines from T-sheets and aerial photographs, we migrated the surveyed HWM from a T-sheet to a LWM position using data from beach topographic profile surveys. The offset used to migrate the T-sheet HWM to a LWM is the median distance between HWM and LWM positions measured in surveys at a beach. The uncertainty in this conversion, E_{tc}, is the standard deviation of the distances between surveyed HWM and LWM positions. For beaches without profiles, the offset and E_{tc} value from a similar nearby littoral areas is used (Fletcher *et al.,* 2003). E_{tc} values for southeast Oahu range from ±3.4 to ±5.7 m.

Calculating Shoreline Change Rates

Single Transect

In previous studies, our research team and other coastal research groups have utilized the single-transect (ST) method to calculate shoreline change rates (*e.g.,* Fletcher *et al.,* 2003; Hapke *et al.,* 2006; Hapke and Reid, 2007; Morton and Miller, 2005; Morton, Miller, and Moore, 2004) (Figure 3). ST calculates a shoreline change rate and rate uncertainty at each transect using various methods to fit a trend line to the time series of historical shoreline positions (*e.g.,* end point rate, average of rates, least squares).

Our group employs weighted least squares regression with the ST method, which accounts for uncertainty in each shoreline position when calculating a trend line (Fletcher *et al.,* 2003; Genz *et al.,* 2007). The weight for each shoreline position is the inverse of the total shoreline positional uncertainty squared (*e.g.,* $w_i = 1/E_i^2$). Shoreline positions with higher uncertainty will, therefore, have less of an influence on the trend line than data points with smaller uncertainty. The slope of the line is the shoreline change rate. Model (rate) uncertainties are calculated at the 95% confidence interval.

Recent work by Frazer *et al.* (2009) and Genz *et al.* (2009)

identifies a number of shortcomings with the ST method. ST tends to overfit the data by using more mathematical parameters than necessary. Models that overfit data are unparsimonious. The principle of parsimony, when applied to mathematical modeling, states that a model with the smallest number of parameters that provides a satisfactory fit to the data is preferred. Satisfactory fit is quantified by minimizing the residuals of the model fit. The classic example of an unparsimonious model is an $n - 1$ degree polynomial used to fit n noisy data points: The model fit to the data is perfect, but the model is so sensitive to noise that its predictions are usually poor. The problem of overfitting with ST is made worse by limited data (often less than 10 historical shorelines) and high uncertainty (noise) in shoreline positions, both typical of shoreline studies.

Another problem with the ST method is that it treats the beach as if it were a set of isolated blocks of sand centered on each transect, which do not share sand with adjacent transects and move independently of adjacent transects. However, on an actual continuous beach, the positions of each transect share sand with adjacent positions along the shore. Thus, the shoreline positions and shoreline change rates at each transect on a beach are related. Shoreline transects need to be closely spaced to effectively characterize shoreline change along a beach. We use a 20-m transect spacing for easy comparison of our methods and results with other recent studies.

The rates calculated using the ST method tend to have high uncertainty because ST is modeling shoreline change independently at each transect. High rate uncertainty can result in rates at many transects that are not statistically significant. For this study we consider a rate to be insignificant if it is indistinguishable from a rate of 0 m/y (*i.e.,* ± rate uncertainty overlaps 0 m/y). If we can reduce the uncertainty in shoreline change rates, we will aid coastal managers in making better-informed decisions in planning for future erosion hazards.

Polynomial Methods

Here we provide a summary of the recently developed polynomial methods to assist the reader in interpreting the results and conclusions in this study. Please refer to Frazer *et al.* (2009) and Genz *et al.* (2009) for more detailed information on these rate calculation methods.

The ST method calculates a rate at each transect by fitting a linear trend to shoreline positions plotted in distance along a transect and time. Shoreline change rates vary independently along the shore (from transect to transect) with the ST method. Polynomials can be used to model this variation in shoreline change rates in the alongshore direction. By modeling shoreline data in the alongshore direction as well, we can incorporate shoreline positions from all transects on a beach in a single model. The single model will invariably require fewer mathematical parameters to calculate change rates at each transect than the ST method, leading to more parsimonious models (reducing overfitting). In addition, a single polynomial model correctly assumes that the shoreline data from adjacent transects is related (*e.g.,* dependent).

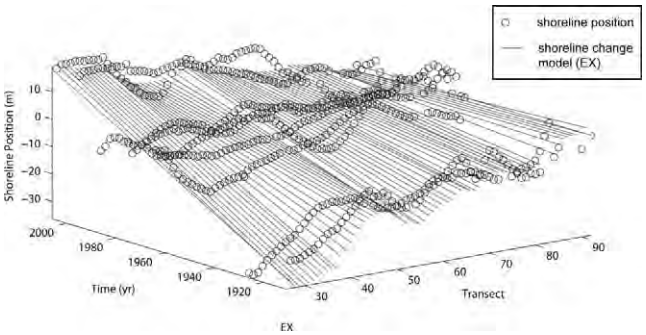

Figure 4. PX (EX) shoreline change model for North Bellows Beach. Rates (slope) vary continuously in the alongshore direction but are constant (linear) in time (no acceleration).

Frazer *et al.* (2009) and Genz *et al.* (2009) have developed polynomial shoreline change rate calculation methods that include the alongshore variation of shoreline change rates in their models. These methods build polynomial models in the alongshore direction using linear combinations of mathematical basis functions. These methods employ data from all transects along a beach to calculate a rate at any one location. Similar to ST, a line is fit in the time and cross-shore dimension at each transect. However, unlike ST, calculation of this line is dependent on data from all transects on a beach.

The polynomial methods allow detection of rate variations (acceleration in time), in addition to modeling rate variations spatially alongshore. Detecting acceleration in the rates is easier with these methods because of the reduced number of parameters in the model compared with ST. The ± uncertainties with the rates calculated using the polynomial methods are invariably lower than with the ST method because they use all of the data on a beach to calculate the rates. Thus, the basis function methods produce statistically significant rates at a higher percentage of transects than ST.

The polynomial methods use one of three types of basis functions, combined in a finite linear combination, to build a model for the alongshore variation of rates. All of the methods use generalized least squares regression (GLS) to calculate the parameters of the model. GLS incorporates the uncertainty (E_i) of each shoreline position in weighting each shoreline's influence on the model. LXT uses Legendre polynomials as the basis functions. RXT utilizes trigonometric functions (*e.g.,* sines and cosines) as the basis functions. EXT, also known as "eigenbeaches" utilizes eigenvectors (*i.e.,* principal components) of the shoreline data as the basis functions. The eigenvectors are calculated from the shoreline data using all transects on a beach.

Models that do not include acceleration in their rates are referred to as LX, RX, and EX, respectively. Generally, we refer to these as PX models (Figure 4). The rates from PX models are constant in time but vary continuously in the alongshore direction. The rates from the LXT, RXT, and EXT models vary continuously with time as well as in the alongshore dimension, and we refer to these models generally as PXT models (Figure 5). A PXT model that does not identify

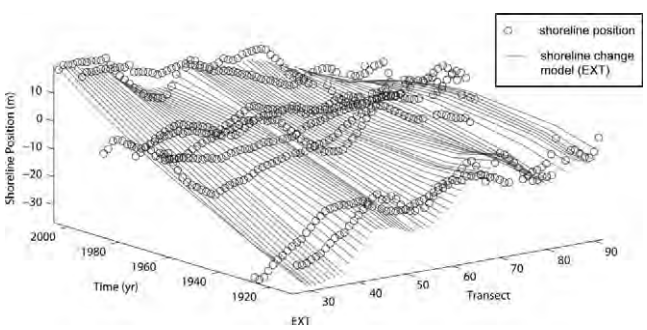

Figure 5. PXT (EXT, includes acceleration in the rate with time) shoreline change model for North Bellows Beach. Rates (slope) vary continuously in the alongshore direction and with time.

acceleration in the rates at a particular beach reverts to a PX model.

Rates are first calculated using the ST method for comparison with the rates from the PX and PXT rates. In addition, results from the ST model are used in estimating the spatial (alongshore) correlation of the noise for the polynomial models. A decaying exponential function is fit to the autocorrelation of the ST data residuals. The best-fit exponential decay function is incorporated in the alongshore polynomial model to represent decreasing dependence of the shoreline data with distance from each transect.

With the Matlab codes developed by Frazer *et al.* (2009) and Genz *et al.* (2009), many possible models are calculated for the three basis function model types, with and without acceleration in the rates (LXT, RXT, EXT, LX, RX, EX). The models vary in the number (parameters) of basis functions of each type used in linear combination.

An information criterion (IC) is used to compare the parsimony of the various models. We use a version of Akaike information criterion (AICu) (Burnham and Anderson, 2002; Frazer *et al.,* 2009; Genz *et al.,* 2009). In general, an IC is a comparative statistic or score based on the residual errors of the model (*i.e.,* "goodness of fit") and the number of mathematical parameters used in the model. As a measure of parsimony or, more accurately, the lack of it, the IC score is increased for models with a greater number of model parameters and reduced for improved fit to the data. The model with the lowest IC score is the most parsimonious model and is the best model to describe shoreline change at a beach. A model with a rate of 0 m/y (showing no change) is also given an IC score for comparison with the models with rates.

The IC scores are used to select the best model within each of the six polynomial model types (LXT, RXT, EXT, LX, RX, EX). The ST model and its IC score are calculated for comparison with the polynomial models. The polynomial models invariably produce results with lower IC scores than ST. Rates from the seven model types (including ST) are plotted together for comparison (Figure 6a), providing a qualitative assessment of the agreement of the rates from the various models. The results may be considered more robust if most or all of the models agree in their rates.

We attempt to provide the best information about long-term and more recent shoreline change occurring at a beach to help shoreline managers in planning for future erosion hazards. The favored model among the PX models (*i.e.,* models without rate acceleration) and the PXT models (*i.e.,* models with rate acceleration) are identified using IC scores. The PX models provide a better assessment of the trend of the whole time series of historical shorelines. Inspection of PXT models shows that these models typically capture the trend of the most recent few shorelines. Therefore, we use the PX models to estimate the long-term rate and the PXT models to obtain additional information about more recent shoreline change and how the rates may have varied with time. As with the ST method, bounds for the rates are calculated at the 95% confidence interval.

Using the PXT models we attempt to identify erosion hazards not recognized by the PX models. For example, a beach that is shown to be accreting over the long term (with PX) may still present a future erosion hazard if the PXT model indicates the rate of accretion is slowing (decelerating). Conversely, a beach that is eroding presents less of a future erosion hazard if the PXT model indicates the erosion rate is decelerating. We use the rate acceleration from the PXT models to provide more information about the "fitness" of the littoral sediment budget at a beach. Beaches with decelerating erosion rates and accelerating accretion rates have improving fitness because these beaches present less of a future erosion hazard. Beaches with accelerating erosion rates and decelerating accretion rates have deteriorating fitness because they present a greater future erosion hazard.

Rates presented from the PXT models (*e.g.,* Figure 6) are from time of the most recent shoreline and are referred to as the "present rate." This distinction is important because the rates from the PXT models can vary with time and a rate may be calculated for any point in the time series of historical shorelines. In any case, it is helpful to compare the model fit to individual transect plots (ST) to better understand the shoreline change behavior through time as described by the PX and PXT models.

Shoreline change rates are reported to the nearest tenth of a meter resulting in some rates with uncertainty ± 0.0 m/y. To clarify for the reader, these rates do not have zero uncertainty. This is simply a result of rounding to the nearest tenth of a meter.

RESULTS

Historical Shoreline Change

Kailua Beach

The EX shoreline change model has the lowest IC score among the PX (nonaccelerated) models at both beach study segments at Kailua Beach (separated by Kaelepulu Stream). The EX method calculates erosion rates similar to those of the ST method (Figure 6b–6d), indicating long-term accretion throughout most of Kailua Beach. However, the average rate uncertainty is reduced with the EX model compared with the ST model (± 0.1 m/y *vs.* ± 0.2 m/y, respectively) (Table 1), resulting in a greater percentage of transects that have significant rates with the EX model (Figure 7).

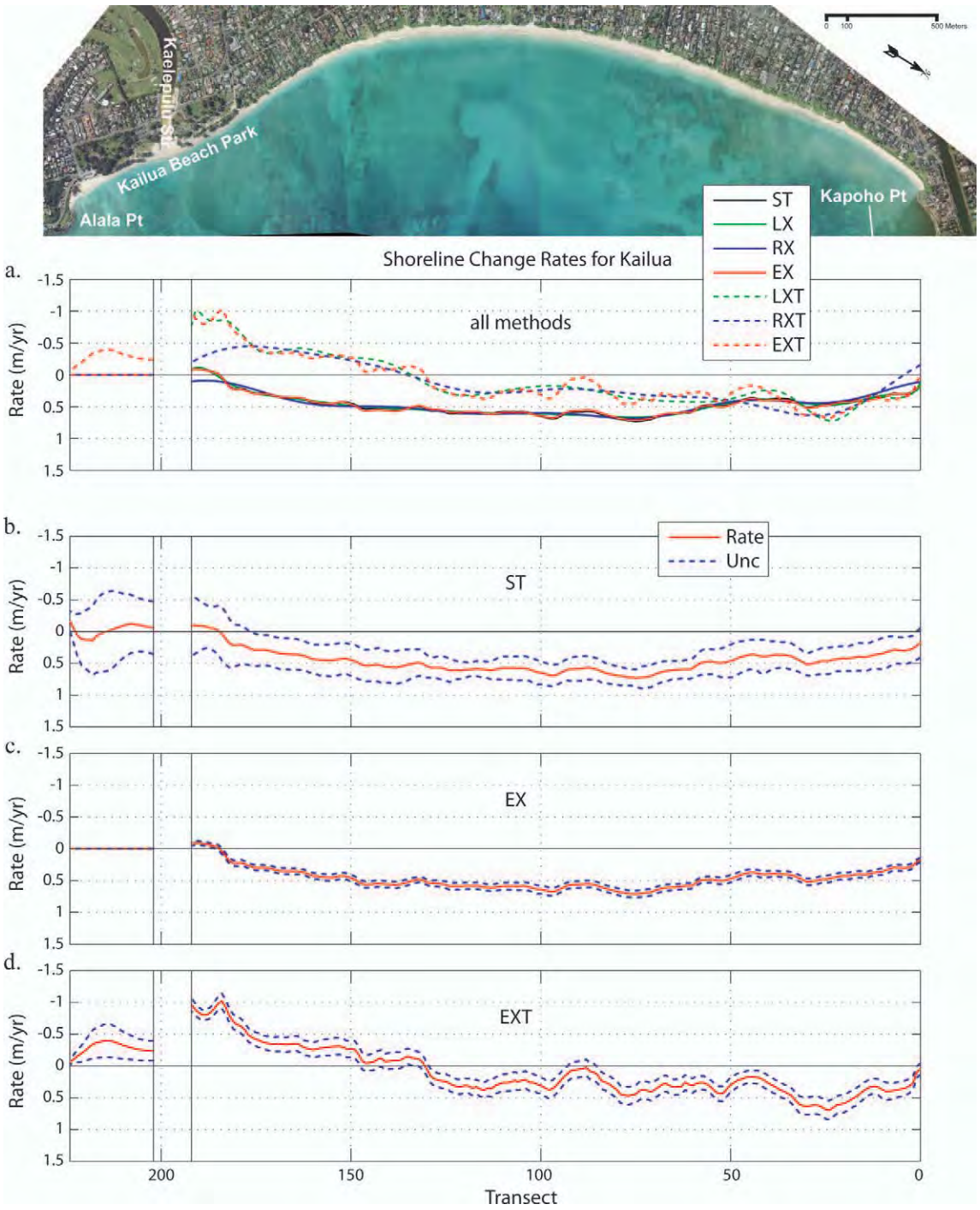

Figure 6. Shoreline change rates (m/y) at Kailua Beach, 1928–2005. Negative rates indicate annual erosion. (a) Rates from ST, PX, and PXT models (±uncertainties not shown). (b) ST rates with ±uncertainties. (c) EX (lowest IC score among the PX models) rates with ±uncertainties. (d) EXT (lowest IC score among the PXT models) rates with ±uncertainties.

In the segment south of Kaelepulu Stream, the EX model shows no long-term change, in contrast to results from the ST model and previous studies. The selection of an EX model (based on IC scores) that shows no significant change may be interpreted two ways. One, the historical shorelines data for this portion of beach is too highly variable (noisy) to calculate a statistically significant long-term trend. Or, two, this segment of beach is stable in the long term, and any erosion or accretion is episodic within the time frame of the study. The ST method (which always produces a model with rates) has

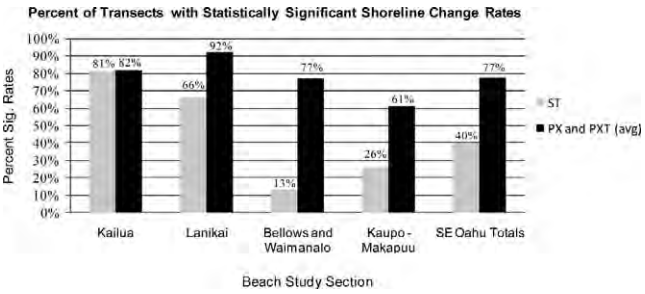

Figure 7. Percentage of transects with statistically significant shoreline change rates using the ST method and PX and PXT methods. Statistically significant rates are those with a ±uncertainty that does not overlap a rate of 0 m/y.

higher rate uncertainties in this segment, further suggesting a highly variable data set. High uncertainty with the ST model results in insignificant rates (± uncertainties overlap 0 m/y) at all transects, essentially in agreement with the EX model results showing no long-term change.

EXT has the lowest IC score among the PXT models. In contrast to ST and EX, EXT estimates recent erosion at Kailua Beach Park with rates up to −1.0 ± 0.1 m/y. EXT also indicates that the extent of erosion may be spreading north from Kailua Beach Park toward central Kailua. Recent beach erosion (2006–2008) has cut a scarp and undermined trees in the beachfront dunes at Kailua Beach Park. Looking at the movement of historical shorelines in an individual transect plot from Kailua Beach Park, we see a previous episode of accretion from 1947 to 1967 and erosion from 1967 to 1978 (Figure 8). According to the EXT model, erosion rates at Kailua Beach Park have been accelerating since the late 1960s or early 1970s. Inspection of the shoreline data in the transect plots shows that the trend toward erosion probably began more recently, beginning with the 1988 or 1996 historical shoreline.

EXT results for Kailua Beach provide a warning of potential erosion hazards not indicated by the EX model. EXT results indicate recent accelerating erosion at 39% of transects (all in the south). EXT also shows recent decelerating accretion at 48% of transects (in the center area). These transects could become erosive if the trend of deceleration continues. Therefore, based on EXT results, the fitness of the littoral sediment budget along most of Kailua Beach (87% of transects) has recently deteriorated.

Lanikai

At Lanikai, 1229 m of beach were lost to erosion in the time span of this study (306 m at north Lanikai, 923 m at south Lanikai) (Figures 9a–9c). Present-day Lanikai Beach is bounded on both ends by extensive seawalls constructed in areas where the beach has been lost to erosion. Aerial photographs show the beach at north Lanikai was completely lost to erosion between 1975 and 1982 and has not returned. At south Lanikai, the shoreline advanced seaward between 1949 and 1975 forming an accretion point similar in size to the

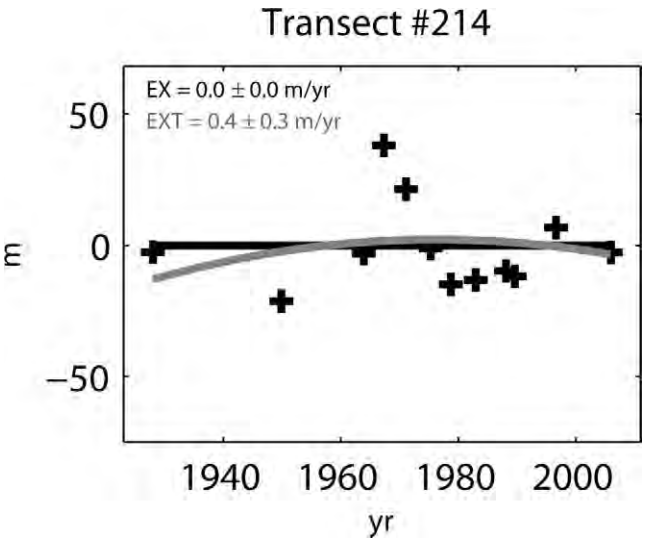

Figure 8. Individual transect plot (transect 214) from Kailua Beach Park showing the fit of the EX and EXT model. Note apparent previous episode of accretion (1949–1967) and erosion (1967–1978).

accretion point presently growing in the north-central portion of Lanikai Beach. Accretion ended and erosion took over in the late 1970s and much of the beach was lost by 1989. We

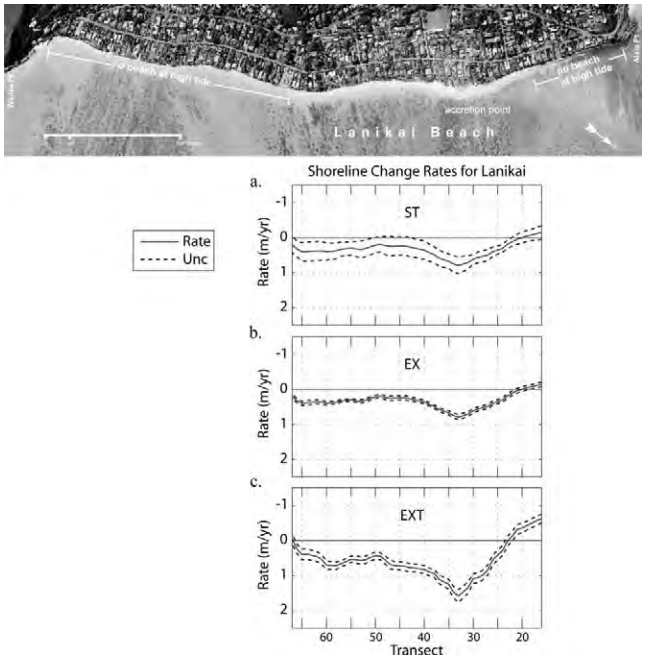

Figure 9. Shoreline change rates (m/y) at Lanikai Beach, 1911–2005. Negative rates indicate annual erosion. (a) ST rates with ±uncertainties. (b) EX (lowest IC score among the PX models) rates with ±uncertainties. (c) EXT (lowest IC score among the PXT models) rates with ±uncertainties.

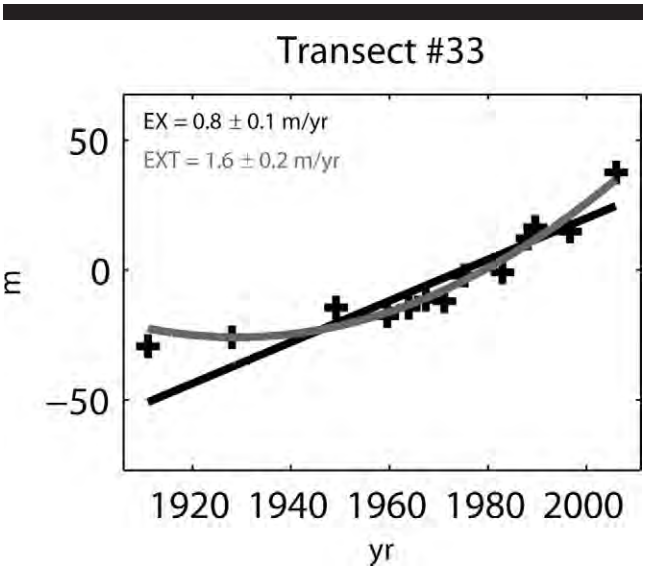

Figure 10. Individual transect plot (transect 33) from north-central Lanikai Beach. The EXT model results indicate accelerating accretion in this area beginning prior to 1949.

calculate shoreline change rates only for the remaining portion of Lanikai Beach.

At Lanikai, the EX model has the lowest IC score among the PX models. EX measures long-term accretion at all transects at Lanikai Beach, except for a small area of erosion at the northern end of the beach. EX calculates the highest accretion rates (up to 0.8 ± 0.1 m/y) aligned with the middle of the accretion point in the north central portion of the beach.

The EXT model has the lowest IC score among the PXT models at Lanikai Beach. Similar to EX, the EXT model calculates the highest accretion rates (up to 1.6 ± 0.2 m/y) at the center of the accretion point in north central Lanikai Beach. The EXT model indicates accelerating erosion at the north end of Lanikai Beach. Based on the EXT model, the central portion of Lanikai Beach began undergoing accelerating accretion prior to 1949 (Figure 10). The EXT model at the southernmost transects indicates that accretion is slowing in this area and may be turning to accelerating erosion. Recent beach profile surveys have shown that the extent of beach loss in south Lanikai continues to expand to the north. All of Lanikai Beach could eventually disappear if the pattern of encroaching beach loss continues.

Bellows and Waimanalo Beaches

At north Bellows (Figure 11), the northern end (690 m) of the beach was lost to erosion prior to 1996. Waves break against stone revetments at high tide in this area. At the remaining portion of north Bellows Beach (Wailea Point to Waimanalo Stream) and central Bellows Beach (Waimanalo Stream to Inaole Stream), the EX model has the lowest IC score among the PX models. At south Bellows and Waimanalo beaches (Inaole Stream to Kaiona Beach Park) (Figure 12), the LX model has the lowest IC score among the PX models.

The EX model indicates long-term erosion at nearly all transects at north Bellows with the highest erosion rates at the northern end of the beach (up to −0.4 ± 0.1 m/y). The EX model at central Bellows indicates long-term erosion in the northern half of the beach study segment and long-term accretion in much of the southern half of the segment. At south Bellows and Waimanalo the LX model indicates long-term accretion in the northern half of this beach study segment and an area of long-term erosion (up to −0.4 ± 0.1 m/y) in the south at Kaiona Beach Park. Again, the alongshore pattern of shoreline change rates from PX models is similar to rates from the ST model. However, the PX models result in a higher percentage of transects with significant rates because the rate uncertainties are reduced compared with ST results.

EXT has the lowest IC scores among the PXT models in the three study segments at Bellows and Waimanalo beaches. In the northern end of Bellows Beach (area of beach loss) the EXT model indicates accelerating erosion throughout the time series of historical shorelines (Figure 13), with the highest rates at the north end of the beach adjacent to the revetments (up to −0.7 ± 0.2 m/y). The extent of recent erosion indicated by the EXT model in northern Bellows is similar to the extent of erosion indicated by the ST and EX models. Agreement among the three models in this area further supports the indication that the remaining beach at north Bellows is threatened by continued erosion and potential beach loss. The EXT model indicates accelerating accretion in the south of the north Bellows segment (against Waimanalo Stream jetty), suggesting that eroded sediment is being transported from the north end of the beach to the south and is accumulating against the jetty.

In the south Bellows and Waimanalo segment, the EXT model indicates a pattern of recent erosion that is significantly different than indicated by the ST and LX models over the long term. At the south end of Bellows Field Beach Park, the EXT model finds an area of recent erosion with rates up to −0.7 ± 0.1 m/y. Recent (1994–2007) biannual beach profile surveys near the middle of this erosive area (as modeled by EXT) do not indicate significant erosion in this area. The EXT model indicates recent accretion in the south of Waimanalo Beach near Waimanalo Bay Beach Park. Beach profile surveys (1994–2007) at Waimanalo Bay Beach Park have shown recent erosion, evidenced by a steep scarp in the beachfront dunes causing undermining of large trees on the dunes. The EXT models and beach surveys at south Bellows and Waimanalo provide a warning that this beach may be subject to episodic erosion even if the beach is relatively stable over the long term (as modeled by ST and LX).

The EXT models indicate recent accelerating erosion at 43% of transects and recent decelerating accretion at 14% of transects. Thus, the EXT models indicate deteriorating fitness of the littoral sediment budget at 57% of transects at Bellows and Waimanalo beaches. The areas of deteriorating fitness are in the northern portion of each the three beach study segments, whereas the areas of improving fitness (43% of transects) are in the south of each study segment.

Kaupo and Makapuu Beaches

At Kaupo and Makapuu beaches the ST models and PX find a similar alongshore pattern of shoreline change for all

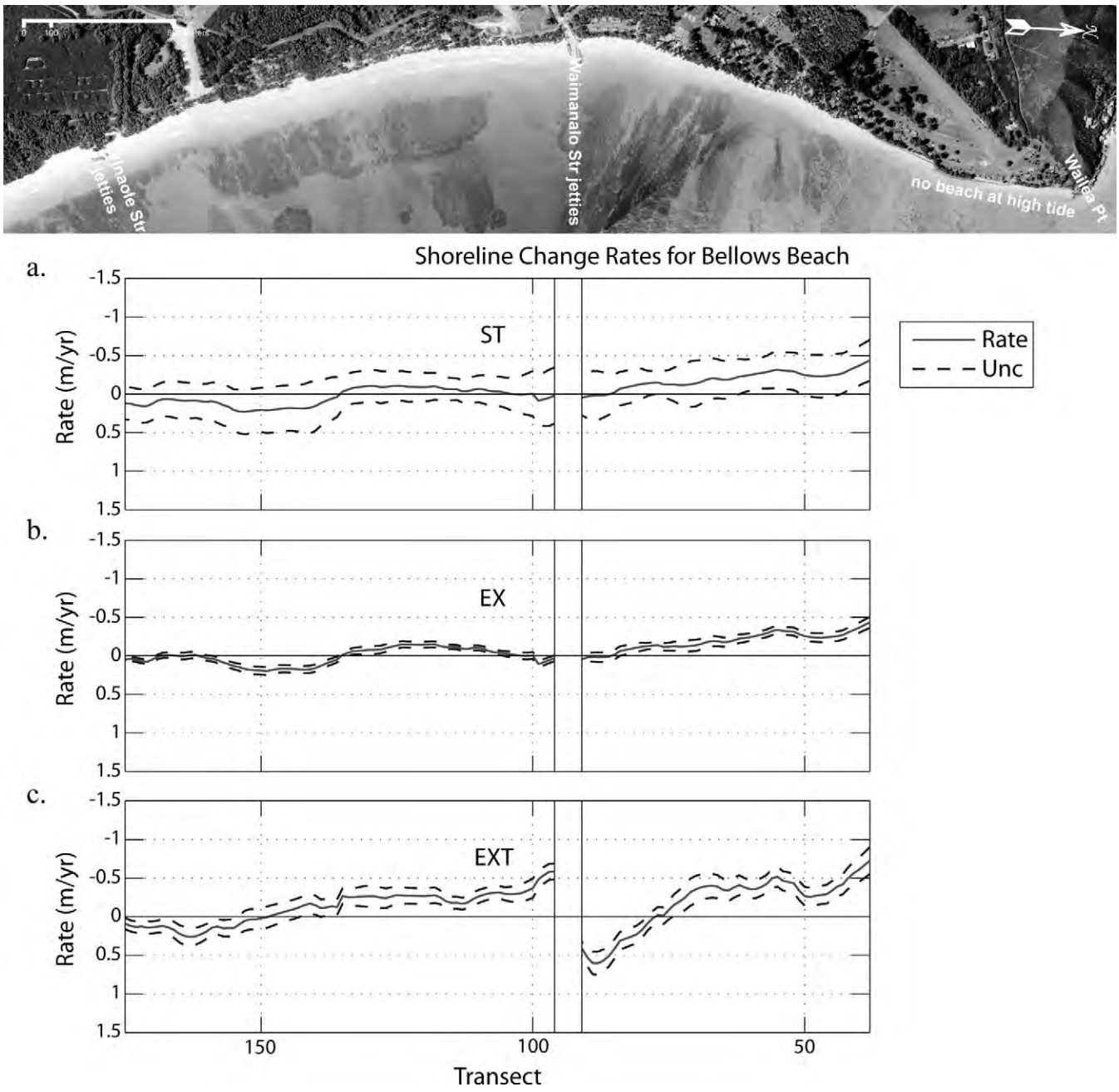

Figure 11. Shoreline change rates (m/y) at Bellows Beach, 1911–2005. Negative rates indicate annual erosion. (a) ST rates with ±uncertainties. Note the high number of transects with insignificant rates (±rate uncertainties overlap 0 m/y) with ST at this beach. (b) EX (lowest IC score among the PX models) rates with ±uncertainties. (c) EXT (lowest IC score among the PXT models) rates with ±uncertainties.

beaches, except at Kaupo Beach Park (Figures 14a–14c). Other than at Kaupo Beach Park, the ST and PX models with the lowest IC scores estimate erosion rates under 0.3 m/y or find no significant change. The rate uncertainty is improved with PX models compared with ST models, resulting in significant rates at a greater percentage of transects. The PXT models with the lowest IC scores detect recent accretion or find no significant change at all beaches, except Kaupo Beach Park.

At Kaupo Beach Park the RX model has the lowest IC score among the PX models. Here, the RX model finds long-term erosion (up to -1.7 ± 0.2 m/y) at the southern end of the beach and long-term accretion at the northern end of the beach (up to 1.2 ± 0.1 m/y). The LXT model, with the lowest

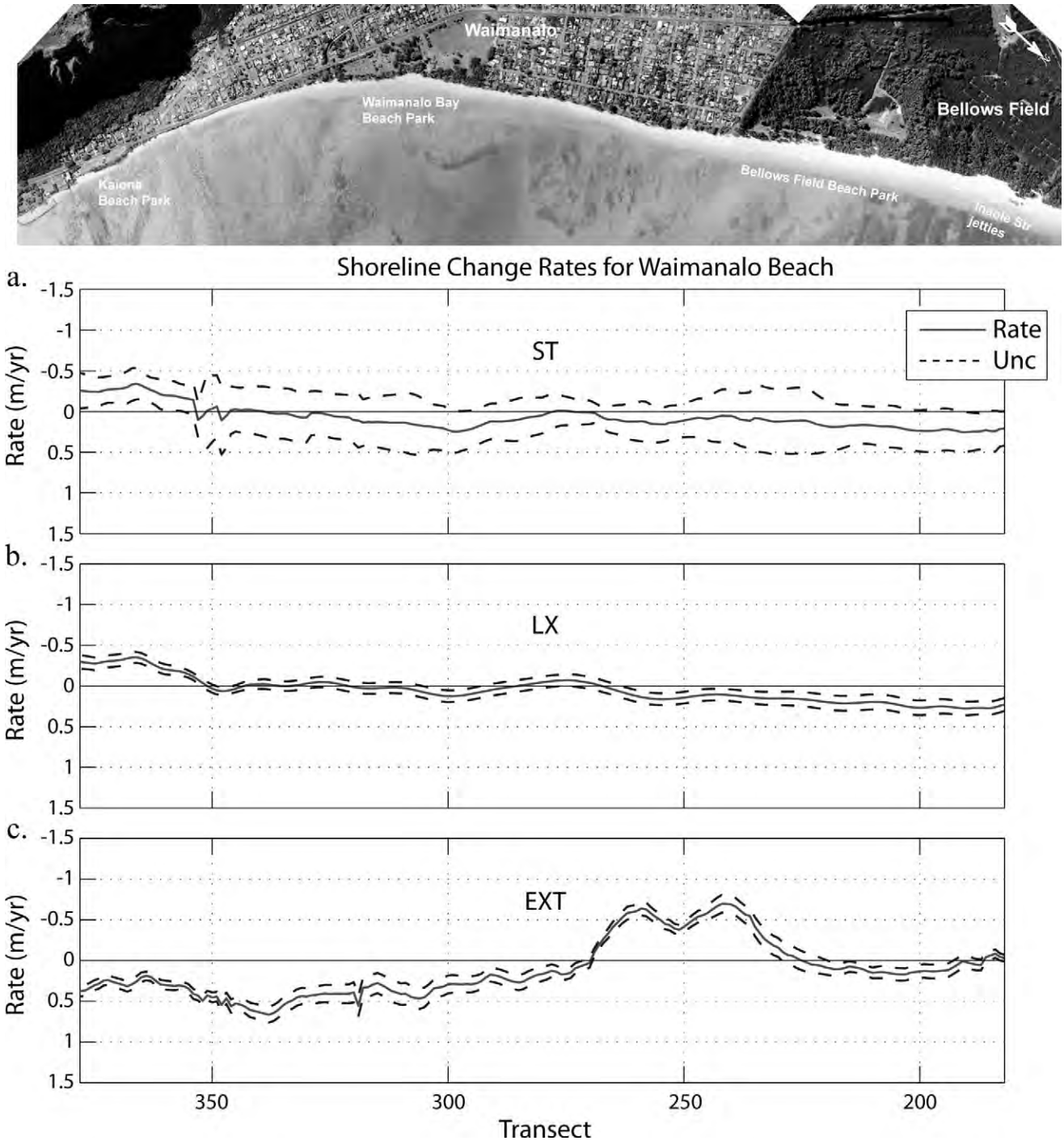

Figure 12. Shoreline change rates (m/y) at south Bellows and Waimanalo beaches, 1911–2005. Negative rates indicate annual erosion. (a) ST rates with ±uncertainties. Note the high number of transects with insignificant rates (±rate uncertainties overlap 0 m/y) with ST at this beach. (b) LX (lowest IC score among the PX models) rates with ±uncertainties. (c) EXT (lowest IC score among the PXT models) rates with ±uncertainties.

IC score among the PXT models, indicates a pattern of shoreline change rates at this beach that is similar to the results of the RX model, with erosion in the south and accretion in the north. However, the results of the RX and LXT models do not agree with the results of the ST, EX, nor EXT models at Kaupo Beach Park, bringing into question the validity of the RX and LXT models at this beach. Nonetheless, the results of the RX and LXT models here point out that Kaupo Beach Park should be monitored closely for future erosion hazards.

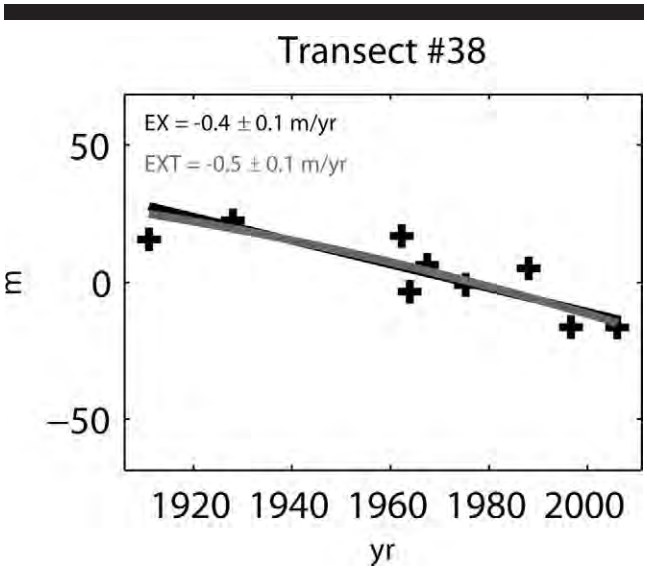

Figure 13. Individual transect plot (transect 38) from northern Bellows Beach. The EXT model results indicate accelerating erosion throughout the time series of historical shorelines in this area.

At Makapuu Beach the PX and PXT models indicating no significant change (rates = 0 m/y) have the lowest IC scores. The LX model (0 m/y) has the lowest IC score among the PX models. The LXT model reverts to the LX model (0 m/y and finds no acceleration) and has the lowest IC score among the PXT models. The ST model rates at Makapuu are statistically insignificant at all transects. Examination of the historical shorelines shows high variability in their position throughout the time span of the study (Figure 15). High seasonal variability is also recorded in beach profile surveys at Makapuu Beach. A lack of available shoreline data (six historical shorelines) for Makapuu may also be limiting our ability to calculate a long-term trend.

DISCUSSION

The EX model has the lowest IC score among the PX models in eight of fourteen beach segments in this study. The EXT model has the lowest IC score among the PXT models in 11 of 14 beach segments. EX and EXT may be calculating models with better fit to the data and fewer parameters because the alongshore polynomial model is composed of basis functions that are derived from the shoreline data itself. The other PX and PXT methods (LX, RX, LXT, RXT), which attempt to fit a series of predetermined mathematical basis functions to the data, often require a greater number of these basis functions (parameters) to produce a satisfactory fit to the data, resulting in higher IC scores. This may be especially true at beaches with one or more sudden sign changes in the shoreline change rates along the shore (*e.g.,* erosion to accretion from one transect to the next). The LX and RX models may fit the shoreline data better where the rates vary smoothly alongshore (*e.g.,* South Bellows and Waimanalo Beach).

Model parameters should be constrained by our knowledge of the physics and/or limits of a system. For example, periodic phenomena such as tides and waves are best modeled using linear combinations of sine and cosine functions. The temporal dynamics of shoreline change are unknown. Because they are calculated from the beach data, eigenvectors (in EX and EXT) may provide a better description of the unknown dynamics of change at a beach than a model with predetermined basis functions (*e.g.,* LX and RX).

Whether the EX and EXT methods actually produce better shoreline change models at most beaches is an area of ongoing research. Further research could include comparison of predictions of the most recent shoreline(s) in truncated shoreline data sets by the various PX and PXT models, as in Genz *et al.* (2009). Updates to this study using modern shorelines (new aerial photography) are necessary to continue monitoring Oahu's beaches for changes in shoreline trends. New shoreline data may be used to test predictions of future shoreline positions made by the models in this study.

Inspection of the PXT models from this study in individual transect plots shows that the most recent trend of accelerating or decelerating rates, as indicated by these models, is often less than 50 years. In other words, the present rates (*i.e.,* rates from the most recent shoreline time) from the PXT models are strongly influenced by the trend of the last several shorelines. Thus, the PXT models are better suited for describing the recent change at a beach and for showing how the rates may have changed throughout the time series of shorelines. The PX models, with a linear fit to the entire time series of shoreline data, provide a better characterization of the long-term change occurring at a beach.

In three of fourteen beach segments in this study, the model showing no change (0 m/y) had the lowest IC score among the PX models. IC's selection of a model showing no change may be interpreted two ways. One, the historical shoreline data are not adequately configured (not enough shorelines, too much positional uncertainty) to calculate statistically defensible shoreline change rates. Or, two, the beach is stable over the time span of the study. For the purpose of shoreline management, a model without rates provides statistically supported evidence that a beach has not changed significantly in the time span of the study. Thus, a result showing no significant change may be as valuable for erosion hazard planning as a model that indicates significant erosion or accretion.

Here we provide the rates and uncertainties from the PX and PXT model with the lowest IC score. However, the specific goals of an agency's coastal management plan may influence planners to choose another of the parsimonious PX or PXT models for erosion hazard planning. It is important that coastal scientists and coastal managers are clear on what question is being asked regarding shoreline change at a beach before reporting shoreline change results. Are we interested in long-term change or more recent change? Are we looking for the worst-case scenario or the most likely scenario? For example, an agency may determine that the most conservative or safest course is to select the model that calculates the highest erosion rates and predicts the greatest erosion hazard. Or, coastal planners may use results from several shoreline change rate calculation methods to present a range of

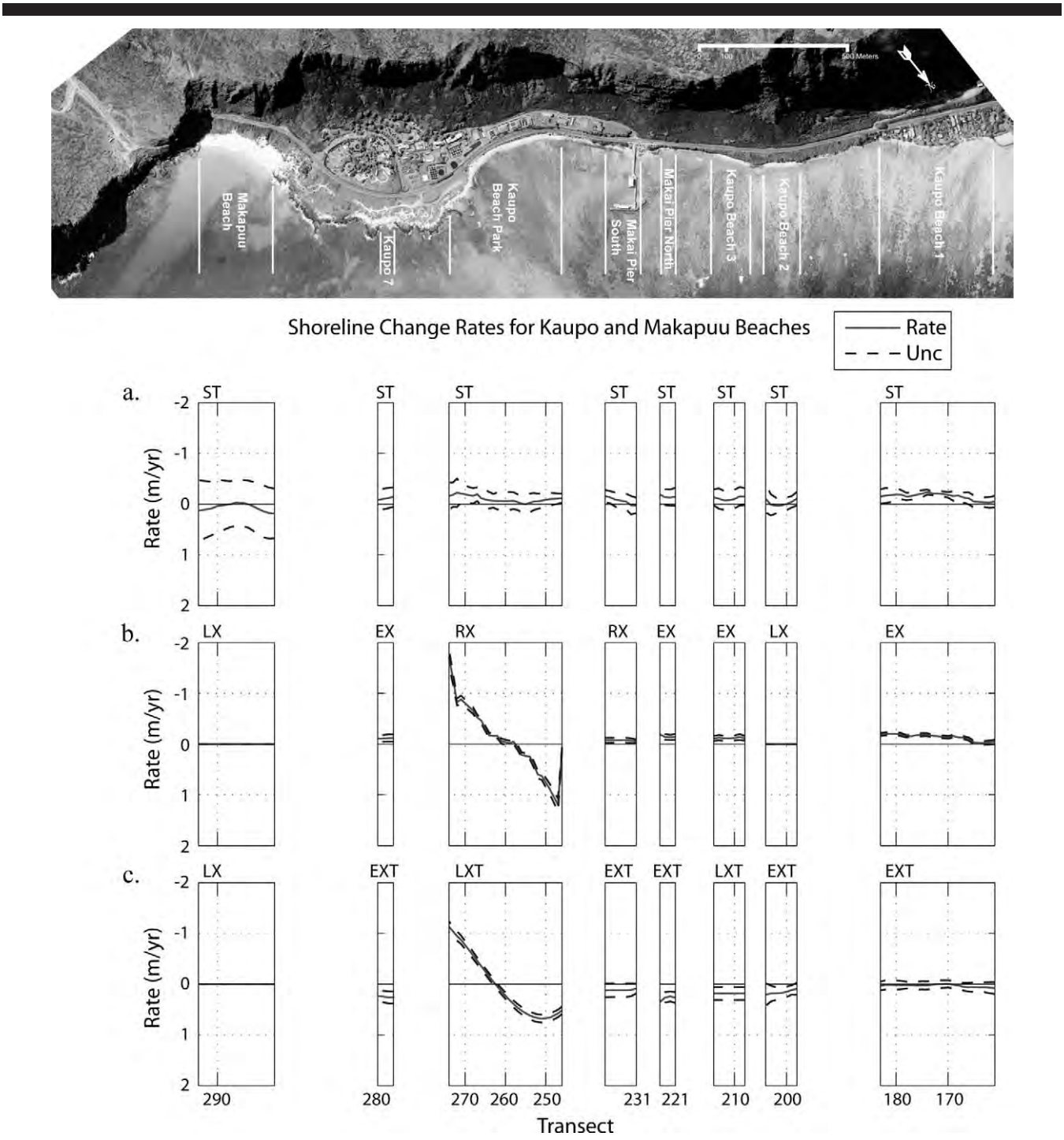

Figure 14. Shoreline change rates (m/y) at Kaupo and Makapuu beaches, 1911–2005. Negative rates indicate annual erosion. (a) ST rates with ±uncertainties. (b) Rates and ±uncertainties calculated by PX model with lowest IC score in each study segment. (c) Rates and ±uncertainties calculated by PXT model with lowest IC score in each study segment.

possible future shoreline change scenarios. Ultimately, the credibility of erosion rates and erosion hazard forecasts is improved if the results from various shoreline change rate calculation methods agree.

Time series of historical shorelines in this study span nearly 100 years. As discussed previously, the recent trend in PXT models often illustrates an erosion or accretion trend of the most recent shorelines (<50 years). Littoral processes along most Hawaiian beaches are driven primarily by waves from frequent easterly trade winds and powerful seasonal swells

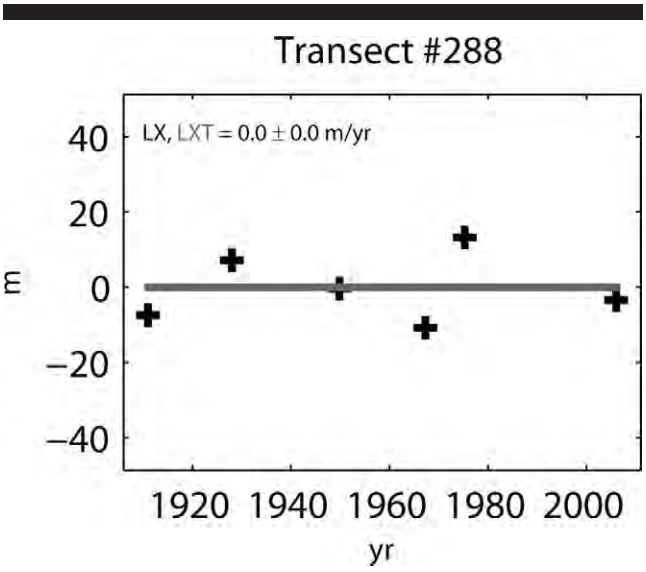

Figure 15. Individual transect plot (transect 288) from Makapuu Beach. The LX and LXT models (with the lowest IC scores among the PX and PXT models) find no significant change at Makapuu Beach, likely a result of the high temporal variability of the shoreline position here.

(Vitousek and Fletcher, 2008). It is possible that some PXT models are detecting shorter term (*e.g.,* decadal) fluctuations in shoreline position related to atmospheric variability (*e.g.,* ENSO, PDO, trade wind oscillations) at some beaches (Rooney *et al.,* 2003), as opposed to chronic, *i.e.,* long-term, shoreline change. An example of this may be the most recent episode of accelerated erosion as modeled by PXT at Kailua Beach Park. There we see at least one other prior episode of erosion and accretion in the movement of the historical shoreline positions. The PXT models (and the PX models) cannot identify multiple erosion and accretion events in a data set. Doing so would require fitting more complex models (*e.g.,* a sinusoid) to a limited shoreline data set, leading to overfitting of the data. In addition, the PXT models are limited by their inability to model the inevitable deceleration that should follow any period of accelerated shoreline change, such as seen at Kailua Beach Park. Theoretically, a rate that continues to accelerate into the future will eventually become unrealistically high. Therefore, the PXT models may not be appropriate for forecasting future shoreline positions in the long term (*e.g.,* 50 years) at most beaches.

Because the PXT methods can detect acceleration, these methods have the prospect of detecting accelerating shoreline change that should be expected with accelerating sea-level rise from global temperature increase (Church and White, 2006). We will attempt to investigate shoreline change due to sea-level rise in our continued studies of all the beaches in the Hawaiian Islands with the PX and PXT methods. Thus far, it appears shoreline change at Hawaii beaches is dominated by the dynamics of the local littoral sediment budget. If Hawaii beaches are changing because of sea-level rise, it appears difficult, at present, to detect this change signal in the background of typically noisy historical shoreline data.

CONCLUSIONS

The EX and EXT methods are the preferred methods for calculating shoreline change rates from historical shoreline data. The most parsimonious model is selected from a range of models utilizing IC. The EX and EXT models have the lowest IC scores among the PX and PXT models (with and without rate acceleration) at most southeast Oahu beaches.

The PX method, with a linear fit to the time series of historical shoreline positions, provides a better characterization of the change that has occurred throughout the time series of shorelines (*i.e.,* long-term). The PXT method, which is able to detect acceleration in the shoreline change rates, may provide additional information about recent change occurring at a beach and can show how the rates may have varied with time. Ability to detect accelerating shoreline change is an important advance because a beach may not change at a constant (linear) rate. The PXT models may identify potential erosion hazards not detected by the ST and PX models. Recent accelerated shoreline change detected by the PXT models provides additional valuable information that will help shoreline managers better plan for future erosion hazards.

The PX and PXT methods calculate shoreline change rates from an improved data set, compared with the ST method, by utilizing data from all shoreline transects on a beach. Therefore, the PX and PXT methods invariably calculate rates with lower uncertainties than the ST method. The result is a greater percentage of transects with significant rates and increased confidence in results from these models. Improved confidence in results from shoreline change studies will help shoreline managers to make better-informed decisions to protect against future erosion hazards.

In the time span of this study (1911–2005) nearly 2 km (1919 m) of beach were lost to erosion along the southeast Oahu shoreline, most notably at Lanikai and North Bellows. Calculating shoreline change rates with the PX methods indicates areas of significant long-term erosion at northern and central Bellows Beach and in the south of Waimanalo Beach. The PX methods indicate long-term accretion along most of Kailua Beach and Lanikai Beach. The PXT methods detect recent accelerating erosion at southern Kailua Beach, northern Bellows Beach, and at Kaupo Beach Park.

ACKNOWLEDGMENTS

Funding for this study was made available by U.S. Geological Survey National Shoreline Assessment Project, State of Hawaii Department of Land and Natural Resources, City and County of Honolulu, Hawaii Sea Grant College, U.S. Army Corps of Engineers, Harold K.L. Castle Foundation, and Hawaii Coastal Zone Management Program. We thank Matthew Dyer, Tiffany Anderson, Chris Bochicchio, Sean Vitousek, Amanda Vinson, and Craig Senter of the University of Hawaii Coastal Geology Group for their support on this project.

LITERATURE CITED

Bochicchio, C.; Fletcher, C.; Dyer, M.; and Smith, T., 2009. Reef top sediment bodies: windward Oahu, Hawaii. *Pacific Science,* 63, 61–82.

Bodge, K. and Sullivan, S., 1999. Hawaii pilot beach restoration pro-

C3

ject: Coastal engineering investigation. Prepared for State of Hawai'i, Department of Land and Natural Resources, Honolulu.
Burnham, K.P. and Anderson, D.R., 2002. *Model Selection and Multimodel Inference,* 2nd edition. New York: Springer-Verlag.
Church, J.A. and White, N.J., 2006. A 20th century acceleration in global sea-level rise. *Geophysical Research Letters,* 33(L01602).
Crowell, M.; Leatherman, S.P., and Buckley, M.K., 1991. Historical shoreline change: error analysis and mapping accuracy. *Journal of Coastal Research,* 7(3), 839–852.
Daniels, R.C. and Huxford, R.H., 2001. An error assessment of vector data derived from scanned National Ocean Service topographic sheets. *Journal of Coastal Research,* 17(3), 611–619.
Draper, N.R. and Smith, H., 1998. *Applied Regression Analysis,* 3rd edition. New York: John Wiley & Sons, Inc.
Ellis, M.Y., 1978. *Coastal Mapping Handbook,* U.S. Department of the Interior, Geological Survey; U.S. Department of Commerce, National Ocean Survey. Washington, D.C.: U.S. Government Printing Office, 199p.
Fletcher, C.; Mullane, R.; and Richmond, B., 1997. Beach loss along armored shorelines on Oahu, Hawaiian Islands. *Journal of Coastal Research,* 13, 209–215.
Fletcher, C.H.; Rooney, J.J.B.; Barbee, M.; Lim, S.-C., and Richmond, B.M., 2003. Mapping shoreline change using digital orthophotogrammetry on Maui, Hawaii. *Journal of Coastal Research,* Special Issue No. 38, pp. 106–124.
Frazer, L.N.; Genz, A.S., and Fletcher, C.H., 2009. Toward parsimony in shoreline change prediction (I): new methods. *Journal of Coastal Research.* In press.
Genz, A.S.; Fletcher, C.H.; Dunn, R.A.; Frazer, L.N., and Rooney, J.J., 2007. The predictive accuracy of shoreline change rate methods and alongshore beach variation on Maui, Hawaii. *Journal of Coastal Research,* 23(1), 87–105.
Genz, A.S.; Frazer, L.N., and Fletcher, C.H., 2009. Toward parsimony in shoreline change prediction (II): applying statistical methods to real and synthetic data. *Journal of Coastal Research.* In press.
Hapke, C.J. and Reid, D., 2007. National Assessment of Shoreline Change: Part 4: Historical Coastal Cliff Retreat along the California Coast. U.S. Geological Survey Open File Report 2005-401. http://pubs.usgs.gov/of/2007/1133/ (accessed May 14, 2006).
Hapke, C.J.; Reid, D.; Richmond, B.M.; Ruggiero, P., and List, J., 2006. National Assessment of Shoreline Change: Part 3: Historical Shoreline Change and Associated Coastal Land Loss along Sandy Shorelines of the California Coast. U.S. Geological Survey Open File Report 2005-1401. http://pubs.usgs.gov/of/2006/1219/ (accessed September 15, 2006).
Harney, J.N. and Fletcher, C.H., 2003. A budget of carbonate framework and sediment production, Kailua Bay, Oahu, Hawaii. *Journal of Sedimentary Research,* 73(6), 856–868.
Hwang, D., 1981. Beach Changes on Oahu as Revealed by Aerial Photographs. Prepared by the Urban Regional Planning Program, Hawaii Institute of Geophysics, and Sea Grant Program, University of Hawaii for the Dept. of Planning and Economic Development, State of Hawaii. Technical Supplement 22—Hawaii Coastal Zone Management Program; HIG-81-3; UNIHI-SEAGRANT-CR-81-07. Hawaii, USA.
Morton, R.A. and Miller, T.A., 2005. National Assessment of Shoreline Change: Part 2: Historical Shoreline Changes and Associated Coastal Land Loss along the U.S. Southeast Atlantic Coast. U.S. Geological Survey Open File Report 2005-1401. http://pubs.usgs.gov/of/2005/1401/ (accessed March 3, 2006).
Morton, R.A.; Miller, T.A., and Moore, L.J., 2004. National Assessment of Shoreline Change: Part 1: Historical Shoreline Changes and Associated Coastal Land Loss along the U.S. Gulf of Mexico. U.S. Geological Survey Open File Report 2004-1043. http://pubs.usgs.gov/of/2004/1043 (accessed September 15, 2006).
National Academy of Sciences, 1990. *Managing Coastal Erosion.* Washington D.C.: National Research Council, Committee on Coastal Erosion Zone Management, National Academy Press.
Norcross-Nu'u, Z.M. and Abbott, T., 2005. Adoption of Erosion Rate-Based Setbacks in Maui, Hawaii: Observations and Lessons Learned. *Solutions to Coastal Disasters Conference.* (Charleston, S.C).
Norcross, Z. M. and Abbott, T., 2005. Adoption of Erosion Rate-Based Setbacks in Maui, Hawaii: Observations and Lessons Learned. *Solutions to Coastal Disasters 2005.* pp. 697–705. American Society of Civil Engineers, Virginia, USA.
PCI Geomatica Orthoengine, v.10. www.pcigeomatics.com (accessed September 10, 2007).
Rooney, J.J.B.; Fletcher, C.H.; Barbee, M.; Eversole, D.; Lim, S.-C.; Richmond, B.M., and Gibbs, A., 2003. Dynamics of Sandy Shorelines in Maui, Hawaii: Consequences and Causes. *Coastal Sediments '03 Proceedings* Clearwater Beach, Florida.
Sea Engineering, 1988. Oahu Shoreline Study. City and County of Honolulu. Honolulu, Hawaii: Department of Land Utilization.
Shalowitz, A.L., 1964. *Shore and Sea Boundaries.* Publication 10–1. Washington D.C.: U.S. Department of Commerce.
Sherrod, D.R.; Sinton, J.M.; Watkins, S.E., and Brunt, K.M., 2007. Geologic Map of the State of Hawaii. U.S. Geological Survey, Open-File Report 2007-1089, v 1.0.
Vitousek, S. and Fletcher, C., 2008. Maximum annually recurring wave heights in Hawaii. *Pacific Science,* 62(4) 541–554.

APPENDIX G

CMB REPORT 06-014: RESULTS OF OFFSHORE SAND INVESTIGATION FOR THE SOUTHEAST OAHU REGIONAL SEDIMENT MANAGEMENT DEMONSTRATION PROJECT, HAWAII, HONOLULU DISTRICT

GEOTECHNICAL AND STRUCTURES LABORATORY
ENGINEER RESEARCH AND DEVELOPMENT CENTER
US ARMY CORPS OF ENGINEERS

Geotechnical and Structures Laboratory

US Army Corps of Engineers®
Engineer Research and Development Center

Concrete and Materials Branch
Testing and Evaluation Program

CMB Report 06-014: Results of Offshore Sand Investigation for the Southeast Oahu Regional Sediment Management Demonstration Project, Hawaii, Honolulu District

Joe G. Tom and Judy C. Tom

September 2006

Concrete and Materials Branch
Testing and Evaluation Program

September 2006

CMB Report 06-014: Results of Offshore Sand Investigation for the Southeast Oahu Regional Sediment Management Demonstration Project, Hawaii, Honolulu District

Prepared For

US Army Engineer District, Honolulu

By Joe G. Tom and Judy C. Tom

US Army Engineer Research and Development Center
3909 Halls Ferry Road
Vicksburg, MS 39180-6199

Contents

Preface

The work described in this report was authorized by the US Army Engineer District, Honolulu, (POH) for the Southeast Oahu Regional Sediment Management (SEO/RSM) Demonstration Project. The work was performed under MIPR No. W81HEM50275957, managed at the US Army Engineer Research and Development Center (ERDC), Vicksburg, MS. Mr. Joe G. Tom, ERDC, Geotechnical and Structures Laboratory (GSL), was the Principal Investigator. Mr. Tom and Ms. Judy C. Tom prepared this report. Drs. Philip G. Malone and Charles A. Weiss, Jr., GSL, consulted on the investigation.

Dr. W. Allen Roberson, Chief, Concrete and Materials Branch (CMB), monitored the investigation at ERDC, GSL, under the general supervision of Dr. Albert J. Bush, Chief, Engineering Systems and Materials Division, and Dr. David W. Pittman, Director, GSL.

1 Introduction

Background

The US Army Engineer Research and Development Center (ERDC) have the responsibility of quality assurance for construction materials on US Army Corps of Engineers projects. That responsibility includes the assurance that all construction materials meet the minimum requirements of the project specifications. The ERDC performs this function for the Districts through its Laboratories. The quality assurance responsibility also includes preliminary investigations of construction materials in preparation of the Materials Design Memorandum for the Districts. Construction materials include portland-cement concretes, asphalt concrete, soils, stones, joint materials, steel reinforcements, and other materials as requested.

This investigation is being conducted to determine the general movement of sediment offshore of Wailea Point (which is located in the central portion of the region).

Analysis of sediment grain size trends; Benthic sand samples will be collected around target SEO/RSM areas for grain size determination. Analysis of the resulting grain size distributions will reveal trends (i.e., coarse vs. fine) of long-term sediment erosion and deposition within adjacent areas of the sample regions. Sediment sampling will be carried out in two locations: (1) ~2.0 km^2 vicinity of Wailea Point. (250 samples) and (2) a smaller study on the shoreward opening of the Kailua sand channel (100 samples).

Sample spacing will be denser in areas of more specific interest, such as a 37.5 m spacing applied in the immediate vicinity of Wailea Point. changing to 75 m spacing in the off shore sand fields and 150 m spacing in the regions between sand fields. The resulting sediment transport vectors will have resolutions varying with sample spacing, such that vectors near shore will be plotted every 75 m and vectors in offshore sand fields will be plotted every 150 m. A final report containing all data, procedures, results, and interpretations from the grain size trend analysis will be

delivered. The approach and theory behind grain size trend analysis is published in McLaren and Bowles (1985), Goa and Collins (1992), Le Roux (1994), Hughes (2005).

Authorization

This work is authorized under US Army Engineer District, Honolulu, MIPR No. W81HEM50275957. Mr. Thomas D. Smith, CEPOH-EC-T, made the request for the offshore sediment sampling investigations.

Objective

The objective of this report is to provide specific results of tests and evaluations performed on the sand samples that are to be used in the sediment trend analysis.

Samples

The Concrete and Materials Branch (CMB) of the Geotechnical and Structures Laboratory, ERDC, received 224 samples of various beach sands taken from offshore of Wailea Point as shown on the maps in Appendix A. The samples were assigned CMB Serial Number 060166 supplemented with the POH sample number as shown in Appendix B, Table B1. The sand samples were collected by students from the University of Hawaii at Manoa under the direction of Mr. Christopher Bochiccho, Department of Geology and Geophysics, and Mr. Thomas D. Smith, CEPOH-EC-T, and sent to ERDC. Appendix B, Table B1 lists the initial mass determinations from the University of Hawaii and also the results determined from the as-received mass in their original bags and the oven-dry mass of each sample. Numerically, the samples are listed as 0 to 295, with many samples not sent to ERDC for analysis; those are indicated with a zero reading rather than a blank or deleted listing. Two samples, No. 76 and No. 144, were indicated as having been sent for analysis, however the samples were not found in the shipping containers. Another sample, No. 293, was indicated as having no sample sent for analysis; however, the sample numbered as 293 was found in the shipping containers and evaluated with the other samples.

Tests

The sand samples were tested and evaluated for particle size distribution with the current version of the following test methods or specifications:

a. ASTM C 136, “Standard Test Method for Sieve Analysis of Fine and Coarse Aggregates.”

b. ASTM C 702, “Standard Practice for Reducing Samples of Aggregate to Testing Size.”

2 Evaluation

Sand Samples

The 224 samples of various beach sands (CMB Serial No. 060166) were evaluated in accordance with the standard test method, ASTM C 136. Each sample was removed from the zip-lock bag and surface-dried in a 100-degree F environmental room for approximately 24 hours to allow the wet dust material adhering to the interior of the bag to dry so that it could be easily removed without lost. The dry dust material was added back to the original sample and the entire sample was oven-dried to a constant mass. The larger samples of beach sand were reduced to testing size using a mechanical splitter in accordance with ASTM C 702.

The standard method requires the use of sieves designated in SI units and listed in units of millimeters and microns with an alternate listing in US inches. The SI sieves were converted to Phi, Φ, units as required by the Honolulu District personnel. The conversion on the sieve sizes are listed in Table 1 below. The nest of sieves started with -2.0-Phi down to 5.0-Phi sieve size in 0.5-Phi intervals. The nest of sieves included 15 individual sieves plus a collecting pan. Due to the large number of sieves, the analysis was divided into two operations, one set of sieves from -2.0-Phi to 2.0-Phi, and another set of sieves from 2.5-Phi to 5.0-Phi. Therefore, each sample or split portion was sieved twice, once in the larger sieves and then the material remaining in the collecting pan was placed in the second set of sieves and tested.

The material retained on each individual sieve was weighed and final mass recorded. The results were calculated as a percentage of the total sample sieved. All of the material from each sample was returned to the original bag and will be shipped back to Mr. Thomas D. Smith, CEPOH-EC-T, in Honolulu, Hawaii, upon completion of this investigation.

Table 1. Phi units with conversions to SI units and US equivalent units

Phi Units	Conversion to SI units	Standard Sieve Designation	Alternative US Designation
Φ	mm	mm / μm	No.
-2.0	4.00	4.00	No. 5
-1.5	2.83	2.80	No. 7
-1.0	2.00	2.00	No. 10
-0.5	1.41	1.40	No. 14
0.0	1.00	1.00	No. 18
0.5	0.707	710	No. 25
1.0	0.500	500	No. 35
1.5	0.354	355	No. 45
2.0	0.250	250	No. 60
2.5	0.177	180	No. 80
3.0	0.125	125	No. 120
3.5	0.088	90	No. 170
4.0	0.063	63	No. 230
4.5	0.044	45	No. 325
5.0	0.031	32	No. 450

3 Conclusions and Recommendations

Sand Samples

The 224 samples of beach sand (CMB Serial No. 060166) were tested and evaluated for particle size distribution in accordance with the project requirements. The sample results are provided as the results of the percentage of the total amount sieved per sieve size. The results are shown in graphic format to display the distribution of the particles sizes throughout the range of the sample as presented in Appendix C. The numerical results are provided in Appendix D.

POH personnel indicated 225 samples were sent; however, only 224 samples were received. Sample numbers 76 and 144 were not received with the other samples. Sample number 293 was not listed as being sent; however, a sample identified as number 293 was received and analyzed. A total of 224 samples were received and analyzed for particle size distribution.

Appendix A

Maps of Sand Sample Locations

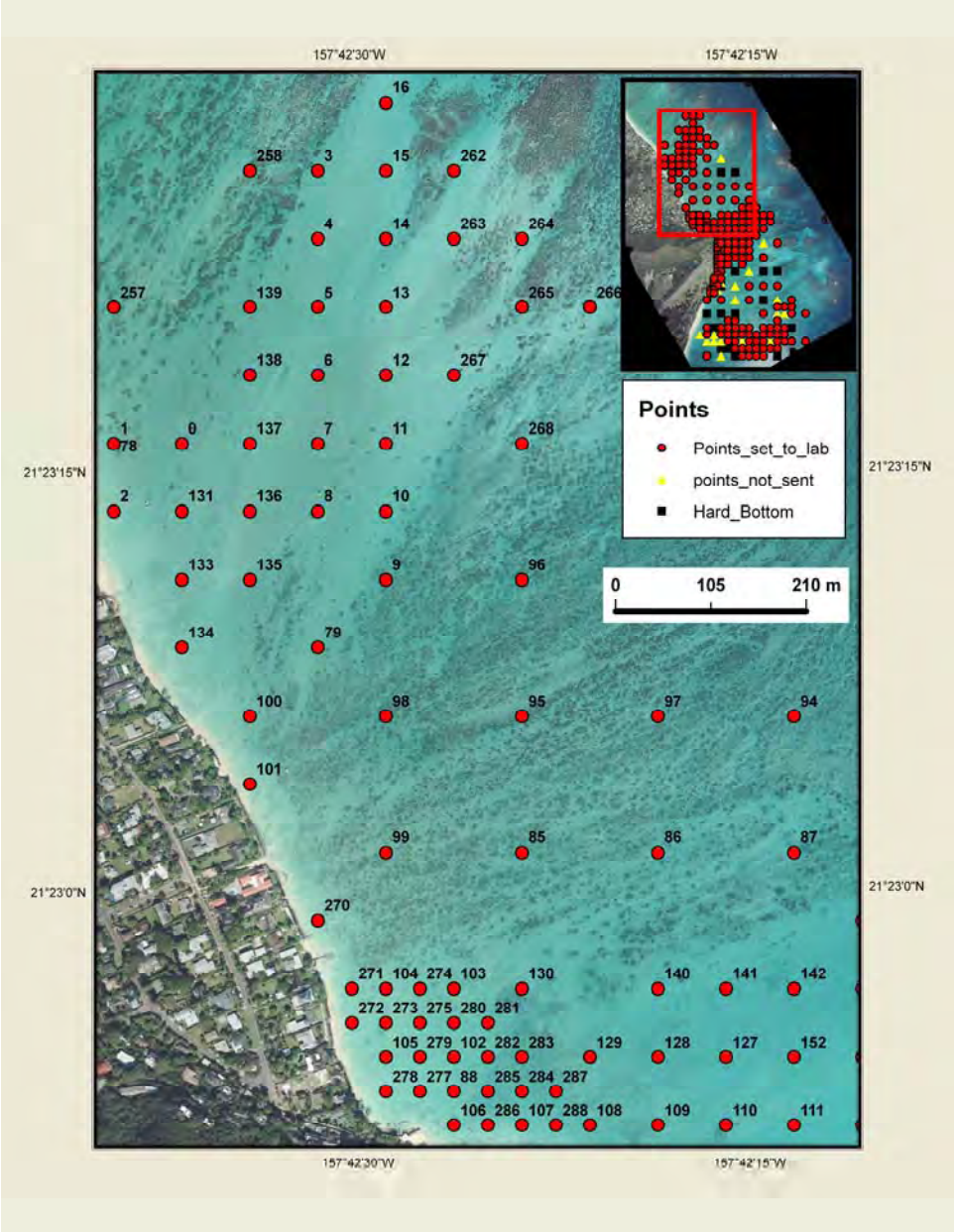
157°42'30"W
157°42'15"W
21°23'15"N
21°23'0"N
Points
Points_set_to_lab
points_not_sent
Hard_Bottom
0
105
210 m

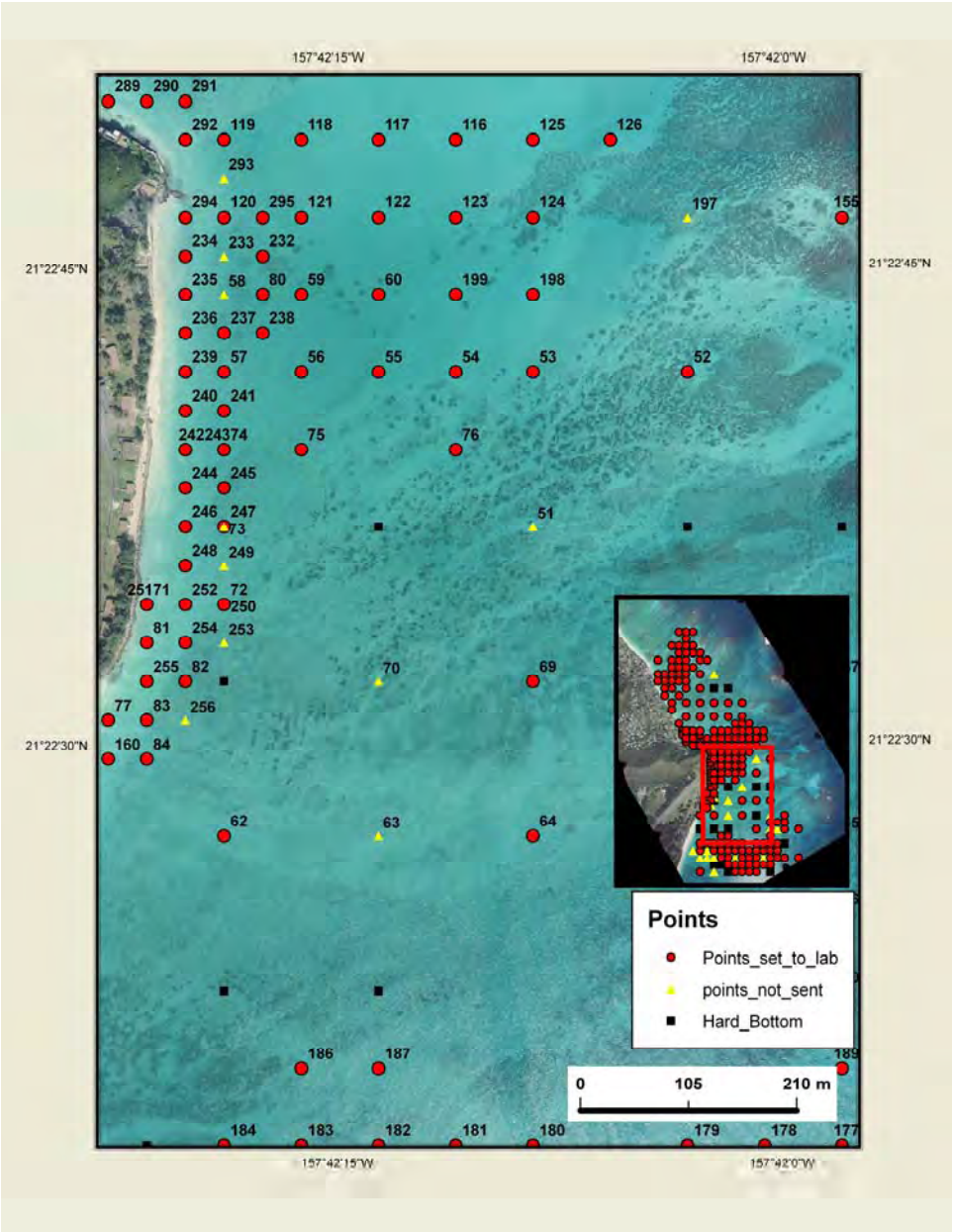
157°42'15"W
157°42'0"W
21°22'45"N
21°22'30"N
289 290 291
292 119 118 117 116 125 126
293
294 120 295 121 122 123 124 197 155
234 233 232
235 58 80 59 60 199 198
236 237 238
239 57 56 55 54 53 52
240 241
24224374 75 76
244 245
246 247 73 51
248 249
25171 252 72 250
81 254 253
255 82 70 69
77 83 256
160 84
62 63 64
186 187 189
184 183 182 181 180 179 178 177
Points
Points_set_to_lab
points_not_sent
Hard_Bottom
0 105 210 m

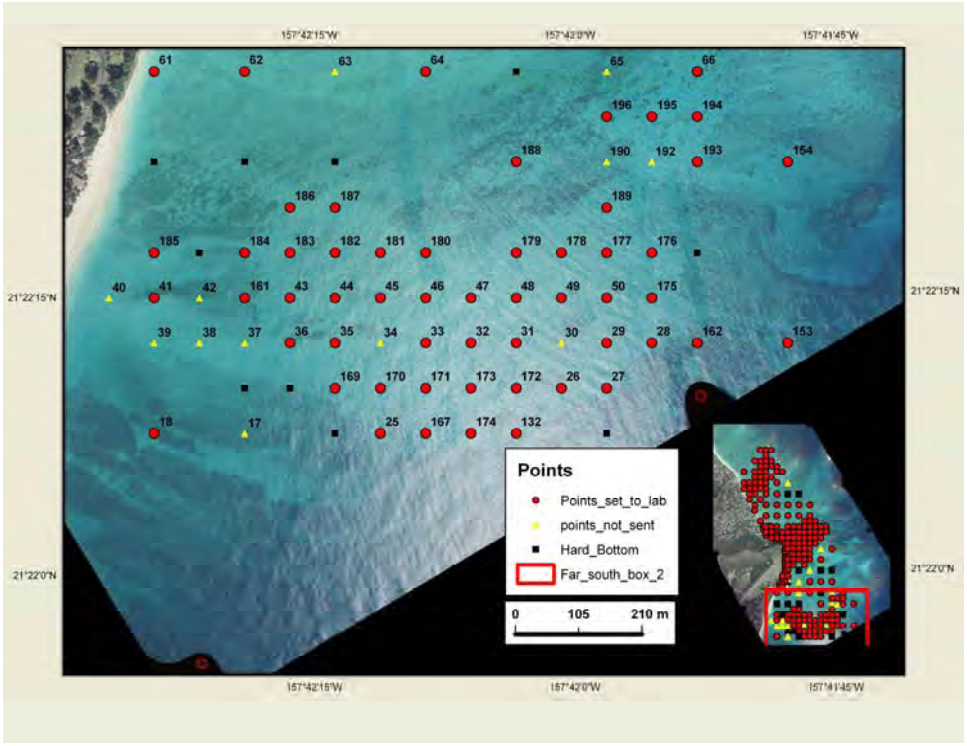
157°42'15"W
157°42'0"W
157°41'45"W
21°22'15"N
21°22'0"N
61
62
63
64
65
66
196
195
194
188
190
192
193
154
186
187
189
185
184
183
182
181
180
179
178
177
176
40
41
42
161
43
44
45
46
47
48
49
50
175
39
38
37
36
35
34
33
32
31
30
29
28
162
153
169
170
171
173
172
26
27
18
17
25
167
174
132
Points
Points_set_to_lab
points_not_sent
Hard_Bottom
Far_south_box_2
0
105
210 m

Appendix B

Sand Sample Identification and Masses

Table 2. Sand Samples, CMB Serial Number 060166				
CMB Serial Supplement No.	**Field Identification**	**POH Mass, g**	**As-Received Mass in Bag, g**	**Oven-Dry Mass, g**
0	0	615	586	432.0
1	1	538	511	376.10
2	2	630	626	450.2
3	3	452	441	309.40
4	4	604	583	423.4
5	5	650	606	452.2
6	6	568	545	435.5
7	7	716	617	501.9
8	8	705	646	489.1
9	9	625	562	381.90
10	10	672	685	478.7
11	11	747	695	522.7
12	12	780	718	511.5
13	13	611	553	421.3
14	14	768	709	534.2
15	15	584	557	399.90
16	16	589	523	416.0
17	No Sample	No Sample	0	0
18	18	708	715	521.1
19	No Sample	No Sample	0	0
20	No Sample	No Sample	0	0
21	No Sample	No Sample	0	0
22	No Sample	No Sample	0	0
23	No Sample	No Sample	0	0
24	No Sample	No Sample	0	0
25	25	759	758	580.0
26	26	645	646	509.8
27	27	836	846	649.5
28	28	504	504	425.6
29	29	605	622	477.5
30	No Sample	No Sample	0	0
31	31	601	591	415.3
32	32	643	642	448.7
33	33	632	635	436.2
34	No Sample	No Sample	0	0
35	35	566	566	406.3
36	36	558	558	400.4
37	No Sample	No Sample	0	0
38	No Sample	No Sample	0	0
39	No Sample	No Sample	0	0
40	No Sample	No Sample	0	0
41	41	553	558	426.4
42	No Sample	No Sample	0	0
43	43	498	499	444.8
CMB Serial	**Field**	**POH Mass, g**	**As-Received**	**Oven-Dry**

Supplement No.	Identification		Mass in Bag, g	Mass, g
44	44	814	785	539.9
45	45	574	576	460.8
46	46	479	478	411.8
47	47	560	555	400.5
48	48	639	625	438.2
49	49	563	562	434.0
50	50	753	732	533.0
51	No Sample	No Sample	0	0
52	52	598	542	410.1
53	53	481	419	322.74
54	54	577	548	359.91
55	55	646	613	476.6
56	56	529	503	374.43
57	57	627	597	459.3
58	No Sample	No Sample	0	0
59	59	554	521	343.28
60	60	530	518	364.77
61	61	650	649	470.9
62	62	769	723	501.1
63	No Sample	No Sample	0	0
64	64	553	552	388.24
65	No Sample	No Sample	0	0
66	66	709	642	454.6
67	67	946	880	624.9
68	68	479	334	306.37
69	No Sample	No Sample	0	0
70	No Sample	No Sample	0	0
71	71	848	800	592.7
72	72	513	427	315.3
73	No Sample	No Sample	0	0
74	74	443	402	278.15
75	75	779	686	469.6
76	76	430	Not Received	Not Received
77	77	1052	1020	743.8
78	78	1183	1082	886.1
79	79	1041	985	746.8
80	80	>2100	2529	1857.2
81	81	>2100	2461	1838.3
82	82	2065	1851	1371.9
83	83	1654	1592	1225.9
84	84	>2100	2327	1711.7
85	85	1560	1544	1126.5
86	86	>2100	2255	1437.7
87	87	>2100	1975	1469.6
88	88	1324	1205	873.8
CMB Serial Supplement	**Field Identification**	**POH Mass, g**	**As-Received Mass in Bag, g**	**Oven-Dry Mass, g**

No.				
89	89	1116	1050	776.7
90	90	>2100	2716	2137.5
91	91	>2100	1942	1294.2
92	92	888	835	605.4
93	93	1268	1177	880.5
94	94	>2100	2147	1620.9
95	95	>2100	2037	1665.9
96	96	2006	1882	1225.8
97	97	1413	1337	1032.5
98	98	1759	1575	1274.5
99	99	>2100	1840	1452.2
100	100	755	720	536.1
101	101	1774	1754	1233.3
102	102	555	506	368.02
103	103	644	610	473.3
104	104	477	468	315.88
105	105	610	556	398.90
106	106	687	671	501.5
107	107	616	588	424.6
108	108	729	712	509.5
109	109	503	484	332.49
110	110	561	548	377.64
111	111	620	616	430.7
112	112	605	591	412.1
113	113	651	638	452.2
114	114	577	519	366.41
115	115	478	471	306.62
116	116	567	543	381.01
117	117	551	531	363.26
118	118	624	589	414.8
119	119	624	561	398.80
120	120	605	567	410.3
121	121	435	402	280.01
122	122	607	602	402.6
123	123	560	524	389.19
124	124	639	570	444.2
125	125	521	490	349.93
126	126	583	534	348.16
127	127	603	545	386.73
128	128	520	480	368.42
129	129	442	399	298.89
130	130	604	551	371.51
131	131	718	641	484.1
132	132	480	456	324.24
133	133	713	609	485.5
CMB Serial Supplement No.	**Field Identification**	**POH Mass, g**	**As-Received Mass in Bag, g**	**Oven-Dry Mass, g**

134	134	520	505	380.99
135	135	650	606	469.2
136	136	622	577	490.7
137	137	720	656	505.0
138	138	665	565	456.0
139	139	487	433	339.82
140	140	783	734	524.7
141	141	514	487	365.02
142	142	547	508	348.48
143	143	566	522	371.96
144	144	558	Not Received	Not Received
145	145	532	462	352.46
146	146	528	512	354.39
147	147	666	647	492.9
148	148	561	549	430.7
149	149	604	567	409.6
150	150	639	619	443.2
151	151	582	557	390.11
152	152	561	521	376.17
153	153	1947	1887	1323.4
154	154	1056	989	714.2
155	155	1884	1796	1263.1
156	No Sample	No Sample	0	0
157	No Sample	No Sample	0	0
158	158	>2100	2016	1704.5
159	No Sample	No Sample	0	0
160	160	489	464	347.42
161	161	1254	1134	898.1
162	162	>2100	2386	1722.0
163	No Sample	No Sample	0	0
164	No Sample	No Sample	0	0
165	No Sample	No Sample	0	0
166	No Sample	No Sample	0	0
167	167	892	885	657.8
168	No Sample	No Sample	0	0
169	169	579	572	419.7
170	170	702	696	577.1
171	171	722	704	527
172	172	815	777	564.4
173	173	759	754	549.7
174	174	976	893	635.3
175	175	637	619	458.2
176	176	467	474	391.0
177	177	658	650	466.8
178	178	515	511	386.76
CMB Serial Supplement No.	**Field Identification**	**POH Mass, g**	**As-Received Mass in Bag, g**	**Oven-Dry Mass, g**
179	179	701	694	488.1

180	180	569	568	459.2
181	181	1103	1117	890.5
182	182	527	513	369.88
183	183	741	733	537.8
184	184	640	653	522.5
185	185	1011	1007	821.9
186	186	565	561	453.7
187	187	600	597	463.8
188	188	545	541	370.63
189	189	774	772	573.2
190	No Sample	No Sample	0	0
191	No Sample	No Sample	0	0
192	No Sample	No Sample	0	0
193	193	463	453	335.94
194	194	532	530	462.0
195	195	466	467	405.3
196	196	752	750	568.3
197	No Sample	No Sample	0	0
198	198	521	479	327.65
199	199	545	528	365.54
200	No Sample	No Sample	0	0
201	No Sample	No Sample	0	0
202	No Sample	No Sample	0	0
203	No Sample	No Sample	0	0
204	No Sample	No Sample	0	0
205	No Sample	No Sample	0	0
206	No Sample	No Sample	0	0
207	No Sample	No Sample	0	0
208	No Sample	No Sample	0	0
209	No Sample	No Sample	0	0
210	No Sample	No Sample	0	0
211	No Sample	No Sample	0	0
212	No Sample	No Sample	0	0
213	No Sample	No Sample	0	0
214	No Sample	No Sample	0	0
215	No Sample	No Sample	0	0
216	No Sample	No Sample	0	0
217	No Sample	No Sample	0	0
218	No Sample	No Sample	0	0
219	No Sample	No Sample	0	0
220	No Sample	No Sample	0	0
221	No Sample	No Sample	0	0
222	No Sample	No Sample	0	0
223	No Sample	No Sample	0	0
CMB Serial Supplement No.	**Field Identification**	**POH Mass, g**	**As-Received Mass in Bag, g**	**Oven-Dry Mass, g**
224	No Sample	No Sample	0	0
225	No Sample	No Sample	0	0

226	No Sample	No Sample	0	0
227	No Sample	No Sample	0	0
228	No Sample	No Sample	0	0
229	No Sample	No Sample	0	0
230	No Sample	No Sample	0	0
231	No Sample	No Sample	0	0
232	232	588	576	389.22
233	No Sample	No Sample	0	0
234	234	811	781	575.3
235	235	588	612	444.8
236	236	519	510	371.03
237	237	863	742	562.3
238	238	772	728	507.0
239	239	743	672	497.8
240	240	854	864	644.7
241	241	1087	1013	768.2
242	242	735	687	504.0
243	243	997	939	739.1
244	244	823	806	613.9
245	245	460	455	286.84
246	246	833	798	621.0
247	247	469	450	325.89
248	248	822	800	587.5
249	No Sample	No Sample	0	0
250	250	548	482	332.20
251	251	797	778	579.7
252	252	852	831	610.0
253	No Sample	No Sample	0	0
254	254	747	735	536.5
255	255	783	739	547.2
256	No Sample	No Sample	0	0
257	257	1100	1019	743.8
258	258	543	516	413.7
259	259	591	536	410.7
260	260	988	847	674.5
261	261	753	705	547.5
262	262	737	698	506.7
263	263	719	642	523.3
264	264	624	550	444.9
265	265	733	646	526.2
266	266	605	598	418.0
267	267	672	638	444.2
268	268	738	690	517.1
CMB Serial Supplement No.	**Field Identification**	**POH Mass, g**	**As-Received Mass in Bag, g**	**Oven-Dry Mass, g**
269	No Sample	No Sample	0	0
270	270	667	636	467.7
271	271	829	793	569.5

272	272	798	732	542.0
273	273	731	653	475.7
274	274	667	583	431.4
275	275	786	746	553.8
276	276	646	613	454.6
277	277	1005	1024	760.8
278	278	754	680	506.3
279	279	677	651	508.0
280	280	654	580	423.9
281	281	690	661	535.2
282	282	1113	1031	793.3
283	283	770	715	555.0
284	284	1240	1178	917.4
285	285	1058	995	779.1
286	286	662	661	502.6
287	287	580	554	408.1
288	288	915	872	645.4
289	289	882	873	653.6
290	290	518	509	349.36
291	291	612	580	414.5
292	292	802	801	606.1
293	293	Received	1034	740.9
294	294	680	675	498.2
295	295	774	746	533.3

Appendix C

Sand Sample Graphic Results

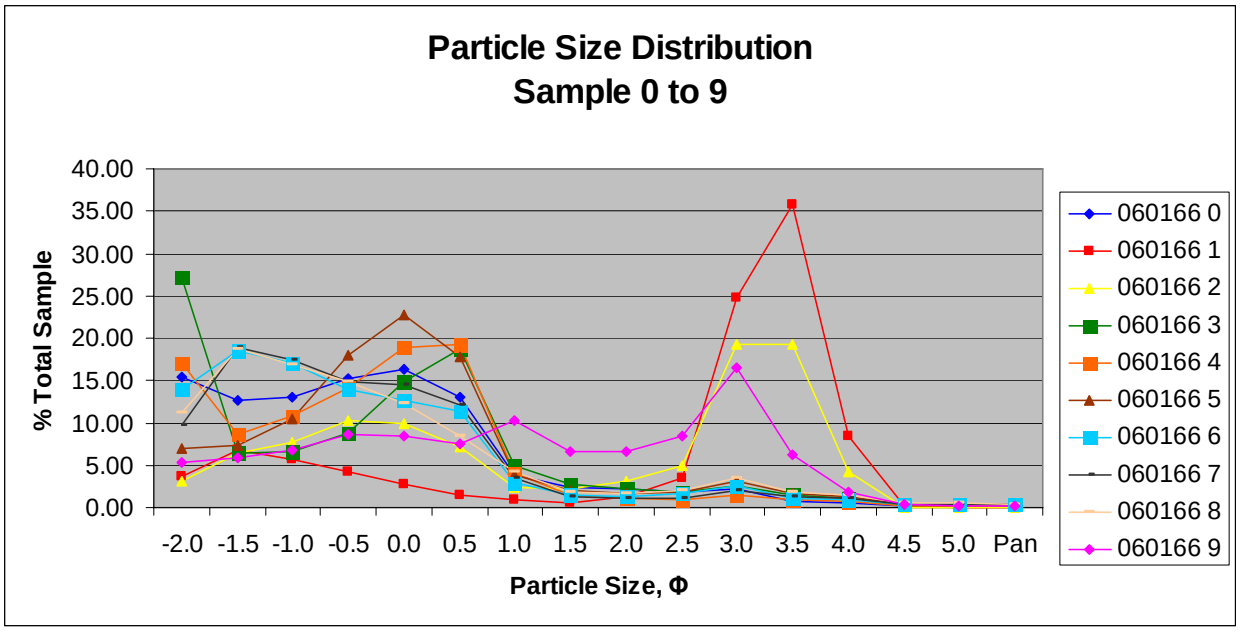
Particle Size Distribution
Sample 0 to 9
% Total Sample
40.00
35.00
30.00
25.00
20.00
15.00
10.00
5.00
0.00
-2.0 -1.5 -1.0 -0.5 0.0 0.5 1.0 1.5 2.0 2.5 3.0 3.5 4.0 4.5 5.0 Pan
Particle Size, Φ
060166 0
060166 1
060166 2
060166 3
060166 4
060166 5
060166 6
060166 7
060166 8
060166 9

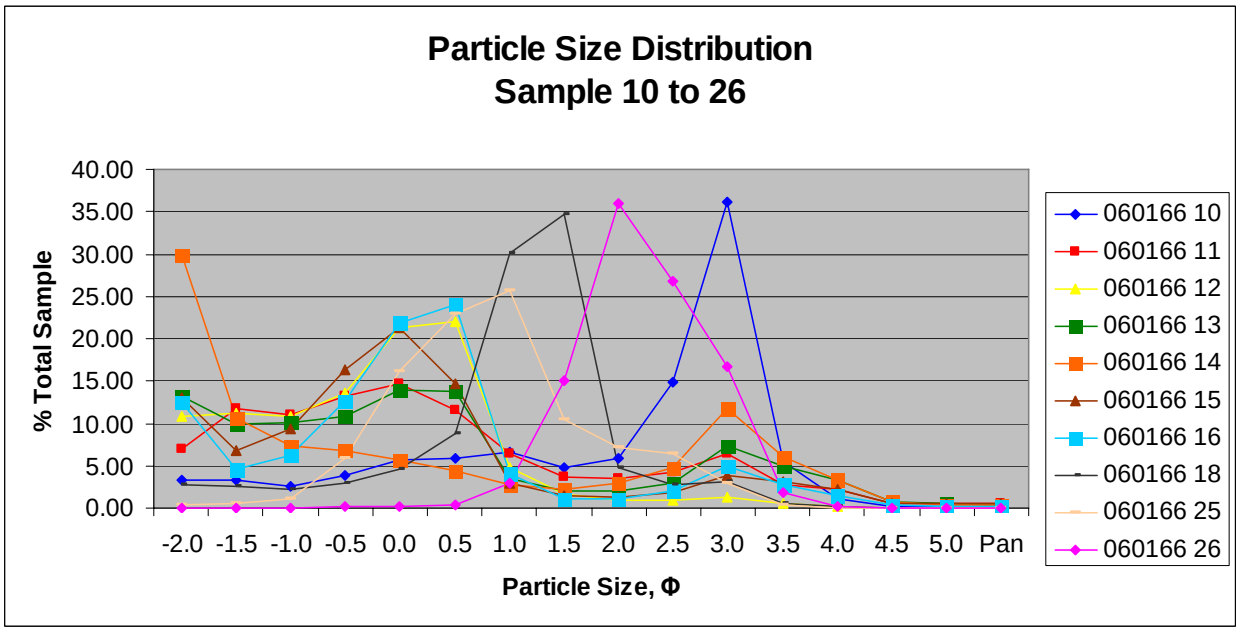
Particle Size Distribution
Sample 10 to 26
% Total Sample
40.00
35.00
30.00
25.00
20.00
15.00
10.00
5.00
0.00
-2.0 -1.5 -1.0 -0.5 0.0 0.5 1.0 1.5 2.0 2.5 3.0 3.5 4.0 4.5 5.0 Pan
Particle Size, Φ
060166 10
060166 11
060166 12
060166 13
060166 14
060166 15
060166 16
060166 18
060166 25
060166 26

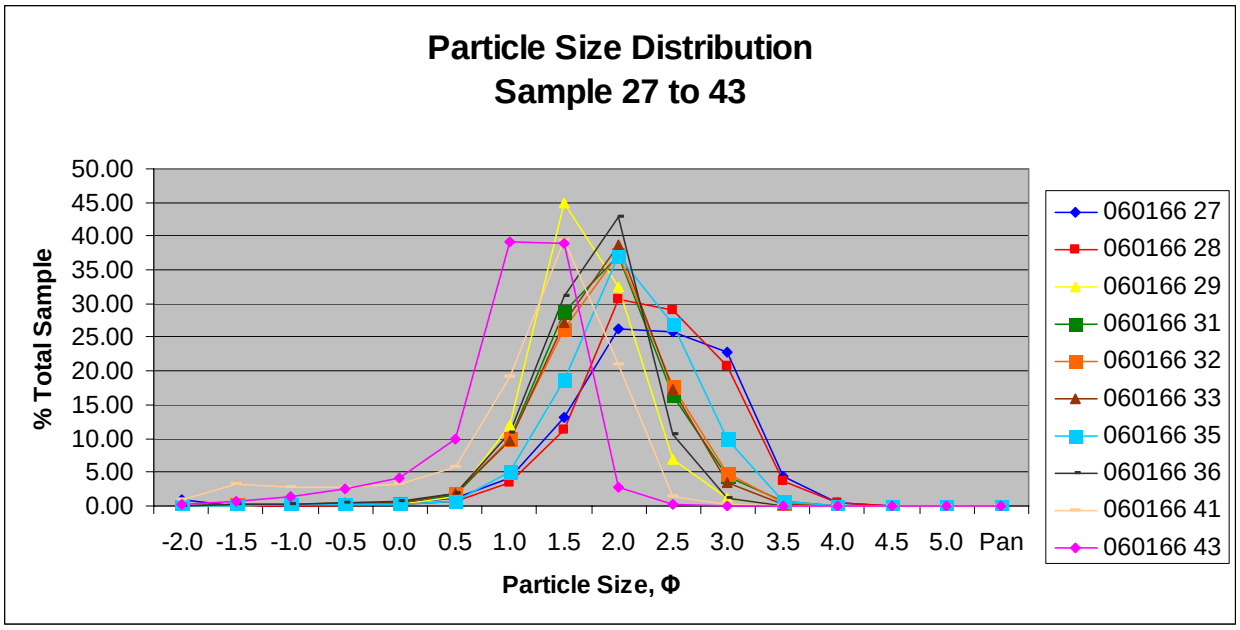
Particle Size Distribution
Sample 27 to 43
% Total Sample
50.00
45.00
40.00
35.00
30.00
25.00
20.00
15.00
10.00
5.00
0.00
-2.0 -1.5 -1.0 -0.5 0.0 0.5 1.0 1.5 2.0 2.5 3.0 3.5 4.0 4.5 5.0 Pan
Particle Size, Φ
060166 27
060166 28
060166 29
060166 31
060166 32
060166 33
060166 35
060166 36
060166 41
060166 43

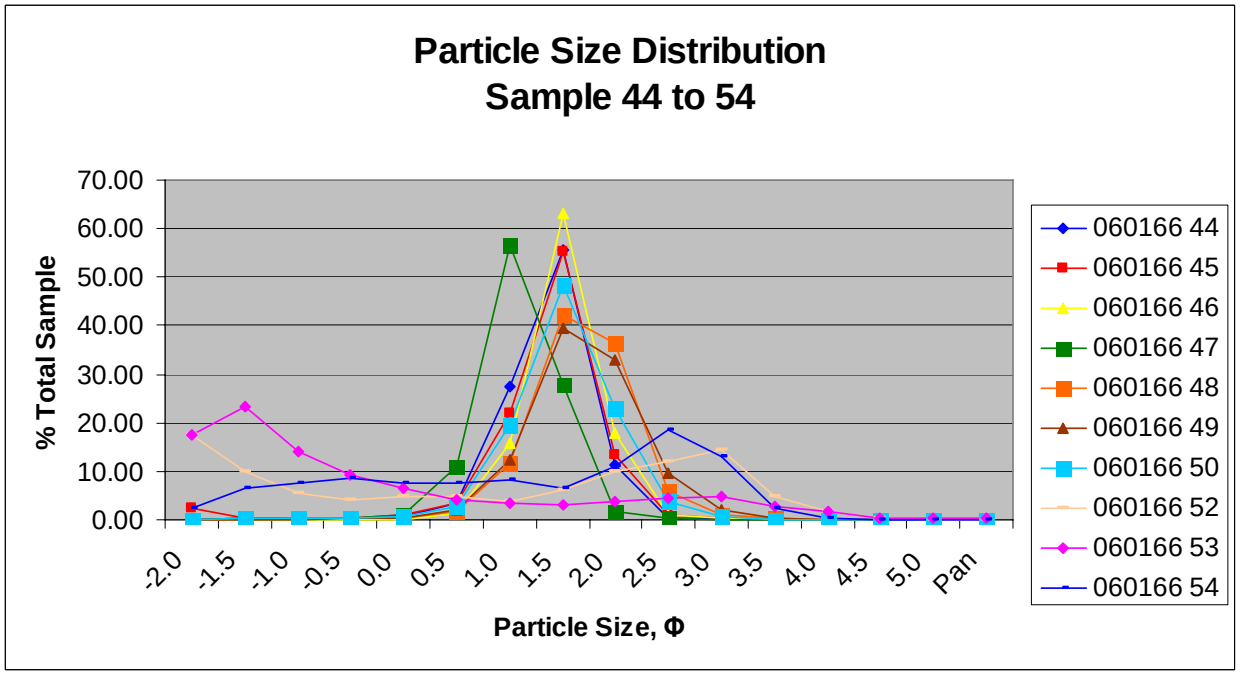
Particle Size Distribution
Sample 44 to 54
% Total Sample
70.00
60.00
50.00
40.00
30.00
20.00
10.00
0.00
-2.0 -1.5 -1.0 -0.5 0.0 0.5 1.0 1.5 2.0 2.5 3.0 3.5 4.0 4.5 5.0 Pan
Particle Size, Φ
060166 44
060166 45
060166 46
060166 47
060166 48
060166 49
060166 50
060166 52
060166 53
060166 54

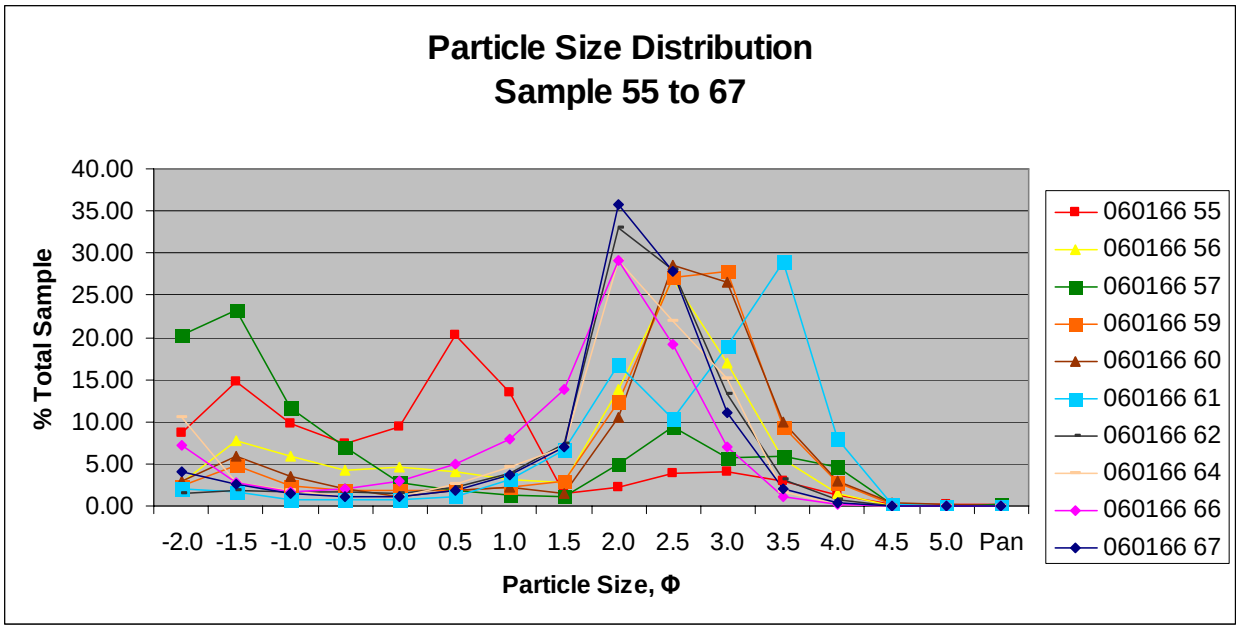
Particle Size Distribution
Sample 55 to 67
% Total Sample
40.00
35.00
30.00
25.00
20.00
15.00
10.00
5.00
0.00
-2.0 -1.5 -1.0 -0.5 0.0 0.5 1.0 1.5 2.0 2.5 3.0 3.5 4.0 4.5 5.0 Pan
Particle Size, Φ
060166 55
060166 56
060166 57
060166 59
060166 60
060166 61
060166 62
060166 64
060166 66
060166 67

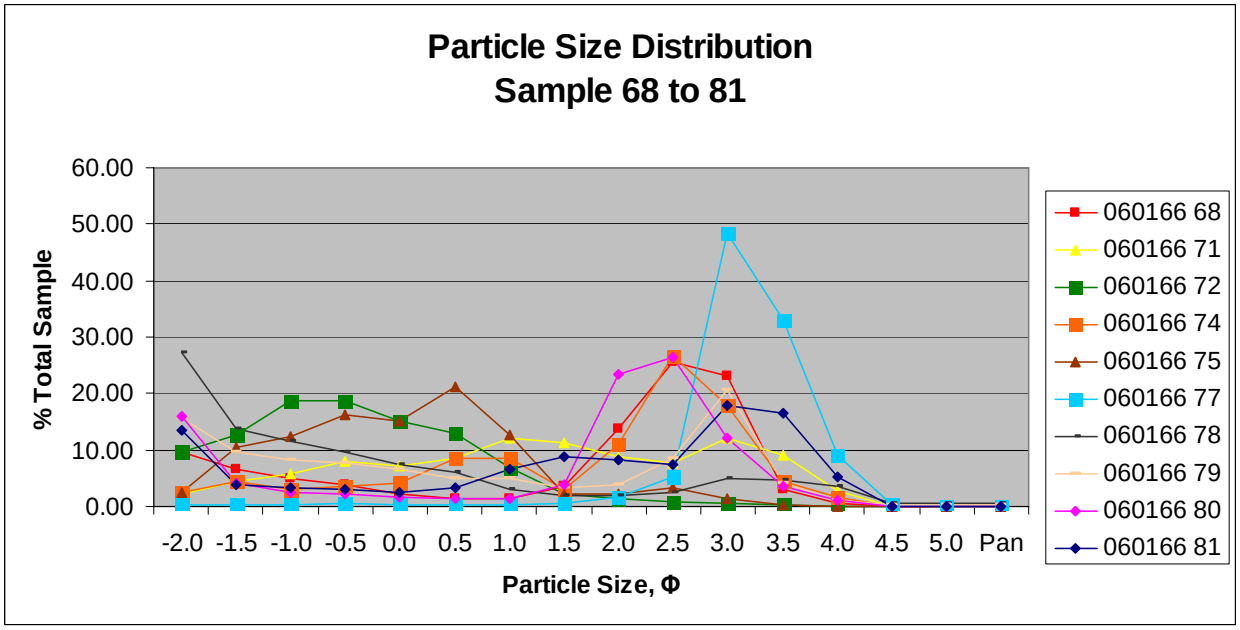
Particle Size Distribution
Sample 68 to 81
% Total Sample
60.00
50.00
40.00
30.00
20.00
10.00
0.00
-2.0 -1.5 -1.0 -0.5 0.0 0.5 1.0 1.5 2.0 2.5 3.0 3.5 4.0 4.5 5.0 Pan
Particle Size, Φ
060166 68
060166 71
060166 72
060166 74
060166 75
060166 77
060166 78
060166 79
060166 80
060166 81

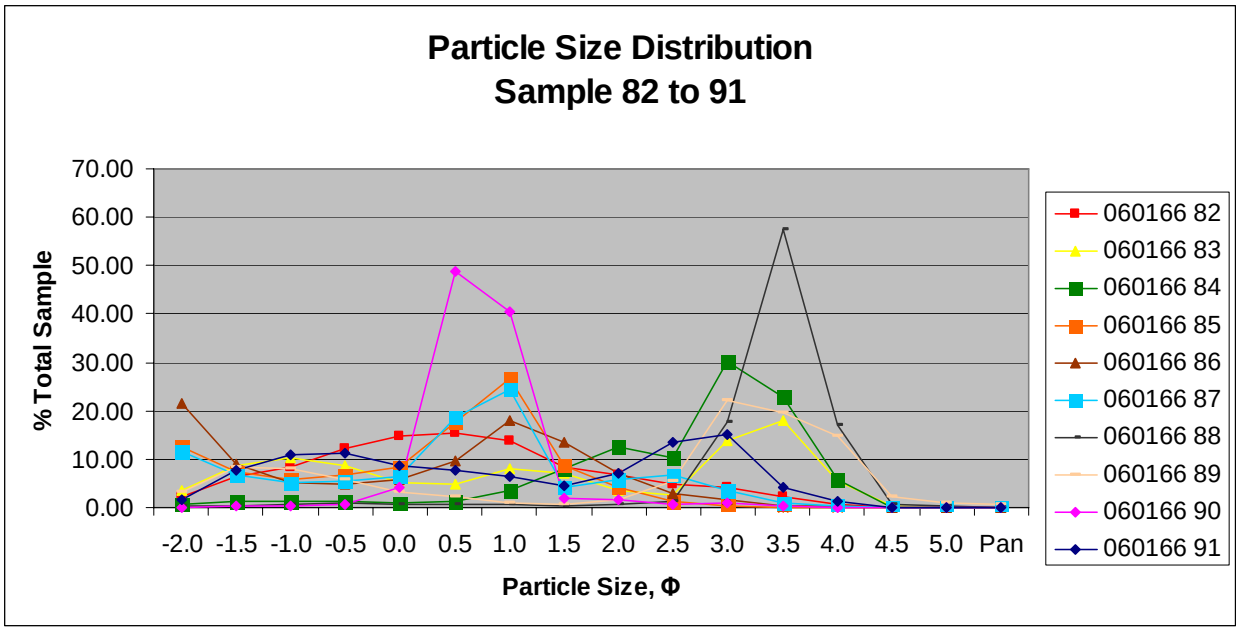
Particle Size Distribution
Sample 82 to 91
% Total Sample
70.00
60.00
50.00
40.00
30.00
20.00
10.00
0.00
-2.0 -1.5 -1.0 -0.5 0.0 0.5 1.0 1.5 2.0 2.5 3.0 3.5 4.0 4.5 5.0 Pan
Particle Size, Φ
060166 82
060166 83
060166 84
060166 85
060166 86
060166 87
060166 88
060166 89
060166 90
060166 91

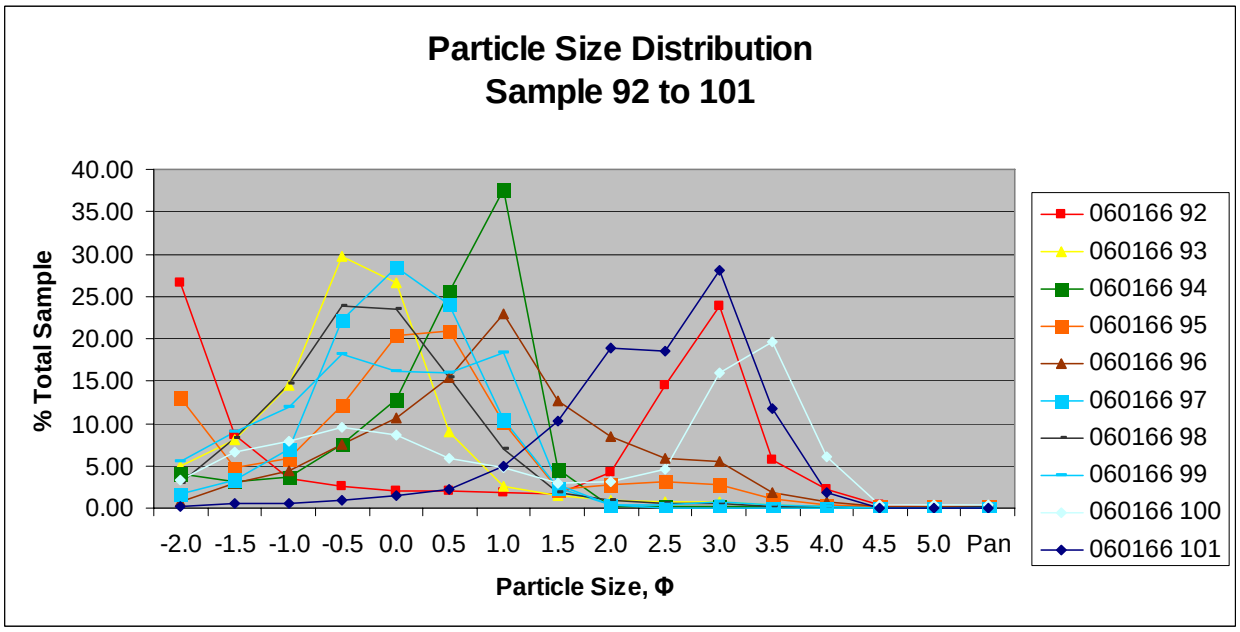
Particle Size Distribution
Sample 92 to 101
% Total Sample
40.00
35.00
30.00
25.00
20.00
15.00
10.00
5.00
0.00
-2.0 -1.5 -1.0 -0.5 0.0 0.5 1.0 1.5 2.0 2.5 3.0 3.5 4.0 4.5 5.0 Pan
Particle Size, Φ
060166 92
060166 93
060166 94
060166 95
060166 96
060166 97
060166 98
060166 99
060166 100
060166 101

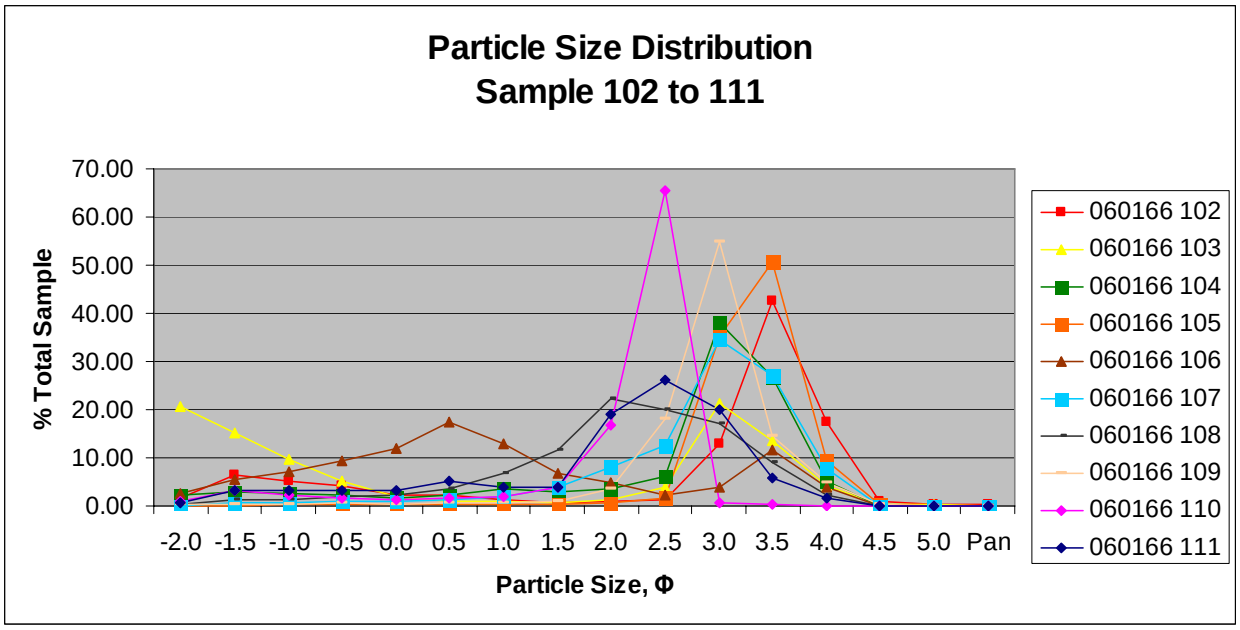
Particle Size Distribution
Sample 102 to 111
% Total Sample
70.00
60.00
50.00
40.00
30.00
20.00
10.00
0.00
-2.0 -1.5 -1.0 -0.5 0.0 0.5 1.0 1.5 2.0 2.5 3.0 3.5 4.0 4.5 5.0 Pan
Particle Size, Φ
060166 102
060166 103
060166 104
060166 105
060166 106
060166 107
060166 108
060166 109
060166 110
060166 111

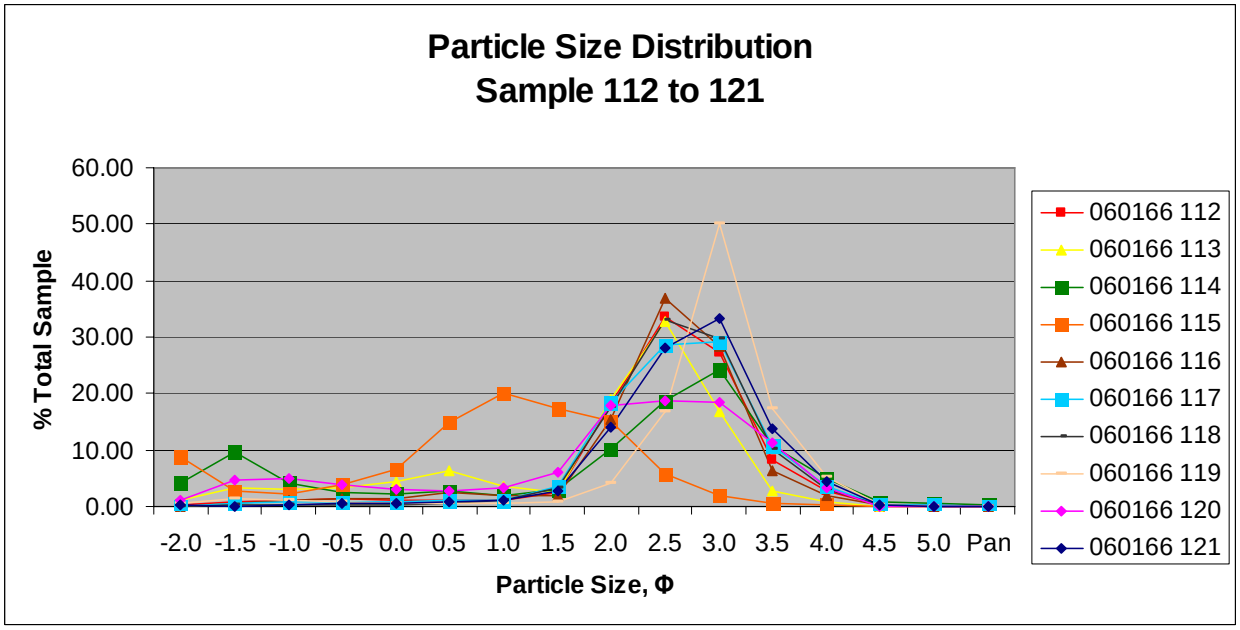
Particle Size Distribution
Sample 112 to 121
% Total Sample
60.00
50.00
40.00
30.00
20.00
10.00
0.00
-2.0 -1.5 -1.0 -0.5 0.0 0.5 1.0 1.5 2.0 2.5 3.0 3.5 4.0 4.5 5.0 Pan
Particle Size, Φ
060166 112
060166 113
060166 114
060166 115
060166 116
060166 117
060166 118
060166 119
060166 120
060166 121

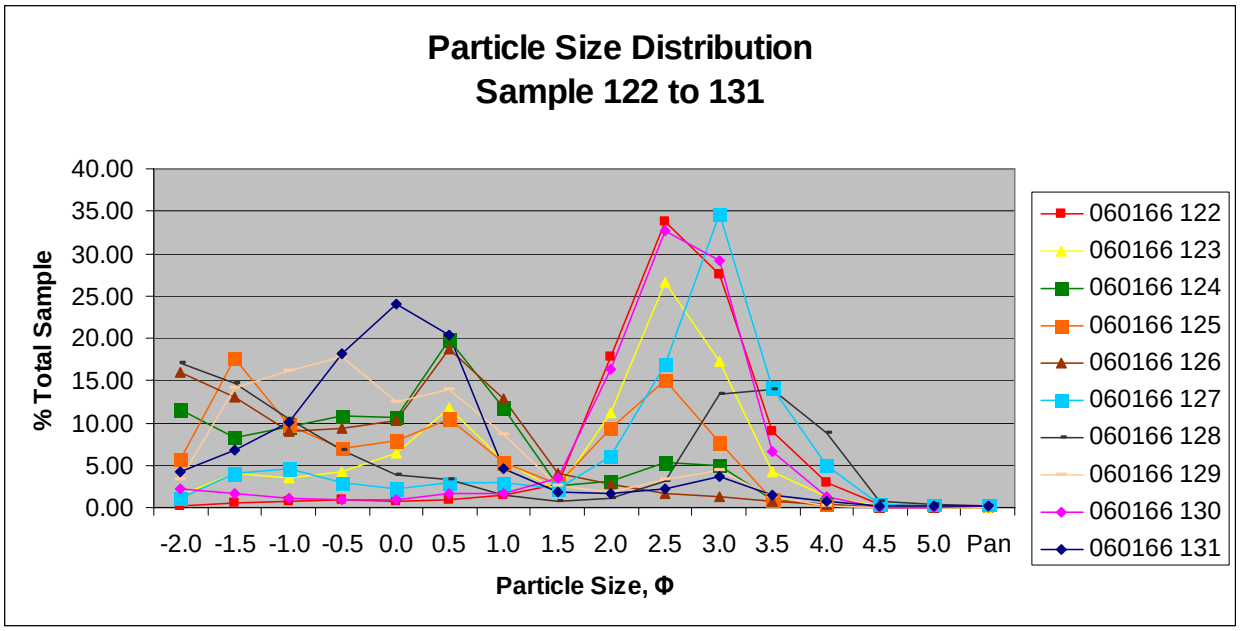
Particle Size Distribution
Sample 122 to 131
% Total Sample
40.00
35.00
30.00
25.00
20.00
15.00
10.00
5.00
0.00
-2.0 -1.5 -1.0 -0.5 0.0 0.5 1.0 1.5 2.0 2.5 3.0 3.5 4.0 4.5 5.0 Pan
Particle Size, Φ
060166 122
060166 123
060166 124
060166 125
060166 126
060166 127
060166 128
060166 129
060166 130
060166 131

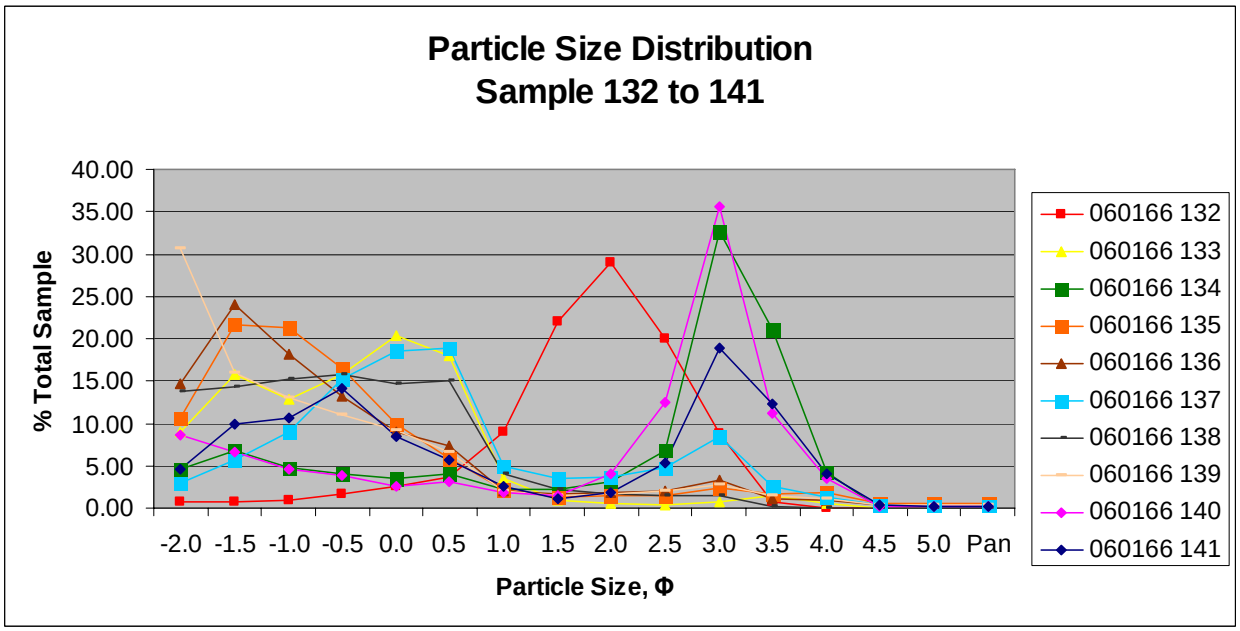
Particle Size Distribution
Sample 132 to 141
% Total Sample
40.00
35.00
30.00
25.00
20.00
15.00
10.00
5.00
0.00
-2.0 -1.5 -1.0 -0.5 0.0 0.5 1.0 1.5 2.0 2.5 3.0 3.5 4.0 4.5 5.0 Pan
Particle Size, Φ
060166 132
060166 133
060166 134
060166 135
060166 136
060166 137
060166 138
060166 139
060166 140
060166 141

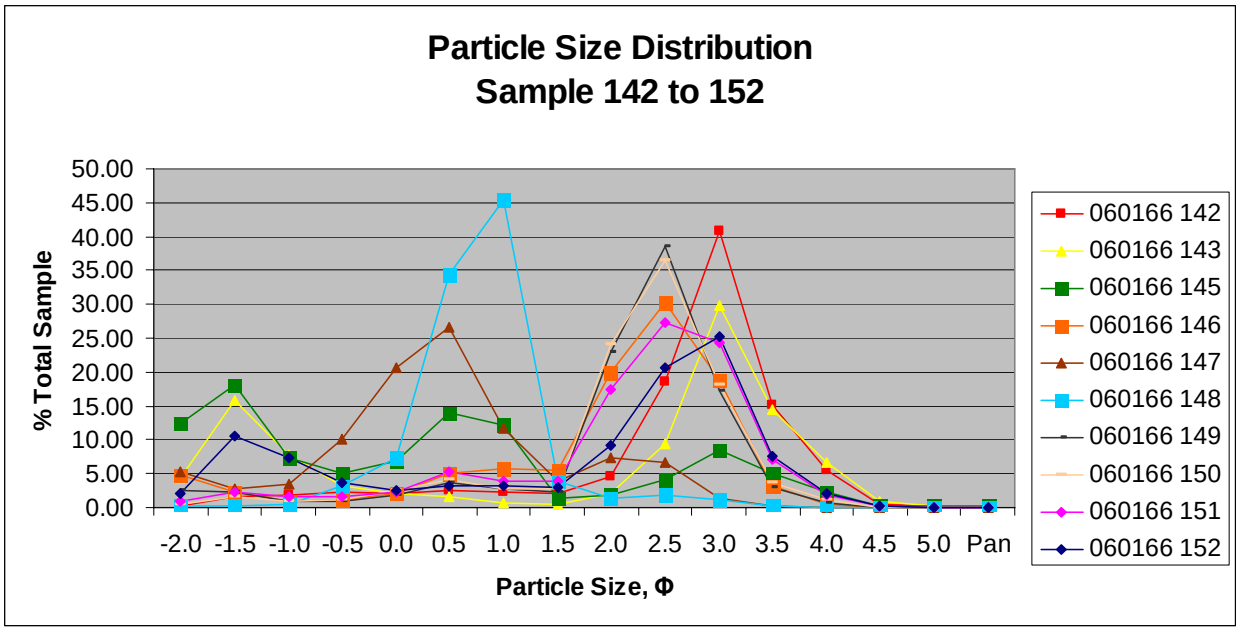
Particle Size Distribution
Sample 142 to 152
% Total Sample
50.00
45.00
40.00
35.00
30.00
25.00
20.00
15.00
10.00
5.00
0.00
-2.0 -1.5 -1.0 -0.5 0.0 0.5 1.0 1.5 2.0 2.5 3.0 3.5 4.0 4.5 5.0 Pan
Particle Size, Φ
060166 142
060166 143
060166 145
060166 146
060166 147
060166 148
060166 149
060166 150
060166 151
060166 152

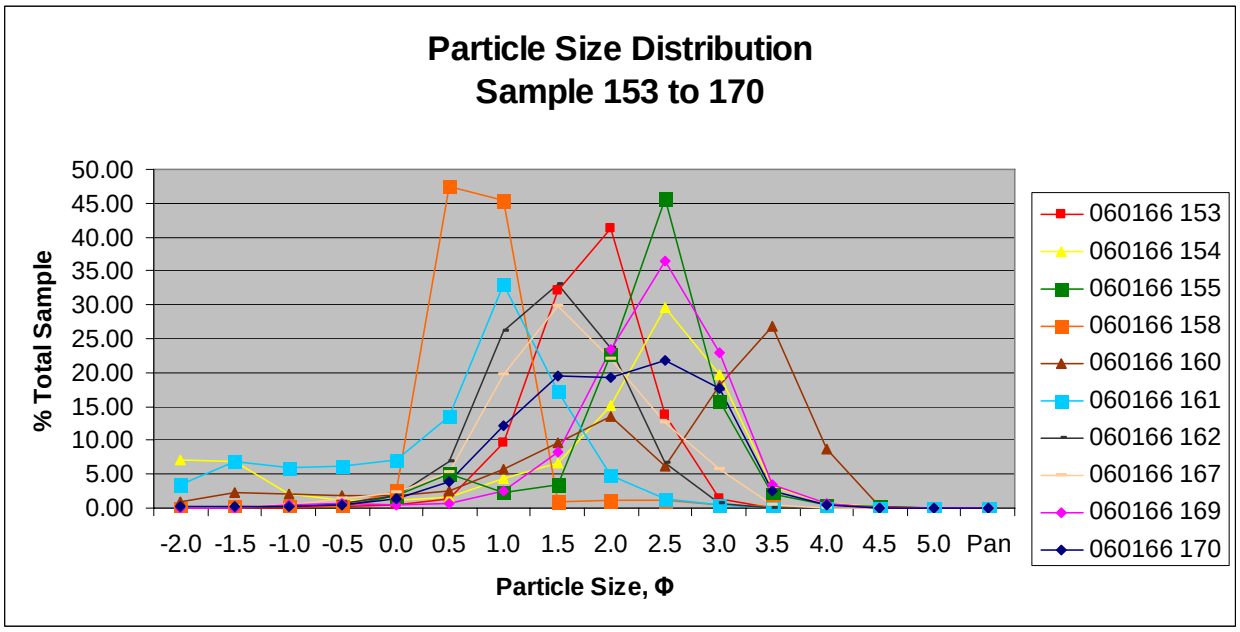
Particle Size Distribution
Sample 153 to 170
% Total Sample
50.00
45.00
40.00
35.00
30.00
25.00
20.00
15.00
10.00
5.00
0.00
-2.0 -1.5 -1.0 -0.5 0.0 0.5 1.0 1.5 2.0 2.5 3.0 3.5 4.0 4.5 5.0 Pan
Particle Size, Φ
060166 153
060166 154
060166 155
060166 158
060166 160
060166 161
060166 162
060166 167
060166 169
060166 170

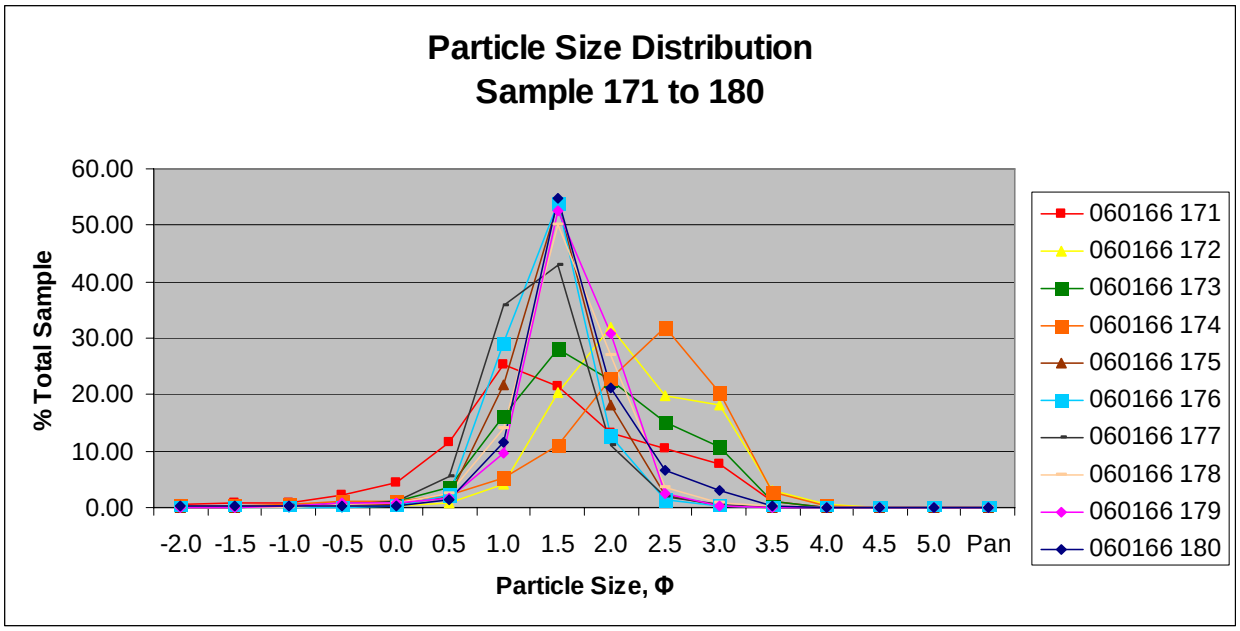
Particle Size Distribution
Sample 171 to 180
% Total Sample
60.00
50.00
40.00
30.00
20.00
10.00
0.00
-2.0 -1.5 -1.0 -0.5 0.0 0.5 1.0 1.5 2.0 2.5 3.0 3.5 4.0 4.5 5.0 Pan
Particle Size, Φ
060166 171
060166 172
060166 173
060166 174
060166 175
060166 176
060166 177
060166 178
060166 179
060166 180

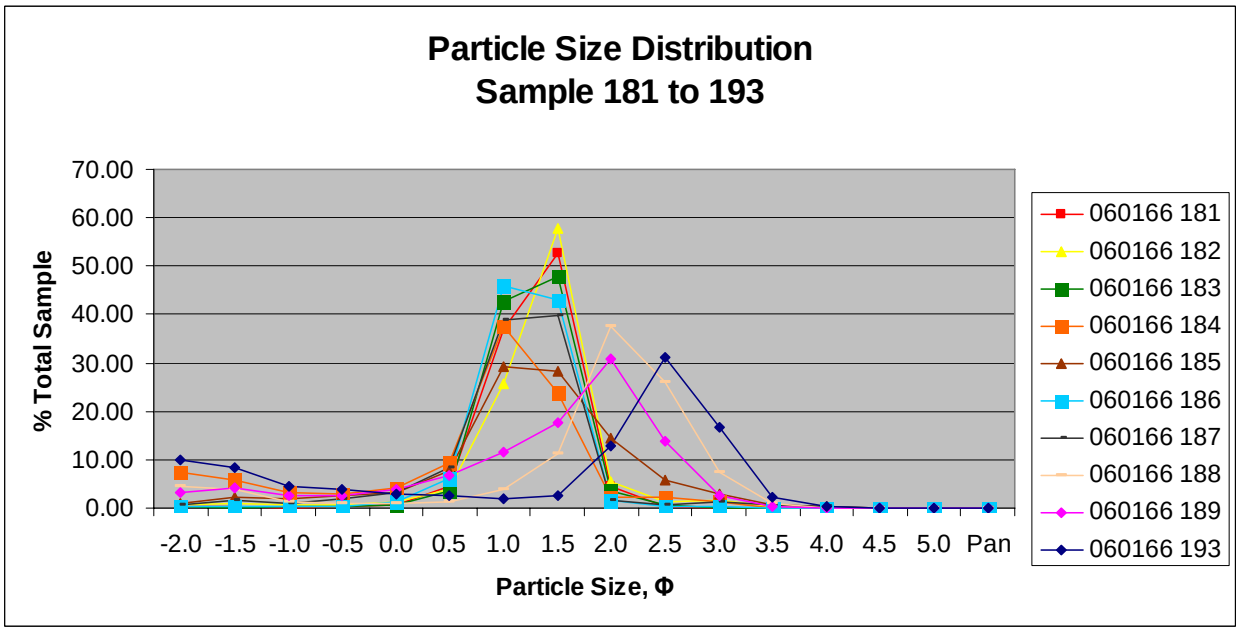
Particle Size Distribution
Sample 181 to 193
% Total Sample
70.00
60.00
50.00
40.00
30.00
20.00
10.00
0.00
-2.0 -1.5 -1.0 -0.5 0.0 0.5 1.0 1.5 2.0 2.5 3.0 3.5 4.0 4.5 5.0 Pan
Particle Size, Φ
060166 181
060166 182
060166 183
060166 184
060166 185
060166 186
060166 187
060166 188
060166 189
060166 193

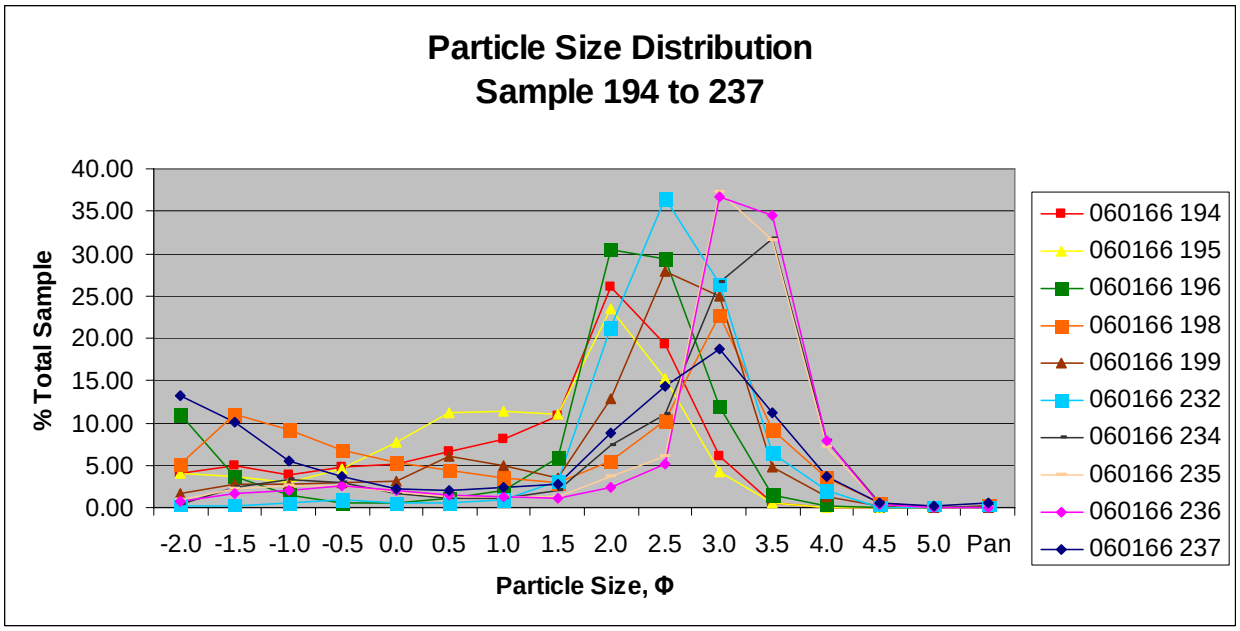
Particle Size Distribution
Sample 194 to 237
% Total Sample
40.00
35.00
30.00
25.00
20.00
15.00
10.00
5.00
0.00
-2.0 -1.5 -1.0 -0.5 0.0 0.5 1.0 1.5 2.0 2.5 3.0 3.5 4.0 4.5 5.0 Pan
Particle Size, Φ
060166 194
060166 195
060166 196
060166 198
060166 199
060166 232
060166 234
060166 235
060166 236
060166 237

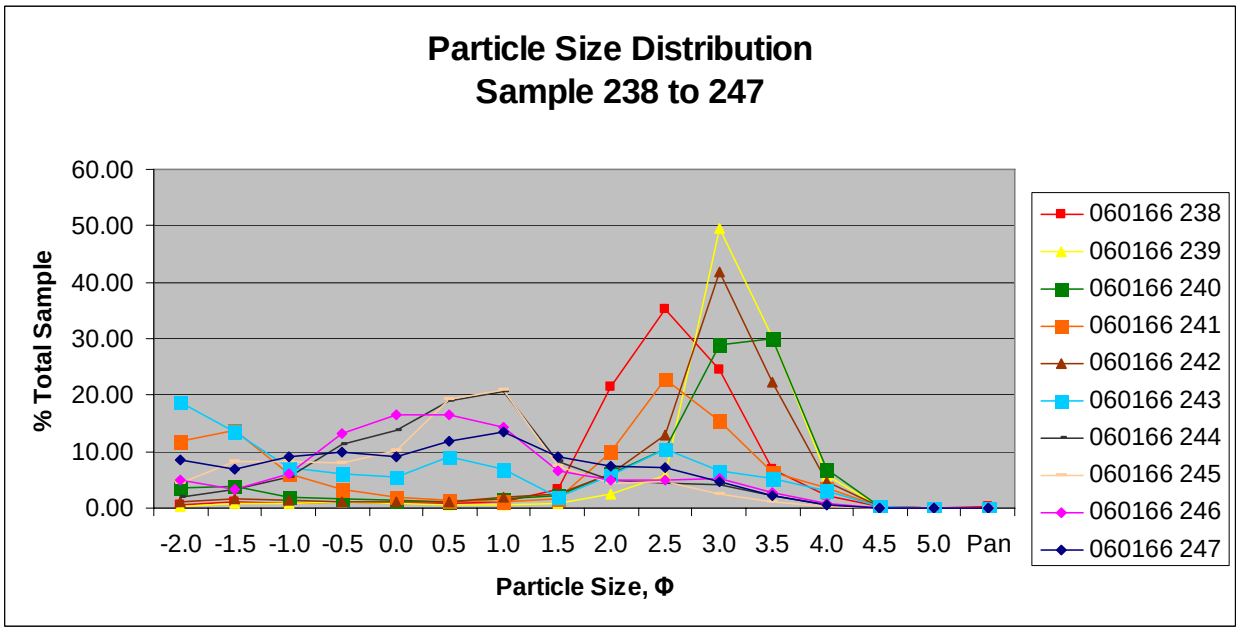
Particle Size Distribution
Sample 238 to 247
% Total Sample
60.00
50.00
40.00
30.00
20.00
10.00
0.00
-2.0 -1.5 -1.0 -0.5 0.0 0.5 1.0 1.5 2.0 2.5 3.0 3.5 4.0 4.5 5.0 Pan
Particle Size, Φ
060166 238
060166 239
060166 240
060166 241
060166 242
060166 243
060166 244
060166 245
060166 246
060166 247

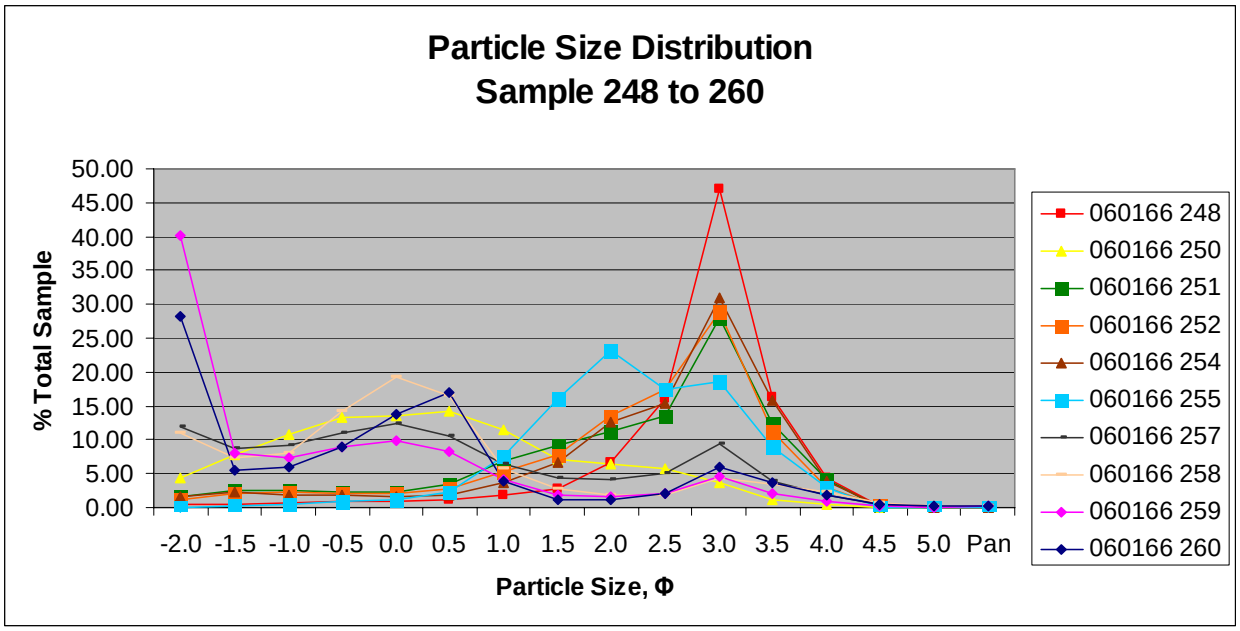
Particle Size Distribution
Sample 248 to 260
% Total Sample
50.00
45.00
40.00
35.00
30.00
25.00
20.00
15.00
10.00
5.00
0.00
-2.0 -1.5 -1.0 -0.5 0.0 0.5 1.0 1.5 2.0 2.5 3.0 3.5 4.0 4.5 5.0 Pan
Particle Size, Φ
060166 248
060166 250
060166 251
060166 252
060166 254
060166 255
060166 257
060166 258
060166 259
060166 260

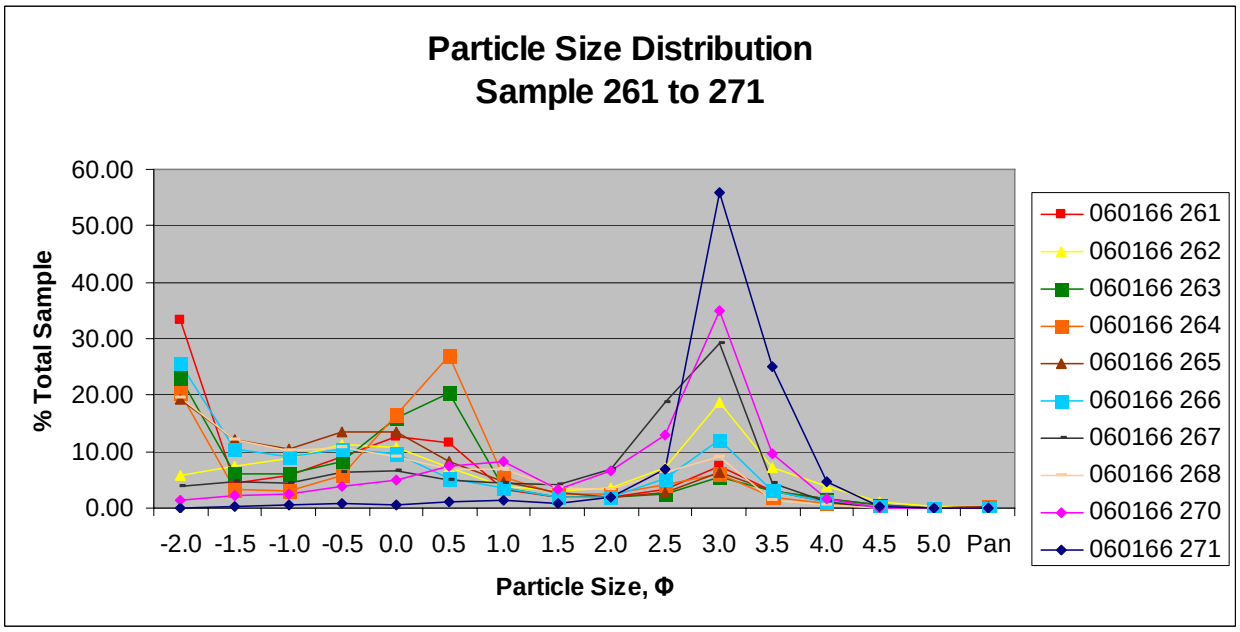
Particle Size Distribution
Sample 261 to 271
% Total Sample
60.00
50.00
40.00
30.00
20.00
10.00
0.00
-2.0 -1.5 -1.0 -0.5 0.0 0.5 1.0 1.5 2.0 2.5 3.0 3.5 4.0 4.5 5.0 Pan
Particle Size, Φ
060166 261
060166 262
060166 263
060166 264
060166 265
060166 266
060166 267
060166 268
060166 270
060166 271

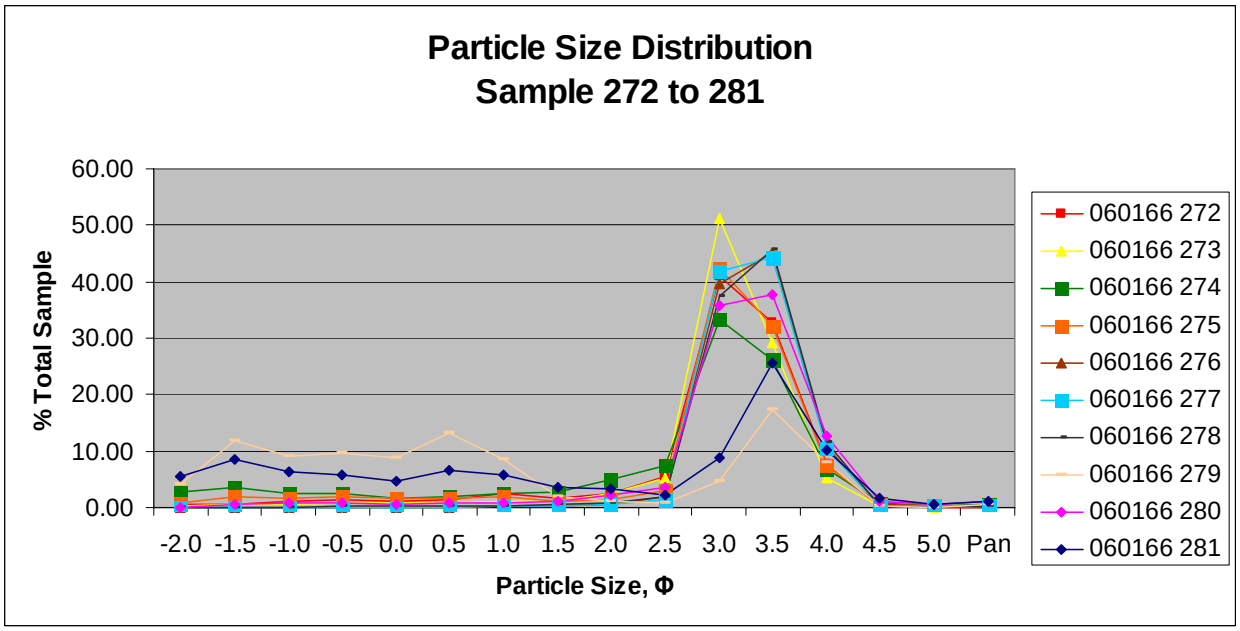
Particle Size Distribution
Sample 272 to 281
% Total Sample
60.00
50.00
40.00
30.00
20.00
10.00
0.00
-2.0 -1.5 -1.0 -0.5 0.0 0.5 1.0 1.5 2.0 2.5 3.0 3.5 4.0 4.5 5.0 Pan
Particle Size, Φ
060166 272
060166 273
060166 274
060166 275
060166 276
060166 277
060166 278
060166 279
060166 280
060166 281

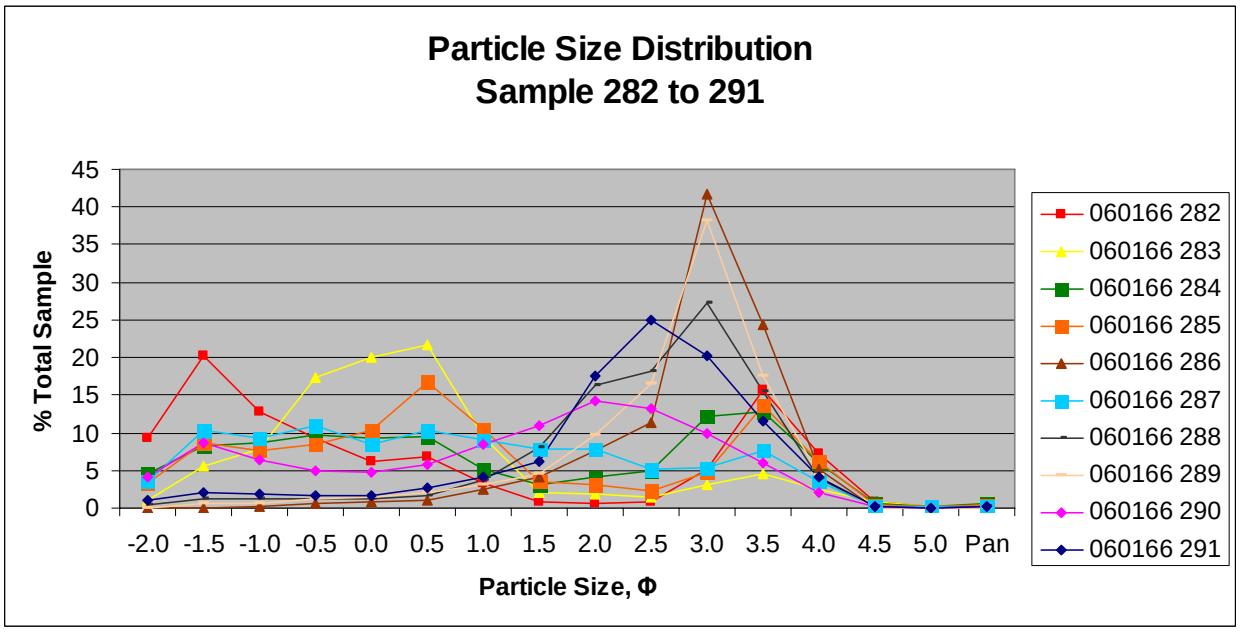
Particle Size Distribution
Sample 282 to 291
% Total Sample
45
40
35
30
25
20
15
10
5
0
-2.0 -1.5 -1.0 -0.5 0.0 0.5 1.0 1.5 2.0 2.5 3.0 3.5 4.0 4.5 5.0 Pan
Particle Size, Φ
060166 282
060166 283
060166 284
060166 285
060166 286
060166 287
060166 288
060166 289
060166 290
060166 291

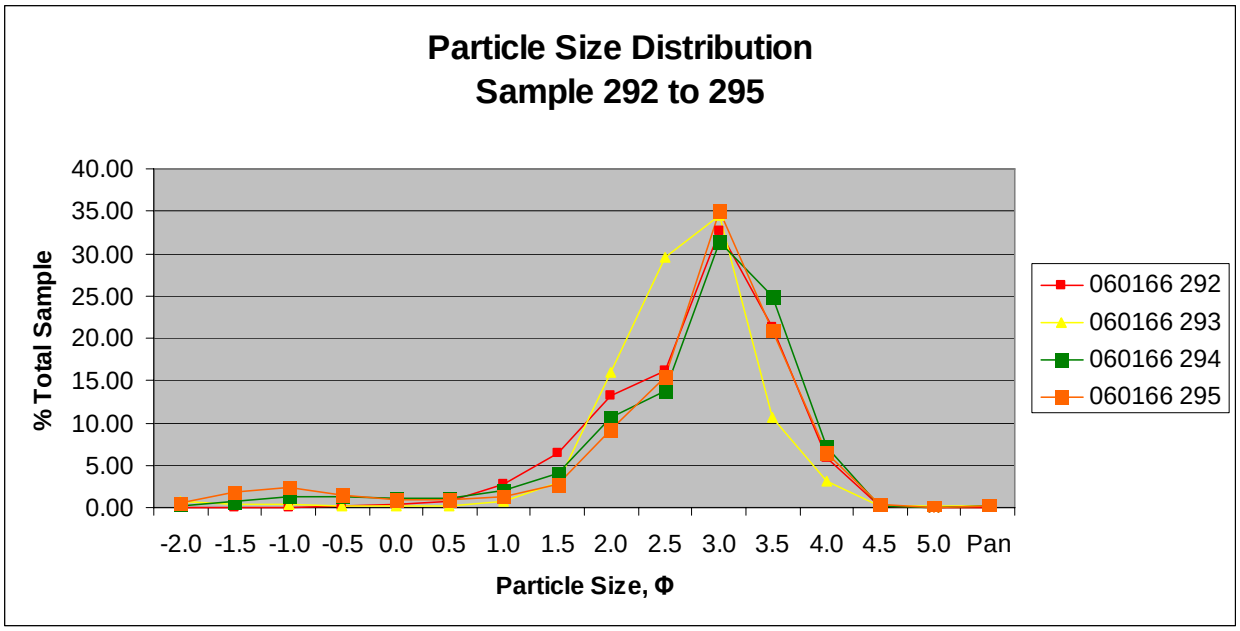
Particle Size Distribution
Sample 292 to 295
% Total Sample
40.00
35.00
30.00
25.00
20.00
15.00
10.00
5.00
0.00
-2.0 -1.5 -1.0 -0.5 0.0 0.5 1.0 1.5 2.0 2.5 3.0 3.5 4.0 4.5 5.0 Pan
Particle Size, Φ
060166 292
060166 293
060166 294
060166 295

Appendix D

Sand Sample Numerical Results

Table C1. Numerical Results of Particle Size Distribution for Samples 0 to 9

Particle Size, Φ	060166 0	060166 1	060166 2	060166 3	060166 4	060166 5	060166 6	060166 7	060166 8	060166 9
-2.0	15.41	3.65	3.16	27.07	17.02	7.02	13.94	9.68	11.14	5.41
-1.5	12.67	6.86	6.34	6.47	8.63	7.41	18.48	18.82	18.69	5.94
-1.0	12.96	5.72	7.76	6.62	10.82	10.45	17.00	17.39	16.85	6.76
-0.5	15.25	4.26	10.28	8.73	14.17	18.04	13.92	14.94	14.93	8.64
0.0	16.35	2.67	9.88	14.95	18.84	22.72	12.64	14.50	12.25	8.41
0.5	12.94	1.49	7.12	18.68	19.34	17.87	11.29	12.19	8.44	7.61
1.0	3.86	0.86	2.40	4.94	3.97	3.80	2.85	3.50	4.27	10.20
1.5	2.46	0.64	2.12	2.73	1.46	2.01	1.39	1.29	1.81	6.61
2.0	2.24	1.30	3.06	2.24	1.12	1.71	1.33	1.04	1.56	6.68
2.5	1.91	3.42	4.95	1.75	0.97	1.91	1.59	1.17	1.93	8.42
3.0	2.17	24.74	19.18	2.57	1.48	3.16	2.58	2.08	3.43	16.49
3.5	0.72	35.74	19.32	1.53	0.96	1.61	1.19	1.21	1.80	6.20
4.0	0.56	8.42	4.25	1.02	0.70	1.26	0.93	1.10	1.47	1.85
4.5	0.16	0.13	0.07	0.26	0.20	0.39	0.30	0.39	0.50	0.33
5.0	0.16	0.05	0.04	0.23	0.16	0.34	0.28	0.37	0.50	0.24
Pan	0.18	0.05	0.07	0.21	0.16	0.30	0.29	0.33	0.43	0.21
	100.0	100.0	100.0	100.0	100.0	100.0	100.0	100.0	100.0	100.0

Table C2. Numerical Results of Particle Size Distribution for Samples 10 to 26

Particle Size, Φ	060166 10	060166 11	060166 12	060166 13	060166 14	060166 15	060166 16	060166 18	060166 25	060166 26
-2.0	3.28	7.02	10.76	13.23	29.96	12.94	12.50	2.71	0.29	0.00
-1.5	3.33	11.67	11.26	9.99	10.62	6.87	4.51	2.62	0.48	0.01
-1.0	2.60	11.08	10.75	10.16	7.29	9.32	6.23	2.20	1.10	0.02
-0.5	3.94	13.13	13.54	10.83	6.78	16.24	12.62	2.96	5.89	0.11
0.0	5.65	14.60	21.28	13.96	5.75	21.33	21.90	4.60	16.09	0.17
0.5	5.92	11.54	22.06	13.79	4.33	14.68	23.95	8.87	22.89	0.44
1.0	6.69	6.45	4.73	3.55	2.76	2.99	4.09	30.13	25.70	2.89
1.5	4.82	3.74	1.65	2.02	2.25	1.49	1.12	34.61	10.50	14.96
2.0	5.94	3.40	1.00	2.01	2.88	1.34	1.13	4.79	7.11	36.03
2.5	14.81	4.21	0.84	2.96	4.76	1.82	1.98	2.74	6.49	26.72
3.0	36.10	6.47	1.23	7.34	11.80	3.94	4.89	3.16	3.00	16.67
3.5	5.51	2.80	0.48	5.04	6.13	3.05	2.73	0.50	0.35	1.78
4.0	1.01	2.17	0.22	3.39	3.22	2.29	1.43	0.10	0.09	0.20
4.5	0.16	0.62	0.05	0.76	0.65	0.61	0.36	0.00	0.01	0.01
5.0	0.11	0.55	0.04	0.55	0.45	0.56	0.27	0.00	0.01	0.00
Pan	0.13	0.55	0.11	0.42	0.37	0.53	0.27	0.01	0.01	0.00
	100.0	100.0	100.0	100.0	100	100.0	100.0	100.0	100.0	100.0

Table C3. Numerical Results of Particle Size Distribution for Samples 27 to 43

Particle Size, Φ	060166 27	060166 28	060166 29	060166 31	060166 32	060166 33	060166 35	060166 36	060166 41	060166 43
-2.0	0.90	0.00	0.00	0.00	0.03	0.05	0.05	0.05	0.95	0.18
-1.5	0.04	0.02	0.09	0.13	0.13	0.28	0.01	0.22	3.27	0.71
-1.0	0.10	0.04	0.18	0.20	0.24	0.29	0.15	0.31	2.75	1.31
-0.5	0.26	0.05	0.26	0.31	0.31	0.35	0.17	0.40	2.65	2.51
0.0	0.45	0.22	0.33	0.47	0.54	0.57	0.24	0.64	3.15	4.21
0.5	1.04	0.75	1.28	1.70	1.93	1.84	0.65	1.95	5.69	9.82
1.0	4.09	3.37	12.05	9.86	9.88	9.62	5.17	10.74	19.21	39.12
1.5	13.07	11.26	44.96	28.82	26.30	27.17	18.69	31.04	39.48	38.95
2.0	26.38	30.68	32.60	37.14	37.23	38.60	37.05	42.89	21.03	2.88
2.5	25.85	28.94	6.94	16.36	17.83	17.36	26.94	10.63	1.37	0.16
3.0	22.85	20.65	1.14	4.32	4.92	3.54	10.01	1.04	0.34	0.11
3.5	4.48	3.64	0.09	0.58	0.56	0.28	0.77	0.11	0.08	0.04
4.0	0.45	0.38	0.02	0.10	0.08	0.05	0.10	0.00	0.02	0.00
4.5	0.02	0.00	0.00	0.01	0.01	0.01	0.00	0.00	0.01	0.00
5.0	0.01	0.00	0.06	0.00	0.00	0.00	0.00	0.00	0.01	0.00
Pan	0.01	0.00	0.00	0.01	0.01	0.00	0.01	0.00	0.01	0.00
	100.0	100.0	100.0	100.0	100.0	100.01	100.0	100.0	100.0	100.0

Table C4. Numerical Results of Particle Size Distribution for Samples 44 to 53

Particle Size, Φ	060166 44	060166 45	060166 46	060166 47	060166 48	060166 49	060166 50	060166 51	060166 52	060166 53
-2.0	0.04	2.48	0.00	0.17	0.02	0.06	0.09	0.05	17.42	17.64
-1.5	0.32	0.42	0.01	0.29	0.16	0.14	0.29	0.01	9.88	23.24
-1.0	0.32	0.35	0.01	0.31	0.18	0.14	0.34	0.15	5.57	14.19
-0.5	0.34	0.42	0.03	0.37	0.19	0.22	0.39	0.17	4.27	9.31
0.0	0.55	0.91	0.15	1.14	0.42	0.51	0.69	0.24	4.89	6.52
0.5	3.41	3.37	1.21	10.98	1.69	2.01	2.84	0.65	4.70	4.21
1.0	27.53	22.03	15.82	56.61	11.66	12.27	19.45	5.17	3.71	3.50
1.5	55.55	55.27	63.15	27.83	42.16	39.61	48.47	18.69	6.01	2.95
2.0	11.34	13.26	17.94	1.88	36.32	32.86	23.05	37.05	10.01	3.94
2.5	0.34	0.93	1.20	0.36	5.93	9.70	3.69	26.94	11.90	4.39
3.0	0.21	0.43	0.43	0.05	1.02	2.08	0.59	10.01	14.43	4.97
3.5	0.05	0.10	0.06	0.00	0.20	0.31	0.09	0.77	4.94	2.79
4.0	0.01	0.02	0.00	0.00	0.03	0.05	0.02	0.10	1.74	1.68
4.5	0.01	0.00	0.00	0.00	0.00	0.01	0.00	0.00	0.25	0.30
5.0	0.01	0.00	0.00	0.00	0.00	0.00	0.00	0.00	0.13	0.18
Pan	0.00	0.00	0.00	0.00	0.00	0.01	0.00	0.01	0.13	0.20
	100.0	100.0	100.0	100.0	100.0	100.0	100.0	100.0	100.0	100.0

Table C5. Numerical Results of Particle Size Distribution for Samples 54 to 66

Particle Size, Φ	060166 54	060166 55	060166 56	060166 57	060166 59	060166 60	060166 61	060166 62	060166 64	060166 66
-2.0	2.28	8.72	2.72	20.28	2.31	2.87	2.03	1.54	10.42	7.24
-1.5	6.65	14.80	7.75	23.19	4.77	5.95	1.63	1.87	2.73	2.68
-1.0	7.59	9.72	5.84	11.55	2.48	3.47	0.80	1.58	1.85	1.70
-0.5	8.60	7.38	4.28	7.02	1.91	1.97	0.77	1.60	1.19	2.03
0.0	7.45	9.45	4.52	2.85	1.80	1.17	0.74	1.53	1.13	2.97
0.5	7.70	20.25	4.01	1.82	1.84	1.84	1.10	2.22	2.67	4.95
1.0	8.12	13.52	3.14	1.28	2.24	2.25	3.20	3.81	4.65	7.98
1.5	6.36	1.50	2.85	1.15	2.95	1.46	6.61	7.35	6.95	13.77
2.0	10.91	2.23	13.75	4.96	12.39	10.50	16.69	33.06	29.17	29.14
2.5	18.42	3.78	27.00	9.40	27.06	28.56	10.30	28.08	22.00	19.15
3.0	12.96	4.03	17.01	5.76	27.84	26.49	19.01	13.36	15.17	6.99
3.5	2.32	2.95	5.45	5.85	9.34	9.98	28.88	3.20	1.71	1.07
4.0	0.45	1.25	1.52	4.52	2.76	3.02	7.87	0.70	0.25	0.23
4.5	0.06	0.17	0.07	0.19	0.17	0.31	0.24	0.04	0.05	0.04
5.0	0.04	0.11	0.04	0.09	0.07	0.11	0.07	0.02	0.02	0.02
Pan	0.08	0.14	0.05	0.10	0.07	0.07	0.04	0.04	0.04	0.04
	100.0	100.0	100.0	100.0	100.0	100.0	100.0	100.0	100.0	100.0

Table C6. Numerical Results of Particle Size Distribution for Samples 67 to 80

Particle Size, Φ	060166 67	060166 68	060166 71	060166 72	060166 74	060166 75	060166 77	060166 78	060166 79	060166 80
-2.0	4.14	9.74	2.31	9.66	2.56	2.36	0.18	27.35	15.59	16.05
-1.5	2.65	6.50	4.35	12.60	4.38	10.57	0.30	13.75	9.64	4.02
-1.0	1.40	4.98	5.90	18.64	3.09	12.25	0.21	11.52	8.25	2.61
-0.5	1.04	3.85	8.02	18.66	3.53	16.36	0.43	9.65	7.80	2.22
0.0	1.07	2.16	7.20	15.03	4.14	15.07	0.29	7.44	6.61	1.62
0.5	1.92	1.45	8.61	12.93	8.57	21.11	0.21	6.01	5.09	1.26
1.0	3.60	1.49	12.00	6.96	8.61	12.78	0.27	3.13	4.82	1.49
1.5	6.93	3.65	11.25	2.31	3.11	2.31	0.45	1.99	3.33	3.84
2.0	35.85	13.66	8.79	1.29	11.08	2.17	1.62	2.01	3.79	23.46
2.5	27.86	25.71	7.71	0.85	26.76	3.21	5.36	2.42	8.48	26.39
3.0	11.09	22.99	12.00	0.53	17.91	1.28	48.38	5.09	20.76	11.99
3.5	1.95	3.11	9.19	0.26	4.50	0.29	33.02	4.70	4.01	3.65
4.0	0.40	0.50	2.62	0.13	1.62	0.10	9.08	3.51	1.12	1.19
4.5	0.05	0.07	0.03	0.03	0.04	0.02	0.18	0.52	0.21	0.07
5.0	0.02	0.06	0.00	0.02	0.03	0.02	0.01	0.43	0.21	0.05
Pan	0.04	0.08	0.02	0.10	0.06	0.10	0.01	0.49	0.29	0.07
	100.0	100.0	100.0	100.0	100.0	100.0	100.0	100.0	100.0	100.0

Table C7. Numerical Results of Particle Size Distribution for Samples 81 to 90

Particle Size, Φ	060166 81	060166 82	060166 83	060166 84	060166 85	060166 86	060166 87	060166 88	060166 89	060166 90
-2.0	13.39	2.17	3.52	0.67	12.64	21.37	11.52	0.23	3.27	0.09
-1.5	3.72	6.36	8.75	1.42	7.34	9.10	6.59	0.44	8.38	0.19
-1.0	3.23	8.32	10.20	1.26	5.92	5.28	5.18	0.68	8.15	0.38
-0.5	2.89	12.26	8.58	1.23	6.68	4.82	5.44	1.06	5.76	0.65
0.0	2.49	14.66	5.03	0.99	8.35	5.62	6.49	0.76	3.10	4.09
0.5	3.32	15.41	4.76	1.34	17.64	9.71	18.50	0.65	2.13	48.79
1.0	6.52	13.85	7.97	3.48	26.51	17.99	24.28	0.54	0.98	40.33
1.5	8.72	8.34	7.16	8.01	8.72	13.55	4.32	0.46	0.61	2.05
2.0	8.34	6.64	3.62	12.45	4.19	7.13	5.84	0.76	1.65	1.45
2.5	7.54	4.94	2.65	10.32	1.18	3.03	6.74	1.13	5.55	0.79
3.0	17.96	4.33	13.83	30.09	0.46	1.57	3.50	17.57	22.11	0.84
3.5	16.46	2.09	18.06	22.65	0.15	0.40	0.82	57.46	19.63	0.24
4.0	5.25	0.52	5.61	5.89	0.08	0.18	0.44	17.15	14.90	0.08
4.5	0.12	0.03	0.17	0.12	0.03	0.06	0.10	0.67	2.22	0.01
5.0	0.02	0.02	0.05	0.03	0.03	0.06	0.08	0.27	1.09	0.00
Pan	0.04	0.05	0.04	0.04	0.09	0.13	0.14	0.16	0.49	0.00
	100.0	100.0	100.0	100.0	100.0	100.0	100.0	100.0	100.0	100.0

Table C8. Numerical Results of Particle Size Distribution for Samples 91 to 100

Particle Size, Φ	060166 91	060166 92	060166 93	060166 94	060166 95	060166 96	060166 97	060166 98	060166 99	060166 100
-2.0	1.62	26.52	5.04	3.97	13.01	0.69	1.64	2.97	5.57	3.25
-1.5	7.67	8.54	8.07	3.11	4.84	2.85	3.23	8.27	8.92	6.57
-1.0	10.78	3.56	14.51	3.75	5.93	4.33	7.03	14.62	11.89	7.89
-0.5	11.23	2.57	29.74	7.53	12.06	7.46	22.16	23.79	18.22	9.63
0.0	8.77	2.04	26.62	12.84	20.29	10.71	28.45	23.46	16.16	8.70
0.5	7.64	2.11	8.97	25.59	20.93	15.43	23.95	15.44	15.99	5.93
1.0	6.33	1.85	2.66	37.64	10.11	22.91	10.55	6.98	18.38	4.74
1.5	4.34	1.69	1.43	4.60	2.20	12.69	2.37	1.84	2.69	2.85
2.0	7.19	4.13	0.87	0.22	2.76	8.48	0.31	0.86	0.42	3.08
2.5	13.37	14.51	0.66	0.19	3.07	5.83	0.08	0.49	0.40	4.54
3.0	15.24	23.93	0.72	0.27	2.84	5.59	0.06	0.60	0.68	16.00
3.5	4.30	5.67	0.35	0.13	1.09	1.82	0.04	0.24	0.41	19.64
4.0	1.16	2.12	0.17	0.06	0.44	0.73	0.03	0.15	0.13	6.08
4.5	0.13	0.35	0.04	0.02	0.10	0.18	0.01	0.05	0.02	0.41
5.0	0.09	0.20	0.05	0.02	0.11	0.16	0.01	0.07	0.02	0.30
Pan	0.13	0.20	0.10	0.05	0.23	0.14	0.06	0.16	0.08	0.37
	100.0	100.0	100.0	100.0	100.0	100.0	100.0	100.0	100.0	100.0

Table C9. Numerical Results of Particle Size Distribution for Samples 101 to 110

Particle Size, Φ	060166 101	060166 102	060166 103	060166 104	060166 105	060166 106	060166 107	060166 108	060166 109	060166 110
-2.0	0.20	1.49	20.79	2.13	0.02	2.62	0.11	0.46	0.43	0.94
-1.5	0.46	6.53	15.25	3.00	0.10	5.64	0.49	1.32	0.31	3.15
-1.0	0.49	5.25	9.69	2.60	0.19	7.17	0.56	1.38	0.31	2.27
-0.5	0.92	4.06	5.15	2.25	0.25	9.24	0.87	1.86	0.50	1.73
0.0	1.40	2.26	1.86	1.67	0.26	11.81	0.92	2.19	0.47	1.39
0.5	2.16	2.11	0.97	2.22	0.31	17.45	1.29	3.55	0.53	1.72
1.0	4.94	1.21	0.85	3.47	0.43	12.90	2.08	6.65	0.66	1.94
1.5	10.35	0.59	0.73	2.85	0.45	6.62	3.74	11.72	0.84	3.74
2.0	18.82	0.83	1.43	3.41	0.72	4.70	8.06	22.10	3.55	16.67
2.5	18.58	1.37	3.79	6.17	1.65	2.32	12.44	20.05	18.02	65.62
3.0	28.03	12.75	21.27	37.99	35.27	3.96	34.46	17.19	54.98	0.62
3.5	11.75	42.58	13.47	26.79	50.51	11.70	27.10	9.09	14.36	0.19
4.0	1.83	17.39	4.16	5.25	9.47	3.72	7.65	2.36	4.74	0.03
4.5	0.03	0.94	0.26	0.10	0.25	0.06	0.15	0.04	0.17	0.00
5.0	0.02	0.39	0.17	0.04	0.07	0.04	0.05	0.01	0.07	0.00
Pan	0.03	0.26	0.16	0.06	0.06	0.06	0.04	0.03	0.05	0.00
	100.0	100.0	100.0	100.0	100.0	100.0	100.0	100.0	100.0	100.0

Table C9. Numerical Results of Particle Size Distribution for Samples 111 to 120

Particle Size, Φ	060166 111	060166 112	060166 113	060166 114	060166 115	060166 116	060166 117	060166 118	060166 119	060166 120
-2.0	0.68	0.24	1.10	4.19	8.94	0.09	0.06	0.04	0.58	1.19
-1.5	3.24	0.89	3.42	9.66	2.68	0.64	0.48	0.15	1.33	4.78
-1.0	3.19	1.07	2.92	4.02	2.22	1.06	0.69	0.33	1.15	4.98
-0.5	3.38	1.44	3.27	2.35	3.80	1.31	0.75	0.35	0.75	3.98
0.0	3.38	1.22	4.30	2.19	6.47	1.41	0.92	0.30	0.45	3.04
0.5	5.15	1.20	6.44	2.68	14.97	2.41	1.19	0.52	0.44	2.70
1.0	3.90	1.14	3.67	1.99	20.05	1.85	1.19	1.17	0.53	3.41
1.5	3.90	2.38	2.52	2.92	17.41	2.06	3.47	3.31	0.90	6.11
2.0	19.07	18.15	19.10	10.18	15.08	15.52	18.49	17.74	4.01	17.82
2.5	26.28	33.59	32.88	18.58	5.69	36.99	28.72	33.00	16.88	18.62
3.0	20.03	27.19	16.81	24.14	1.87	28.22	29.15	29.61	50.21	18.52
3.5	5.96	8.12	2.67	10.65	0.53	6.24	10.64	10.12	17.27	11.36
4.0	1.65	2.79	0.74	4.93	0.20	1.82	3.56	3.05	5.26	3.33
4.5	0.12	0.34	0.08	0.79	0.03	0.21	0.41	0.17	0.14	0.08
5.0	0.04	0.16	0.04	0.44	0.03	0.09	0.18	0.07	0.06	0.04
Pan	0.03	0.07	0.03	0.31	0.04	0.08	0.09	0.06	0.05	0.06
	100.0	100.0	100.0	100.0	100.0	100.0	100.0	100.0	100.0	100.0

Table C10. Numerical Results of Particle Size Distribution for Samples 121 to 130

Particle Size, Φ	060166 121	060166 122	060166 123	060166 124	060166 125	060166 126	060166 127	060166 128	060166 129	060166 130
-2.0	0.14	0.25	1.50	11.47	5.68	15.89	1.02	17.14	3.38	2.21
-1.5	0.00	0.53	4.00	8.34	17.57	13.01	4.08	14.66	14.05	1.66
-1.0	0.18	0.82	3.51	9.50	9.70	9.08	4.63	10.54	16.17	1.12
-0.5	0.53	0.98	4.31	10.85	6.90	9.34	2.99	6.74	17.82	0.96
0.0	0.64	0.80	6.43	10.73	7.86	10.19	2.24	3.79	12.44	0.95
0.5	0.69	0.89	11.67	19.86	10.51	18.66	2.97	3.33	13.86	1.57
1.0	1.06	1.45	5.55	11.81	5.33	12.85	2.87	1.55	8.65	1.71
1.5	2.70	2.67	2.05	2.59	2.83	4.12	2.16	0.68	2.60	3.45
2.0	14.17	17.88	11.25	3.18	9.43	2.72	6.06	1.11	1.85	16.39
2.5	28.02	33.73	26.59	5.23	15.11	1.60	16.80	3.07	3.23	32.60
3.0	33.35	27.45	17.24	4.96	7.72	1.23	34.62	13.33	4.34	29.15
3.5	13.76	9.01	4.24	0.98	0.99	0.68	14.12	13.95	1.23	6.64
4.0	4.47	2.97	1.34	0.29	0.21	0.38	4.88	8.76	0.27	1.36
4.5	0.16	0.36	0.18	0.06	0.05	0.07	0.34	0.75	0.02	0.07
5.0	0.06	0.14	0.07	0.04	0.03	0.06	0.13	0.37	0.02	0.05
Pan	0.07	0.07	0.07	0.10	0.08	0.11	0.10	0.22	0.07	0.10
	100.0	100.0	100.0	100.0	100.0	100.0	100.0	100.0	100.0	100.0

Table C11. Numerical Results of Particle Size Distribution for Samples 131 to 140

Particle Size, Φ	060166 131	060166 132	060166 133	060166 134	060166 135	060166 136	060166 137	060166 138	060166 139	060166 140
-2.0	4.20	0.80	9.01	4.55	10.68	14.64	2.93	13.71	30.73	8.66
-1.5	6.71	0.76	15.70	6.82	21.62	24.01	5.61	14.39	15.89	6.65
-1.0	10.08	0.93	12.76	4.79	21.29	18.17	8.90	15.14	12.96	4.58
-0.5	18.21	1.72	15.82	3.95	16.54	13.21	15.18	15.79	10.97	3.78
0.0	24.00	2.58	20.39	3.55	9.87	8.93	18.62	14.69	9.25	2.65
0.5	20.29	3.67	17.97	3.97	5.89	7.28	18.91	15.06	6.68	3.19
1.0	4.54	8.97	3.43	2.19	2.25	2.01	4.87	3.97	2.10	1.85
1.5	1.92	22.08	0.94	2.28	1.35	1.64	3.50	2.20	1.51	1.45
2.0	1.72	28.95	0.52	3.12	1.41	1.88	3.60	1.61	1.74	3.95
2.5	2.19	20.05	0.36	6.85	1.42	2.10	4.68	1.43	1.93	12.47
3.0	3.63	8.78	0.78	32.63	2.41	3.32	8.39	1.53	2.81	35.51
3.5	1.39	0.67	1.53	21.03	1.68	1.12	2.63	0.22	1.40	11.28
4.0	0.72	0.06	0.58	4.18	1.88	0.89	1.35	0.08	1.14	3.52
4.5	0.13	0.00	0.02	0.05	0.57	0.28	0.32	0.03	0.32	0.24
5.0	0.11	0.00	0.02	0.02	0.55	0.25	0.26	0.04	0.28	0.12
Pan	0.18	0.00	0.16	0.03	0.60	0.27	0.24	0.09	0.29	0.12
	100.0	100.0	100.0	100.0	100.0	100.0	100.0	100.0	100.0	100.0

Table C12. Numerical Results of Particle Size Distribution for Samples 141 to 151

Particle Size, Φ	060166 141	060166 142	060166 143	060166 145	060166 146	060166 147	060166 148	060166 149	060166 150	060166 151
-2.0	4.63	0.24	4.34	12.35	4.83	5.29	0.23	2.52	0.51	0.96
-1.5	9.94	1.56	15.81	18.16	2.25	2.64	0.17	2.28	1.57	2.31
-1.0	10.58	1.90	7.79	7.28	0.81	3.47	0.52	0.89	0.93	1.62
-0.5	14.07	2.35	3.21	4.99	1.10	10.02	3.29	0.94	1.17	1.57
0.0	8.41	1.98	2.09	6.95	1.95	20.64	7.30	1.73	2.45	2.38
0.5	5.60	2.48	1.52	14.08	5.12	26.50	34.47	3.76	4.17	5.17
1.0	2.64	2.34	0.78	12.15	5.64	11.80	45.49	2.79	2.77	3.83
1.5	1.18	1.99	0.55	1.29	5.40	3.86	3.89	2.38	2.74	3.87
2.0	1.89	4.54	2.11	1.75	20.01	7.28	1.37	22.89	24.07	17.54
2.5	5.26	18.53	9.50	4.15	30.17	6.74	1.73	38.61	36.54	27.29
3.0	18.88	40.72	29.77	8.58	18.72	1.49	1.06	17.31	18.06	24.33
3.5	12.28	15.13	14.45	5.14	3.30	0.14	0.27	2.99	3.78	7.05
4.0	4.07	5.56	6.73	2.36	0.50	0.05	0.11	0.73	1.06	1.81
4.5	0.33	0.45	0.81	0.33	0.07	0.02	0.02	0.08	0.09	0.13
5.0	0.12	0.13	0.34	0.20	0.06	0.02	0.03	0.05	0.05	0.07
Pan	0.12	0.09	0.20	0.23	0.07	0.03	0.03	0.05	0.03	0.07
	100.0	100.0	100.0	100.0	100.0	100.0	100.0	100.0	100.0	100.0

Table C13. Numerical Results of Particle Size Distribution for Samples 152 to 169

Particle Size, Φ	060166 152	060166 153	060166 154	060166 155	060166 158	060166 160	060166 161	060166 162	060166 167	060166 169
-2.0	1.98	0.00	7.21	0.03	0.02	0.96	3.47	0.07	0.07	0.00
-1.5	10.52	0.00	6.86	0.11	0.15	2.27	6.85	0.25	0.12	0.06
-1.0	7.33	0.00	2.12	0.14	0.17	1.97	5.90	0.32	0.35	0.38
-0.5	3.66	0.27	1.20	0.28	0.28	1.82	6.30	0.67	1.30	0.65
0.0	2.43	0.36	1.14	1.88	2.59	1.77	7.09	1.79	2.30	0.57
0.5	3.13	1.30	1.70	4.99	47.47	2.46	13.42	6.81	5.23	0.72
1.0	3.10	9.52	4.30	2.30	45.47	5.65	33.00	26.06	19.66	2.51
1.5	3.05	32.00	6.74	3.35	0.82	9.56	17.21	33.10	29.89	8.34
2.0	9.12	41.19	15.08	22.82	1.22	13.47	4.88	23.54	22.04	23.29
2.5	20.56	13.76	29.61	45.64	1.08	6.09	1.40	6.60	12.60	36.37
3.0	25.15	1.46	19.78	15.77	0.50	18.05	0.36	0.74	5.83	22.87
3.5	7.47	0.07	3.17	1.99	0.15	26.93	0.09	0.04	0.53	3.54
4.0	2.17	0.04	0.79	0.49	0.06	8.75	0.02	0.01	0.07	0.66
4.5	0.21	0.02	0.18	0.12	0.03	0.21	0.01	0.00	0.01	0.03
5.0	0.03	0.00	0.03	0.02	0.00	0.01	0.00	0.00	0.00	0.00
Pan	0.08	0.02	0.10	0.08	0.00	0.03	0.01	0.02	0.00	0.01
	100.0	100.0	100.0	100.0	100.0	100.0	100.0	100.0	100.0	100.0

Table C14. Numerical Results of Particle Size Distribution for Samples 170 to 179

Particle Size, Φ	060166 170	060166 171	060166 172	060166 173	060166 174	060166 175	060166 176	060166 177	060166 178	060166 179
-2.0	0.22	0.53	0.04	0.12	0.18	0.00	0.01	0.07	0.05	0.01
-1.5	0.28	0.96	0.03	0.08	0.25	0.00	0.00	0.07	0.11	0.09
-1.0	0.26	0.86	0.15	0.34	0.65	0.19	0.01	0.20	0.12	0.34
-0.5	0.56	2.12	0.24	0.85	1.01	0.65	0.09	0.63	0.54	0.77
0.0	1.46	4.50	0.37	1.19	1.11	0.66	0.39	1.23	0.91	0.80
0.5	3.93	11.62	0.84	3.55	2.10	1.83	2.23	5.61	2.48	1.75
1.0	12.26	25.37	4.19	16.22	5.36	21.72	29.04	35.77	13.93	9.67
1.5	19.41	21.49	20.47	28.01	10.98	54.00	54.08	42.99	50.03	52.70
2.0	19.38	13.25	31.99	22.51	22.81	18.25	12.55	11.03	26.97	30.84
2.5	21.81	10.33	19.91	15.22	31.86	2.30	1.31	1.84	3.71	2.60
3.0	17.59	7.82	18.28	10.61	20.35	0.36	0.28	0.47	0.89	0.36
3.5	2.41	1.02	3.01	1.16	2.88	0.04	0.02	0.07	0.19	0.07
4.0	0.39	0.13	0.47	0.12	0.41	0.00	0.00	0.01	0.04	0.01
4.5	0.02	0.01	0.03	0.01	0.04	0.00	0.00	0.00	0.02	0.00
5.0	0.00	0.00	0.00	0.00	0.01	0.00	0.01	0.00	0.00	0.00
Pan	0.00	0.01	0.00	0.00	0.01	0.00	0.00	0.01	0.01	0.00
	100.0	100.0	100.0	100.0	100.0	100.0	100.0	100.0	100.0	100.0

Table C15. Numerical Results of Particle Size Distribution for Samples 180 to 189

Particle Size, Φ	060166 180	060166 181	060166 182	060166 183	060166 184	060166 185	060166 186	060166 187	060166 188	060166 189
-2.0	0.14	0.18	0.76	0.44	7.54	1.06	0.19	0.68	4.47	3.10
-1.5	0.40	0.20	1.01	0.15	5.72	2.22	0.32	1.56	3.86	4.15
-1.0	0.22	0.10	0.67	0.18	3.31	1.89	0.23	1.02	1.43	2.51
-0.5	0.24	0.20	0.75	0.23	2.86	2.42	0.41	1.83	0.93	2.70
0.0	0.41	0.59	1.15	0.57	4.03	3.35	1.29	3.26	0.81	3.86
0.5	1.30	4.39	3.72	3.68	9.37	7.72	6.25	8.43	1.32	6.60
1.0	11.48	36.87	25.57	42.68	37.42	29.14	45.97	38.92	3.74	11.70
1.5	54.64	52.57	57.81	47.78	23.73	28.14	43.06	39.73	11.39	17.75
2.0	21.17	4.57	5.57	3.65	2.30	14.50	1.68	1.72	37.44	30.67
2.5	6.73	0.17	1.22	0.51	2.36	5.64	0.20	0.60	26.14	13.95
3.0	2.97	0.13	1.49	0.10	1.19	3.01	0.30	1.31	7.29	2.66
3.5	0.30	0.03	0.23	0.02	0.14	0.66	0.07	0.65	1.01	0.28
4.0	0.02	0.00	0.03	0.01	0.04	0.24	0.02	0.22	0.14	0.05
4.5	0.01	0.00	0.00	0.00	0.01	0.00	0.01	0.04	0.02	0.00
5.0	0.00	0.00	0.00	0.00	0.00	0.00	0.00	0.01	0.00	0.00
Pan	0.00	0.00	0.00	0.00	0.00	0.00	0.00	0.02	0.01	0.01
	100.0	100.0	100.0	100.0	100.0	100.0	100.0	100.0	100.0	100.0

Table C16. Numerical Results of Particle Size Distribution for Samples 193 to 236

Particle Size, Φ	060166 193	060166 194	060166 195	060166 196	060166 198	060166 199	060166 232	060166 234	060166 235	060166 236
-2.0	10.08	3.97	3.99	10.97	5.07	1.74	0.27	0.43	0.96	0.79
-1.5	8.26	4.91	3.68	3.68	10.96	2.72	0.26	2.38	2.19	1.72
-1.0	4.43	3.93	2.95	1.53	9.10	2.83	0.61	3.26	2.53	2.04
-0.5	3.88	4.74	4.65	0.60	6.85	2.96	0.84	2.98	2.57	2.52
0.0	2.86	5.13	7.65	0.56	5.32	3.16	0.55	1.67	1.80	2.11
0.5	2.51	6.58	11.16	1.05	4.41	6.13	0.52	1.17	1.35	1.46
1.0	2.05	8.02	11.43	2.07	3.54	4.93	0.90	1.13	1.20	1.25
1.5	2.44	10.80	10.93	5.94	2.90	3.56	3.19	2.00	1.30	1.04
2.0	12.91	26.08	23.42	30.40	5.48	12.78	21.31	7.30	3.67	2.46
2.5	31.20	19.18	15.25	29.40	10.24	27.90	36.54	10.94	5.97	5.12
3.0	16.72	6.10	4.30	12.01	22.72	25.02	26.43	26.60	37.25	36.75
3.5	2.20	0.48	0.49	1.51	9.26	4.68	6.45	31.67	31.51	34.44
4.0	0.38	0.09	0.09	0.23	3.43	1.31	2.03	7.82	7.17	7.92
4.5	0.06	0.01	0.01	0.02	0.51	0.21	0.03	0.47	0.40	0.29
5.0	0.00	0.00	0.00	0.01	0.09	0.02	0.02	0.07	0.07	0.06
Pan	0.02	0.00	0.00	0.00	0.11	0.06	0.06	0.12	0.07	0.05
	100.0	100.0	100.0	100.0	100.0	100.0	100.0	100.0	100.0	100.0

Table C17. Numerical Results of Particle Size Distribution for Samples 237 to 246

Particle Size, Φ	060166 237	060166 238	060166 239	060166 240	060166 241	060166 242	060166 243	060166 244	060166 245	060166 246
-2.0	13.29	0.48	0.30	3.52	11.96	1.11	18.58	1.94	4.51	4.86
-1.5	10.04	1.12	0.83	3.96	13.86	1.76	13.46	3.35	8.16	3.22
-1.0	5.51	0.76	0.91	1.91	5.96	1.26	7.04	5.37	8.12	6.09
-0.5	3.76	1.01	1.00	1.62	3.36	1.14	5.95	11.37	7.99	13.21
0.0	2.24	0.90	0.80	1.32	1.90	1.10	5.60	13.68	10.28	16.53
0.5	1.97	0.82	0.64	1.23	1.42	1.16	9.19	19.08	19.14	16.50
1.0	2.41	1.09	0.68	1.63	1.23	1.93	6.88	20.64	21.05	14.27
1.5	2.80	3.17	0.76	2.15	1.68	2.60	1.79	8.36	7.41	6.72
2.0	8.88	21.46	2.39	5.96	9.93	6.00	5.71	5.00	4.52	4.94
2.5	14.31	35.30	5.75	10.50	22.95	12.80	10.47	4.29	4.70	4.82
3.0	18.73	24.38	49.44	28.79	15.47	41.96	6.71	4.20	2.56	5.34
3.5	11.21	6.78	30.23	30.08	6.38	22.19	5.21	2.12	1.13	2.79
4.0	3.59	2.28	5.91	6.93	3.45	4.79	3.00	0.57	0.35	0.69
4.5	0.50	0.19	0.28	0.29	0.31	0.15	0.23	0.01	0.01	0.01
5.0	0.17	0.10	0.03	0.06	0.04	0.03	0.04	0.00	0.02	0.00
Pan	0.59	0.15	0.04	0.05	0.11	0.02	0.13	0.00	0.03	0.01
	100.0	100.0	100.0	100.0	100.0	100.0	100.0	100.0	100.0	100.0

Table C18. Numerical Results of Particle Size Distribution for Samples 247 to 259

Particle Size, Φ	060166 247	060166 248	060166 250	060166 251	060166 252	060166 254	060166 255	060166 257	060166 258	060166 259
-2.0	8.63	0.49	4.43	1.51	1.07	1.62	0.04	11.99	11.09	40.11
-1.5	6.83	0.49	7.90	2.48	2.17	2.18	0.29	8.73	7.42	7.92
-1.0	9.13	0.66	10.72	2.41	2.34	1.91	0.36	9.24	8.06	7.32
-0.5	9.99	0.90	13.22	2.26	2.11	1.74	0.86	10.98	14.25	8.94
0.0	9.12	1.02	13.57	2.32	2.05	1.53	1.13	12.49	19.22	9.95
0.5	11.70	1.17	14.15	3.50	2.75	1.75	2.29	10.59	16.54	8.20
1.0	13.50	1.89	11.40	6.91	5.18	3.76	7.47	6.34	5.73	4.05
1.5	9.14	2.77	7.21	9.17	7.76	6.69	16.07	4.39	2.69	1.74
2.0	7.40	6.74	6.40	11.21	13.63	12.65	23.24	4.23	1.93	1.63
2.5	7.17	15.98	5.78	13.54	17.47	15.34	17.40	4.97	1.88	2.02
3.0	4.55	47.04	3.57	28.05	28.91	30.94	18.64	9.36	4.42	4.54
3.5	2.07	16.33	1.24	12.33	11.33	15.76	9.03	3.97	3.39	2.06
4.0	0.65	4.39	0.35	4.18	3.06	3.82	3.09	1.78	2.26	0.99
4.5	0.06	0.13	0.02	0.09	0.12	0.21	0.07	0.51	0.68	0.31
5.0	0.02	0.01	0.01	0.01	0.02	0.02	0.02	0.13	0.12	0.06
Pan	0.06	0.00	0.06	0.01	0.03	0.06	0.01	0.30	0.31	0.15
	100.0	100.0	100.0	100.0	100.0	100.0	100.0	100.0	100.0	100.0

Table C19. Numerical Results of Particle Size Distribution for Samples 260 to 270

Particle Size, Φ	060166 260	060166 261	060166 262	060166 263	060166 264	060166 265	060166 266	060166 267	060166 268	060166 270
-2.0	28.31	33.17	5.69	23.00	20.23	19.18	25.50	3.98	19.62	1.51
-1.5	5.41	4.45	7.47	5.93	3.30	12.05	10.46	4.72	12.10	2.16
-1.0	5.92	5.86	8.72	5.95	3.03	10.39	8.96	4.41	10.29	2.46
-0.5	9.03	9.12	11.37	8.12	5.78	13.60	10.48	6.41	10.65	3.88
0.0	13.83	12.54	10.86	15.90	16.65	13.60	9.75	6.49	9.18	4.99
0.5	16.87	11.69	7.26	20.36	27.02	8.14	5.32	4.85	6.88	7.42
1.0	3.79	3.27	3.99	3.56	5.52	4.80	3.67	4.31	6.77	8.20
1.5	1.26	1.87	2.96	1.91	2.56	2.73	1.99	4.13	3.50	3.36
2.0	1.25	1.90	3.50	1.79	2.59	1.85	2.06	6.93	3.23	6.63
2.5	2.00	3.20	7.15	2.37	4.10	2.73	5.12	18.80	6.38	12.96
3.0	6.05	7.40	18.61	5.43	6.04	6.22	12.16	29.14	9.17	34.99
3.5	3.70	3.13	7.16	3.09	1.79	2.95	3.14	4.45	1.46	9.53
4.0	1.76	1.54	3.78	1.78	0.86	1.23	0.97	1.08	0.49	1.67
4.5	0.42	0.50	0.99	0.54	0.30	0.31	0.24	0.11	0.12	0.13
5.0	0.16	0.10	0.17	0.11	0.05	0.04	0.06	0.09	0.04	0.05
Pan	0.23	0.26	0.34	0.16	0.18	0.18	0.12	0.10	0.11	0.06
	100.0	100.0	100.0	100.0	100.0	100.0	100.0	100.0	100.0	100.0

Table C20. Numerical Results of Particle Size Distribution for Samples 271 to 280

Particle Size, Φ	060166 271	060166 272	060166 273	060166 274	060166 275	060166 276	060166 277	060166 278	060166 279	060166 280
-2.0	0.04	0.46	0.22	2.71	0.71	0.00	0.01	0.02	4.16	0.06
-1.5	0.22	0.54	0.47	3.55	1.81	0.04	0.02	0.08	11.91	0.56
-1.0	0.51	0.97	0.58	2.59	1.62	0.05	0.04	0.12	9.20	0.76
-0.5	0.74	1.47	0.85	2.40	1.98	0.07	0.07	0.21	9.62	0.90
0.0	0.68	1.21	0.71	1.78	1.62	0.11	0.09	0.23	8.83	0.67
0.5	1.00	1.44	0.77	1.83	1.73	0.11	0.11	0.22	13.28	0.70
1.0	1.36	2.46	1.20	2.46	2.00	0.18	0.17	0.37	8.44	0.89
1.5	0.80	1.74	1.21	2.69	1.23	0.24	0.23	0.50	1.86	1.15
2.0	1.97	2.45	2.35	4.82	1.34	0.65	0.54	0.90	1.10	2.08
2.5	6.95	5.51	5.25	7.33	2.89	1.95	1.50	1.98	0.78	3.47
3.0	55.77	40.99	51.20	33.28	42.35	39.70	41.93	37.45	4.60	35.80
3.5	24.91	32.67	29.24	26.07	32.20	45.15	44.23	45.59	17.22	37.62
4.0	4.67	7.58	5.36	6.90	7.49	10.84	10.35	11.61	8.00	12.72
4.5	0.25	0.33	0.26	0.81	0.62	0.48	0.36	0.41	0.39	1.12
5.0	0.05	0.08	0.09	0.29	0.15	0.15	0.14	0.11	0.13	0.42
Pan	0.07	0.11	0.25	0.48	0.26	0.27	0.19	0.18	0.46	1.09
	100.0	100.0	100.0	100.0	100.0	100.0	100.0	100.0	100.0	100.0

Table C21. Numerical Results of Particle Size Distribution for Samples 281 to 290

Particle Size, Φ	060166 281	060166 282	060166 283	060166 284	060166 285	060166 286	060166 287	060166 288	060166 289	060166 290
-2.0	5.53	9.25	1.07	4.54	3.28	0.05	3.58	0.48	0.09	4.16
-1.5	8.61	20.29	5.57	8.29	8.76	0.04	10.32	1.17	0.52	8.66
-1.0	6.24	12.78	7.91	8.64	7.62	0.2	9.27	1.15	0.669	6.31
-0.5	5.73	9.29	17.24	9.78	8.49	0.67	10.86	1.33	1.21	4.99
0.0	4.76	6.29	20.08	9.33	10.25	0.77	8.54	1.23	1.38	4.66
0.5	6.71	6.77	21.64	9.41	16.63	1.08	10.26	1.71	2.04	5.74
1.0	5.67	3.38	9.45	5.13	10.61	2.4	9.09	3.65	3.17	8.56
1.5	3.46	0.8	2.13	3.13	3.43	4.21	7.87	8.1	4.53	10.85
2.0	3.2	0.71	1.81	4.16	3.16	7.73	7.9	16.21	9.67	14.25
2.5	2.13	0.77	1.38	5.01	2.36	11.36	5.11	18.07	16.46	13.21
3.0	8.85	5.21	3	12.19	4.8	41.8	5.31	27.19	38.24	9.89
3.5	25.64	15.72	4.51	12.74	13.55	24.31	7.61	15.43	17.59	6.07
4.0	10.21	7.26	2.52	6.05	6.12	5.25	3.57	3.89	4.32	2.11
4.5	1.56	0.79	0.74	0.66	0.37	0.09	0.28	0.17	0.08	0.21
5.0	0.49	0.22	0.23	0.22	0.15	0.01	0.17	0.05	0.02	0.08
Pan	1.21	0.48	0.7	0.72	0.42	0.03	0.24	0.14	0.03	0.26
	100.0	100.0	100.0	100.0	100.0	100.0	100.0	100.0	100.0	100.0

Table C22. Numerical Results of Particle Size Distribution for Samples 291 to 295

Particle Size, Φ	060166 291	060166 292	060166 293	060166 294	060166 295
-2.0	1.05	0.02	0.75	0.23	0.60
-1.5	2.00	0.07	0.29	0.82	1.92
-1.0	1.79	0.09	0.28	1.23	2.36
-0.5	1.72	0.20	0.25	1.26	1.53
0.0	1.70	0.33	0.22	1.01	0.95
0.5	2.71	0.74	0.24	1.09	0.89
1.0	4.11	2.75	0.65	1.95	1.33
1.5	6.12	6.47	2.87	4.06	2.78
2.0	17.56	13.12	16.01	10.71	9.20
2.5	25.01	16.19	29.60	13.70	15.38
3.0	20.16	32.74	34.58	31.33	35.03
3.5	11.57	21.20	10.67	24.95	20.93
4.0	4.06	5.85	3.16	7.24	6.51
4.5	0.19	0.12	0.18	0.24	0.32
5.0	0.10	0.08	0.11	0.08	0.08
Pan	0.15	0.05	0.16	0.11	0.18
	100.0	100.0	100.0	100.0	100.0

APPENDIX H

REGIONAL SEDIMENT MANAGEMENT BULLETIN
VOL 4, WINTER/SPRING 2006

Regional Sediment Management

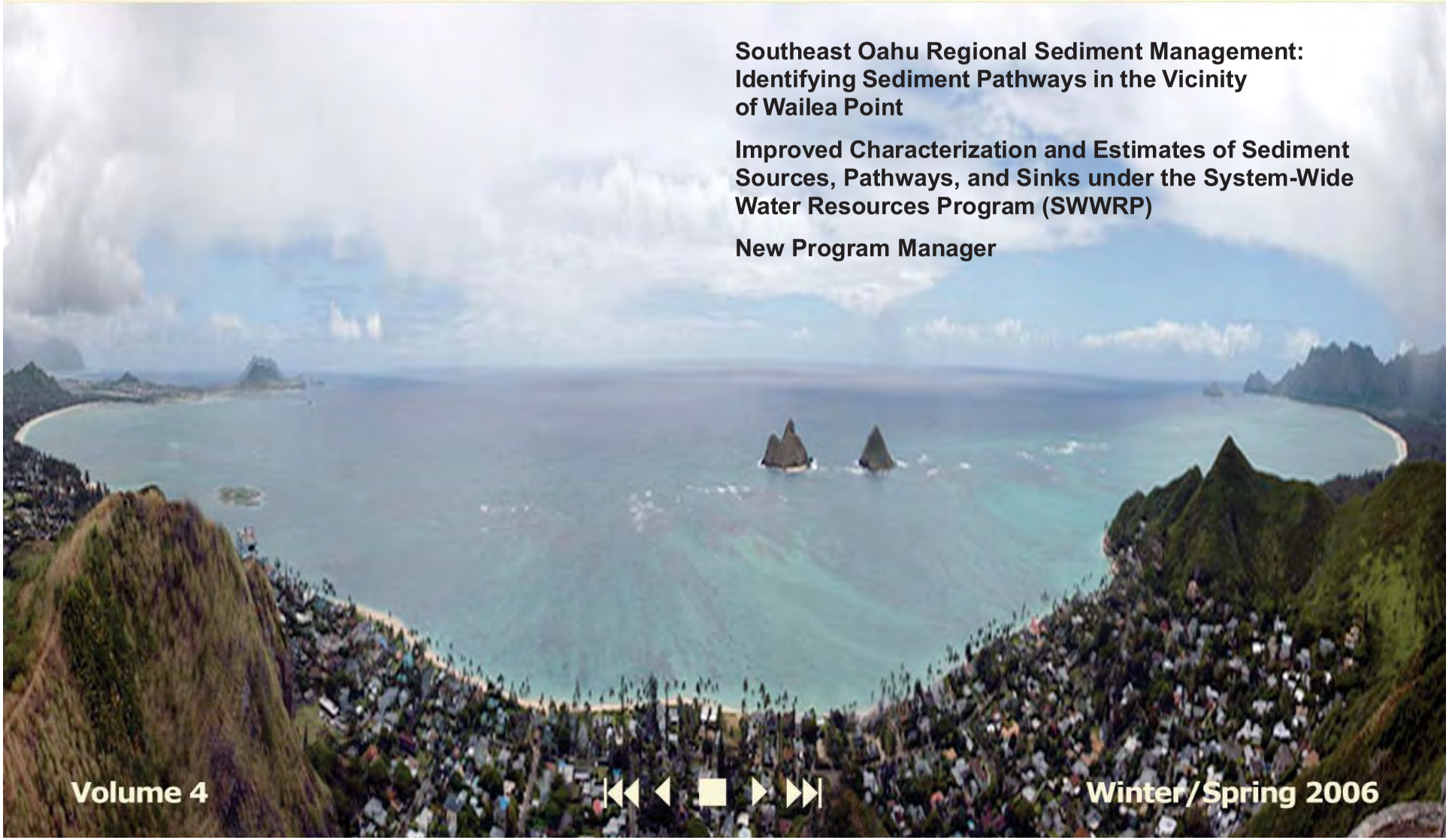

Southeast Oahu Regional Sediment Management: Identifying Sediment Pathways in the Vicinity of Wailea Point

Improved Characterization and Estimates of Sediment Sources, Pathways, and Sinks under the System-Wide Water Resources Program (SWWRP)

New Program Manager

Volume 4 · Winter/Spring 2006

Southeast Oahu Regional Sediment Management: Identifying Sediment Pathways in the Vicinity of Wailea Point

by Thomas D. Smith and Jessica R. Hays, U.S. Army Engineer District, Honolulu

Initial regional sediment management efforts in Hawaii have been focused along the southeast O'ahu (Hawaiian for the gathering place) coast. The Southeast O'ahu Regional Sediment Management (SEO/RSM) study area extends along approximately 12 miles of shoreline from Mokapu (taboo) Point to the north and Mokapu'u (hilltop) to the south. Towns within the region include Kailua (whole in the sea), Lanikai (sky and sea) and Waimanalo (sweet water). Military installations within the area are Marine Corps Base Hawaii and Bellow Air Force Station (AFS). The region experiences prevailing trade winds from the northeast, associated trade showers, and locally generated wind waves. A broad shallow nearshore reef extends along the length of the region. The reef is nominally 2,000 feet wide and has an average depth of about 4 feet. Small offshore islets such as Manana (buoyant), Kaohikaipu (hold back breaking waves), Na Mokulua (calmed, two adjacent islands), Popoi'a, and Mokolea (filled with water) Rock are scattered throughout the reef flat.

Generally, wide sand beaches are a rare sight in Hawaii, but within the SEO region there are a number of long stretches of pristine kahaone (sandy beach). These areas include numerous State of Hawaii-owned beach parks and portions of Bellow AFS. Beach sand in the region primarily comprises calcium carbonate grains derived from shells, corals, and other aquatic organisms. Basalt from the eroding island mountains can also be found in sand samples taken within the active beach profile. At the northern limit of the region, significant quantities of olivine are also present along the upper reaches of the beach.

This is not to say the region does not have erosion and sediment management issues. At Ka'elepulu (hollow and wet) stream mouth, sand from the adjacent shorelines accumulates and blocks the flow of water from Enchanted Lake upstream. The existing sediment management practice is to periodically excavate the sand from the mouth of the stream and place it along the adjacent streambanks. Not only does this practice take the material out of the active profile, strong trade winds blow the sand mauka (toward the mountain) and out of the system. On either side of Wailae (happy water) Point, coastal structures have been constructed such as seawalls, groins, revetments and jetties. Beaches in these areas (including portions of both Lanikai and Bellows AFS) are narrow to nonexistent. At the southern end of the region, the shoreline is eroding and currently within a few feet of Kalanianna'ole Highway along Kaupo (a variety of native banana) and Kaiona (sea mite) beaches. The highway is a major transit route and provides the only access to much of the windward O'ahu coastal margin. The scarcity

of beach quality sand and environmental concerns in Hawaii limit the opportunities for beach nourishment.

A major goal of the SEO/RSM study is to quantify the movement of sand offshore of Wailea (happy waters) Point. The point is located in the central portion of the region and divides the town of Lanikai to the north and Bellows AFS to the south. At the present, the portion of Lanikai beach located adjacent to Wailea Point is awash at high tide and a continuous series of seawalls has been built to protect oceanfront singe-family homes. Further to the north, the beach widens significantly until one reaches Alala (a variety of sweet potato) Point. Beyond Alala Point, the beaches of Kailua are from 100 feet to 200 feet wide and the oceanfront houses are set back up to 300 feet from the mean high water shoreline.

Similarly, south of the point the shoreline has been armored through construction of a revetment along approximately 2,000 feet of the Bellows AFS shoreline. A 50-foot-long groin has been constructed at the point which retains a small pocket beach in front of an officer's beach cottage rental unit. Jetties have also been constructed at the mouth of Waimanalo stream in an attempt to keep the mouth of the stream from being plugged by the influx of sand from adjacent beaches. In order to quantify sediment transport in the vicinity of Wailea Point, the SEO/RMS study strives to incorporate multiple assessment techniques to attain an understanding of the regional coastal processes at work, assess anthropogenic impacts to the system and develop a sediment budget for the area and ultimately the entire region.

In pursuit of a regional sediment budget for SEO, wave, current, and sediment data have been collected, a wave transformation model has been coupled to a water circulation model, and a historical shoreline change analysis is underway. Field data collection was conducted for a one month period in the fall of 2005. Data collection consisted of deployment of Acoustic Doppler Current Profilers (ADCP) and currents) and Acoustic Doppler Velocimeters (ADV) gauges and the tracking of drogues following their release at various locations within Kailua and Waimanalo bays. Instrument locations are shown in Figure 1. Deployment was on 9 Aug 2005 and retrieval was on 14 Sep 2005. Each gauge successfully collected a minimum of one month of time series data.

The ADCP gauges were RD Instruments 1,200 kilohertz Workhorse, bottom mounted facing upward with the sensor head approximately 0.4 meters off the bottom. Figure 2 shows the custom built

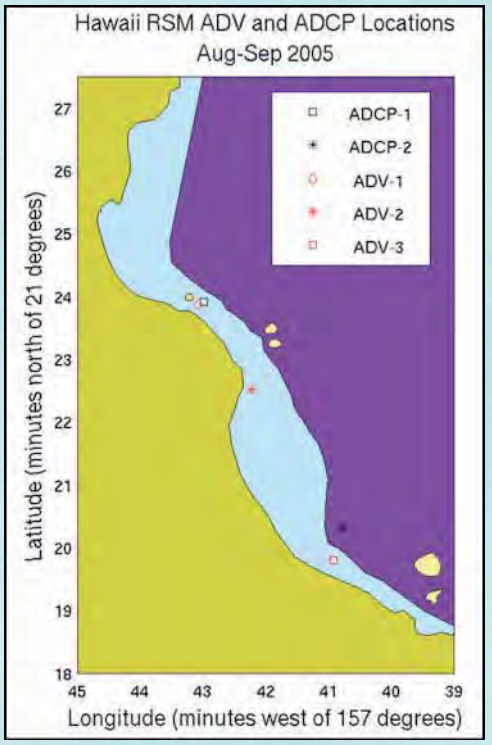

Figure 1. ADCP and ADV locations.

Figure 2. ADCP in frame (left) and close-up of transducer head with biofouling (right).

Figure 3. Hydra ADV in frame (left) and closer view of the biofouled sensor head (right).

mount that was held to the bottom with about 80 pounds of lead weight. These gauges have four acoustic transducers for measuring currents and a pressure sensor, from which horizontal and vertical current profiles were computed at 0.2-meter vertical spacing. These units sampled at 2 kilohertz for directional wave measurements. Each hourly wave burst was approximately 34 minutes long, starting at the top of each hour, and consisted of 4,096 points. There is a 0.44-meter blanking distance from the transducer head, and with a 0.2-meter bin width, this makes the first sample 0.72 meter past the transducer, or about 1.12 meters off the bottom. Current profiles were collected every 10 minutes from a 200-point average.

The three ADV gauges were the Sontek's Hydra model that sample a single point current velocity (U, V, and W) and contained an external pressure sensor. The instrument frame and ADV transducer are shown in Figure 3 (after gauge retrieval). The sample volume for the current measurement is approximately 1 to 2 centimeters in size and about 0.17 meters from the center transducer. This unit uses three beams to determine the three current components.

Four inexpensive current drogues (drifters) were designed and built at the USACE Coastal and Hydraulics Laboratory (CHL) Field Research Facility (FRF) that used Global Positioning System (GPS) tracking and radio telemetry for positioning. They were constructed with off-the-shelf plumbing supplies (PVC pipe, vertical risers, rubber unions, hose clamps), Garmin Geko GPS

Figure 4. GPC current drogue with traditional drifter (grapefruit) and Hawaiian drifter (coconut). Drifter floats just below the surface.

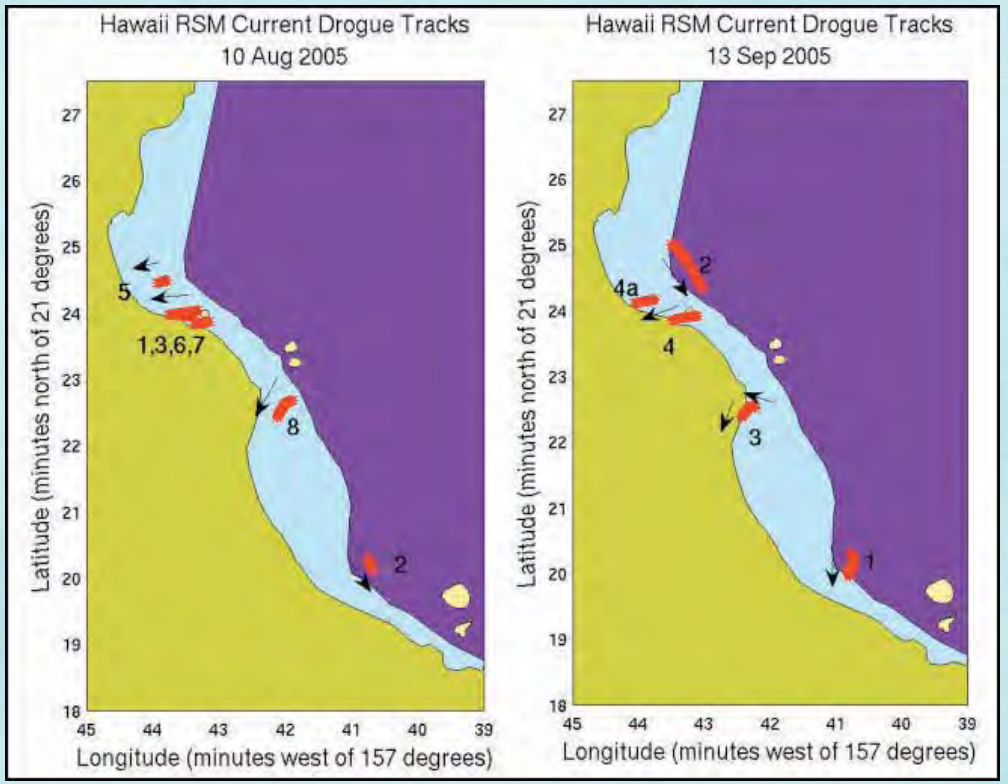

Figure 5. Drogue tracks with track number for 10 August (left) and 13 September (right).

receivers, and MaxStream (model XStream-PKG-R) radio modems (Figure 4). The sails had about a 1-meter cross section. The lower vertical PCV pipe (submerged) contained the modem and batteries, the upper horizontal pipe contained the GPS receiver and radio antennas. A National Electrical Manufactures Association (NEMA) GPS data string was transmitted once per second and the Garmin Fround Control Points (GCP) unit internally recorded positions every 30 seconds. These GPS units are Wide Area Augmentation System

(WAAS) enabled and have a horizontal accuracy of about 3 meters. The radio tracking required line of sight, and it was not possible to simultaneously receive drifters signals in the Kailua and Waimanalo bays.

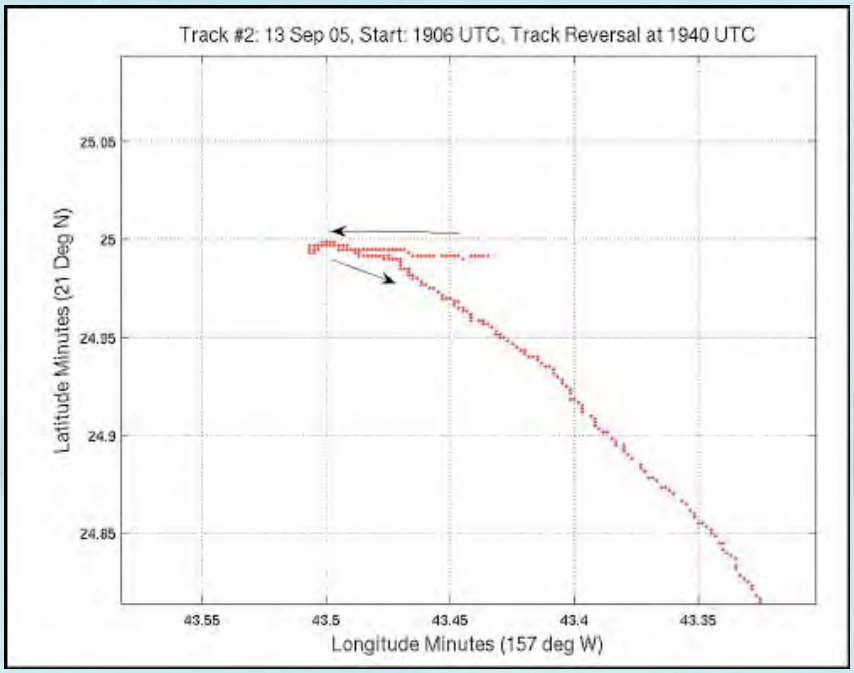

Figure 6. Drouge track reversal on 13 September.

Drogue tracks with track numbers are shown in Figure 5. Some drogues were deployed in the vicinity of the ADV and ADCP gauges for interomparison. An interesting reversal of drogue No. 2 was observed shortly after deployment on 13 Sep (Figure 6), starting off on a nearly due west tract and then turning back to a southeast trajectory.

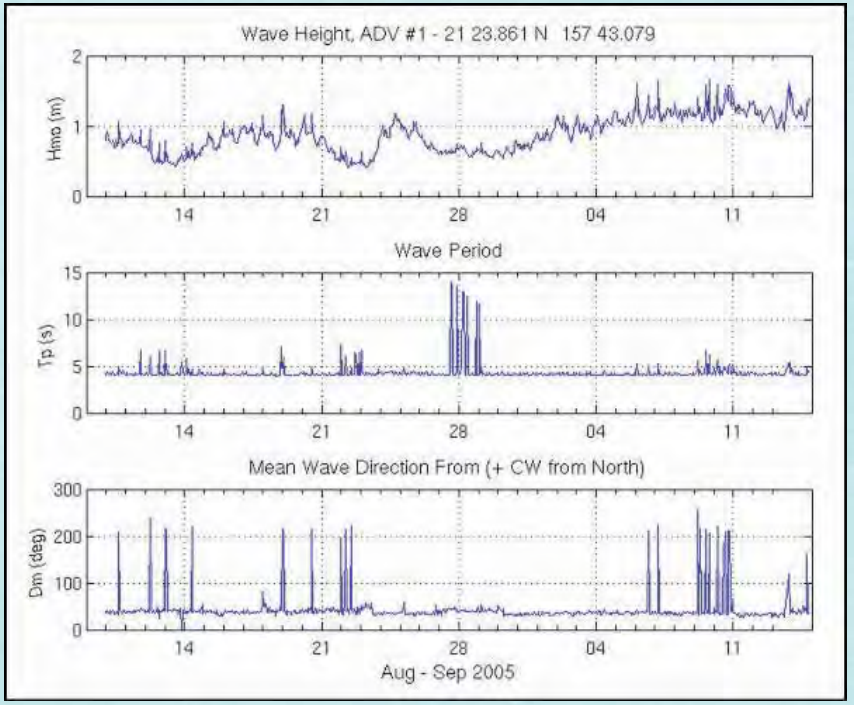

Figure 7. Wave height, period, and direction for ADCP No. 1.

Figure 7 is a plot wave height (Hmo), peak period (Tp), and mean direction (Dm) for ADV No. 1. Figure 8 compares Hmo for the three ADVs and shows ADV No. 3 as having the smallest wave heights. Current directions for ADV No. 2 appear to be mainly north or south which may be due to placing the gauge between coral heads that restricts flows to those directions.

The field data is being utilized to calibrate and verify the results of ongoing wave transformation and water circulation modeling. Bathymetric data used in the generation of model grids were derived from various sources. National

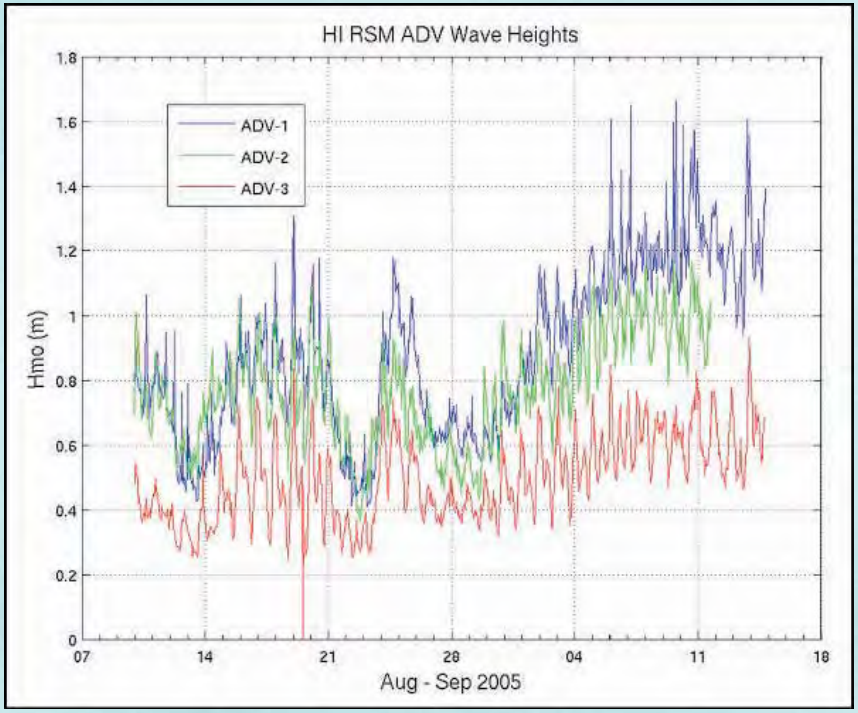

Figure 8. Wave height (Hmo) comparison of the three ADVs.

Geophysical Data Center data sets including ETOPO2 and GEODAS were used in the deep ocean while National Oceanic and Atmospheric Administration (NOAA) digital nautical charts and SHOAL were used for intermediate and nearshore waters, respectively. Grid element size for the circulation model ranged from 75 miles to 80 feet. Bathymetric data were interpolated onto the circulation model grid and hand-edited to ensure accuracy.

Tidal constituents from an established database were used to force the model boundary water levels as well as hindcast winds procured from Ocean Weather, Inc. Tide levels generated by the model compared favorably to NOAA tide gauge data from Kaneohe (bamboo god) Bay and Honolulu (calm bay) Harbor. Wave transformation modeling was conducted over a grid incorporating the SEO region as well as additional area both longshore and makai (oceanward). A directional wave gauge (University of Hawaii/Coastal Data Information Program (CDIP) gauge 098) has been operational at the boundary of the grid from August 2000 to the present and has provided valuable boundary conditions for use in model calibration/verification with nearshore field gauge data acquired as

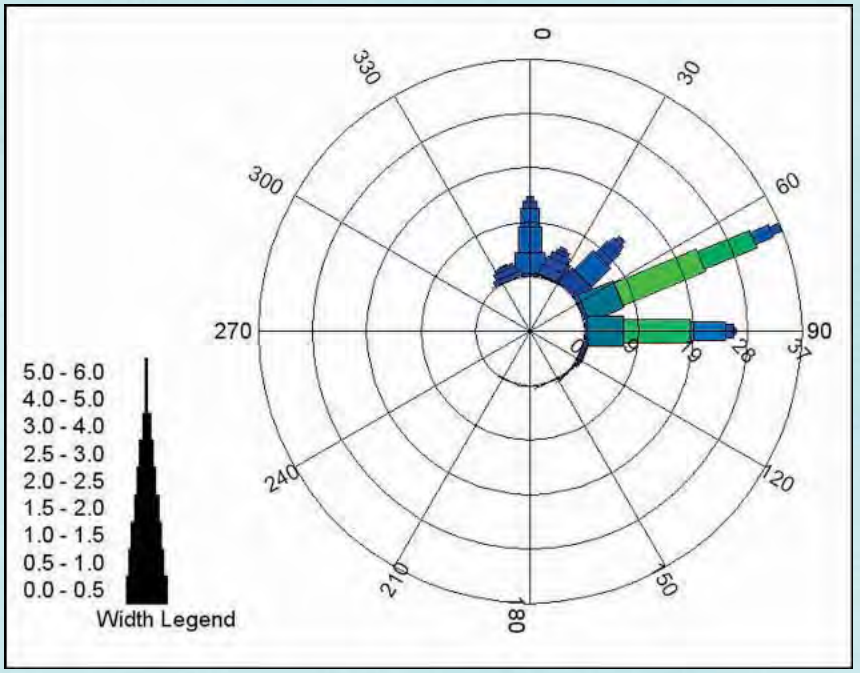

Figure 9. Wave rose for UH/CDIP bouy in RSM demo area.

previously described. As shown in Figure 9, waves recorded by the University of Hawaii gauge were generally from the northeast quadrant and ranged in height from 0.5 to 1.5 meters. Wave periods were on the order of 6 to 16 seconds. Currently, the wave transformation and water circulation modeling is being refined based upon comparison to the field data. Once calibrated, the models will be used to hindcast the wave/wind/tide induced water circulation within the SEO/RSM study area for the year 2004.

The historical shoreline change analysis being conducted for SEO/RSM by the University of Hawaii consists of determining the rate of shoreline change at 20-meter intervals alongshore over the period of early 20th century to 2005. NOAA "T" sheets dating from the early 20th century are being orthorectified using modern GPS ground control and used in comparison with four to eight orthorectified aerial photographs from the post-World War II era to determine a long-term rate of shoreline change. Reweighted weighted least median of squares linear regression technique is being used to determine the long-term trend of historical change. This technique eliminates outlier points from the linear regression and combines measurement and positional uncertainties with regression uncertainties in calculating the standard deviation of the trend.

New aerial photographs from 2005 with a scale of 1:8400 digitally scanned at 10 microns will be acquired for the study. These aerials will cover a coastal strip approximately 800 to 1,000 meters wide centered on the shoreline. Stereo-photogrammetry using orthorectified pairs of photos, with GPS ground control, will be used to create coastal digital terrain models (DTMs). These DTMs will be digitally combined with offshore SHOALS data (where such data exist) to create a seamless topographic/bathymetric DEM for the region. Historical photography and "T" sheets will be orthorectified using the 2005 DEM so that all derived shoreline data are based on orthorectified positions, thus minimizing positional errors. Root mean square positional error of final orthorectified photographs is typically about 1 to 2 meters. Using topographic field profiles to measure beach and dune volume shoreline change rates can be converted to rates of sand volume change over time. Along with historical shoreline change data presented at a 20-meter interval along the entire region a sediment budget for the period of study (approximately 80 years) will be produced.

Sediment Trend Analysis (STA) is a technique that derives patterns of net sediment transport from relative changes in grain-size distributions of aquatic sediments. STA also determines the dynamic behavior or stability (i.e., erosion, dynamic equilibrium, accretion or deposition) of the sediments. Sediment Trend Analysis is used to derive the following information:

- Grain size characteristics of surficial sediment encompassing the entire area of study
- Sediment sources and sinks
- Zones of influence of sediment sources

- Sediment transport pathways
- Sediment stability (i.e., erosion, accretion, dynamic equilibrium, etc.)
- Links between intertidal or beach areas and offshore sediments

For the SEO/RSM study, STA will be utilized as another means to identify sediment pathways in the vicinity of Wailea Point. Sediment sampling is to consist of acquisition of 250 grab samples by the University of Hawaii, analysis of the sediment samples by the CHL and the ultimate use of STA methodology by the University of Hawaii to qualitatively describe how sand moves around and offshore of Wailea Point.

Comparison and correlation of the field data, numerical model results, historical shoreline change analysis, and STA will unlock the mystery of sediment transport within the Wailea Point subregion of the SO/RSM study area. Given an accurate understanding of sediment transport and coastal processes in and around Wailea Point, stakeholders and decision-makers will be able to forge realistic goals in the management of beach resources along the Lanikai and Bellows Air Force Stations shorelines. With a regional sediment management plan in hand, the remaining question will be "Loa'a One? (Got Sand?)".

Loa'a One? (Got Sand?)

APPENDIX I

KAILUA BEACH/KAELEPULU STREAM INFORMATION MEETING MINUTES AND NEWSPAPER ARTICLES

CEPOH-EC-T 19 September 2008

MEMORANDUM For Record

SUBJECT: Recap of September 18, 2008 meeting on Kailua Beach Erosion

1) Attendees:

- USACE Honolulu District – Jessica Podoski (EC-T), Farley Watanabe (EC-R)
- Representative Cynthia Thielen (Kailua/Kaneohe Bay)
- Congresswoman Hirono's Office – Josh Wisch
- University of Hawaii Coastal Geology Dept. – Chip Fletcher, Ph.D.
- UH Sea Grant – Darren Lerner
- DLNR Office of Conservation of Coastal Lands – Dolan Eversole, Chris Conger (Sea Grant Extension Agents)
- DOH Clean Water Branch – Alec Wong
- City & County of Honolulu:
  Dept. of Design/Construction – Terry Hildebrand, Clifford Lau
  Dept. of Parks/Recreation – Wilfred Ho
  Dept. of Facilities Maintenance – Tyler Sugihara, Craig Nishimura, Les Chang
  Dept of Pubic Safety – Kevin Allen (Lifeguard Captain)

2) Discussion focused primarily on regulatory issues that will affect backpassing of sand from Kaelepulu Stream mouth to the eroded area adjacent to the boat ramp (below high water mark) on a regular basis in an effort to address worsening erosion problem. USACE (Watanabe) noted that a Statewide Programmatic General Permit from USACE is effective until 2010 and that DOH Clean Water Branch has the responsibility to enforce the Clean Water Act under this permit (i.e., USACE is not posing a regulatory barrier to backpassing material).

3) Group agreed to draft a Memorandum of Understanding between DLNR/USACE/DOH to outline issues of placing sand at the boat ramp (logistics, monitoring, etc.) and to ensure that all parties have agreed beforehand on procedures in the event that a complaint is registered with DOH following placement. (This occurred during the last attempt at backpassing and stopped sand placement due to suggestion of water quality impairment). Other action considered was to request an emergency declaration from the Governor to get things moving more quickly; however, it is uncertain whether this would exempt enforcement of Clean Water Act.

4) Following drafting and preliminary review of the MOU, group suggests another meeting to be attended by Department/Division heads so that agreement may be approved and forwarded for legal review. Date given for follow-up meeting was approximately 30 days (o/a 20 Oct 08). A follow up meeting to discuss long-term erosion solutions will also be scheduled.

5) For additional information, please see summary provided by meeting organizer (attached) or contact Thomas Smith (438-0581)/Jessica Podoski (438-1680) of Civil Works Technical Branch or Farley Watanabe (438-7701) of Regulatory Branch.

/s/
JESSICA H. PODOSKI, P.E
Coastal Engineer

Podoski, Jessica H POH

From: Dolan.Eversole@hawaii.gov

Sent: Thursday, September 18, 2008 5:32 PM

To: Dolan.Eversole@hawaii.gov

Cc: alec.wong@doh.hawaii.gov; Chris.L.Conger@hawaii.gov; Ikehara, Carolyn T; Mayeda, Craig S.; fletcher@soest.hawaii.edu; Podoski, Jessica H POH; kallen@honolulu.gov; Laurence.K.Lau@hawaii.gov; Chang, Lester K C; repthielen@capitol.hawaii.gov; Sam.J.Lemmo@hawaii.gov; Smith, Thomas D POH; Ho, Wilfred M.Y.; joshua.wisch@mail.house.gov; tsugihara@honolulu.gov; Rep. Cynthia Thielen; Watanabe, Farley K POH; thildebrand@honolulu.gov; lerner@hawaii.edu

Subject: Recap September 18 meeting on Kailua Beach park

I want to thank you all for coming to today's special meeting on the Kailua Beach erosion. I feel we made some progress today in understanding what needs to be done to place beach sand at the erosion site near the boat ramp. As a follow up to the discussion here is a brief summary:

1. The need to supplement with boat ramp area with sand is clear. The best available source is to backpass sand from the Kaelepulu stream either from the stream mouth clearing directly or from the dried stockpiled dune sand and along the banks of the stream (preferred).
2. The erosion occurring at Kailua Beach appears to be worsening and may have crossed a threshold becoming a chronic rather than episodic erosion problem. The erosion may be attributed to a lack of sediment in the system that may be partially alleviated by altering the current sand management practices at the Kaelepulu stream mouth so sand is mechanically redistributed back to the southern portion of the beach park near the boat ramp.
3. The erosion appears to spreading in either direction from the stream mouth and has required the removal of trees as well and the relocation of the lifeguard tower several times.
4. The DLNR and Army Corps of Engineers each have the discretion to allow the sand backpassing under periodic stream maintenance and this would not require a permit to backpass sand to the south.
5. The Department of Health, Clean Water Branch (DOH) is responsible for enforcing Federal and state water quality standards. Due to this fiduciary responsibility to uphold the Federal Clean Water Act the DOH is compelled to enforce if there is a violation of the state water quality standards.
6. It is not clear if the DOH has the discretion to determine at what level and to what degree exceeding the water quality standards constitutes an "violation"
7. The City and County Parks does not want to proceed with a project to bypass sand until there is some assurance they will not be in violation of the DOH's rules.
8. Need to weigh the risk of utilizing sand from stream area vs. impact of no action.
9. Conducting a conceptual feasibility study and project benefit vs. risk analysis may help illustrate the risk of no action.
10. As part of any future action to backpass sand Dolan will assist the City with development of a water quality monitoring plan to address potential concerns of water quality impacts related to the backpassing of sand. Initial estimates for regular water quality monitoring by qualified contractors are on the order $1000 per event.

Future Action Items (with timeline).
1. (Week 1) Dolan Eversole will draft a draft MOU between the DLNR/ CORPS/DOH to outline the issues and how we might all agree to move forward with the project so the sand can be placed below the highwater mark without constituting a violation.
2. (Week 2-3) Upon completion of the draft MOU Dolan will send out for review and comments to this committee.

3. (Week 4) Once the initial comments and concerns have been reviewed another administrative meeting (with each Department/Division head) will be held to discuss the issues raised in the initial review and find expedited solutions.
4. (Week 5-?) Final MOU goes out for legal council review. The MOU will need to be reviewed by the City Corp

Council and the State Attorney General office and may take up to 60-90 days in total.

Other (Interim) Alternatives:

1. Governor's emergency declaration may not supersede Federal Water quality laws.
2. City might be able to proceed with sand placement with understanding of risk of DOH investigation if a complaint is generated. Need to discuss with DOH administration to obtain understanding of investigation and enforcement procedures.
3. Need to weigh the risk of utilizing sand from stream area vs. impact of no action.

Dolan Eversole
Coastal Geologist
University of Hawaii Sea Grant College Program
1151 PunchBowl St Rm 131
Honolulu Hawaii 96813
(808) 587-0321
(808) 587-0322 fax

Posted on: Monday, September 8, 2008

PROBLEM UNSOLVED

Kailua's sandy shore fading

Photo gallery: Kailua Beach Erosion Worsening

By Eloise Aguiar
Advertiser Staff Writer

KAILUA — Erosion at Kailua Beach has reached startling proportions, revealing a 60-foot-long sand trap installed 30 years ago at its southernmost end and buried until recently, and raising concern that the problem could work its way north along the entire beach if something isn't done.

The shore at the end of Kailua Bay, where a boat ramp juts out into the sea, is gone. In its place is a sheer dropoff to a narrow beach lined with a "sand grabber" placed there in the 1970s with the intention of catching and holding sand in place.

It was government's response to the problem and it seemed to work, until recently.

The boat ramp is also taking a hit where water is undermining its left edge, exposing its boulder foundation and causing parts of the asphalt surface to collapse.

About 100 feet of sandy shore from the dropoff out to sea is no longer there. For hundreds of feet along the shore, the roots of ironwood trees are exposed and several ironwood trees have had to be removed for safety reasons.

People thought the sand grabber was working but there was always seasonal movement of the sand, said Raul Fallau, who has lived in Kailua for 50 years and seen it go through many changes. Eventually the sand grabber was totally covered and beachgoers forgot it was there.

"As time went on it started eroding but it would always come back. But this time it isn't coming back," Fallau said. "They brought in sand and tried to fill it up, but you can't compete with Mother Nature."

The "sand grabber" extending from Kailua Beach's small boat launch ramp was installed 30 years ago to stave off erosion and has been covered by sand for so long that most beachgoers forgot it was there. Now, the sea has reached beyond the grabber's concrete blocks and eaten away the beach, leaving a 5-foot dropoff.

Photos by BRUCE ASATO | The Honolulu Advertiser

But leaving the beach as it is could be dangerous to tourists and kids, said Steven and Carol Ann Inouye, who heard about the problem and were at the beach recently to see the damage for themselves.

Kailua Beach is seen from the boat launch ramp.

"I was surprised to see the tiles (of the sand grabber) and the erosion," Steven Inouye said. He had thought the sand grabber, a sort of wall made up of concrete tile blocks, was recently installed. "I don't think the tiles will stop big water from taking the sand."

The beach is part of the city's Kailua Beach Park. But the ocean and up to the high-water mark are the jurisdiction of the state.

The city has asked the state for recommendations about the sand grabber and whether to remove it or repair it, said Lester Chang, director of the city Department of Parks and Recreation. Chang said he's not sure that the sand grabber really worked but is deferring to the state because his department has no expertise on the issue.

When the erosion began, the city moved sand piling up at Kaelepulu Stream to the boat ramp area. However, the state Department of Health halted that, saying the sand, once moved, could not be allowed to come into contact with ocean water.

Kailua isn't the only beach that is eroding, Chang said. Areas in Hau'ula and Hale'iwa are experiencing similar problems. Over the years and at other beaches, he said, he's noticed that sand comes and goes — but what's happening at Kailua is different.

"Usually most of it comes back, but this last two years it seems like it's taking one step forward and three backward," he said.

At a workshop last week hosted by the Army Corps of Engineers on the broader subject of coastal sediment transport, Kailua's erosion problem was raised, said Joseph Bonfiglio, spokesman for the Army Corps.

"The workshop participants agreed on the need to form a focus group with all agencies involved to further discuss issues and alternatives to sediment management at the Kaelepulu Stream mouth," Bonfiglio said in an e-mail.

Chip Fletcher, a University of Hawai'i professor who is conducting a study of the historical shoreline changes of every beach on O'ahu, said the group needs to help develop best management practices for clearing sand from the stream mouth.

Fletcher said the erosion is chronic and creeping north but a plan to manage sand clearing might stem that progress.

"The longer we wait, the longer the erosion will work its way north and affect the entire beach," he said.

Reach Eloise Aguiar at eaguiar@honoluluadvertiser.com.

Ocean Watch

Friday, December 26, 2008

Lesson on why Hawaii's sandy beaches change

When I moved to Hawaii in 1983, I took an oceanography class at UH-Manoa from the chairman of the Oceanography Department, E.D. Stroup.

His fine lectures answered my questions about the ocean so precisely, I even remember where I was sitting when I learned certain facts.

I was front and center the day Stroup explained why Hawaii's sand beaches often change dramatically from season to season. Sand beaches are sediment in motion, changing with the size and direction of waves. Big waves move sand seaward, making beaches narrow. Small waves move sand shoreward, making beaches wide. This phenomenon is called longshore transport.

I'm reminded of that lecture often lately as I read and listen to laments about Kailua Beach. The formerly wide, white beach, the best in Hawaii in many opinions, is going away. The big-wave-little-wave thing isn't working.

There are several possible reasons for this. Some experts think a sea level rise due to global warming might be causing this unusual and, perhaps, permanent erosion. But no one knows for sure that the rate of erosion on Kailua Beach is increasing. This could be one of those natural spikes that happen occasionally, and the beach will eventually fix itself.

Or not. We have man-made structures along the beach that are themselves slowly changing. One is Kaelepulu Stream, a canal that once emptied into the bay but is now sand-choked and stagnant.

Whether the stream ever flowed much naturally is hard to say since it has such a long history of human manipulation.

Enchanted Lake was once a 190-acre body of water called Kaelepulu Pond, a thriving fishpond supporting mullet and other aquatic species. About 90 acres of marshland surrounded this clear pond.

Ancient Hawaiians diverted water in this wetland area for taro farming. Later, sugar planters dammed Kaelepulu Stream, filled the pond and then pumped 2 million gallons of water from it daily to irrigate fields. After the sugar industry left, developers in the 1960s drained water from much of the marsh, filled it with soil and built the community we now call Enchanted Lake.

Over the years, silt from yards, pollution from streets and sand from Kailua Beach collected in the pond and stream. Now these once deep, clear bodies of water are shallow and murky.

Since the stream has too much sand and the beach not enough, it seems logical to dredge the stream, dump the sand back into the ocean and let the waves sort it out. But since the sand in the stream possibly contains pollutants, when workers dredge its mouth, they pile the sand in the beach park. Then wind and rain gradually deposit it back in the stream.

Nature gets away with flushing polluted water and sand into Kailua Bay during storms like we had last week, and we can see the gloomy results: brown water, bobbing trash and warning signs about contaminated water.

Besides the clogged stream, some Lanikai houses and a boat ramp also interfere with the shoreline's natural currents.

State officials are working on solutions to restore the beach, but there are no easy answers.

When Stroup explained beaches in motion, he made one point perfectly clearly: Mess with longshore transport and you'll pay a price.

In this case the price is dear.

Marine biologist Susan Scott writes the newspaper column,
"Ocean Watch", for the Honolulu Star-Bulletin, www.starbulletin.com

Kailua stream nearly overflows canal

Heavy rain frequently causes blockages of Kaelepulu Stream, an area resident says

STORY SUMMARY | READ THE FULL STORY

Firefighters opened the mouth of Kaelepulu Stream at Kailua Beach yesterday after waters rose to hazardous levels, a Fire Department spokesman said.

Firefighters with rubber boots and shovels dug a trench in the sand to allow the stream to drain into Kailua Bay.

Lifelong Kailua resident Bob Thurston, who lives on Kawailoa Road a few lanes from Buzz's, thanked the firefighters yesterday for opening a channel through the sand that had built up across the mouth of the stream into Kailua Bay.

But he said he would rather the city open the stream mouth before heavy rain.

— Leila Fujimori

FULL STORY >>

By Leila Fujimori

POSTED: 01:30 a.m. HST, Jan 03, 2009

(Single Page View) | Return to Paginated View

A fire crew checking Kaelepulu Stream in Kailua after heavy rainfall Thursday night discovered the waters had risen to a dangerously high level yesterday.

Water was beginning to lap over the canal wall onto the parking lot behind Buzz's Original Steakhouse, located across from Kailua Beach Park, Battalion Chief Lionel Camara said at the scene.

Honolulu Fire Department crews opened the mouth of the stream after getting approval from the city Facilities Maintenance and Emergency Management departments.

Firefighters wearing rubber boots and armed with shovels dug a trench about 50 feet long and 3 feet wide, working from noon to 2 p.m. and monitoring the flow until 3 p.m.

The water gushed through the narrow trench into the ocean.

Lifelong Kailua resident Bob Thurston, who lives on Kawailoa Road a few lanes from Buzz's, thanked the firefighters yesterday for opening a channel through the sand that had built up across the mouth of the stream into Kailua Bay.

"All it takes is heavy rains, and the stream starts to overflow back into the neighborhood," Thurston said.

He complained that the city, despite prior flood warnings, failed in the past to open the stream mouth before heavy rain, which led to flooding.

Leslie Muirhead, manager at Buzz's, said the stream "does fill up fast."

"The last big rain, the Friday after Thanksgiving, it flooded the parking lot," she said.

By 3 p.m. the water level in the canal had visibly dropped by about a foot, leaving a wet watermark on the concrete pilings that hold up the bridge running over the stream.

"We frequently drive throughout the communities looking for any unusual situations ... and also to see what the roads and streets look like," said fire Capt. Terry Seelig, adding they are familiar with the flooding problems in the area.

The city also opened the stream mouth Nov. 22 after heavy rain. The storm runoff prompted warning signs at Kailua Beach due to contaminated water.

In December 2007 there were a couple of instances of flooding in the area, and firefighters used portable pumps to move water from lanes on Kawailoa Road.

Camara said that the city's heavy equipment was standing by in case firefighters were unable to accomplish the job. He said it takes some time to haul out the equipment.

The relatively narrow trench will eventually widen by eroding through the sandbar and

CINDY ELLEN RUSSELL / CRUSSELL@STARBULLETIN.COM
Honolulu Fire Department personnel from Companies 18 (Kailua) and 19 (Aikahi) cleared the channel at Kailua Beach Park yesterday morning to prevent flooding. Firefighters noticed the water level beginning to breach the embankment of Kaelepulu Stream and decided to clear the channel. The city also opened the stream mouth Nov. 22 after heavy rain.

View more photos >>

Star Bulletin mobile edition

Monday, January 12, 2009

JAMM AQUINO / JAQUINO@STARBULLETIN.COM

Chip Fletcher, professor of geology and geophysics at the University of Hawaii at Manoa, described yesterday the erosion that has exposed the hollow-tile bricks, known as “sandgrabbers,” at Kailua Beach.

KAILUA'S SAND SLIPPING AWAY

Saving Kailua Beach

The rapid erosion of one of Oahu's most popular beaches spurs multiagency action

STORY SUMMARY | READ THE FULL STORY

The city, state and federal government are taking steps that could eventually counteract the erosion of Kailua Beach.

The Army Corps of Engineers, the state Department of Land and Natural Resources and the state Department of Health are working together to get needed permits and clearances to allow sand from Kaelepulu Stream to be used to replenish the rapidly disappearing beach. A public meeting was held last summer.

The state also hired a consultant to examine the problem and come up with options by 2010.

Beach users say something needs to be done soon.

"In the last two to three years, the shoreline has dramatically eroded," said Chip Fletcher, a professor in the Geology and Geophysics Department at the University of Hawaii at Manoa.

By Robert Shikina

FULL STORY >>

By Robert Shikina

POSTED: 01:30 a.m. HST, Jan 11, 2009

Kailua resident David Brezel, 89, has been swimming daily at Kailua Beach for the past seven years.

Until recently, he entered the water near the boat ramp near the entrance to Lanikai.

Now, exposed cinder blocks stick out where sand used to be, forcing a detour in his routine. He now starts his twice-daily swim on the Kaneohe side of Kaelepulu Stream.

"The waves are smashing onto (the blocks), and it's dangerous, and I can't go swim there anymore," said Brezel, a retired eye doctor. "I like to swim there."

It's just one sign of erosion that's eating away Kailua Beach, which in 1998 was ranked as America's best beach.

Now, erosion has created a drop of about 6 feet before patrons can reach the sandy beach. Roots and pipes extend out of the sandy wall into midair.

The city recently removed 10 ironwood trees because they were being undermined by erosion, said city spokesman Bill Brennan. More trees might also be removed.

Some trees had fallen over because of the loss of beach, said Will Ho, the Windward District manager for the city's parks.

Charles "Chip" Fletcher, a professor in the Geology and Geophysics department at the University of Hawaii at Manoa, said erosion at Kailua has made it difficult to walk across the beach during high tide.

"It's a beach park, for god sakes," he said. "It's severe. It's been unrelenting for the last two years. It's approaching three years now."

The exposed cinder blocks, he said, are "sandgrabbers" built about three decades ago. They were meant to hold sand on the beach.

Now crumbling, the blocks are held together by corroded iron rebar.

Fletcher, a coastal erosion expert, said Kailua Beach had been growing for decades, but the southern portion started to erode the past 10 to 20 years. The erosion near the boat ramp has accelerated in the past two to three years and is now washing away the beach at a rate of 1 to 3 feet a year, he said.

The cause remains elusive.

There are a number of factors from a change in wind patterns to high surf that can lead to erosion, he said.

Fletcher thinks one culprit could be sand going into the mouth of Kaelepulu Stream.

The city regularly dredges the stream, but cannot use sand from the canal to replenish the beach because of federal clean-water requirements.

At the same time, the city dredges only a narrow portion of the stream, Fletcher said. While a heavy runoff could push the sand in Kaelepulu Stream back into the ocean, a dike upstream diverts some of the water to another canal in Kailua, Fletcher said.

The dike was built in the 1980s after flooding damaged the Coconut Grove neighborhood in Kailua.

The state Department of Health is seeking permission to allow the city to use sand recovered from the stream mouth for replenishing the beach.

"The redepositing of the dredged sand from the stream, it can be done, but there are permits, certifications and clearances needed from different agencies," said Joanna Seto, engineering section supervisor of the Health Department's clean-water branch.

Dolan Eversole, a state coastal geologist, said erosion has been increasing around the state, not just at Kailua Beach.

"In the last five years, there seems to be a sudden shift to erosion. Many of the beaches that were formerly stable like Kailua are now beginning to erode," he said.

Factors in the erosion could be locking up of sand by human activity, such as building structures, or the rising sea level, he said.

The state has recently hired a consultant for $45,000 to create a Kailua Beach management plan to provide options for dealing with erosion that has been damaging the beach, said Eversole, who is on loan to the state land department from the University of Hawaii Sea Grant program.

A company called Plan Pacific will create recommendations for management strategies by 2010. The plan will look at erosion, beach management and land use.

"We're hoping that this will be the first of many more strategic beach management plans for the state," Eversole said.

There will be public meetings and workshops with the consultant to solicit concerns from the public .

Meanwhile, state officials still don't know why Kailua Beach's sand is slipping away.

It's unlikely that restoring the sand from the stream mouth will solve the erosion problem, but it could help, Eversole said. "It's the first thing to try."

APPENDIX J

RSM WORKSHOP #4 ATTENDEE LIST AND MINUTES

Hawaii Regional Sediment Management
Southeast Oahu Demonstration Project
Workshop #4

Workshop date: August 27, 2008

Workshop minutes (list of attendees is attached)

Welcome and Introductions (Tom Smith and Sam Lemmo)

Tom Smith welcomed the workshop participants to the fourth and final workshop. He introduced Sam Lemmo, who explained that southeast Oahu is a unique area and an understanding of the sedimentation of the region is needed to understand shoreline change, sand budget, and sand sources, and to develop economical solutions. Mr. Lemmo described the three previous workshops.

Southeast Oahu Regional Sediment Management Overview (Tom Smith)

Tom Smith continued by providing an overview of the SEO/RSM and the topics that would be covered in the workshop. The RSM is an integrated approach from mountains to sea and from Mokapu Peninsula to Makapuu Point. The final products of the SEO/RSM are shoreline change maps, sediment budget, modeling, GIS, demonstration projects, and an RSM plan. He mentioned the potential demonstration projects at Kaupo, Kaiona, Bellows, Lanikai, and Kaelepulu Stream and provided photos of those shorelines.

Field Investigations

Wave and Current Data Collection (Jessica Podoski)

Jessica Podoski presented a description of the data collection program undertaken by the USACE in August and September of 2005. Five weeks of data were collected using three ADVs, 2 ADCPs, and drogues. The CDIP wave buoy was used to determine the input conditions. Wave and current results were presented.

Shoreline Change Analysis (Brad Romine)

Brad Romine presented his results of the shoreline change analysis. He explained that he used historical aerial photographs, using the beach toe as the SCRF (shoreline change reference feature). The shoreline was divided into 20 meter intervals and the change along the SCRF was measured. The data was analyzed using the EX model and the EXT model, which includes acceleration. He explained how to interpret the results. Tom Smith asked which method would be better to use in developing a sediment budget. Mr. Romine explained that EX is better for

identifying the long-term trend, while the EXT is better as showing more recent trends. The areas covered by this work are Kailua, Lanikai, Waimanalo, Kaiona, Kaupo, and Makapuu.

Offshore Sand Sources and Sediment Trend Analysis (Chris Bochicchio)

Chris Bochicchio briefly presented his findings on sediment sources from Kailua Bay through Waimanalo Bay, showing locations and estimated volumes. The largest volume of sand is found in the Kailua sand channel. There were also karst deposits and sand fields throughout the study area.

He continued with a discussion of sediment trend analysis (STA). He explained how sediment size distributions could be interpreted to provide direction and intensity of sediment transport. He presented a color contour plot showing the shoreline change at Bellows and Lanikai. He pointed out that erosion in the location of the Bellows revetments preceded accretion at Lanikai by several years, and then following revetment construction at Bellows, Lanikai experienced erosion. The figure also showed how trends in the shoreline change could be tracked alongshore with time. He also presented a time series plot of weekly average wind direction which showed that the tradewinds have a tendency to oscillate between northeast and east over several years (or longer).

Numerical Modeling Results

Water Circulation and Wave Transformation (Jessica Podoski)

Jessica Podoski presented the water circulation modeling results that were performed using ADCIRC. The currents in the SEO region, modeled under tide and tradewind conditions, are not very strong, and along Lanikai, the currents are typically toward the north. A gyre was found in Kailua Bay. Animations were shown.

She continued with the wave modeling results from STWAVE. The input conditions were wave heights measured by the CDIP wave buoy for 2000 through 2004. The model results were compared with the data collected during the 2005 field experiment. The model included bottom friction as an input, and this value was iterated to determine which value produced the best data fit. A value of $n = 0.2$ (Manning's n) gave good correlation with the measured data, and this was a big improvement over $n=0$. It was also important to include tide in the model. Comparison with the JONSWAP friction coefficient produced similar results.

Regional Sediment Budget (Tom Smith)

Tom Smith presented his sediment budgets for SEO. The calculations were based on the shoreline change analyses presented by the UH Coastal Geology Group and wave modeling results produced by the USACE. He began his analyses at the northern extent of Kailua Beach and worked southward to Makapuu Point.

Mr. Smith pointed out sand sources, sinks, and the limits of littoral cells, which all played roles in the sediment budget. He asked for a discussion of his assumptions as he presented the analyses. In general, there were questions about how much sand, if any, moves around Alala Point between Kailua Bay and Lanikai, and around Wailea Point between Bellows AFS and Lanikai.

SEO/Regional Sediment Management Focus Areas

Kaupo and Kaiona Beaches (Tom Smith)

Tom Smith presented Kaupo Beach as having unstable shoreline along Kalanianaole Highway. DOT installed piles in 2006 to mitigate the erosion threat against the road. This stretch of beach is not believed to be able to hold a beach without structures, so Mr. Smith declared that there was nothing USACE could do at that site.

He continued with Kaiona Beach, which still has a generally sandy shoreline. Some of the properties south of Kaiona Beach Park contain seawalls and north of the beach park, the beach has eroded close to the road. He did not see much potential for a demonstration project at this location.

Kaelepulu Stream (Chip Fletcher)

Dr. Fletcher discussed the situation at Kailua Beach Park, including the erosion on the north side of the boat ramp and the sand buildup in the Kaelepulu Stream mouth.

The City is considering removing the sand grabbers, which have become exposed over the past two years. There is concern whether this would threaten the parking lot inshore. If so, should the parking lot and Ironwood trees be sacrificed to allow the natural progression of the shoreline to occur? He presented that the erosion trend was moving northward.

Will Ho of the C&C Dept. of Parks and Recreation reported that the City's plan for managing the Kaelepulu Stream mouth was to clear it monthly and the sand is piled on the banks adjacent to the stream. The stream mouth fills back in within a few days. State Dept. of Health regulations prohibit placing the sand at any other location on the beach. A heavy rain event might flush the sand back into the littoral system; however, there may not be enough flow, due to re-routing of water out Kawainui Stream. He also noted that the sand is finer than when he was a kid and that the sand has migrated inshore up the stream.

Dr. Fletcher reported on a sand field containing 50,000 to 100,000 cubic yards of sand that is not within the littoral zone and could be mined for beach nourishment.

Ideas that were discussed were removal of the boat ramp, new Best Management Practices, and a focus group to address the stream mouth.

DLNR is conducting a Kailua dune and beach management plan study. Scope of work includes study of sand processes, vegetation, etc.

Tom Smith offered that possibility of their 1135 authority, which would provide the first $100,000 to study the situation. A representative from Congresswoman Hirono's office offered their assistance.

Bellows AFS (David Smith)

David Smith presented three conceptual plans for shoreline restoration at Bellows AFS. The first involved nourishing the beach by following the last stable shoreline (1987) with a minimum dry beach width of 30 feet. The second concept involved nourishing only in front of the revetments, as the southern portion of the shoreline did not need nourishing. This concept required significantly less sand. The third concept showed the effect of removing the revetment and the subsequent equilibrium shoreline location. At this location, there were several buildings that would be threatened by erosion.

Lanikai Beach (David Smith)

David Smith presented two conceptual plans for shoreline restoration at Lanikai Beach. The first concept involved nourishing the beach without the use of structures. This concept produced a 30-foot dry beach width. The second concept involved building tuned T-head groins and nourishing between the groins to produce a more stable beach. This concept produced arc-shaped beach cells with a desired minimum width of 30 feet.

Estimated costs were presented, with Concept 1 requiring renourishment every 8 to 9 years. This greatly increases the cost over 50 years. The 50 year cost for Concept 1 was estimated to be $109,000,000 versus the estimated $42,000,000 for Concept 2.

A question was asked regarding the ability to walk along the beach without obstruction. Dr. Smith replied that the dry beach area was one foot higher than the groin crest elevation. This would produce a continuous walking area with a minimum width of 30 feet, expanding to approximately 100 feet near the groins. Another question was asked regarding the effects of turbidity if the beach was nourished with offshore sand. Dr. Smith replied that the sand mined from the reef flat would likely not cause turbidity problems because the sand is already in a dynamic environment and fines would have been already removed from the sand. Additionally, matching the source sand to the native sand alleviates such concerns.

Tom Smith continued by introducing the Lanikai Beach Restoration Pilot Project. This would involve design of a two-groin system with beach nourishment. The groins would be made of a "soft" material such as a geotextile filled with sand and would be considered temporary. The project site would be centered at the beach access across from Pokole Way.

Future Work (Tom Smith)

Tom Smith presented a list of future work that builds upon the SEO/RSM. Work included investigating sand mining from Kaelepulu Stream, the Lanikai Beach Restoration Pilot Project, review of the SEO sediment budget, updating of the RSM plan, and preliminary development of a Maui RSM plan.

The participants were thanked and the workshop was adjourned.

Workshop #4 List of Attendees
August 27, 2008

FIRST NAME	LAST NAME	ORGANIZATION
Darin	Aihara	U.S. Army Corps of Engineers – intern
Laurie	Baron	
Gail	Baron	
Christopher	Bochicchio	University of Hawaii
Ned	Dewey	The Mills Group
Dianne	Drigot	Marine Corps Base Hawaii
Derek	Esibill	Kailua Intermediate School
Charles (Chip)	Fletcher	University of Hawaii
Peter C.	Galloway	U.S. Army Corps of Engineers – Regulatory Branch
Justin A.	Goo	U.S. Army Corps of Engineers – intern
Lynn	Graybeal	Earth Tech AECOM
Jarrett	Hara	U.S. Army Corps of Engineers – Civil Works Tech Branch
Terry	Hildebrand	Design and Construction City of Honolulu
Wilfred	Ho	City and County of Honolulu
Jamie	Ho	State of Hawaii, Department of Transportation
Sam	Lemmo	State of Hawaii, Department of Land and Natural Resources
Jennifer	Lutz	Earth Tech AECOM
Chadman	Maio	City and County of Honolulu
Frederick	Millen	Hickam Air Force Base
Sharon	Nekoba	Department of Land and Natural Resources
Jessica H.	Podoski	U.S. Army Corps of Engineers – Civil Works Tech Branch
Bradley	Romine	UH Coastal Geology Program
Thomas	Smith	U.S. Army Corps of Engineers – Civil Works Tech Branch
David	Smith	Sea Engineering
Kenneth	Tseutsch	Department of Transportation
Randall	Wakumoto	C&C of Honolulu, Dept. of Environmental Services
Jason	Wische	Representative for Congresswoman Mazie Hirono
Michael F.	Wong	U.S. Army Corps of Engineers – Civil Works Tech Branch